



Methods to incorporate silicon for the direct fluorination of proteins

by

Kymerley R. Scroggie

College of Science and Engineering

Thesis submitted for the fulfilment of the Degree of

Doctor of Philosophy

on 21 October 2020

Table of contents

<i>Thesis summary</i>	<i>vi</i>
<i>Declaration</i>	<i>viii</i>
<i>Acknowledgements</i>	<i>ix</i>
<i>Published work</i>	<i>xi</i>
<i>Glossary of abbreviations and non-standard terms</i>	<i>xiii</i>
1. Fluorinating proteins and their use in positron emission tomography	1
1.1 Introduction	1
1.2 Positron emission tomography (PET)	2
1.3 Biomarkers as diagnostic imaging agents for PET	3
1.4 Properties of positron emitting radionuclides for PET	4
1.4.1 Modes of decay	4
1.4.2 Positron energy	4
1.4.3 Half-life	5
1.4.4 Availability and production	5
1.5 Fluorine-18	6
1.6 Radiolabelling proteins with fluorine-18	7
1.6.1 Electrophilic vs nucleophilic	7
1.6.2 Indirect vs direct	8
1.7 Radiolabelling through Si-F bond formation	10
1.8 Radiolabelling through B-F bond formation	16
1.9 Radiolabelling with fluorine through metal complexes	20

1.10 Radiolabelling through S-F bond formation.....	25
1.11 Radiolabelling through P-F bond formation.....	28
1.12 Concluding remarks	28
1.13 Doctoral research contributions to knowledge	30
2. Design, synthesis and direct aqueous fluorination of a silanol-based prosthetic group..	31
2.1 Introduction.....	31
2.2 Proposed strategy for the direct aqueous fluorination of proteins.....	32
2.3 Direct aqueous fluorination of a model silanol	32
2.4 Designing a silanol for the chemical modification of proteins	35
2.5 Synthesis of 1-[(4-diisopropylsilanol)benzyl]amine (49).....	36
2.5.1 Lithium halogen exchange, silylation and synthesis of a mesylate intermediate	36
2.5.2 Optimisation of metalation and silylation.....	37
2.5.3 Mesylate displacement to introduce amine functionality.....	38
2.5.4 Oxidation of the silane to the silanol.....	39
2.6 Direct aqueous fluorination of 1-[(4-diisopropylsilanol)benzyl]amine (49).....	39
2.7 Concluding remarks and chapter summary.....	42
2.8 Experimental procedures	43
2.8.1 General experimental details.....	43
2.8.2 Direct aqueous fluorination of triisopropylsilanol (47).....	44
2.8.3 Synthetic procedures and analytical data	46
2.8.3 Direct aqueous fluorination of 1-[(4-diisopropylsilanol)benzyl]amine (49).....	52
3. Chemical incorporation of silicon into proteins and their direct aqueous fluorination	61
3.1 Introduction.....	61
3.2 Incorporating silicon into proteins at cysteine	62
3.2.1 Ubiquitin(K63C)	63
3.2.2 C2Am(S78C)	65
3.2.3 Annexin V	67

3.2.4 Bovine serum albumin (BSA)	70
3.3 Incorporating silicon into proteins at lysine	75
3.3.1 Lysozyme	76
3.4 Direct fluorination of proteins at silicon	79
3.4.1 Lysozyme	80
3.5 Concluding remarks and chapter summary.....	82
3.6 Experimental procedures	83
3.6.1 General experimental details.....	83
3.6.2 Synthetic procedures and analytical data.....	84
3.6.3 Proteins used in this study.....	86
3.6.4 Chemical modifications of ubiquitin(K63C)	91
3.6.5 Chemical modifications of C2Am(S78C).....	96
3.6.6 Chemical modifications of annexin V	102
3.6.7 Chemical modifications of BSA	106
3.6.8 Chemical modifications of lysozyme.....	115
3.6.9 Direct fluorination of lysozyme	120
4. Design, synthesis and direct aqueous fluorination of a silanol-based amino acid	122
4.1 Introduction.....	122
4.2 Genetic incorporation of unnatural amino acids	122
4.3 Designing a silanol-based amino acid for genetic incorporation into proteins	123
4.4 Synthesis of 2-amino[3-(4-diisopropylsilanol)phenyl]propanoic acid (72)	125
4.4.1 Installing the silicon core	125
4.4.2 Oxidation studies of homobenzylic alcohols	126
4.4.3 Strecker synthesis	132
4.5 Aqueous fluorination of 2-amino[3-(4-diisopropylsilanol)phenyl]propanoic acid (72).....	133
4.6 Concluding remarks and chapter summary.....	135
4.7 Experimental procedures	135

4.7.1 General experimental details.....	135
4.7.2 Synthetic procedures and analytical data.....	137
4.7.3 Oxidative cleavage studies.....	141
4.7.4 Aqueous fluorination studies of 2-amino[3-(4-diisopropylfluorosilyl)phenyl]propanoic acid (72)	152
5. Genetic incorporation of a silicon-based amino acid.....	161
5.1 Introduction.....	161
5.2 C321.ΔA <i>E.coli</i> cells.....	163
5.2.1 Incorporation using existing aminoacyl-tRNA synthetase and tRNA pairs.....	163
5.2.2 Directed evolution of a new aminoacyl-tRNA synthetase and tRNA pair.....	167
5.3 DH10B <i>E.coli</i> cells.....	172
5.3.1 Incorporation using existing aminoacyl-tRNA synthetase and tRNA pairs.....	172
5.4 Concluding remarks and chapter summary.....	174
5.5 Experimental procedures.....	174
5.5.1 General experimental details.....	174
5.5.2 Plasmids used in this study.....	177
5.5.3 Genetic incorporation of the 72 using an existing aminoacyl-tRNA synthetase.....	182
5.5.4 Directed evolution of an orthogonal aminoacyl-tRNA synthetase/tRNA pair.....	184
6. Conclusions and future directions.....	186
6.1 Introduction.....	186
6.2 Confirming the site of chemical modification and fluorination.....	186
6.3 Direct evolution of aminoacyl-tRNA synthetase and tRNA pairs.....	187
6.4 Hydrolytic stability studies and 2 nd generation silanols.....	188
6.5 Radiolabelling proteins with fluorine-18.....	189
6.6 Concluding remarks.....	189
7. References.....	191
8. Appendices.....	207
8.1 Appendix A.....	207

Thesis summary

The direct fluorination of native proteins is a notoriously difficult task. The aqueous environments required by proteins severely hampers fluorination while the dry, organic environments that promote fluorination denature the proteins. To circumvent these issues, indirect fluorination methods whereby a prosthetic group is first fluorinated and then conjugated to a protein have become common place. However, when it comes to the radiofluorination of proteins these indirect methods are not well suited to the short half-life of the fluorine-18 radionuclide (110 minutes). This doctoral thesis explores the incorporation of silicon, an inorganic fluoride acceptor, into proteins as a means towards their direct fluorination.

This thesis reports the design and synthesis of silanol derivatives and their incorporated into proteins via site-selective chemical modifications at cysteine and lysine residues. The chemically modified proteins were found to undergo direct fluorination at the new incorporated silicon via substitution of the silanol hydroxide group. The direct fluorination proceeds in 100% aqueous conditions in time frames compatible with the half-life of the fluorine-18 radionuclide. These results support the use silanols for the direct, aqueous fluorination of proteins and represents, for the first time, their use for this purpose.

This thesis also reports the site-selective incorporation of a silanol into proteins via amber codon suppression. Using an existing tRNA and tRNA synthetase pair a silanol-based unnatural amino acid was incorporated into green fluorescent protein. With a minimal incorporation efficiency, future work aimed at increasing the incorporation efficiency through the evolution of a tRNA and tRNA synthetase pair specific for the silanol-based unnatural amino acid is required. Nevertheless, this research provides strong evidence for the continual investigation into the use of amber codon suppression for the incorporation of silanols into proteins.

The results presented within this thesis provides a constructive basis for further exploration into the use of silanols for the direct and aqueous fluorination of biomolecules. The results of this work give valuable insights into using silanols for the late-stage radiofluorination of biomolecules and could lead to future advancements in the targeted and early detection of disease within the field of nuclear medicine.

Declaration

I certify that this thesis does not incorporate, without acknowledgment, any material submitted for a degree of diploma in any university; and to the best of my knowledge and belief does not contain any material previously published or written by another person except where due reference is made in the text.

Kymberley R. Scroggie

16 August 2020

Acknowledgements

Firstly, I would like to thank my supervisors Associate Professor Justin Chalker and Associate Professor Michael Perkins. It has been a long, enjoyable journey and it goes without saying that I could never have completed this PhD without your continual encouragement. The support and guidance you have both given me in all my endeavours both in and outside the world of chemistry (no matter how crazy you thought they were) has been vital to my development, both personal and professional. For this and your friendship, I thank you!

I also wish to express my gratitude to Associate Professor Hui-wang Ai (University of Virginia) and Dr Gonalo Bernardes (University of Cambridge) who both welcomed me into their laboratories for a short time during my doctoral studies. Working in your research groups was an exhilarating opportunity where I was able to extend my knowledge and technical skill sets in the fields of molecular biology and chemical biology. I am grateful for the knowledge of the international science community I gained from these experiences, which have been instrumental to my career development.

Secondly, I would like to thank all those within Chemical and Physical Sciences. I could not have asked for a more friendly and supportive environment to work in. Thanks to Simone Madaras, Patryk Syta, Dylan Innes and Kyle Farrell, the Chalker-Perkins Lab was a pleasure to be a member of. Special thanks to Flinders Analytical's Jason Young and Dr Daniel Jardine for their assistance with mass spectroscopy analysis, Associate Professor Martin Johnston who always kept the NMR up and running, Dr Maria Matos from the University of Cambridge for her guidance in protein modifications and Tan Truong from the University of Virginia for teaching me all the molecular biology technical skills I now have.

Thirdly, I would like to acknowledge the generous funding bodies that made my doctoral studies possible. The Australian Government for providing the Research Training Scheme, the

Faculty of Science and Engineering who awarded me The Faculty of Science and Engineering Research Award, Flinders University who awarded me the Flinders University Research Scholarship and, the Australian Federation of University Women who selected me as a recipient for the South Australia Graduate Centenary Scholarship to conduct part of my doctoral studies at the University of Virginia.

And finally, I wish to thank my friends and family. To Lisa Alcock and Renata Kučera, thank you for the coffee breaks, chats, laughs and everything else. In this crazy world we live in, your friendship keeps me sane! To my Mum and Dad, you have always supported and encouraged me to do the things I have wanted to do for which I am forever grateful. This has been no different, thank you. To my partner Nathan, words cannot describe how thankful I am to have you by my side. You are my biggest advocate and have encouraged and pushed me to achieve things I never thought possible. This one is for both of us!

Published work

The following is a list of peer-reviewed articles that were published, and conference presentations that were presented during the candidate's candidature.

Peer-reviewed articles related to the work presented in this thesis

1. K. R. Scroggie, L. J. Alcock, M. J. Matos, G. J. L. Bernardes, M. V. Perkins & J. M. Chalker, 2018, A silicon-labelled amino acid suitable for late-stage fluorination and unexpected oxidative cleavage reactions in the preparation of a key intermediate in the Strecker synthesis, *Peptide Science*, 62, E24069–6, DOI: 10.1002/Pep2.24069.

Peer-reviewed articles not related to the work presented in this thesis

1. N. A. Lundquist, M. J. Sweetman, K. R. Scroggie, M. J. H. Worthington, L. J. Esdaile, S. F. K. Alboaiji, S. E. Plush, J. D. Hayball & J. M. Chalker, 2019, Polymer supported carbon for safe and effective remediation of PFOA- and PFOS- contaminated water, *ACS Sustainable Chemistry & Engineering*, 7(13), 11044-11049, DOI: 10.1021/acssuschemeng.9b01793.

Conference presentations

1. K. R. Scroggie, M. V. Perkins, HW. Ai and J. M. Chalker, 2019, Incorporation of Silicon into Proteins for Direct Fluorine Labelling, invited speaker at the inaugural Fringe Festival Lectures in Adelaide, Australia.
2. K. R. Scroggie, M. J. Matos, M. V. Perkins, HW. Ai, G. J. L. Bernardes And J. M. Chalker, 2018, Silicon Incorporation for Direct Fluorine Labelling of Proteins, invited flash talk at the EMBO Chemical Biology Workshop in Heidelberg, Germany.

3. K. R. Scroggie, M. J. Matos, M. V. Perkins, HW. Ai, G. J. L. Bernardes And J. M. Chalker, 2018, Silicon Incorporation for Direct Fluorine Labelling of Proteins, poster presentation at the EMBO Chemical Biology Workshop in Heidelberg, Germany.
4. K. R. Scroggie, M. J. Matos, G. J. L. Bernardes, M. V. Perkins And J. M. Chalker, 2017, The site-selective and direct fluorine labelling of proteins under aqueous conditions, poster presentation at the Royal Australia Chemical Institute Congress Meeting in Melbourne, Australia.
5. K. R. Scroggie, M. V. Perkins And J. M. Chalker, 2016, Studies Towards the Direct Labelling of Proteins with ^{18}F for PET Imaging, poster presentation at the Royal Australia Chemical Institute Medicinal Chemistry and Chemical Biology Conference in Sydney, Australia.

Glossary of abbreviations and non-standard terms

APCI	atmospheric pressure chemical ionisation
Ar	aromatic
CAT	chloramphenicol acetyltransferase
COSY	correlated spectroscopy
Da	Daltons
DABCO	1,4-diazabicyclo[2.2.2]octane
Dha	dehydroalanine
DMF	dimethylformamide
DMP	Dess-Martin periodinane
DMSO	dimethyl sulphoxide
DSA	direct sample analysis
equiv.	equivalents
ESI	electrospray ionisation
FEP	fluorinated ethylene polypropylene
FTIR	Fourier transform infrared

HDMS	high definition mass spectroscopy
hr	hour/s
HMBC	heteronuclear multiple-bond correlation
HRMS	high resolution mass spectroscopy
HSQC	heteronuclear single-quantum correlation
iPr	isopropyl
IR	infrared spectroscopy
<i>J</i>	coupling constant
LB	Luria-Bertani lysogeny broth
LC-MS	liquid chromatography mass spectroscopy
min	minute/s
<i>M.jannaschii</i>	<i>Methanocaldococcus jannaschii</i>
mp	melting point (°C)
MS	mass spectroscopy
Ms	mesyl
MWCO	molecular weight cut off
m/z	mass to charge ratio
NaP _i	sodium phosphate buffer
NMR	nuclear magnetic resonance
PBS	phosphate buffer saline
PCC	pyridinium chlorochromate

PDC	pyridinium dichromate
PET	positron emission tomography
pK_a	acid dissociation constant
R_f	retention factor
RPM	revolutions per minute
rt	room temperature
sec	second/s
TBS	<i>tert</i> -butyldimethylsilyl
TCEP	tris(2-carboxyethyl)phosphine
TEMPO	(2,2,6,6-tetramethylpiperidin-1-yl)oxyl
THF	tetrahydrofuran
TLC	thin layer chromatography
ToF	time of flight
Tris HCl	tris(hydroxymethyl)aminomethane hydrochloride
UPLC	ultra performance liquid chromatography
UV	ultraviolet
δ	chemical shift (ppm)
ν_{max}	wavenumber at maximum absorption (cm^{-1})

Chapter One

Fluorinating proteins and their use in positron emission tomography

1.1 Introduction

Positron emission tomography (PET) is a powerful, non-invasive molecular imaging modality. First used to detect brain tumours prior to surgical removal in the 1950's,^{1,2} it is now used in the study of cardiac diseases³ and myocardial perfusions,⁴ neurodegenerative diseases such as Parkinson's,⁵ Alzheimer's⁶ and Huntington's,⁷ inflammatory diseases,⁸ cancers including those that affect the breasts,^{9,10} lungs,¹¹ skin¹² and prostate,¹³ as well as diseases caused by bacterial infections.¹⁴

Central to molecular imaging with PET is the development of suitable PET imaging agents. With endless opportunities to use PET for molecular diagnostic and therapeutic procedures¹⁵ this has become a key area of research within the fields of medicine, chemistry and biology. Finding suitable molecular probes and the radiolabelling of these probes with positron emitting radionuclides, however, still represents one of the most significant challenges faced by the research community.¹⁶ In this Chapter we present a review of the literature discussing

protein-based imaging agents for PET and the strategies for radiolabelling them with fluorine-18 with a particular focus on non-carbon approaches and their potential for the direct labelling of these biomolecules.

1.2 Positron emission tomography (PET)

PET is primarily based on radiolabelled molecular probes that serve as imaging agents. These imaging agents, radiolabelled with a radionuclide that decays via β^+ decay, release a positron (β^+) and a neutrino (ν_e) upon a decay event. After being ejected from the nucleus the positron releases kinetic energy as it moves throughout the surrounding matter. When at a low enough energy, a collision with an electron in the surrounding matter results in annihilation. In this process, the positron and electron are converted into a pair of photons with energies of 511 keV which are emitted at ca. 180° apart (Figure 1.1). Coincidence detection of these photon pairs allows the point at which annihilation occurred to be determined.¹⁷

The coincidence detection of a high magnitude of photon pairs provides information that can be used to reconstruct three dimensional images. The exact location of the positron at the time of decay is unknown as it travels a short distance (millimetres) before annihilation. Nevertheless, coincidence detection gives an approximation of the temporal and spatial distribution of the imaging agent¹⁵ and the reconstructed images can provide functional information about the biological processes that are or are not occurring within the body. What information can be obtained is dependent on the molecular probe that is used. Which molecular probe is used is itself, dependent on the question trying to be answered.

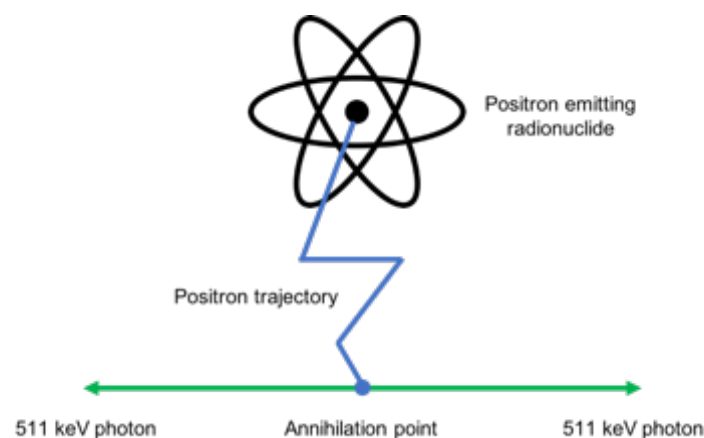


Figure 1.1 Fundamentals of PET imaging; a single positron emission event.

1.3 Biomarkers as diagnostic imaging agents for PET

Biomarkers have been essential to our current understanding of disease and to our endless endeavour to improve human health. Described as 'a characteristic that is objectively measured and evaluated as an indicator of normal biological processes, pathogenic processes, or pharmacological responses to a therapeutic intervention',¹⁸ biomarker is a reasonably new term. Their use in medicine, however, is well versed. Blood glucose levels for example have long been used as a biomarker for diabetes¹⁹ as has cholesterol levels to assess cardiovascular risk²⁰ (though hotly debated for years) and the presence of antibodies for infection.²¹

Biomarkers that indicate pathogenic processes are particularly useful as PET imaging agents for the detection, characterisation and staging of disease. Unquestionably, the most prominent in PET is 2-[¹⁸F]-fluoro-deoxy-D-glucose ([¹⁸F]FDG) used to study glucose metabolism.²² [¹⁸F]FDG has found extensive use in oncology as tumour cells metabolise glucose at a higher rate and in neurology where diminished glucose uptake can signify the onset of neurological diseases.²³ Another is 6-[¹⁸F]-fluoro-3,4-dihydroxyphenylalanine ([¹⁸F]DOPA) used to study the nigrostriatal dopaminergic pathway.²⁴ [¹⁸F]DOPA is the golden standard for staging in Parkinson's disease.²⁵

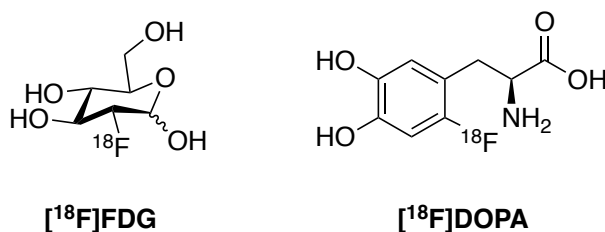


Figure 1.2 Structures of [¹⁸F]FDG and [¹⁸F]DOPA

Small molecules have always held a monopoly as molecular probes for PET, primarily because they are easier to radiolabel. However, interest in using larger biomarkers such as peptides and proteins has grown substantially of late.²⁶ The most attractive properties of these types of biomarkers is that they exhibit high binding affinities and specificities for their molecular targets.²⁷ With recent advances in molecular display techniques, we are now collecting huge amounts of information regarding peptide-protein and protein-protein interactions that are biomarkers of pathogenic process. Furthermore, these advances now allow us to select and evolve peptides and proteins which have higher affinities for their molecular targets than their

natural analogues.²⁸ By translating this knowledge to the development of new imaging agents and pairing it with the sensitivity of PET, peptides and proteins have the potential to be formidable imaging agents in the early detection, staging and unambiguous diagnosis of disease.

1.4 Properties of positron emitting radionuclides for PET

There is a suite of radionuclides that decay via β^+ decay with some more suited to PET studies than others.²⁹ In general, those that are pure positron emitters and have a low maximum positron energy are preferred. However, the half-life must also be adequate for the application. These, along with considerations into the availability and production of radionuclides are discussed in more detail below. The properties of some radionuclides that decay via β^+ decay are illustrated in Table 1.1 at the end of this section.

1.4.1 Modes of decay

Pure positron emitting radionuclides, such as carbon-11, nitrogen-13, fluorine-18 and copper-64 are conventionally used in PET. These radionuclides emit positrons through only a single decay pathway whereby all photons detected are a result of annihilation with energies of 511 keV. For non-pure positron emitting radionuclides (those that emit positrons through multiple decay pathways) their decay cascades are complex and can interfere in data collection. Whereby two photons of different energies are detected in coincidence, known as “prompt gamma” coincidences, artificial data is generated and images generated from that data display inaccurate representations of the imaging agent’s distribution.³⁰ The use of non-pure positron emitting radionuclides is however, becoming more practical with a number of methods to account for prompt gamma coincidences having being reported recently.³¹⁻³⁶ No doubt we will see new applications of PET arise from the use of non-pure positron emitting radionuclides in the not too distant future.

1.4.2 Positron energy

Among other factors, the positron energy impacts the spatial resolution of images acquired in PET. A radionuclide’s positron energy is directly related to the positron’s range; the distance it travels from the nucleus before it undergoes annihilation with an electron in the

surrounding matter. Thus for radionuclides with higher positron energies, annihilation occurs further away from the nucleus resulting in a lower spatial resolution.³⁷ This is less pronounced in human studies than it is in small animal PET imaging purely due to differences in the physical size of the objects.³⁰ Nevertheless, radionuclides with lower positron energies are more favourable as positrons with a high energy can create “ghost” artefacts whereby they exit the organs annihilating in locations where there was no tracer uptake. Ghost artefacts have been observed with the high positron energy radionuclides gallium-68³⁸ and iodine-124.³⁹ As the distance travelled by a positron is dependent on the medium and its energy, this is a significant issue when studying the respiratory system where the positron may exit into air.

1.4.3 Half-life

The half-life is arguably the most important property to consider when selecting which radionuclide to use in PET. It must be adequate for the intended application and is often matched to the biological half-life of the molecular probe. In general, larger biomolecules have slower pharmacokinetics and radionuclides with longer half-lives such as gallium-68 (67.7 min), fluorine-18 (110 min), copper-64 (12.7 hr) and iodine-124 (4.18 days) are more suitable when they are to be used as imaging agents.^{28,40} On the other hand, if the half-life is too long it can result in the patient being exposed to excess radiation unnecessarily. Additionally, the half-life needs to be of adequate length to allow for it to first be incorporated into the molecular probe. For example, the short-lived oxygen-15 has a half-life of 2.03 minutes. After only 14 minutes less than 1% of the starting radiation will still be present. Thus, there is a very limited time for the labelling of complex molecules such as peptides and proteins with oxygen-15.

1.4.4 Availability and production

The availability of a radionuclide is non-negotiable and hence, heavily contributes to their use in PET. The production of most β^+ emitting radionuclides requires a nuclear reactor or particle accelerator. Expensive and laborious, these necessary instruments are restricted to a small number of locations as are those trained to use them. For centres without the equipment to produce their own radionuclides, they must be produced off site and transported to them. Inherently unstable, the radionuclide must have an adequate half-life such that it does not decay

to inapt quantities during transportation. Therefore, it is mandatory for radionuclides produced off site to have longer half-lives.

Some radionuclides can be harvested from a generator, making them available to centres without nuclear reactors and particle accelerators. Generators provide a constant supply of a shorter-lived radionuclide, known as the daughter, from a longer-lived parent radionuclide. The positron emitting radionuclides gallium-68 and rubidium-82 can be obtained in this way, from generators containing the parent radionuclides germanium-68 and strontium-82 respectively.²⁹ By harvesting from generators, the daughter radionuclide can be obtained on demand.

Table 1.1 Properties of positron emitting radionuclides.^{41,42} *non-pure positron emitter; maximum positron energy (MeV) representative of most frequently emitted positron.

Radionuclide	β^+ decay (% of all decay)	Maximum positron energy (MeV)	Half-life	Production
Carbon-11	99.8%	0.960	20.4 min	$^{14}\text{N}(\text{p},\alpha)^{11}\text{C}$
Nitrogen-13	99.8%	1.20	9.97 min	$^{16}\text{O}(\text{p},\alpha)^{13}\text{N}$
Oxygen-15	99.9%	1.73	2.03 min	$^{14}\text{N}(\text{d},\text{n})^{15}\text{O}$
Fluorine-18	96.7%	0.634	110 min	$^{18}\text{O}(\text{p},\text{n})^{18}\text{F}$
Scandium-44	94.3%	1.47	3.97 hr	$^{44}\text{Ti}/^{44}\text{Sc}$ generator
Copper-64	17.6%	0.653	12.7 hr	$^{64}\text{Ni}(\text{n},\text{p})^{64}\text{Cu}$
Gallium-68	88.9%*	1.90	67.7 min	$^{68}\text{Ge}/^{68}\text{Ga}$ generator
Rubidium-82	95.4%*	3.38	1.26 min	$^{82}\text{Sr}/^{82}\text{Rb}$ generator
Zirconium-89	22.7%	0.902	78.4 hr	$^{89}\text{Y}(\text{p},\text{n})^{89}\text{Zr}$
Iodine-124	22.7%*	2.14	4.18 days	$^{124}\text{Te}(\text{p},\text{n})^{124}\text{I}$

1.5 Fluorine-18

Of the positron emitting radionuclides fluorine-18 is often considered to be ideal for PET. Possessing favourable nuclear properties it has a moderate half-life of 110 minutes, a low maximum positron energy at 0.634 MeV and is a pure positron emitter decaying via β^+ decay 96.7% of the time and electron capture the remaining 3.1%.^{41,42} Thanks, in large to the omnipresent use of [^{18}F]FDG, fluorine-18 is now also readily available with the required equipment

for its production in more locations than ever before and logistics in place for its transport to centres without a cyclotron on site.²⁸

Fluorine-18 also possesses favourable chemical and electronic properties. Similar to replacement of non-radioactive carbon with the positron emitting isotope carbon-11, non-radioactive fluorine can be replaced with fluorine-18 with negligible effects on the biological properties and activity of the molecule. While there is a limited number of fluorine atoms found in biological molecules, there are a number of hydrogens and hydroxyl groups. Similar in its size to hydrogen (van der Waals radii fluorine 1.47 Å, hydrogen 1.20 Å) and in electronic nature to the hydroxyl group, fluorine can serve in their bioisosteric replacement. A classic example of the former is [¹⁸F]DOPA with bioisosteric replacement of the C6 hydrogen with fluorine-18. [¹⁸F]FDG is an example of the latter with replacement of the C2 hydroxyl group.

1.6 Radiolabelling proteins with fluorine-18

Naturally, given its ideal nuclear properties and wide availability, researchers have been enticed to radiolabel peptides and proteins with fluorine-18 for use in PET. Fluorine-18 is compatible with peptides and small to intermediate sized proteins (≤ 60 kDa) as they reach their molecular targets within times comparable to its moderate half-life of 110 minutes.^{40,43} However, the complexity of these molecules makes radiolabelling them with fluorine-18 a challenging task. For proteins specifically, this is even more difficult as physiological conditions (an aqueous environment within a pH range of 5-8 and temperatures at or below 37 °C) are generally required to maintain their high specificity and affinity for their molecular targets.

1.6.1 Electrophilic vs nucleophilic

Radiolabelling with fluorine-18 can be conducted via either electrophilic or nucleophilic fluorinations. For electrophilic fluorinations, fluorine-18 is produced by proton irradiation of [¹⁸O]O₂ gas yielding [¹⁸F]F₂. The extremely reactive [¹⁸F]F₂ can then be used as is or converted to a less reactive fluorinating agent such as xenon difluoride ([¹⁸F]XeF₂) or acetylhypofluorite ([¹⁸F]CH₃COOF).⁴⁴ Electrophilic fluorination has played a critical role in the synthesis of imaging agents for PET. [¹⁸F]FDG for example, now the most widely used PET imaging agent, was first synthesised using electrophilic fluorination.⁴⁵ However, the need to add non-radioactive fluorine

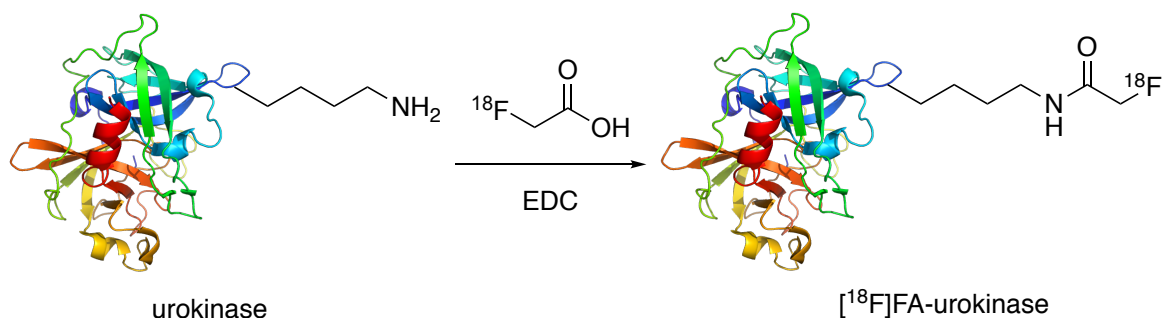
during the synthesis of $[^{18}\text{F}]\text{F}_2$ results in lower specific activities⁴⁶ which has limited its utility. For peptides and proteins to be used in targeted imaging high specific activities are essential as their molecular targets *in vivo* are readily saturated and often expressed in low densities.²⁶ Therefore, radiolabelling is most often conducted via nucleophilic fluorination with fluoride-18.

Nucleophilic fluoride-18 ions are generated through irradiation of 'heavy' water ($[^{18}\text{O}]\text{H}_2\text{O}$). Fluoride ions are poorly nucleophilic in water⁴⁷ however, and rigorous drying procedures are adhered to before the fluoride-18 ion is used in radiolabelling experiments. This is commonly achieved by passing the solution through an ion-exchange cartridge to capture the fluoride-18 ion which is then eluted as its alkali or tetrabutylammonium salt. To further activate the fluoride-18 ion, the alkali salts can be chelated to cryptands. By far the most commonly employed is elution with potassium carbonate giving $[^{18}\text{F}]\text{KF}$ which is then complexed with Kryptofix 222.⁴⁸ In addition to the dry conditions, nucleophilic fluorinations are usually performed at elevated temperatures (50-100 °C) to increase yields and specific activities as well as shorten reaction times.

In general, due to the low specific activities associated with electrophilic fluorinations, the low nucleophilicity of the fluoride ion in water and the high temperatures employed, proteins (and those peptides that also denature under these conditions) are indirectly radiolabelled with fluorine.

1.6.2 Indirect vs direct

Indirect methods of radiolabelling involve the introduction of fluorine-18 through prosthetic groups; small compounds that can be radiolabelled at high temperatures in organic solvents and subsequently conjugated to a biomolecule. The first indirect radiolabelling of a protein with fluorine-18 was reported in 1982 when Müller-Platz and co-workers used $[^{18}\text{F}]\text{fluoroacetic acid}$ as a prosthetic group to radiolabel urokinase. $[^{18}\text{F}]\text{fluoroacetic acid}$ was prepared via nucleophilic fluorination of ethylbromoacetate followed by hydrolysis of the ester at reflux. $[^{18}\text{F}]\text{fluoroacetic acid}$ was then conjugated to the free amino groups of urokinase under physiological conditions through amide coupling mediated by *N*-(3-dimethylaminopropyl)-*N'*-ethylcarbodiimide (EDC) (Scheme 1.1).⁴⁹ An extensive number of prosthetic groups have since been used to radiolabelled proteins with fluorine-18 through indirect labelling methods.^{50,51}



Scheme 1.1 Indirect radiolabelling of urokinase with [^{18}F]fluoroacetic acid.

Notwithstanding the resourcefulness of indirect radiolabelling methods these intrinsic multi-step syntheses are far from optimal, particularly for the short-lived fluorine-18. Furthermore, a number of these indirect methods are not site-selective creating heterogeneously labelled products. As a whole the effects that non-selective modifications have on the biodistribution and pharmacokinetics of the protein are not well understood.⁵² For example, Grierson et al. showed that the binding of annexin V to apoptotic cells is compromised when randomly radiolabelled with a fluorine-18 prosthetic group at multiple lysine residues versus when site-selectively modified at cysteine.⁵³ Tait et al. also found that site-selective radiolabelling with technetium-99m lead to an increase in binding affinity of annexin V when compared to those randomly modified.⁵⁴ In another study however, no difference was found between the random and site-selective modification of annexin V.⁵⁵ Nevertheless, it makes it difficult to characterise the products and good manufacturing practices require a level of quality assurance and quality control to be maintained between batches which is compromised when non site-selective methods are used.

Direct methods on the other hand, at least in principal, offer the time to incorporate a unique prosthetic group site-selectively into proteins that can be subsequently radiolabelled with fluorine-18 in a single step under mild aqueous conditions. It has however, been thought that in general proteins cannot be directly radiolabelled through traditional C-F bond formation as it requires conditions that denature the protein.¹⁵ Recently there has been a number of investigations looking into the radiolabelling of molecules with fluorine-18 through inorganic-fluoride bond formation. As an alternative to traditional C-F bond formation, it has rekindled the prospect of being able to directly radiolabel proteins with fluorine-18.

In the next sections we present a review and discussion of the literature regarding radiolabelling with fluorine-18 through fluorine bond formation with inorganic elements. In the

context of the work detailed in this thesis, a particular focus has been placed on the opportunities they offer towards the direct radiolabelling of proteins.

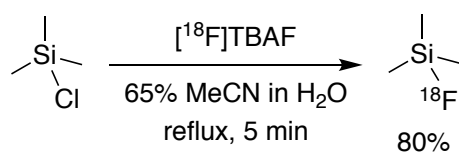
1.7 Radiolabelling through Si-F bond formation

The first report of Si-F bond formation being used in regard to the synthesis of imaging agents for PET was in 1985. Rosenthal and co-workers successfully prepared [¹⁸F]fluorotrimethylsilane by reacting chlorotrimethylsilane with [¹⁸F]tetramethylammonium fluoride ([¹⁸F]TBAF) (Scheme 1.2).⁵⁶ In contrast to C-F bond formation this reaction proceeded even in the presence of water and [¹⁸F]fluorotrimethylsilane was produced in an 80% yield (decay corrected) when performed in a 65% acetonitrile aqueous solution. It would, however, be another 20 years before Si-F bond formation was again used in the radiolabelling of molecules with fluorine-18.

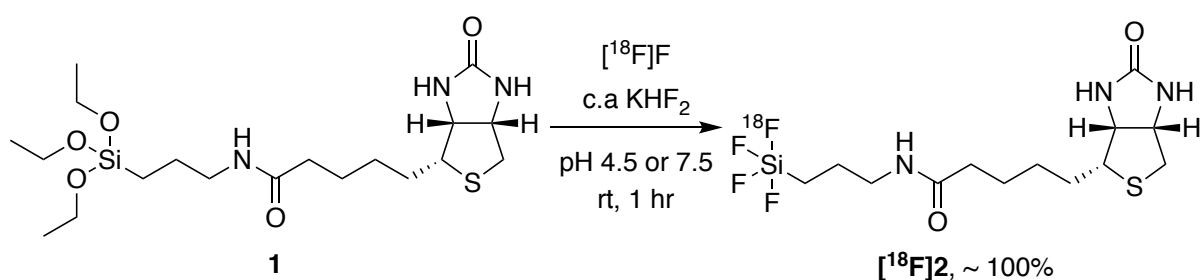
In 2005 Ting *et al.* reported the radiolabelling of the triethoxysilane **1** with fluorine-18 through Si-F bond formation (Scheme 1.3).⁵⁷ This time the fluoride-18 anion was used directly after irradiation without conversion to another fluorinating agent simply added to an aqueous solution of **1**. This single step fluorination resulted in the rapid formation of alkyltetrafluorosilicate [¹⁸F]**2** with yields approaching 100% in buffered aqueous media at both pH 4.5 and 7.5 in less than an hour at room temperature.

These two foundational studies by Rosenthal *et al.* and Ting *et al.* revealed that Si-F bond formation may be a promising alternative to C-F bond formation for the direct radiolabelling of proteins with fluorine-18. In both examples, the Si-F bond formation was high yielding and achieved in time frames suitable to the half-life of fluorine-18, at room temperature and in aqueous solutions. To be useful, however, the Si-F bond would need stability *in vivo*. This is of utmost importance to PET imaging agents as they can no longer be traced throughout the body using PET if the fluorine-18 is cleaved from the molecular probe. Unfortunately, in both the cases described above a low hydrolytic stability of the Si-F bond was observed. *In vivo* [¹⁸F]fluorotrimethylsilane rapidly hydrolysed ($t_{1/2} < 1.5$ minutes) and analysis *in vitro* found that the rate of hydrolysis increased at higher pH.⁵⁶ The alkyltetrafluorosilicate was also found to be

susceptible to hydrolysis *in vitro* with hydrolysis observed within an hour when in a buffered aqueous solution at pH 7.5.⁵⁷



Scheme 1.2 Direct nucleophilic fluorination of chlorotrimethylsilane with fluorine-18 under aqueous conditions.



Scheme 1.3 Direct nucleophilic fluorination of triethoxysilane **1**

Despite that the Si-F bond is one of the strongest σ bonds known, in dilute aqueous environments where water is plentiful, the hydrolysis of Si-F bond is both thermodynamically and kinetically favoured.⁵⁷ It is therefore almost inevitable that the Si-F bond will eventually hydrolyse *in vivo* resulting in the loss of the mandatory radionuclide. Nevertheless, when fluorine-18 decays, it decays to oxygen-18 resulting in the same silanol product that results from hydrolysis. Therefore, the Si-F bond need only be stable for long enough that it outlives the fluorine-18 radionuclide. To alleviate the rate at which the Si-F bond hydrolyses Rosenthal *et al.* suggested incorporating more hindered substituents on the silicon atom.⁵⁶ Presumably, the steric and inductive effects of the substituents would reduce the ease at which the pentacoordinate hydrolysis transition state forms, as is the case for organosilanes.

Independently, Choudhry⁵⁸ and Schirrmacher⁵⁹ showed that indeed, with an increase in sterics comes an increase in the hydrolytic stability of the Si-F bond. In an abstract, Choudhry reported that of the four compounds they tested (**3-6**) only **6** showed satisfactory stability *in vitro* with almost 100% stability observed after 5 hours at 45 °C in water and in PBS. Schirrmacher *et al.* took it one step further also testing **7** and observing the hydrolytic stability of the Si-F bond *in vivo*. It was found that while **6** did have reasonable stability in human serum at 37 °C and pH

7.4-7.6 *in vivo*, hydrolysis occurs with the characteristic uptake of radioactivity in the bones indicating the presence of free fluoride-18. They found that the more sterically hindered **7** was stable in human serum and showed a limited uptake of radioactivity in bone, *in vivo*, 50 minutes post injection.

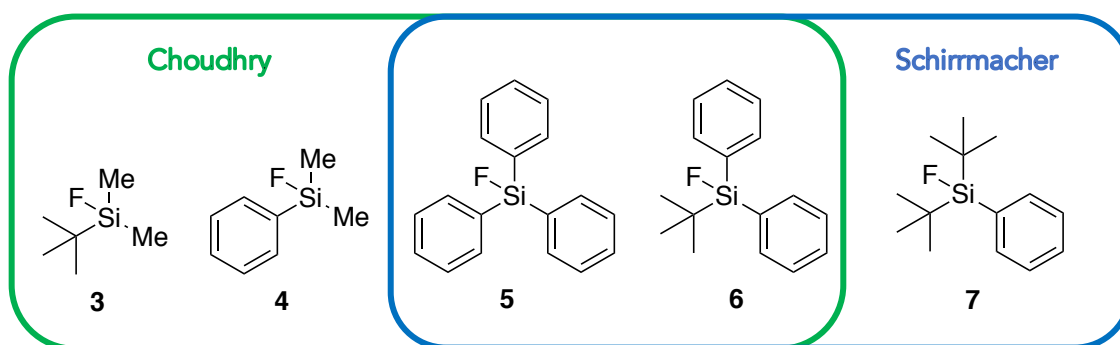


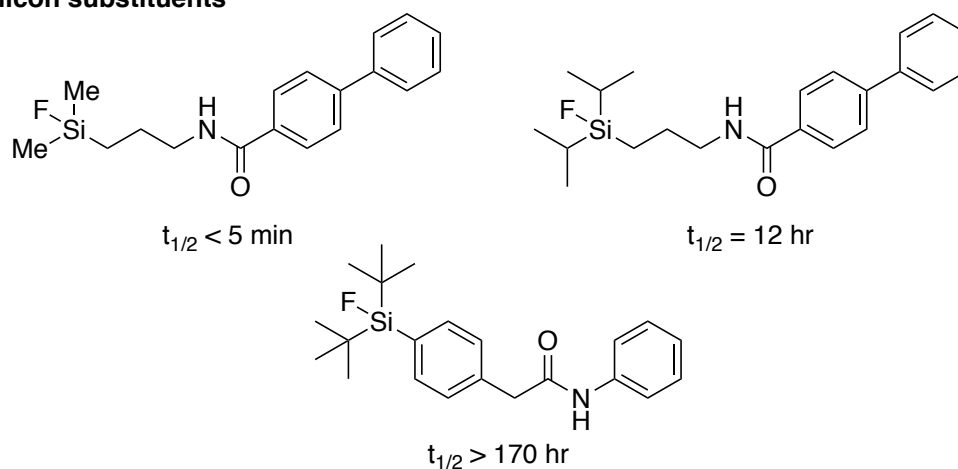
Figure 1.3 Fluorosilanes studies by Choudhry *et al.* and Schirmacher *et al.*

Extending on this, Ametamey and co-workers showed the diisopropyl substituents also increase the hydrolytic stability. They found Si-F bonds with diisopropyl substituents to be more stable against hydrolysis than methyl substituents but less than *tert*-butyl substituents (Figure 1.4A).⁶⁰ In a follow up paper, Ametamey and co-workers further explored the hydrolytic stability of the Si-F bond determined the hydrolytic half-lives of 15 fluorosilanes.⁶¹ Their results corroborated previous studies and assumptions that bulkier substituents on the silicon leads to an increased hydrolytic stability of the Si-F bond. The addition of methyl groups at the *ortho* positions of the phenyl ring were also found to give a significant increase in hydrolytic half-life (Figure 1.4B). Interestingly, the functionality at the *para* position of the phenyl ring had a substantial influence on the hydrolytic stability (Figure 1.4C). This suggests that inductive effects, not just sterics, play a significant role in the hydrolytic stability of Si-F bonds. Outside of this study however, the role inductive effects play in the hydrolytic stability of Si-F bonds has not been explored. Nevertheless, those arylfluorosilanes substituted with either the diisopropyl or di-*tert*-butyl groups displayed a satisfactory hydrolytic half-life to be useful PET imaging agents.

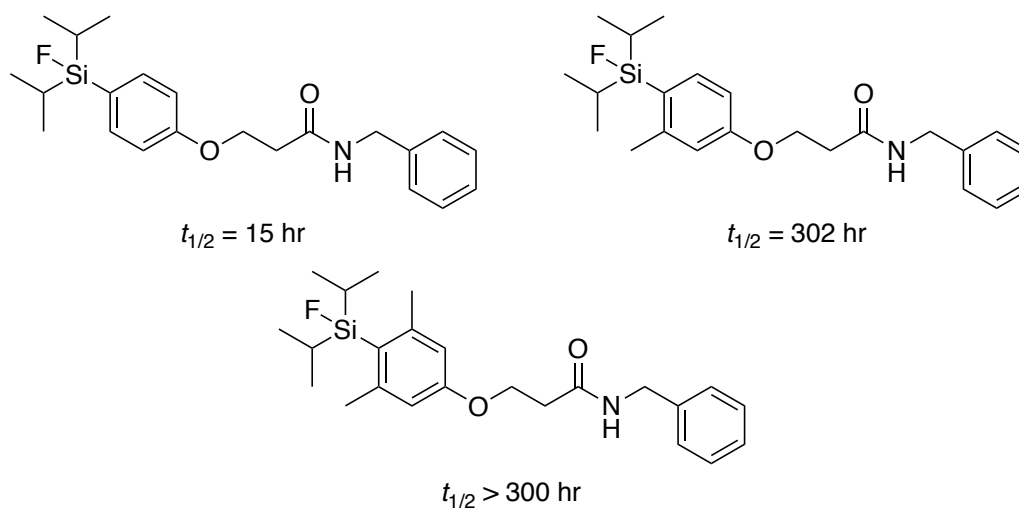
[¹⁸F]arylfluorosilanes can be synthesised from their corresponding silanes, silanols and fluorosilanes. They have also been synthesised from chlorosilanes and alkoxy silanes, but both undergo rapid hydrolysis when in aqueous solutions.^{62,63} Thus, they have a very limited applicability for the direct radiolabelling of proteins. On the other hand, silanes are relatively stable in neutral and slightly acid media. Fluorosilanes with sufficient steric substituents are also

reasonably stable in water as we have seen and silanols are infinitely stable in water.

A) Silicon substituents



B) Ortho substituents



C) Para substituents

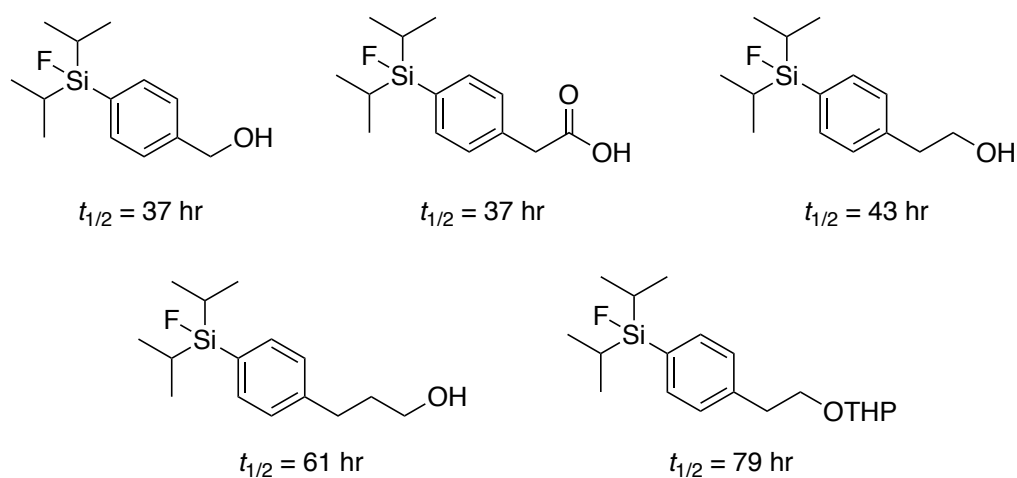
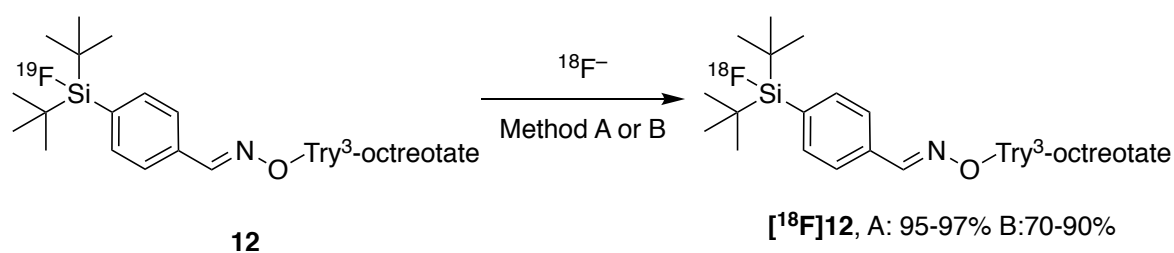


Figure 1.4 Increased steric hinderance around the silicon atom has a positive effect on the hydrolytic half-live of the Si-F bond. Half-lives measured in a 2:1 solution of acetonitrile:aqueous buffer (pH 7).⁶¹

Schirmacher and co-workers were the first to show that $^{19}\text{F}/^{18}\text{F}$ isotopic exchange was applicable to Si-F bond formation. Remarkably, when radiolabelling [^{19}F]di-*tert*-butylphenyl fluorosilane, yields of 80-95% were achieved in just 10 to 15 minutes at room temperature when using the azeotropically dried $^{18}\text{F}[\text{KF}]/\text{Kryptofix 222}$ complex in acetonitrile.⁵⁹ Furthermore when conjugated to Tyr³-octreotate (**12**), yields of 95-97% were obtained (Scheme 1.5). They also tried to radiolabel **12** in a 15% acetonitrile aqueous solution with fluoride-18 in target water directly after irradiation. Unfortunately, at room temperature for 15 minutes this only gave [^{18}F]**12** in a 5% radiochemical yield. However, when the temperature was increased to 95 °C and the reaction time doubled the yields significantly increased to 70-90%.

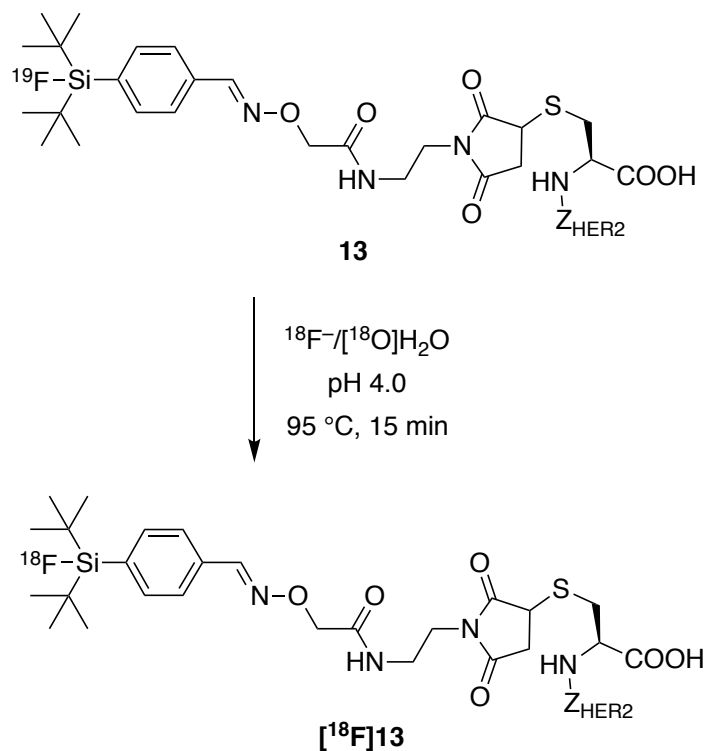


Scheme 1.5 Radiolabelling of **12** via $^{19}\text{F}/^{18}\text{F}$ isotopic exchange. Method A: $^{18}\text{F}[\text{KF}]/\text{Kryptofix 222}$, MeCN, rt, 10-15 min. Method B: $^{18}\text{F}-/[\text{^{18}O}]\text{H}_2\text{O}$, MeCN (15-20% total volume), 95 °C, 30 min.

Requiring such high temperatures to obtain sufficient yields $^{19}\text{F}/^{18}\text{F}$ isotopic exchange has a limited applicability to the direct radiolabelling of proteins. Nevertheless, Glaser *et al.* has used this method to synthesise a fluorine-18 labelled human epidermal growth factor receptor (HER2) specific binding affibody.⁶⁴ Conjugating [^{19}F]di-*tert*-butylphenyl fluorosilane to the affibody using maleimide chemistry followed by isotopic exchange with fluoride-18 in target water yielded the affibody [^{18}F]**13** in a 38% radiochemical yield in just 15 minutes at 95 °C under 100% aqueous conditions, pH 4.0 (Scheme 1.6). Though there was a limited difference in the retention of the radiolabelled affibody in high-HER2-expressing and low-HER2-expressing tumours, the binding affinity remained within a sub nanomolar range. This indicates that the high temperatures used did not affect its specificity nor its affinity for its molecular target. To the best of our knowledge, this example reported by Glaser *et al.* represents the only example of the direct radiolabelling of a protein with fluorine-18 in the chemical literature.

Further efforts towards aqueous Si-F radiolabelling methods are scarcely described in the chemical literature. Katzenellenbogen and co-workers reported the direct radiolabelling of a silylacetate⁶⁵ and Fouquet *et al.* has reported direct radiolabelling of silyl *N*-methyl-imidazoles.⁶⁶

Aqueous solutions of fluoride-18 were used in both cases but ultimately, the reactions were performed in organic solvents (THF or acetonitrile) and at high temperatures (100-110 °C). Bar the single example above, radiolabelling via this method has only been used in for the indirect radiolabelling of proteins with fluorine-18.⁶⁷⁻⁷¹

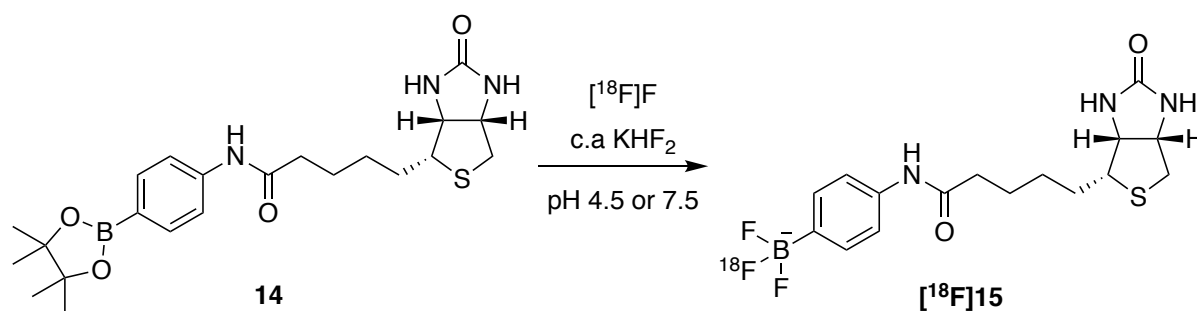


Scheme 1.6 Direct radiolabelling of the HER2 binding affibody through Si-F bond formation performed via $^{19}\text{F}/^{18}\text{F}$ isotopic exchange in a 100% aqueous environment.

1.8 Radiolabelling through B-F bond formation

Along with silicon, boron was one of the first elements to be used as an inorganic fluoride acceptor for radiolabelling with fluorine-18. B-F bond formation for the radiolabelling of small molecules has been around since the 1960's.^{72,73} However, until Ting *et al.* reported the radiolabelling of the biotinylated aryl boronic ester **14** with fluorine-18 in 2005 (Scheme 1.7),⁵⁷ boron's use in the radiolabelling of biomolecules had generated little interest. As with the alkyltetrafluorosilicate **1** (*vide supra*) the authors were able to show that the alkylboronic ester **14** could readily be fluorinated in a single, rapid step with simple addition of fluoride-18, without the need for the rigorous and time-consuming drying generally employed. The fluorination worked

well in aqueous solvents and yields approached 58% and 41% after an hour at pH 4.5 and 7.5 respectively. Additionally, the stability of [^{18}F]15 was measured in blood and serum with no dissociation of fluoride-18 observed up to one hour. Thus, they suggested that [^{18}F]trifluoroborates may be useful as imaging agents in PET and since, a wide range of aryl and alkyltrifluoroborates have all been investigated for this purpose.



Scheme 1.7 Fluorination of **14** occurs in a single, rapid step in water at room temperature.

As with the Si-F bond, the hydrolytic stability of the B-F bond of aryltrifluoroborates is dependent on the substituents on the aryl group and their positions relative to the B-F bond. Perrin *et al.* showed that the B-F bond's half-life can be increased by reducing the electron density that is delocalised into the *p*-orbital of the boron atom.^{74,75} With an increase in the deactivating strength of electron withdrawing groups at the *meta* and *para* positions comes an increase in the half-life of the B-F bond (Figure 1.5A and B). Substituents at *ortho* positions have a large effect on the half-life though both their electronic nature and sterics are expected to play a role here. An *ortho* methoxy substituent increases the half-life from 2 to 15 minutes and an *ortho* fluorine substituent to 50 minutes (Figure 1.5C). Interestingly, the addition of a *para* fluorine substituent to these results in a decrease in the half-life but with fluorine substitution at both *ortho* positions and the *para* position the half-life reaches 4.7 hours (Figure 1.5D). The introduction of endocyclic heteroatoms gives the largest increases in half-life, pushing well into hours rather than minutes, a half-life more suitable for PET (Figure 1.5E). Gabbaï and co-workers further showed that zwitterionic aryltrifluoroborates also offer a greater hydrolytic stability.⁷⁶ Substituted with cationic functionality at the *ortho* position, the close proximity to the trifluoroborate creates strong coulombic interactions that help to stabilise the B-F bond (Figure 1.5F).

A simple relationship between the hydrolytic stability of alkyltrifluoroborates and their corresponding carboxylic acid was discovered by Perrin and co-workers. In a study that looked at the rates of B-F bond hydrolysis using ^{19}F NMR spectroscopy, they found that the higher the

negative logarithm of the hydrolysis rate constant ($pK_{(B-F)}$) the more stable the B-F bond.⁷⁷ Intriguingly, they observed an almost perfect negative correlation ($R=0.984$) between the $pK_{(B-F)}$ and the pK_a of their corresponding carboxylic acids. That is to say, the lower the pK_a of the corresponding carboxylic acid, the greater the hydrolytic stability of the alkyltrifluoroborate's B-F bond. This indicates that as with pK_a a number of factors affect the hydrolytic stability of the B-F bond. Given the prominence of pK_a in organic chemistry, this relationship makes it a simple task to predict the stability of the B-F bond of alkyltrifluoroborates helping to guide the design imaging agents suitable for fluorine-18 PET. A selection of alkyltrifluoroborates, their hydrolytic half-lives and the pK_a of their corresponding carboxylic acids are shown in Figure 1.6.

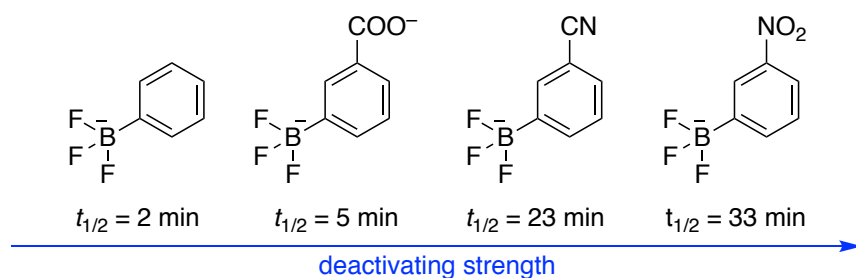
[¹⁸F]trifluoroborates, and their non-radioactive counterparts, can be readily synthesised from their corresponding boronic acids or esters under mildly acidic conditions. Fluorination is optimal at pH 2-3, when the hydroxide and alkoxy substituents are protonated and these acidic conditions can be generated by the addition of the carrier KHF_2 and/or hydrochloric acid. [¹⁸F]trifluoroborates can also be synthesised through ¹⁹F/¹⁸F isotopic exchange. Inspired by the success of ¹⁹F/¹⁸F isotopic exchange in the radiolabelling of fluorosilanes (*infra vide*), Gabbai *et al.* showed that trifluoroborates could also be radiolabelled via ¹⁹F/¹⁸F isotopic exchange by simply mixing together a solution of fluoride-18 in target water and the trifluoroborate in acetonitrile (<15% total volume) (Scheme 1.8).⁷⁶ The reaction proceeded efficiently at room temperature in only 20 minutes but only at a pH of 1.5-3.0 which was achieved by the addition of hydrochloric acid. At higher pH very minimal yields were obtained.

While it has been shown to occur at room temperature and in aqueous solutions, the current methods for direct fluorine-18 fluorination through B-F bond formation are incompatible with most proteins which cannot tolerate the very low pH (ca. pH 2) employed. In light of this, it is quite surprising that the indirect radiolabelling of proteins using these methods has seldom been used. Published recently, a single example was found in the literature describing the indirect radiolabelling of super folded green fluorescent protein.⁷⁸

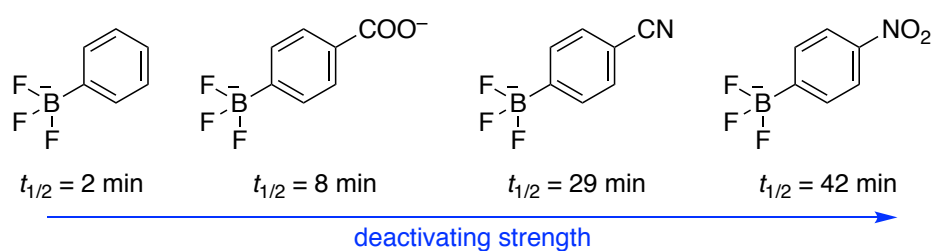
On the contrary there is an overwhelming number of examples of radiolabelling through B-F bond formation involving the radiolabelling of small biomolecules and peptides. These include biotin,^{79,80} rhodamine,⁸¹ marimastat,⁸² panobinostat,⁸³ metalloproteinases,⁸⁴ bombesin⁸⁵ and arginylglycylaspartic acid (RDG).⁸⁶ As the radiolabelling of small molecules and peptides are not limited by the use of high temperatures and organic solvents radiolabelling is normally

conducted at 80 °C and in 50% aqueous organic solvent to increase yields and limit the total synthesis time.⁸⁷

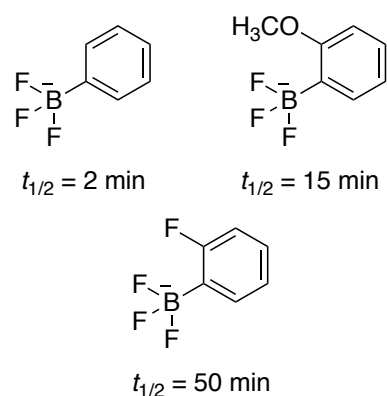
A) *Meta* substituents



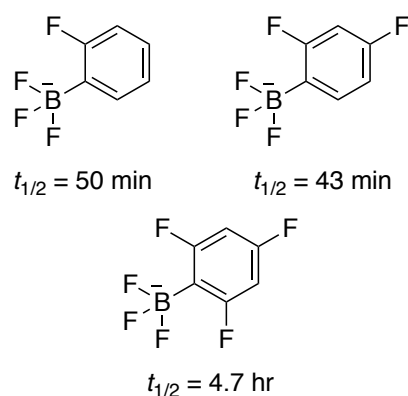
B) *Para* substituents



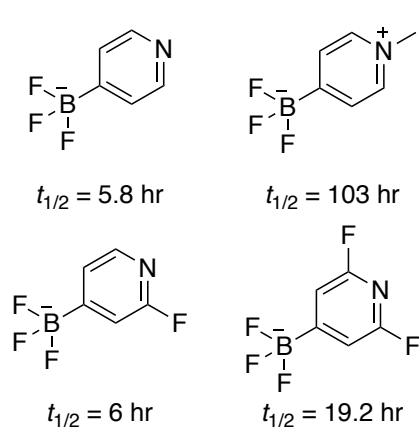
C) *Ortho* substituents



D) Fluorine substituents



E) Heteroaromatic



F) Zwitterionic substituents

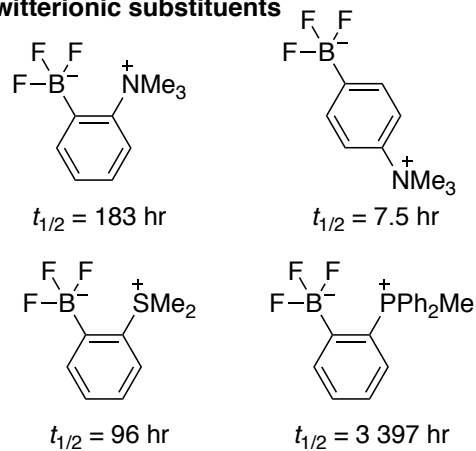


Figure 1.5 The effect aromatic substitution has on the half-life of the B-F bond of aryltrifluoroborates.

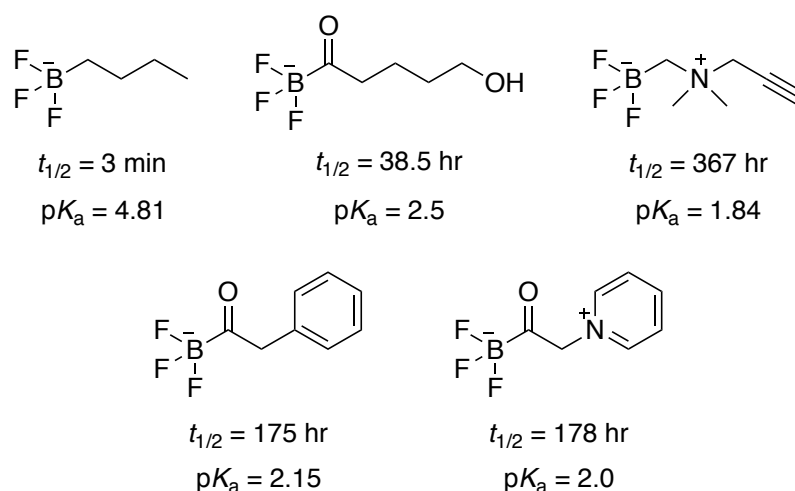
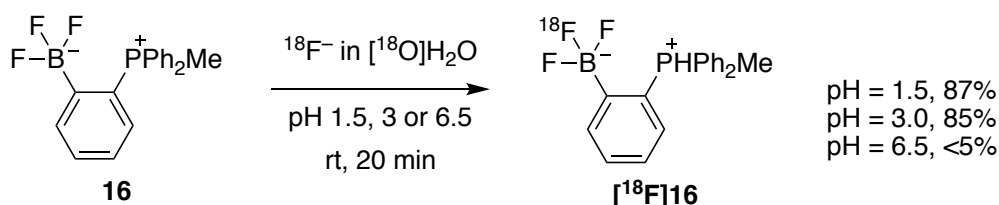


Figure 1.6 A selection of alkyltrifluoroborates and their half-lives and the pK_a of their corresponding carboxylic acids. The lower the pK_a the greater the hydrolytic stability of the B-F bond.



Scheme 1.8 $[^{18}\text{F}]$ trifluoroborates can be synthesised via $^{19}\text{F}/^{18}\text{F}$ isotopic exchange at low pH and room temperature with exceptional yields in only 20 minutes.

1.9 Radiolabelling with fluorine through metal complexes

Metal complexes have gained much attention for the radiolabelling of peptides and proteins with fluorine-18 for PET of late. Envisioned as a method complementary to radiometal labelling,⁸⁸ this makes use of $[^{18}\text{F}]$ fluorine-metal complexes that can be chelated to ligands incorporated into a peptide or protein. Since the first reported use of metal fluorine complexes for radiolabelling with fluorine-18 in 2009⁸⁸ this field of research has moved forward in leaps and bounds with group 13 metals having particular success.

McBride *et al.* were the first to report the use of aluminium fluorine metal complexes for the radiolabelling of compounds with fluorine-18 through chelation.⁸⁸ In this initial study the ability of $[^{18}\text{F}]$ fluorine-metal complex to bind to a diethylenetriaminopentaacetic acid (DTPA) hapten-peptide was investigated. Of the six metals tested (aluminium, gallium, indium, zirconium,

lutetium and yttrium) the aluminium complex bound to the DTPA-hapten-peptide with the greatest affinity, but unfortunately none were stable in water. As aluminium fluoride complexes are known to be stable in water, the authors attributed the low stability to the weak binding of the metal to the DTPA chelate. Thus, they screened a number of other chelates and assessed their stability. In all cases, yields were lower than what could be achieved with DTPA and only when $[^{18}\text{F}]\text{AlF}$ was bound to a 1,4,7-triazacyclononane-1,4,7-triacetic acid (NOTA) hapten-peptide, did it exhibit sufficient stability in serum and *in vivo*. It has since been shown that greater labelling yields can be achieved with the pentadentate NOTA derivative NODA without a loss in stability.⁸⁹⁻⁹¹ Only coordinating with the aluminium ion at five donor atoms instead of six leaves free a final coordination site for the fluoride-18 ion.

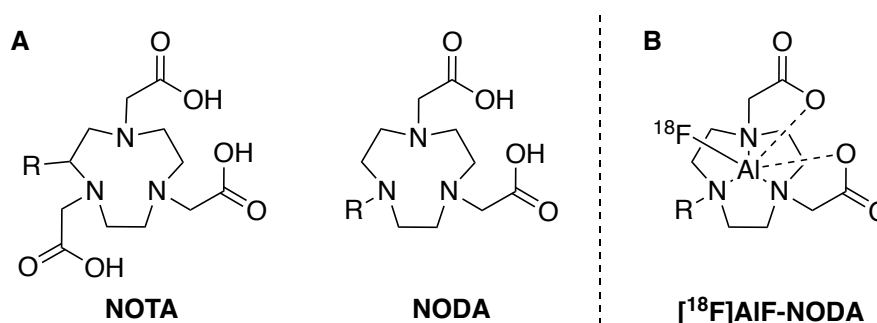
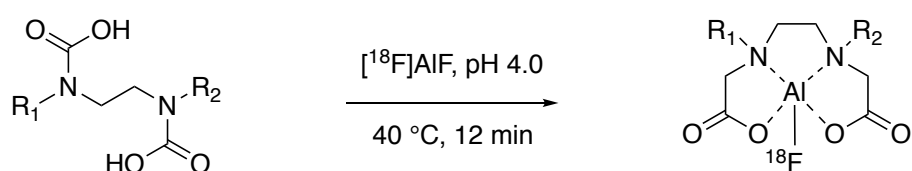


Figure 1.7 A) NOTA and NODA chelates. NOTA offers six donor atoms (N_3O_3) which compete with the fluoride-18 ion in coordination with the aluminium ion. In comparison NODA has only five donor atoms (N_3O_2) leaving a coordination site free for the fluoride-18 ion. **B)** $[^{18}\text{F}]\text{AlF}$ coordinated to the NODA complex.

The $[^{18}\text{F}]\text{AlF}$ metal complex can be synthesised from aluminium trichloride in water at room temperature. This is optimal at pH 4.0 and thus is generally performed in sodium acetate buffer. Binding of the complex with chelates is also optimal at pH 4.0 and though quick (generally 15-30 minute reaction times are all that is needed), it normally requires temperatures of 100 °C. A one-pot method whereby aluminium trichloride, fluoride-18 and the chelate are all added together has been extensively used for the radiolabelling of peptides with fluorine-18 (for recent reviews see Kumar & Ghosh, 2018 and Fersing *et al.*, 2019).^{92,93} Its use with heat sensitive proteins has been limited to indirect radiolabelling with subsequent conjugation of the radiolabelled chelate to the protein.⁹⁴⁻¹⁰⁰ There have, however, been some efforts made towards reducing the temperature and increasing the pH such that radiolabelling through aluminium complexes may be suitable for the direct radiolabelling of heat and acid sensitive proteins.

Huynh *et al.* were able to reduce the temperature required for complexation of [¹⁸F]AlF to NODA chelators by increasing the pH to 5.5. To obtain sufficient yields high levels (>40%) of ethanol were required.¹⁰¹ Nevertheless, they were able to radiolabel the monoclonal antibody trastuzumab at 30 °C in 15 minutes with a 45% radiochemical yield and it showed a greater uptake in HER2 positive cells (9.1 ± 1%) than it did HER2 negative cells (0.8 ± 0.04%), suggesting the high levels of ethanol did not affect its affinity for its molecular target.

In 2016 Cleeren *et al.* synthesised new chelators that were able to bind with [¹⁸F]AlF at 40 °C without any organic co-solvent and at the optimal pH of 4.5.¹⁰² These chelators were designed to be acyclic rather than macrocyclic to reduce the activation energy of the chelation. In order to maintain the stability that may have been lost by this change, they also replaced one nitrogen donor with an oxygen donor (N₂O₃) as it is a more effective aluminium chelator. [¹⁸F]AlF complexed to four of the eight chelators tested in exceptional yields at 40 °C in 12 minutes (Scheme 1.9). At room temperature, **17** could be radiolabelled in a >90% RCY but 40 °C was needed for **18**, **19** and **20**. [¹⁸F]**23** showed sufficient stability *in vitro* (rat serum, 37 °C) and *in vivo* (healthy mice). Therefore, as a proof of concept **19** was conjugated to a urea-based prostate-specific membrane antigen (PSMA) inhibitor. Radiolabelled with [¹⁸F]AlF at pH 4.5, 40°C for 12 minutes resulted in a 25% RCY. Preliminary studies into the stability *in vivo* were promising but require further evaluation.



17 R₁ = CH₂COOH, R₂ = benzyl

18 R₁ = R₂ = 2-hydroxybenzyl

19 R₁ = 2-hydroxybenzyl, R₂ = benzyl

20 R₁ = 2-CH₂C₅H₅N, R₂ = benzyl

[¹⁸F]**21** R₁ = CH₂COOH, R₂ = benzyl, 96%

[¹⁸F]**22** R₁ = R₂ = 2-hydroxybenzyl, 96%

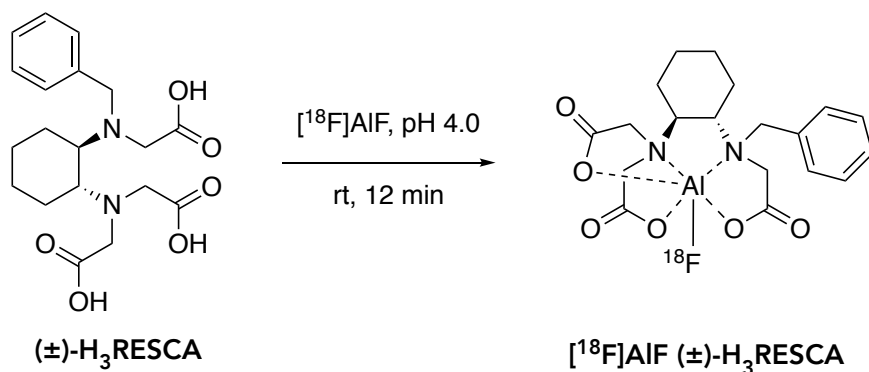
[¹⁸F]**23** R₁ = 2-hydroxybenzyl, R₂ = benzyl, 89%

[¹⁸F]**24** R₁ = 2-CH₂C₅H₅N, R₂ = benzyl, 94%

Scheme 1.9 Chelators synthesised by Cleeren *et al.* that allow for complexation with [¹⁸F]AlF in aqueous solvents at 40 °C, pH 4.0 in 12 minutes.

Cleeren *et al.* have since reported a new restrained chelator, (±)-H₃RESCA, that can be complexed to [¹⁸F]AlF at room temperature in 12 minutes at pH 4.5¹⁰³ (Scheme 1.10) and a protocol for using it to directly radiolabel proteins.¹⁰⁴ This procedure has successfully been used

to directly radiolabel human serum albumin (HAS), Kupffer cell marker CRlg and a HER2 targeting affibody with fluorine-18.¹⁰⁵



Scheme 1.10 Complexation of $[\text{}^{18}\text{F}]\text{AlF}$ to $(\pm)\text{-H}_3\text{RESCA}$ occurs at room temperature, pH 4.0 in only 12 minutes in aqueous solvents.

One downside to the method developed by Cleeren and co-workers for the direct radiolabelling with fluorine-18 is that the reaction is performed at pH 4-5 and thus, is not suitable for acid sensitive proteins. As previously discussed, Huynh *et al.* was able to achieve complexation at pH 5.5 and room temperature though the method used high concentrations of ethanol.¹⁰¹ Russelli *et al.* has recently reported three chelators that can be radiolabelled at higher pH using Cleeren's method in good yields (Figure 1.8).¹⁰⁶ At pH 4.0 only **25** could be efficiently labelled but at pH 5.0 all three were labelled efficiently (81%, 69% and 52% for **25**, **26** and **27** respectively). Even at pH 6.5 radiochemical yields reached ca. 50% for all three chelators. **27** showed the greatest stability *in vitro* and was further studied *in vivo*. Preliminary results indicate that it has an adequate hydrolytic stability with a lower accumulation of free fluorine-18 in bone than observed for previously reported $[\text{}^{18}\text{F}]\text{AlF}$ complexes.¹⁰²

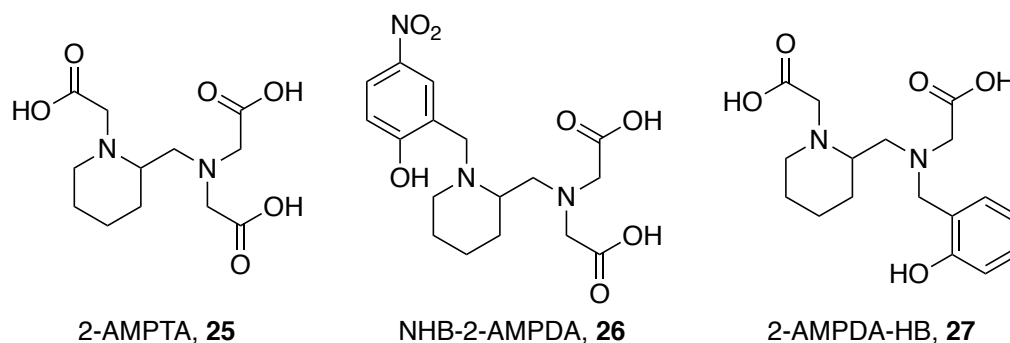


Figure 1.8 Chelators synthesised by Russelli *et al.* that allow for complexation with $[\text{}^{18}\text{F}]\text{AlF}$ in aqueous solvents at 40 °C, in 12 minutes at pH 4.5-6.5.

Alongside aluminium a whole suite of fluorine-metal complexes have been explored for fluorine-18 radiolabelling purposes though none have been quite as successful. Reid and co-workers have been the most prolific team working in this area of research. In 2014 they explored Cl/F halide exchange with aluminium, gallium and indium trichlorides complexed to the macrocyclic (N₃) chelators **28** and **29** (Figure 1.9).¹⁰⁷ All the fluorine-19 complexes could be synthesised from their corresponding trichlorides at room temperature but organic solvent (100% for In, 70% for Al and Ga) were used and only GaCl₃(BnMe₂-tacn) was radiolabelled. In a 1:1 water:acetonitrile mixture at room temperature, a 30% RCY was achieved in 1 hour using carrier added [¹⁸F]KF. Comparatively, when GaCl was complexed to a NODA (N₃O₂) chelator, the same results could be achieved in only 30 minutes at room temperature without the addition of an organic co-solvent.¹⁰⁸ [¹⁸F]GaF₃(BnMe₂-tacn) has also be synthesised through ¹⁹F/¹⁸F isotopic exchange, however, it was performed in a 25% water solution and required heating to 80 °C.¹⁰⁹ Reid *et al.* have also reported the radiolabelling of AlCl₃(BnMe₂-tacn) using McBride's method (pH 4.0, 100 °C) with carrier added [¹⁸F]KF that lead to a RCY of 24% in 60-90 minutes.¹¹⁰

Reid and co-workers have also reported attempts to perform Cl/F halide exchange of the trichloride **28**, **29** and **30** complexes (Figure 1.9) with the metals scandium, yttrium, lanthanum and lutetium, though only the scandium complexes could be synthesised using this method and it required anhydrous conditions.¹¹¹ Most recently they have investigated chromium, manganese, iron and cobalt in their corresponding trichloride **28** and **30** complexes.¹¹² The cobalt and manganese complexes were found to be unstable in water while the halide exchange for the chromium complex did not go to completion even after 24 hours at reflux in acetonitrile. Iron on the other hand underwent exchange in aqueous acetonitrile at room temperature in just 30 minutes when using 4 mole equivalent of potassium fluoride when complexed with **28**. This complex could be radiolabelled in a 6% yield with aqueous fluoride-18 in a 1:4 water:acetonitrile mixture at 80°C in 10 minutes.

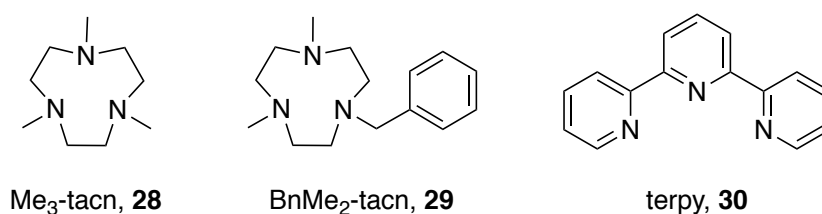


Figure 1.9 A selection of chelators with three nitrogen donors explored by Reid and co-workers.

1.10 Radiolabelling through S-F bond formation

Inkster *et al.* synthesised [^{18}F]**31-34** (Figure 1.10) from their corresponding sulfonyl chlorides through nucleophilic fluorination with [^{18}F]CsF in 1:1 solutions of aqueous Cs_2CO_3 and organic solvents at room temperature in 15 minutes.¹¹³ [^{18}F]**31** was also synthesised with [^{18}F]CsF in 100% aqueous Cs_2CO_3 however, variable yields were obtained (6-19%). The authors attributed this to the limited solubility of **31** in water and that the reaction was analysed directly. When DMSO was added immediately before analysis, excellent radiochemical yields of 80% were recorded. Likely, these high yields are somewhat driven by the precipitation of the product from solution and it is probable that repeated on a protein where there would no longer be solubility issues, yields would be lower.

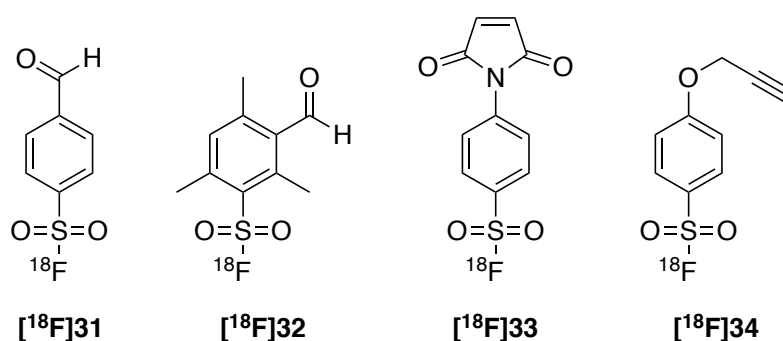
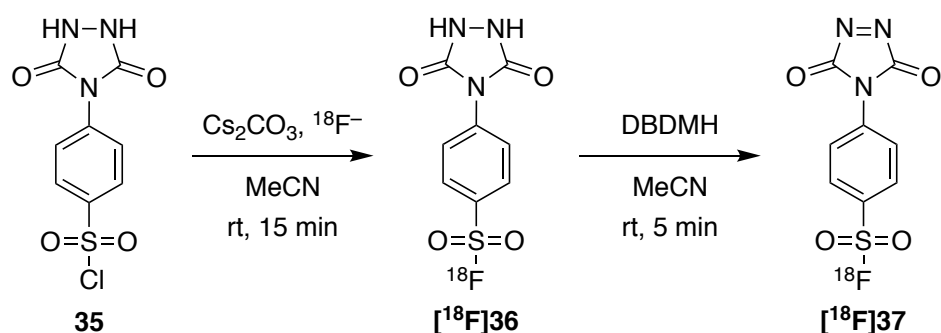


Figure 1.10 [^{18}F]**31-34** can be synthesised in high radiochemical yields from their corresponding sulfonyl chlorides with [^{18}F]CsF in 50% aqueous solutions at room temperature in only 15 minutes.

Despite the ability to radiolabel arylsulfonyl chlorides in good yields under aqueous conditions and at room temperature, they unfortunately are highly susceptible to hydrolysis. Thus, they have a limited applicability to the direct radiolabelling of proteins. The method of radiolabelling an arylsulfonyl chloride described above has however, been used in the synthesis of [^{18}F]**37** (Scheme 1.11), a potential prosthetic group for the indirect radiolabelling of proteins at tyrosine.¹¹⁴

As with the other fluoride bonds we have discussed, S-F bonds also undergo hydrolysis. Inkster *et al.* found **32** and **34** to be hydrolytically stable at pH 7.2 in a 150 mM PBS solution with 10% DMSO over 2.5 hours. **33** showed some hydrolysis (90% remaining) while **31** showed complete hydrolysis. Interestingly, this indicated that not only does steric hinderance protect the S-F bond from hydrolysis but that electronic effects may play a significant role.¹¹³ However, Matesic and co-workers later proved that this is not the case and that while electron-donating

groups may help stabilise the S-F bond, the more significant factor is steric hindrance.¹¹⁵ Nevertheless, at the time given the excellent stability of [¹⁸F]**32**, it was used to indirectly label a bombesin peptide fragment through oxime formation in DMSO. Under identical conditions used for [¹⁸F]**31-34**, the radiolabelled peptide fragment was found to be hydrolytically stable, however, in mouse serum defluorination was observed within 15 minutes.



Scheme 1.11 [¹⁸F]**37** is synthesised from its corresponding sulfonyl chloride **35** using the radiolabelling method reported by Inkster *et al.*¹¹³ followed by oxidation with 1,3-dibromo-5,5-dimethylhy-dantoin (DBDMH). [¹⁸F]**37** reacts with tyrosine under basic (pH 9-10) conditions at room temperature.

Perhaps not surprisingly, the Michael acceptor [¹⁸F]ethenesulfonyl fluoride (**[¹⁸F]38**, Figure 1.11A) which has been investigated as a prosthetic group also shows a low stability in rat serum at 37 °C.¹¹⁶ The stability of the S-F bond was found to be highly dependent on the conjugate. After 15 minutes the purity of the aniline adduct [¹⁸F]**39** had reduced to 70% while complete degradation of the cysteine adduct [¹⁸F]**30** was observed. [¹⁸F]**38** was also used to indirectly radiolabel insulin and bovine serum albumin (BSA). After only 15 minutes the purity of [¹⁸F]Insulin (**[¹⁸F]41**) had reduced to 13% while [¹⁸F]BSA (**[¹⁸F]42**) had completely degraded. This suggest that as with Si-F and B-F bonds the nature of distant functionalities also affect the hydrolytic stability of S-F bonds.

The synthesis of di-*tert*-butyl analogues has been suggested as a way to increase the hydrolytic stability of the S-F bond. Preliminary studies investigating the synthesis of the sterically hindered **43** (Figure 1.12) have, however, been unsuccessful.¹¹⁷ Given the ease of fluorinating sulfonyl chlorides this warrants further investigation but to date no reports have emerged in the chemical literature.

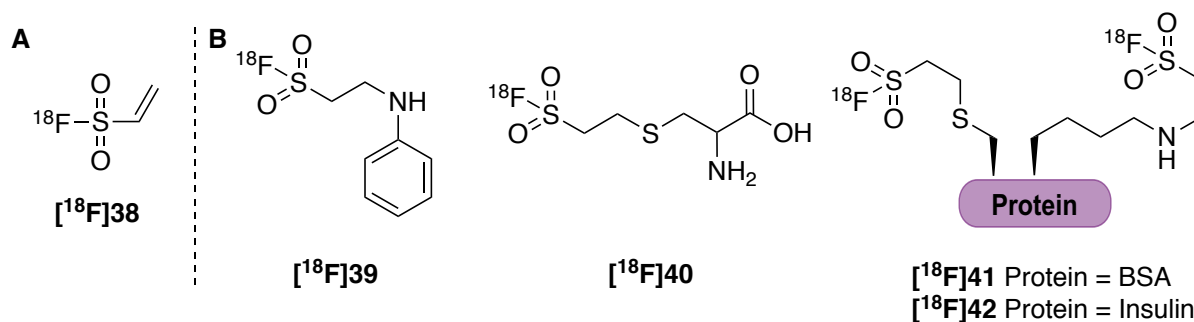


Figure 1.11 A) Structure of [^{18}F]38. B) [^{18}F]38 adducts that exhibited the highest stability of the S-F bond. [^{18}F]38 could be conjugated to aniline as well as the amine of several amino acids, the thiol of cysteine and to insulin and BSA.

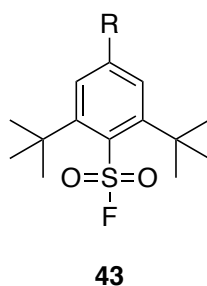
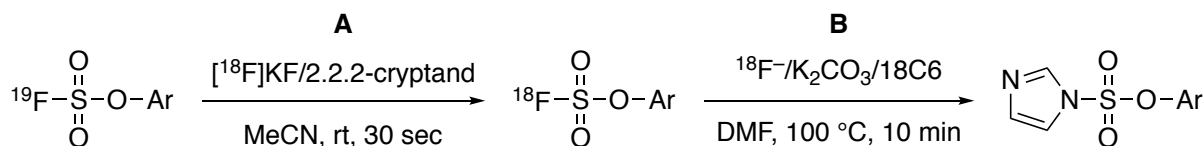


Figure 1.12 The use of di-*tert*-butyl groups have been suggested to increase the stability of the S-F bond.

In addition to arylsulfonylchlorides, arylfluorosulfates have also been radiolabelled with fluorine-18. Remarkably, they can be rapid radiolabelled through $^{19}\text{F}/^{18}\text{F}$ isotopic exchange using the traditional azeotropically dried [^{18}F]KF/Kryptofix 222 in acetonitrile in as little as 30 seconds at room temperature (Scheme 1.12A).¹¹⁸ Furthermore, they show excellent stability *in vivo*. Very recently, Kwon *et al.* also reported the synthesis of fluorine-18 radiolabelled aryl fluorosulfates from their aryl imidazylate precursors.¹¹⁹ In comparison, fluorination was performed at high temperatures (Scheme 1.12B) but greater than 50% yields were frequently obtained with only a few exceptions.



Scheme 1.12 Aryl [^{18}F]fluorosulfates have been synthesised via $^{19}\text{F}/^{18}\text{F}$ isotopic exchange at room temperature in only 30 seconds (**A**) and via their corresponding imidazylates at 100 °C in 10 minutes (**B**). Neither were tested in aqueous conditions.

1.11 Radiolabelling through P-F bond formation

Recently, the radiolabelling of proteins through phosphorus fluorine bond formation was reported.¹²⁰ As with the other inorganic elements we have discussed, phosphorus readily forms bonds with fluorine. Hong *et al.* studied the effects of steric hinderance on radiolabelling yields and hydrolytic stability of the P-F bond in the small organophosphines **44-46** (Figure 1.13). When using ¹⁹F/¹⁸F isotopic exchange, rapid ¹⁸F-labelling occurring at room temperature within 5-15 minutes even with bulky *tert*-butyl substituents on the phosphorous atom. Incredibly, in a 95% aqueous solution (5% DMSO added for solubility of **46**) 50% radiochemical yields were achieved. Again, the use of two *tert*-butyl substituents lead to an improved hydrolytic stability and [¹⁸F]**46** was found to be 100% stable *in vivo* 120 minutes post injection into healthy mice. Using the tetrafluorophenyl ester of **46**, the organophosphine was conjugated to human serum albumin (HAS). No conditions for the procedure for the radiolabelling of the protein conjugate were detailed but a radiochemical yield of >5% was reported.

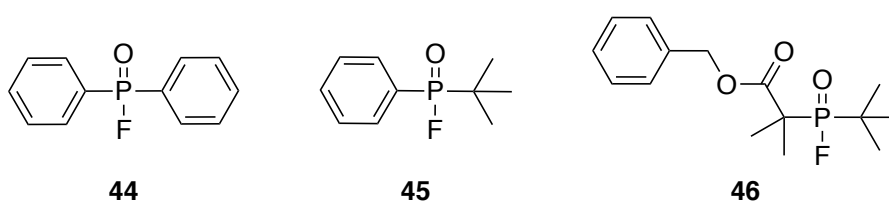


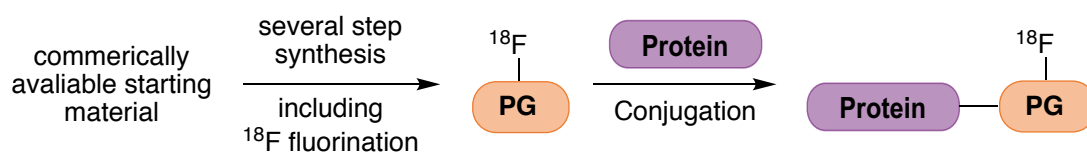
Figure 1.13. Hong *et al.* studied the radiolabelling of these three organophosphines using ¹⁹F/¹⁸F isotopic exchange. **46** offers the greatest hydrolytic stability and can even be radiolabelled in a 50% radiochemical yield in a 95% aqueous solution at room temperature within 5-15 minutes.

1.12 Concluding remarks

PET has emerged as a powerful imaging technique for the detection, diagnosis and staging of disease. With their high specificity and affinity for their molecular targets, peptide and protein biomarkers for disease have gained significant attention as potential imaging agents for targeted PET. In particular, there has been interest in the radiolabelling of these molecules with the 'ideal' radionuclide fluorine-18. For peptides which can withstand the harsh conditions required for C-F bond formation this can be achieved using conventional methods. For proteins however, restricted by the low specific activities obtained from electrophilic fluorination and the low nucleophilicity of the fluoride-18 in aqueous media, this has primarily been accomplished

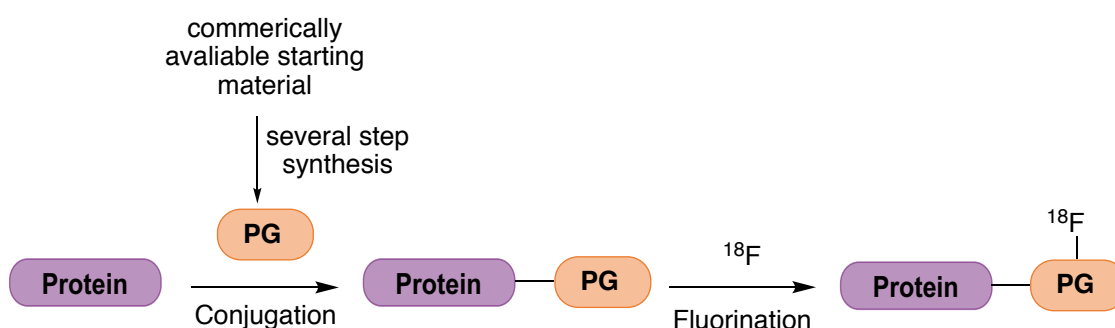
through indirect labelling with prosthetic groups. These multi-step methods are not however, optimal for use with fluorine-18 which has a half-life of only 110 minutes.

A. Indirect radiolabelling



- Organic solvents
- High temperatures
- High yields and specific activity
- Multiple step synthesis
- Early incorporation of fluorine-18
- Lengthy HPLC purification
- Not compatible with fluorine-18 half-life

B. Direct radiolabelling



- Late-stage single step incorporation of fluorine-18
- Simple size exclusion purification
- On demand stable precursors
- Compatible with fluorine-18 half-life
- Low nucleophilicity of fluoride-18 in water
- Low temperatures required

Scheme 1.13 The advantages and disadvantages of indirect (A) and direct (B) methods for the radiolabelling of proteins with fluorine-18.

Recently, efforts have been centred around the exploration of inorganic approaches to radiolabel peptides and proteins with fluorine-18. Predominately these have focused on aluminium, boron and silicon fluoride bond formations. As with traditional C-F bond formation these methods have been used in the indirect radiolabelling of proteins with fluorine-18. They have however, also reignited the possibility of directly radiolabelling proteins with fluorine-18 with reports of fluorine bond formation occurring in aqueous media. With the clear advantages to direct fluorination methods and only a single example of the direct radiolabelling of a protein in the chemical literature, there exists an exciting opportunity to contribute to and build upon this research.

1.13 Doctoral research contributions to knowledge

Although proteins have been radiolabelled with fluorine-18, the indirect strategies generally used to achieve this are not well suited to its half-life. Aiming to address this issue, this thesis concerns the utilisation of silicon in the direct fluorination of proteins. The research described here in this thesis illustrates the candidate's original contributions to knowledge in the field concerning the direct and aqueous fluorination of proteins.

Chapter one provides a context to the contributions to knowledge presented in this thesis. It details a review of the current literature on the fluorination of peptides and proteins with fluorine-18 using inorganic fluoride acceptors. Chapter two explores the design and synthesis of novel silicon-based compounds with consideration into how they may be site-selectively incorporated into proteins through chemical modifications. Their reactivity towards fluorine sources in the presence of water is also assessed to determine their suitability for the direct fluorination of proteins. Chapter three describes the use of these molecules for the site-selective chemical modification of proteins. Fluorination of a chemically modified protein under aqueous conditions demonstrates that the newly designed silicon compounds are viable candidates and represents the first use of silanols for the direct fluorination of proteins. Chapter four addresses issues associated with attaining site-selective chemical modification of proteins, presenting the synthesis of a silicon-based amino acid suitable for incorporation into protein via amber codon suppression. An unexpected oxidative cleavage observed during the synthesis leads to the discovery of a novel reaction converting homobenzylic alcohols to benzaldehydes. The fifth Chapter describes the incorporation of the new silicon-based amino acid into green fluorescent protein using amber codon suppression. Lastly, Chapter six concludes this thesis with a summary of the work completed during this doctorate, the implications it has for the direct and site-selective radiolabelling of proteins with fluorine-18 and possible future directions this project may take.

Chapter Two

Design, synthesis and direct aqueous fluorination of a silanol-based prosthetic group

2.1 Introduction

A review of the literature on radiolabelling with fluorine-18 through bond formation with inorganic elements revealed that many of them can form in the presence of water and at room temperature (Chapter 1). Despite this, they have been used primarily, for the indirect radiolabelling of proteins with only a few examples of their use for the direct radiolabelling of proteins with fluorine-18.^{64,101,105} Thus, there exists an opportunity to explore the direct radiolabelling of proteins through fluorine bond formation with inorganic elements.

Drawn to the direct radiolabelling of a protein via $^{19}\text{F}/^{18}\text{F}$ isotopic exchange at silicon by Glaser *et al.*,⁶⁴ we considered that other silicon-based compounds may also be useful for the direct radiolabelling of proteins. This Chapter details the evaluation and application of silanols as a fluoride acceptor in aqueous media. Successful fluorination of a model silanol encouraged the design and synthesis of a silanol-based molecule that could be incorporated into a protein via chemical modification. Direct fluorination of this molecule was also evaluated and is reported. The chemical modification of proteins with the silanol-based molecule is described in Chapter 3.

The data and conclusions presented here in this Chapter have not been prepared for publication in any scientific journal nor are reported anywhere else on the date of thesis submission. The candidate planned, researched, conducted and prepared the following Chapter with full intellectual and practical contributions unless otherwise state in-text.

2.2 Proposed strategy for the direct aqueous fluorination of proteins

The ideal method for the direct radiolabelling of proteins with fluorine-18 involves the simple addition of fluoride-18 directly from the target water to a shelf-stable precursor that results in rapid fluorination at room temperature in aqueous media. As the nucleophilicity of the fluoride-18 ion is reduced in water, achieving this is not a trivial task. Nevertheless, we propose that many of these attributes could be achieved by fluorinating proteins through Si-F bond formation. Indeed, Si-F bond formation has already been used to achieved radiolabelling of a protein with simple addition of fluoride-18 directly from the target water in aqueous solvents.⁶⁴ However, the fluorosilane precursor used is unstable in water when exposed for extended periods undergoing hydrolysis and radiolabelling was performed at high temperature. Silanols have previously been used as precursors for the radiolabelling of small molecules with fluorine-18, however, they have only been fluorinated with the ¹⁸F[KF]/Kryptofix 222 complex and in organic solvents.⁶⁰ We considered that as silanols are stable in water that they could also be used to synthesis shelf-stable protein precursors and wondered if they could be fluorinated in a single, rapid step at room temperature in aqueous media.

With the trade-off between the ease of fluorination and the hydrolytic stability of the Si-F bond (discussed in Chapter 1) when more sterically hindered substituents on the silicon atom are used and, that hydroxides make poor leaving groups, we propose to use diisopropyl substituents. We envision that this will be required to reach suitable fluorination yields. The use of diisopropyl substituents on the silicon atom has been shown to result in limited hydrolytic stabilities of the Si-F bond.⁶¹ But, the hydrolytic stability of the Si-F bond is highly dependent on the functionality of the fourth substituent⁶¹ and the effect a protein substituent has on the hydrolytic stability of the Si-F bond is currently unknown. Furthermore, there is an opportunity to optimise the hydrolytic stability in future studies. This will be discussed in Chapter 6.

Another key aspect to our strategy is that silanols could be incorporated into proteins via genetic methods as well as through the chemical modification of proteins. Over 200 unnatural amino acids have been incorporated into proteins in response to a unique codon using genetic methods.¹²¹ As prolonged exposure to water will not result in hydrolysis, it is therefore possible for a silanol-based amino acid to be genetically incorporated into recombinant proteins. Chemical modification allows for the silanol to be incorporated quickly but is limited to incorporation at the site of the residue being modified. The benefit to genetic incorporation is that it allows for a greater control over the site of modification. The unique codon can be introduced using site-directed mutagenesis at any chosen site. As such, the silanol could be incorporated site-selectively at a site that will not affect its affinity and specificity for its molecular target. Additionally, this means that genetic incorporation can be used as a general method for the incorporation of a silanol and allow for incorporation into a wider range of proteins. The genetic incorporation of a silanol-based amino acid are the topics for Chapters 4 and 5 of this thesis.

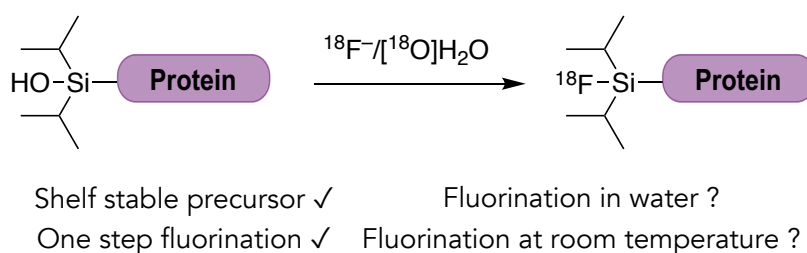


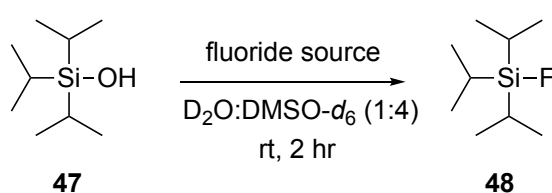
Figure 2.1 Proposed strategy for the direct radiolabelling of proteins through Si-F bond formation from the corresponding silanol. Silanols are stable in water and can be synthesised in one step but, can they be fluorination in water and at room temperature?

2.3 Direct aqueous fluorination of a model silanol

To first confirm whether or not the hydroxide of silanols would undergo displacement reactions with the fluoride anion in aqueous media, we conducted fluorinations on a model silanol. Displacement of the hydroxide by the fluoride ion at silicon has been shown to occur in dimethyl sulphoxide⁶⁰ though no attempts in an aqueous solvent or with an aqueous co-solvent have been reported. Presumably this is because water solvates fluoride ions, reducing their nucleophilicity leading to lower yields.⁴⁷ Thus, it is preferential to conduct these reactions in organic solvents. When performing direct fluorinations on proteins however, an aqueous solvent must be used.

Given that our strategy was based on the use of isopropyl substituents, we chose triisopropylsilanol (**47**) as the model silanol. A limited solubility of **47** in water meant that the fluorinations needed to be performed with an organic co-solvent to avoid precipitation. While not being conducted solely in water as would be the case for proteins, this experiment would still indicate whether it is possible to perform this reaction in the presence of water and at room temperature. As the half-life of fluorine-18 is only 110 minutes, we also chose to limit these reactions to two hours.

Taking triisopropylsilanol, we reacted it with a range of fluoride sources (10 equivalents) in a 1:4 water:dimethyl sulphoxide solution (this was the maximum water content that could be used before **47** precipitated from the solution) at room temperature for 2 hours. Using ^1H and ^{19}F NMR experiments of the reaction mixtures, we were able to provide evidence that supported fluorination of the silicon atom. The conversion was found to be dependent on the fluoride source with hydrogen fluoride in pyridine giving the best results for those tested (Scheme 2.1). Additionally, increasing the temperature to 37 °C increased conversion to 43% when using hydrogen fluoride in water as the fluoride source. However, similar conversion for the fluoride sources ammonium fluoride and hydrogen fluoride in pyridine were obtained at 37 °C. Importantly, these results support our hypothesis that hydroxides would undergo substitution with fluoride ions at silicon atoms in the presence of an aqueous solvent and at room temperature. Gratifyingly, observing conversions within 2 hours also supports our overarching hypothesis that silanols are viable precursors for the direct radiolabelling of proteins with fluorine-18.



Entry	Fluoride source	Conversion	δ_{F} (ppm)
1	NH_4F	6%	-183.55
2	HF (48% in H_2O)	23%	-183.52
3	HF•Pyridine	77%	-183.53

Scheme 2.1 Silanols can be converted to fluorosilanes in the presence of water using a range of fluoride sources. Signals in the ^{19}F NMR spectra at -183.5 ppm were used to support formation of the Si-F bond and conversions were determined via integration of the ^1H NMR spectra.

Potassium fluoride was also tested as a fluoride source, however, it precipitated upon addition to the triisopropylsilanol solution and no signals were present in the ^{19}F NMR spectrum of the reaction mixture. Both the precipitation and the lack of ^{19}F signals in the NMR spectrum indicate that potassium fluoride is not soluble in this solvent system. Similarly, the low yield obtained when using ammonium fluoride was also deemed to be due to its limited solubility in this solvent system. It is foreseeable that higher yields could be achieved with ammonium fluoride and potassium fluoride in solvent system that have a higher aqueous content.

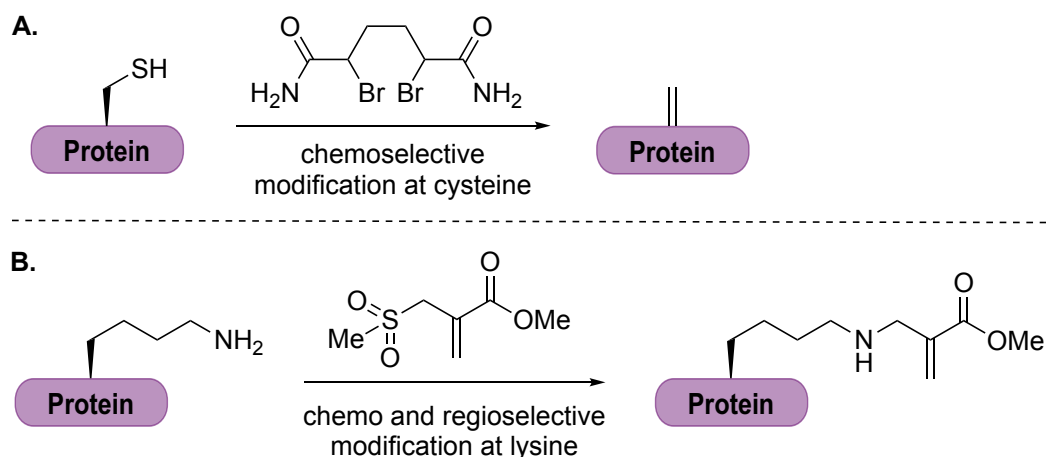
2.4 Designing a silanol for the chemical modification of proteins

With evidence that silanols can be converted to fluorosilanes in the presence of water and at room temperature, the next step was to repeat this on a protein. To do this, a silanol would first have to be incorporated into a protein. The simplest and quickest way to achieve this is through chemical modification. Therefore, we set out to design a silanol that could be incorporated into a protein via chemical modification.

In a bid to use site-selective methods to create homogenous products we chose to chemically modify proteins through the conversion of cysteine to dehydroalanine (Scheme 2.2A).¹²² This method generates a unique electrophilic site that allows for the conjugation of Michael donors to the protein. Complementary to this, our collaborators at the University of Cambridge have developed a method for the chemo- and regioselective installation of a very similar electrophilic site at lysine (Scheme 2.2B).¹²³ Again, this allows for conjugation of Michael donors to the protein. We envision that this method would be useful for proteins that do not contain an available cysteine. Both can undergo Michael additions with benzylamines¹²⁴ and thus we proposed the benzylamine **49** shown in Figure 2.2 for the incorporation silicon into proteins via chemical modification.

Theoretically, using the right intermediate, a diverse range of conjugates could be accessed from a single compound that could be used for the modification of proteins using different chemical modification methods. Therefore, we chose to synthesise a mesylate intermediate that would be able to partake in substitution reactions with myriad nucleophiles. It was envisioned that **50** could simply be obtained by mesylation of the alcohol **51**. This in turn,

could be accessed by lithium halogen exchange on the arylbromide **52** followed by silylation with diisopropylchlorosilane (Scheme 2.3).



Scheme 2.2 **A)** Chemoselective conversion of cysteine to dehydroalanine via chemical modification of native proteins. **B)** Chemo and regioselective chemical modification of native proteins at lysine to install a unique electrophilic site.

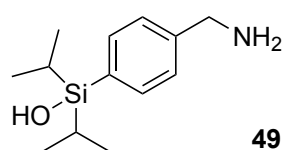
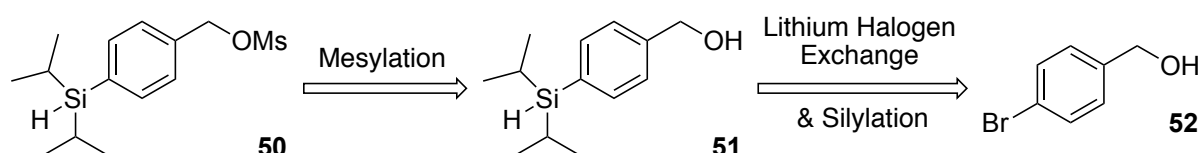


Figure 2.2 Structure of the proposed Michael donor silanol-based prosthetic group **49**.



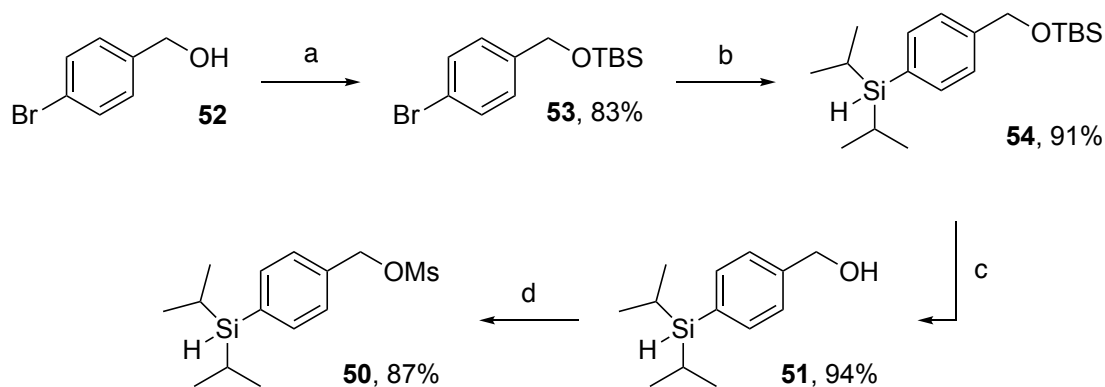
Scheme 2.3 Retrosynthetic analysis of the mesylate intermediate **50**.

2.5 Synthesis of 1-[(4-diisopropylsilyl)benzyl]amine (**49**)

2.5.1 Lithium halogen exchange, silylation and synthesis of a mesylate intermediate

To access **50**, alcohol **52** was first protected as the silyl ether to limit side reactions during the subsequent metalation and silylation. The silyl ether **53** was synthesised using *tert*-butyldimethylsilyl chloride and imidazole in dry dichloromethane and isolated in an 83% yield (Scheme 2.4). Imidazole was added to increase the rate of reaction through the formation of *N-tert*-butyldimethylsilyl imidazole, a more reactive silylation agent than *tert*-butyldimethylsilyl

chloride.¹²⁵ With the alcohol protected, lithium halogen exchange with *n*-butyllithium at $-78\text{ }^{\circ}\text{C}$ and the subsequent silylation with diisopropylchlorosilane successfully produced **54** in an excellent yield of 91%. Cleavage of the silyl ether **54** under acidic conditions in methanol gave the primary alcohol **51** and it was isolated in a 94% yield. Finally, **51** was converted to the sulfonate ester **50** in an 87% yield with methane sulfonyl chloride in the presence of triethylamine (Scheme 2.4).



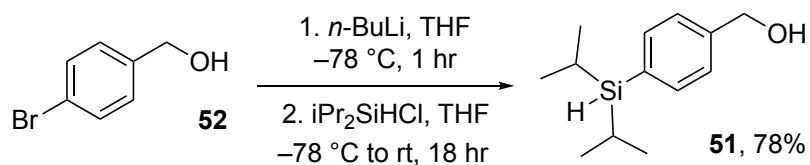
Scheme 2.4 Synthesis of the mesylate intermediate **50**. a) TBS-Cl, imidazole, CH_2Cl_2 , rt, 18 hr; b) *n*-BuLi in hexanes, THF, $-78\text{ }^{\circ}\text{C}$, 1 hr, then *iPr*₂SiHCl, $-78\text{ }^{\circ}\text{C}$ to rt, 22 hr; c) HCl, H_2O , MeOH, rt, 18 hr; d) MsCl, Et_3N , CH_2Cl_2 , $0\text{ }^{\circ}\text{C}$ to rt, 2 hr.

2.5.2 Optimisation of metalation and silylation

Without protection of the alcohol it is possible to produce silyl ethers alongside the desired product during the lithium halogen exchange and silylation step. Formation of silyl ethers, however, is very slow without the addition of a catalyst.¹²⁵ Therefore, if the rate of silylation of the organolithium is faster than that of the formation of the silyl ether it should be possible to produce the desired product **51** in a reasonable yield without substantial formation of the silyl ether. Chen *et al.* had reported **51** synthesised from **52** through metalation and silylation without protection of the alcohol in a 73% yield.¹²⁶ Based on this rationale and the report by Chen, we attempted to optimise the synthesis of **50** reducing the number of steps by eliminating the protection and deprotection.

Under identical conditions to those used by Chen *et al.*¹²⁶ the metalation and silylation of **52** was performed with *n*-butyllithium and diisopropylchlorosilane (Scheme 2.5). Two equivalents of *n*-butyllithium were used, the first acting as a base and deprotonating the alcohol, the second participating in lithium halogen exchange with the arylbromide forming the aryllithium. Followed

by silylation with diisopropylchlorosilane, **51** was obtained without any evidence of the silyl ether. Furthermore, **50** was obtained in a 78% yield, greater than the 71% overall yield obtained from **52** using the 3-step protection and deprotection route discussed above.



Scheme 2.5 Metalation and the subsequent silylation with diisopropylchlorosilane of the unprotected alcohol **52** gives **51** in good yields without formation of the silyl ether.

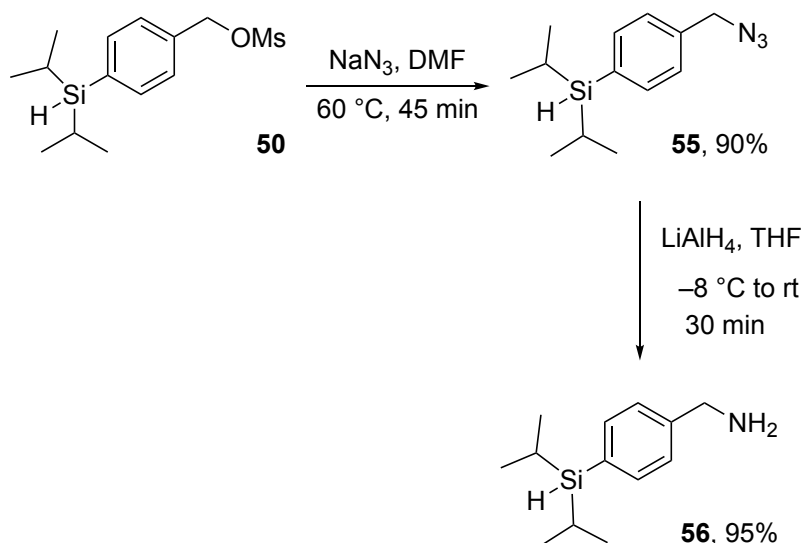
Evidence of a reaction between the organolithium and *n*-butylbromide was observed in the ¹H NMR spectrum obtained after workup. Organolithium reagents are known to react with the *n*-butylbromide formed during halogen lithium exchange with *n*-butyllithium when the organolithium is slow to react with the final reactant.¹²⁷ Presumably, the steric bulk of the silane, which slows the rate of silylation, opens up the opportunity for competing reactions involving the organolithium to occur. Despite this, this method optimised the yield and reduced the number of steps required.

2.5.3 Mesylate displacement to introduce amine functionality

With the mesylate intermediate **50** in hand, we next investigated displacement reactions to introduce amine functionality. The benzylamine **56** could be easily and quickly obtained through azide **55** followed by reduction to the amine with lithium aluminium hydride in excellent yields (Scheme 2.6). The azide **55** was obtained in sufficient purity simply through extraction with ethyl acetate and washing of the organic fractions with a brine solution. Initial attempts at the reduction of the azide to the amine with lithium aluminium hydride in tetrahydrofuran at 0 °C (ice bath) gave the desired products in good yields (65-75%). The reaction was optimised with temperature proving to be extremely important. When conducting the reaction in a salt/ice bath at -8 °C, **56** was obtained in 95% yield. Again, sufficient purity of **56** was achieved via extraction from the aqueous layer and washing of the organic fractions with a brine solution.

It is noted that during mass spectrometry characterisation of the azide compound, using positive atmospheric pressure chemical ionisation (APCI), the expected molecular ion peak ([M+H]) was not observed. Rather the major peak seen for **55** was that of the molecular ion peak

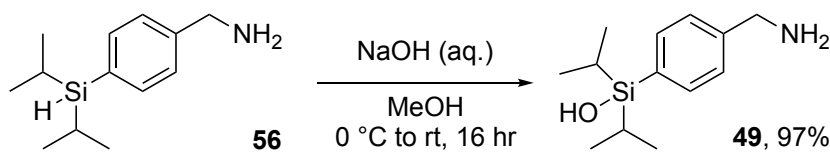
minus 28 Da ($[M+H - 28]$). This is consistent with protonation and the loss of N_2 . The loss of molecular nitrogen is a commonly seen fragmentation of azide.¹²⁸



Scheme 2.6 The benzylamine **56** could be obtained in good yields from the mesylate intermediate **50** via substitution with sodium azide and subsequent reduction with lithium aluminium hydride.

2.5.4 Oxidation of the silane to the silanol

The final step in the synthesis of **49** was to convert the silane into the silanol. Silane **56** was oxidised to the silanol **49** with methanol in a basic solution of water (sodium hydroxide). The silanol was obtained with a 97% yield after 16 hours (Scheme 2.7). The silane was cleanly converted to the silanol and no further purification was required. It also proved to be stable at room temperature and in air with no decomposition observed during the time frame of this project.

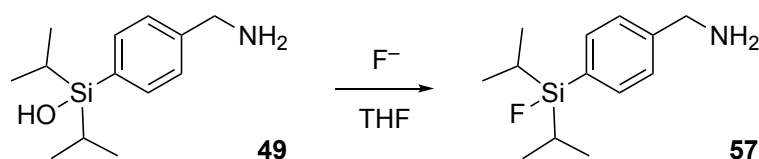


Scheme 2.7 Oxidation of the silane **56** to **49** with methanol in a basic aqueous solution.

2.6 Direct aqueous fluorination of 1-[(4-diisopropylsilanol)benzyl]amine (**49**)

As with triisopropylsilanol, we wanted to confirm that **49** could be fluorinated in the presence of water. Firstly, to support complete conversion of the silanol to the fluorosilane,

fluorination was performed in an organic solvent and at high temperatures. Using HF•Pyridine (~70% HF, ~30% pyridine) as the fluoride source, **49** was completely converted to **57** at 50 °C in 24 hours with 4 equivalents of fluoride in tetrahydrofuran (Scheme 2.8, Entry 1). No other products were observed and **57** was isolated in an 82% yield in sufficient purity without the need for further purification. Increasing the fluoride equivalents to 10 and bringing the temperature up to 95 °C greatly reduced the reaction time giving almost identical results in only an hour (Scheme 2.8, Entry 2).



Entry	Fluoride source	Equivalents	Temperature	Reaction time	Isolated yield
1	HF•Pyridine	4	50 °C	24 hr	82%
2	HF•Pyridine	10	95 °C	1 hr	83%

Scheme 2.8 **49** is completely converted to the fluorosilane **57** in tetrahydrofuran at elevated temperatures.

We next moved toward conditions more suitable to proteins and investigated the fluorination of **49** in the presence of water and at room temperature. Significant differences, chemical shifts of **49** and **57** in the ¹H NMR spectra, meant that conversion could be determined by integration of the ¹H NMR spectra of the reaction mixture. Hence, the fluorinations were conducted in deuterated solvents and analysed directly. Unfortunately, the low solubility of **49** in water limited the maximum aqueous content to 20% with precipitation occurring when values above this were used. Therefore, fluorination could not be tested in 100% aqueous conditions as was desired and instead was studied in a 5:1 solution of dimethyl sulphoxide to water. Considering the prospect of using fluoride-18 the reaction time was also limited to 3.5 hours, approximately double the radioactive half-life of fluorine-18. ¹⁹F NMR spectroscopy was used to support fluorination with the characteristic signal for a Si-F bond around δ_F -185 ppm.

As HF•Pyridine was successful at fluorinating **49** in tetrahydrofuran, we first tested fluorination in the presence of water with HF•Pyridine as the fluoride source. Using 10 (Scheme 2.9, entry 1) and 5 (Scheme 2.9, entry 2) equivalents of the fluoride, complete conversion to **57**

was observed in the ^1H NMR spectra. The Si-F bond was consistent with with a signal at $\delta_{\text{F}} -185.2$ ppm in the ^{19}F NMR spectra. Using fewer equivalents of fluoride reduced the conversion to 83% and 48% for 2 (Scheme 2.9, entry 3) and 1 (Scheme 2.9, entry 4) equivalents respectively. Again, ^{19}F NMR spectroscopy supported Si-F bond formation, albeit at very low intensities.

In the production of $[^{18}\text{F}]\text{F}^-$, enriched $[^{18}\text{O}]\text{H}_2\text{O}$ is commonly used as the target source and $[^{18}\text{F}]\text{F}^-$ is obtained as a solution in water. As such fluorination was also tested using hydrogen fluoride in water (~48% HF) as the fluoride source. Again, complete conversion to **57** was observed when using 10 (Scheme 2.9, entry 5) or 5 (Scheme 2.9, entry 6) equivalents of the fluoride. Using 2 (Scheme 2.9, entry 7) or 1 (Scheme 2.9, entry 8) equivalents gave conversion lower than that for HF•Pyridine but still gave good conversion (66% and 32% respectively). This time no signals were observed in the ^{19}F NMR spectra for the hydrogen fluoride or the product. Presumably, this is due to the lower sensitivity of ^{19}F relative to ^1H , the small (10 mg) reaction scale and the lower yields of these experiments. With sufficient evidence in the ^1H NMR spectra that fluorination was successful these reactions were not repeated on a larger scale.



Entry	Fluoride source	Equivalents	Conversion	δ_{F} (ppm)
1	HF•Pyridine	10	100%	-185.25
2	HF•Pyridine	5	100%	-185.21
3	HF•Pyridine	2	83%	-185.20
4	HF•Pyridine	1	48%	-185.07
5	HF in H ₂ O	10	100%	-185.18
6	HF in H ₂ O	5	100%	-185.16
7	HF in H ₂ O	2	66%	–
8	HF in H ₂ O	1	32%	–

Scheme 2.9 Under 20% aqueous conditions both the fluoride sources HF•Pyridine and HF in H₂O can be used for the fluorination of **49**.

These results, along with those for the fluorination of triisopropylsilanol (**47**) (Section 2.3), supported that silanols can be fluorinated when in the presence of water and at room temperatures.

2.7 Concluding remarks and chapter summary

In this Chapter a model silanol was shown to undergo fluorination in the presence of water and at room temperature. Further, the fluorination could be performed on a time scale suitable for syntheses with fluoride-18. However, the content of water that could be used was limited by the solubility of these silanols in water. Thus, fluorinations were performed in 25% aqueous DMSO solutions. Nevertheless, this result supports the use of silanols for the direct aqueous fluorination of proteins with fluoride-18 and a benzylamine suitable for conjugation to proteins through chemical modification was designed and synthesised. The benzylamine was synthesised from a mesylate intermediate which should give access to a range of functionalities that may be useful for the incorporation of silicon into proteins via chemical modifications. As with the model silanol, the benzylamine could be fluorinated in the presence of water and at room temperature in time frames suitable to syntheses with fluoride-18. The chemical modification of proteins with this benzylamine is presented in Chapter 3.

2.8 Experimental procedures

2.8.1 General experimental details

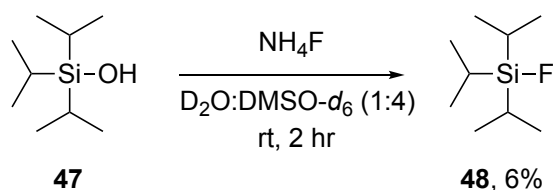
All reactions requiring anhydrous conditions were performed under a nitrogen atmosphere in flame-dried glassware. Dichloromethane and triethylamine were distilled over calcium hydride, tetrahydrofuran and diethyl ether were distilled over sodium and benzophenone. All other solvents and reagents were used as supplied from commercial suppliers without further purification. All fluorination reactions were conducted using plastic reaction vessels to avoid etching of glass with hydrogen fluoride. Fluorination NMR spectroscopy experiments were conducted with a fluorinated ethylene polypropylene (FEP) copolymer NMR tube liner. All fluorination reactions that were heated were carried out on a Grant Bio PMHT Thermoshaker.

Analytical thin layer chromatography was performed on aluminium sheets coated with silica gel containing a fluorescent indicator (0.15-0.2 mm thickness, 8 μm granularity) and were visualised using UV light or developed in a potassium permanganate or ninhydrin dip. Thin layer chromatography sheets used to analyse amines were pre-treated with 0.1% triethylamine in the required solvent system. Column chromatography was performed using silica gel (230-400 mesh, 60 \AA pore diameter).

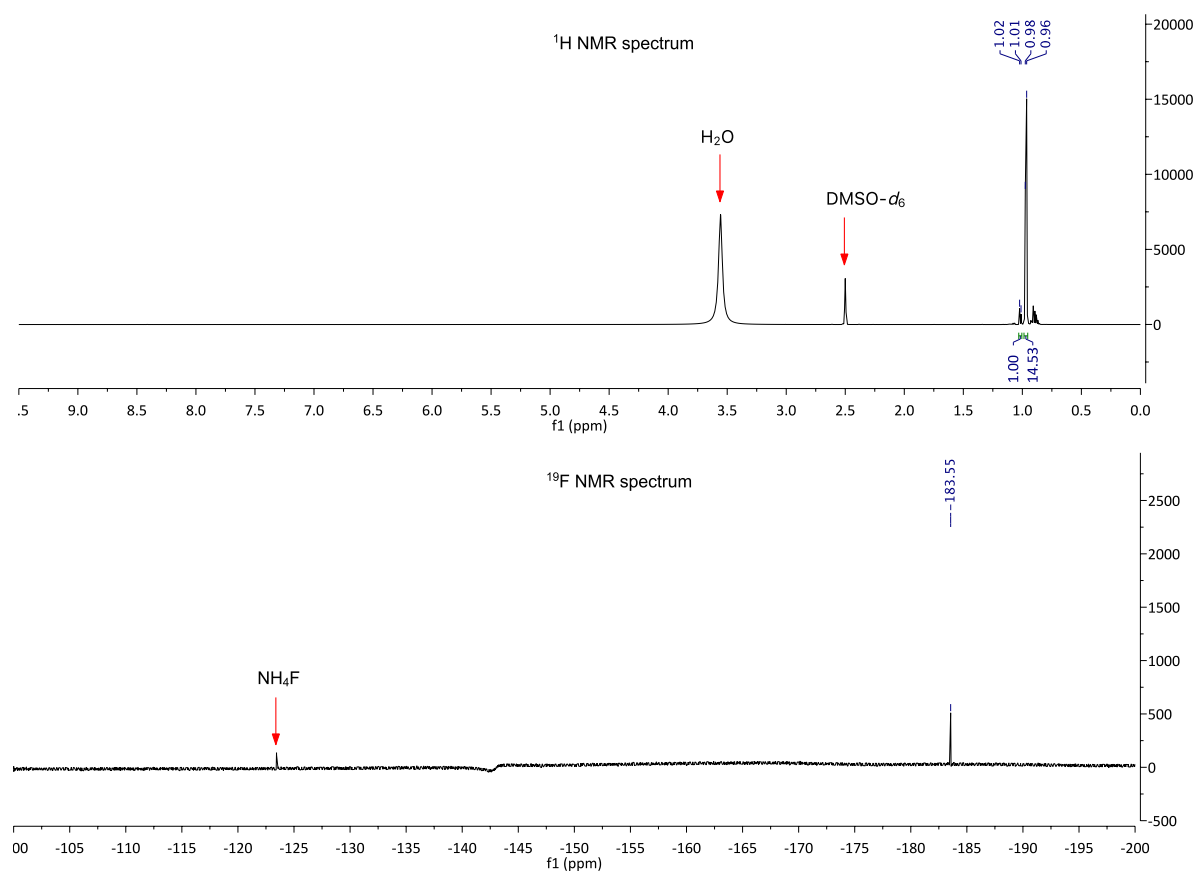
All NMR data were recorded using a Bruker Ultrashield 400 or a Bruker Ultrashield 600. Deuterated chloroform (CDCl_3) or deuterated water (D_2O) were used as the solvent and for internal locking. ^1H NMR chemical shifts were referenced to δ_{H} 7.26 ppm (CDCl_3) or δ_{H} 4.79 ppm (D_2O) and ^{13}C NMR chemical shifts to δ_{C} 77.16 ppm. Chemical shifts (δ) are reported in parts per million (ppm) and coupling constants (J) in hertz (Hz). Multiplicity is reported as s = singlet, d = doublet, t = triplet, m = multiplet and br. s = broad singlet. Infrared spectra were recorded on an FTIR spectrometer with the absorptions reported in wavenumbers (cm^{-1}). High resolution mass spectrometry was recorded using atmospheric pressure chemical ionisation (APCI) on a Perkin Elmer AxION connected to a DSA-ToF or electrospray ionisation (ESI) on a Waters Synapt HDMS. All HRMS data is reported as the observed molecular ion unless otherwise stated. Melting points were recorded on a Gallenkamp melting point apparatus and the values reported are a triplicate average.

2.8.2 Direct aqueous fluorination of triisopropylsilanol (**47**)

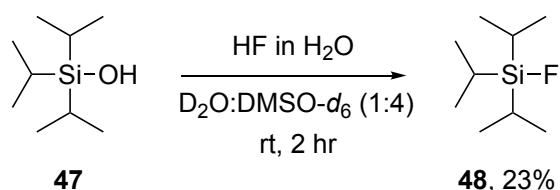
Scheme 2.1, Entry 1



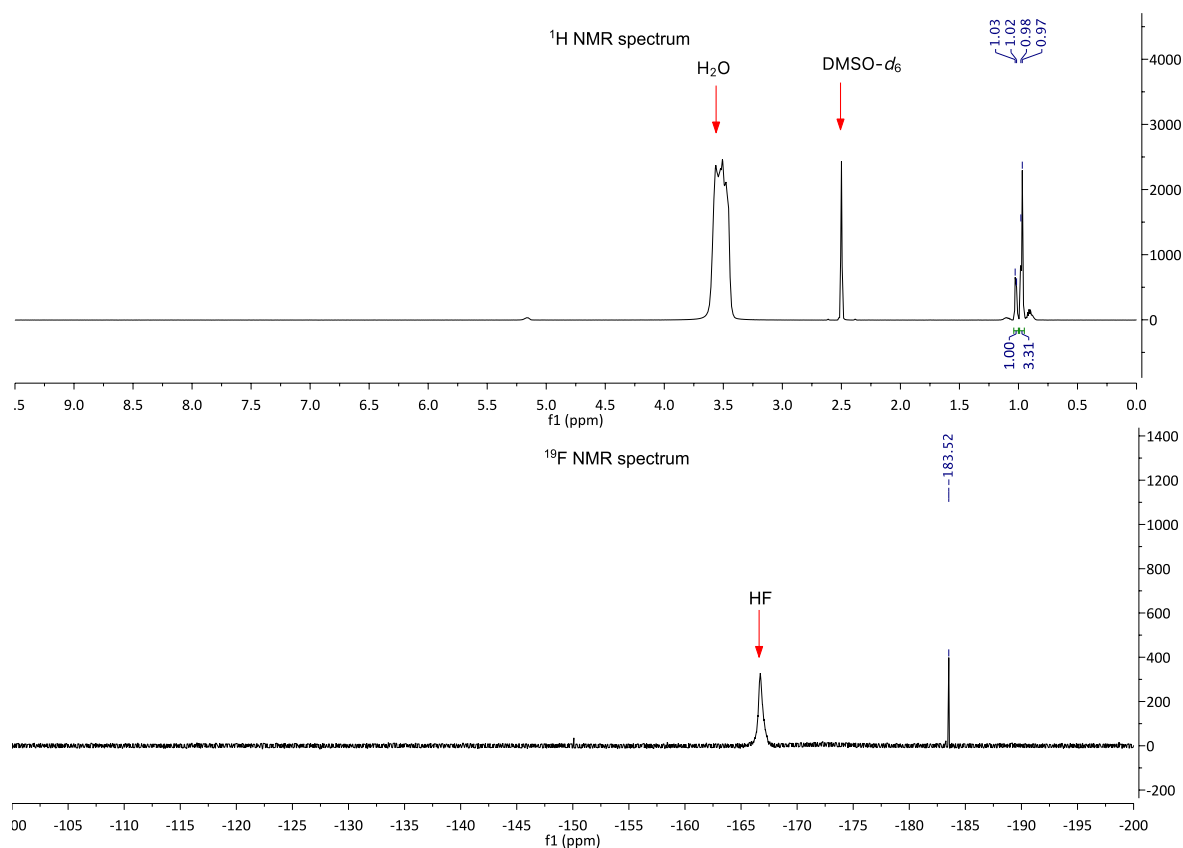
NH_4F (2 mg, 0.057 mmol) was added to a solution of **47** (9.9 mg, 0.057 mmol) in $\text{DMSO-}d_6$ (75 μL) and D_2O (20 μL) in a 0.5 mL microcentrifuge Eppendorf tube. After the addition of NH_4F the reaction was placed on a rotisserie (60 RPM) and allowed to react for 2 hr. After this time the solution was transferred to an FEP liner NMR tube and analysed via NMR spectroscopy. A signal at $\delta_{\text{F}} -183.55$ ppm, consistent with a Si-F bond, in the ^{19}F NMR spectrum supported that fluorination had occurred. Integration of the isopropyl signals in the ^1H NMR spectrum (δ_{H} 1.01-1.02 ppm for **48** and δ_{H} 0.96-0.98 ppm for **47**) revealed a 1:14.5 mixture and 6% conversion to **48**.



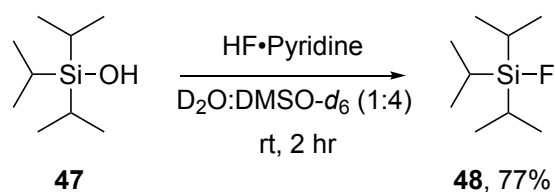
Scheme 2.1, Entry 2



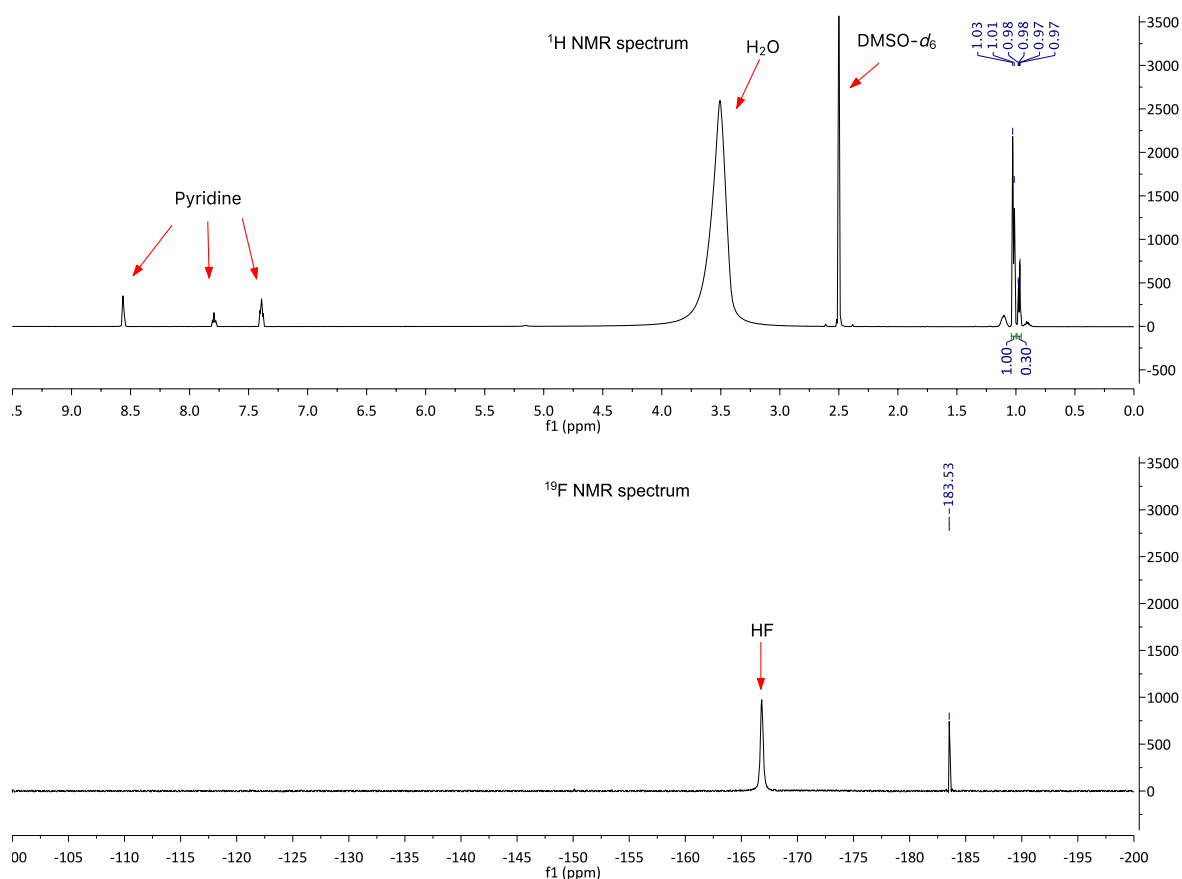
HF in H₂O (~48% HF) (2.9 μ L, 0.069 mmol) was added to a solution of **47** (12.1 mg, 0.069 mmol) in DMSO-*d*₆ (75 μ L) and D₂O (20 μ L) in a 0.5 mL microcentrifuge Eppendorf tube. After the addition of HF in H₂O the reaction was placed on a rotisserie (60 RPM) and allowed to react for 2 hr. After this time the solution was transferred to FEP liner NMR tube and analysed via NMR spectroscopy. A signal at δ_F -183.52 ppm, consistent with a Si-F bond, in the ¹⁹F NMR spectrum supported that fluorination had occurred. Integration of the isopropyl signals in the ¹H NMR spectrum (δ_H 1.02-1.03 ppm for **48** and δ_H 0.97-0.98 ppm for **47**) revealed a 1:3.3 mixture and 23% conversion to **48**.



Scheme 2.1, Entry 3

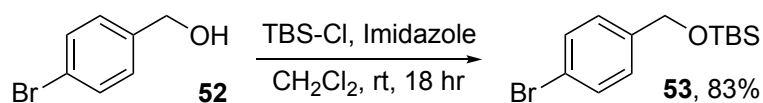


HF•Pyridine (~70% HF) (1.72 μL , 0.057 mmol) was added to a solution of **47** (10.0 mg, 0.057 mmol) in DMSO- d_6 (75 μL) and D₂O (20 μL) in a 0.5 mL microcentrifuge Eppendorf tube. After the addition of HF•Pyridine the reaction was placed on a rotisserie (60 RPM) and allowed to react for 2 hr. After this time the solution was transferred to FEP liner NMR tube and analysed via NMR spectroscopy. A signal at δ_{F} -183.53 ppm, consistent with a Si-F bond, in the ¹⁹F NMR spectrum supported that fluorination had occurred. Integration of the isopropyl signals in the ¹H NMR spectrum (δ_{H} 1.03-1.01 ppm for **48** and δ_{H} 0.97-0.98 ppm for **47**) revealed a 1:0.3 mixture and 77% conversion to **48**.



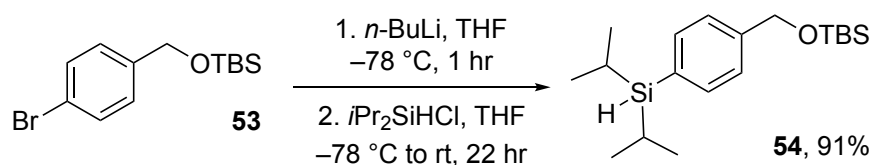
2.8.3 Synthetic procedures and analytical data

1-[(4-Bromo)benzyl]tert-butyldimethylsilyl ether (**53**)



TBS-Cl (0.901 g, 5.98 mmol) was added to a solution of **52** (1.00 g, 5.4 mmol) and imidazole (0.408 g, 5.99 mmol) in CH₂Cl₂ (25 mL) at room temperature. The reaction was stirred for 18 hr and then quenched with H₂O (40 mL) and extracted with CH₂Cl₂ (3 × 20 mL). The organic fractions were combined, washed with brine (30 mL), dried (Na₂SO₄), filtered and the solvent removed under reduced pressure. The residue was purified by column chromatography (10% EtOAc in hexanes) to afford **53** (R_f = 0.72) as a colourless oil (1.35 g, 83%). Spectroscopic data was consistent with that previously reported.^{129,130} IR (ν_{max}): 2955, 2929, 2857, 1486, 1257, 1087, 1012, 838, 797, 777 cm⁻¹; ¹H NMR (600 MHz, Chloroform-*d*) δ_H 7.45 (d, *J* = 8.1 Hz, 2H, ArH), 7.20 (d, *J* = 8.1 Hz, 2H, ArH), 4.68 (s, 2H, CH₂), 0.94 (s, 9H, (CH₃)₃), 0.10 (s, 6H, CH₃); ¹³C NMR (151 MHz, Chloroform-*d*) δ_C 140.60, 131.41, 127.85, 120.71, 64.47, 26.07, 18.54, -5.12.

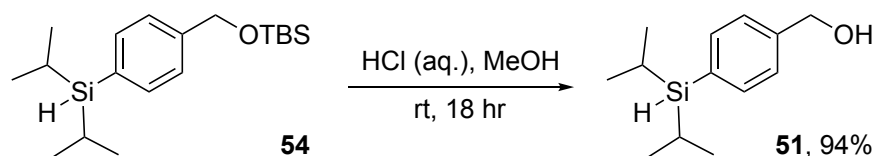
1-[(4-Diisopropylsilyl)benzyl]tert-butyldimethylsilyl ether (**54**)



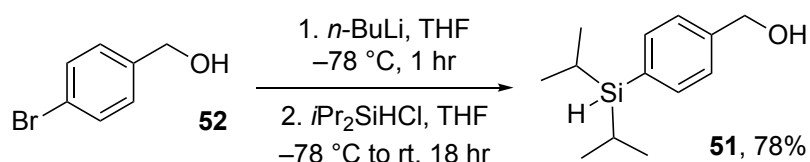
At -78 °C, *n*-BuLi (2.5 M in hexanes, 0.45 mL, 1.12 mmol) was added to a solution of **53** (0.168 g, 0.558 mmol) in THF (10 mL). After an hour, diisopropylchlorosilane (114 μL, 0.669 mmol) was added and the cooling bath removed to warm the reaction to room temperature. After 22 hr the reaction was quenched with a saturated aqueous solution of NaHCO₃ (5 mL) and the aqueous layer extracted with EtOAc (3 × 5 mL). The combined organic layers were washed with brine (20 mL) dried (Na₂SO₄), filtered and then solvent removed under reduced pressure. Purification by column chromatography (gradient elution; 0% to 2% EtOAc in hexanes) afforded **54** (R_f = 0.68, 2% EtOAc in hexanes) as a colourless oil (0.172 g, 91%). IR (ν_{max}): 3448, 2954, 2891, 2863, 2101, 1462, 1257, 1088, 838, 781 cm⁻¹; ¹H NMR (400 MHz, Chloroform-*d*) δ_H 7.48 (d, *J* = 7.9 Hz, 2H, ArH), 7.31 (d, *J* = 7.9 Hz, 2H, ArH), 4.75 (s, 2H, CH₂), 3.94 (t, *J* = 3.1 Hz, 1H, SiH), 1.22 (m, 2H, *i*PrH), 1.06 (d, *J* = 7.3 Hz, 6H, (*i*PrCH₃)), 0.99 (d, *J* = 7.3 Hz, 6H, (*i*PrCH₃)), 0.95 (s, 9H, CH₃), 0.11

(s, 6H, CH_3); ^{13}C NMR (101 MHz, Chloroform-*d*) δ_{C} 142.47, 135.58, 132.50, 125.45, 65.09, 26.13, 18.83, 18.63, 10.87, -5.10; HRMS (APCI) calculated for $[\text{C}_{19}\text{H}_{37}\text{Si}_2\text{O}]^+$ 337.2377; found 337.2371.

1-[(4-Diisopropylsilyl)benzyl]alcohol (**51**)



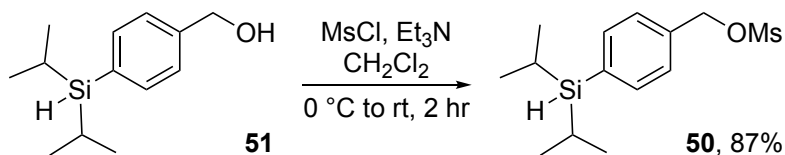
HCl (0.3 mL, 37%) was added to a solution of **54** (0.412 g, 1.22 mmol) in MeOH (10 mL). The reaction was stirred for 18 hr and then the solvent removed under reduced pressure. The resulting residue was diluted with EtOAc (30 mL), washed with saturated aqueous NaHCO_3 (30 mL), dried (Na_2SO_4) and filtered. The solvent was removed under reduced pressure to afford **51** as a white solid (0.256 g, 94%).



At -78 $^\circ\text{C}$, *n*-BuLi (2.5 M in hexanes, 16.1 mL, 40.2 mmol) was added to a solution of **52** (3.01 g, 16.1 mmol) in THF (50 mL). After 1 hour, a solution of diisopropylchlorosilane (3.43 mL, 20.1 mmol) in THF (20 mL) was added and the cold bath removed. The reaction left to warm to room temperature. After 17 hr total reaction time it was quenched with saturated aqueous NaHCO_3 (30 mL). The aqueous layer was extracted with EtOAc (3×40 mL) and the combined organic layers washed with brine (50 mL), dried (Na_2SO_4), filtered and the solvent removed under reduced pressure. The residue was purified by column chromatography (20% EtOAc in hexanes) to afford **51** ($R_f = 0.44$) as a white solid (2.808 g, 78%).

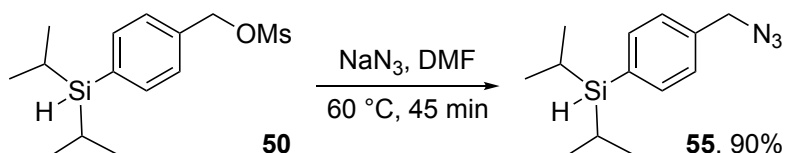
IR (ν_{max}): 3401, 2939, 2861, 2097, 1641, 1460, 999, 781 cm^{-1} ; ^1H NMR (600 MHz, Chloroform-*d*) δ_{H} 7.52 (d, $J = 7.9$ Hz, 2H, ArH), 7.35 (d, $J = 7.6$ Hz, 2H, ArH), 4.70 (s, 2H, CH_2), 3.94 (t, $J = 3.2$ Hz, 1H, SiH), 1.64 (br. s, 1H, OH), 1.23 (m, 2H, *i*PrH), 1.06 (d, $J = 7.4$ Hz, 6H, *i*Pr CH_3), 0.99 (d, $J = 7.4$ Hz, 6H, *i*Pr CH_3); ^{13}C NMR (151 MHz, Chloroform-*d*) δ_{C} 141.80, 135.92, 133.68, 126.38, 65.53, 18.79, 18.60, 10.83.

1-[(4-Diisopropylsilyl)benzyl]methanesulfonate (**50**)



At 0 °C methanesulfonyl chloride (1.95 mL, 25.2 mmol) was added dropwise to a solution of **51** (2.81 g, 12.6 mmol) and triethylamine (3.54 mL, 25.2 mmol) in CH₂Cl₂ (80 mL). The ice bath was removed, and the reaction allowed to warm to room temperature. After 2 hr the reaction was quenched with saturated aqueous NaHCO₃ (sat. 50 mL) and extracted with CH₂Cl₂ (3 × 40 mL). The organic fractions were combined, washed with brine (100 mL), dried (Na₂SO₄), filtered and the solvent removed under reduced pressure. The residue was purified by column chromatography (15% EtOAc in hexanes) to afford **50** (R_f = 0.31) as a clear oil that solidified upon cooling (3.341 g, 88%). Mp: 42 °C; IR (ν_{max}): 3027, 2954, 2937, 2864, 2103, 1460, 1347, 1331, 1177, 997, 813, 786, 667, 528 cm⁻¹; ¹H NMR (600 MHz, Chloroform-*d*) δ_H 7.56 (d, J = 7.9 Hz, 2H, ArH), 7.40 (d, J = 7.9 Hz, 2H, ArH), 5.24 (s, 2H, CH₂), 3.95 (t, J = 3.2 Hz, 1H, SiH), 2.92 (s, 3H, OCH₃), 1.24 (m, 2H, *i*PrH), 1.06 (d, J = 7.4 Hz, 6H, *i*PrCH₃), 0.98 (d, J = 7.4 Hz, 6H, *i*PrCH₃); ¹³C NMR (151 MHz, Chloroform-*d*) δ_C 136.21, 136.12, 134.17, 128.08, 71.58, 38.45, 18.74, 18.56, 10.75; HRMS (ESI) calculated for [C₁₄H₂₄O₃SSiNa]⁺ 323.1113; found 323.1128.

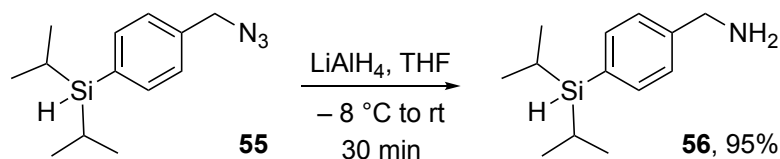
1-[(4-Diisopropylsilyl)benzyl]azide (**55**)



At 60 °C, sodium azide (0.407 g, 6.27 mmol) was added in small portions to a solution of **50** (0.942 g, 3.13 mmol) in DMF (25 mL) in a round bottom flask fitted with a reflux condenser. After the final addition of sodium azide, the reaction was stirred for 45 min before it was removed from the heat source and cool to room temperature. The reaction mixture was diluted with H₂O (50 mL) and extracted with EtOAc (3 × 20 mL). The organic fractions were combined, washed with brine (20 mL), dried (Na₂SO₄) and filtered. Removal of the solvent under reduced pressure at an elevated temperature yielded **55** as a yellow oil (0.698 g, 90%). IR (ν_{max}): 2942, 2891, 2864, 2100, 1730, 1462, 1397, 1249, 1106, 1101, 881, 783, 661 cm⁻¹; ¹H NMR (600 MHz, Chloroform-*d*) δ_H 7.53 (d, J = 8.0 Hz, 2H, ArH), 7.30 (d, J = 7.8 Hz, 2H, ArH), 4.35 (s, 2H, CH₂), 3.95 (t, J = 3.2 Hz,

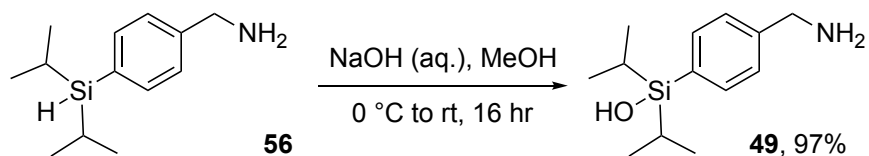
1H, SiH), 1.24 (m, 2H, *i*PrH), 1.07 (d, *J* = 7.4 Hz, 6H, *i*PrCH₃), 0.99 (d, *J* = 7.4 Hz, 6H, *i*PrCH₃); ¹³C NMR (151 MHz, Chloroform-*d*) δ_c 136.37, 136.09, 134.58, 127.48, 54.97, 18.77, 18.60, 10.81 ppm; HRMS (APCI) calculated for [C₁₃H₂₂NSi]⁺ 220.1522; found 220.1516. No molecular ion peak was observed for this compound. The major fragment observed was consistent with protonation and a loss of N₂ commonly seen with azide.¹²⁸

1-[(4-Diisopropylsilyl)benzyl]amine (**56**)



LiAlH₄ (0.925 g, 121.85 mmol) was added in portions to a solution of **55** (3.02 g, 12.2 mmol) in THF (80 mL) at -8 °C. After complete addition of the LiAlH₄ the reaction was left in the ice bath without any temperature control. The reaction was stirred for 30 min before being quenched with dropwise addition of H₂O (25 mL). Na₂SO₄ was added to help clear the emulsion before extraction with EtOAc (3 × 30 mL). The combined organic layers were washed with brine (50 mL), dried (Na₂SO₄) and filtered. Removal of the solvent under reduced pressure afforded **56** as a yellow oil (2.57 g, 95%). IR (ν_{max}) 2941, 2890, 2863, 2100, 1578, 1462, 1382, 1322, 1296, 1106, 1001, 881, 783, 660 cm⁻¹; ¹H NMR (600 MHz, Chloroform-*d*) δ_H 7.48 (d, *J* = 7.8 Hz, 2H, ArH), 7.30 (d, *J* = 7.6 Hz, 2H, ArH), 3.93 (t, *J* = 3.2 Hz, 1H, SiH), 3.87 (s, 2H, CH₂), 1.72 (br. s, 2H, NH₂), 1.22 (m, 2H, *i*PrH), 1.06 (d, *J* = 7.3 Hz, 6H, *i*PrCH₃), 0.98 (d, *J* = 7.4 Hz, 6H, *i*PrCH₃); ¹³C NMR (151 MHz, Chloroform-*d*) δ_c 144.04, 135.93, 132.54, 126.56, 46.57, 18.77, 18.62, 10.84; HRMS (ESI) calculated for [C₁₃H₂₄NSi]⁺ 222.1668; found 222.1678.

1-[(4-Diisopropylsilanol)benzyl]amine (**49**)

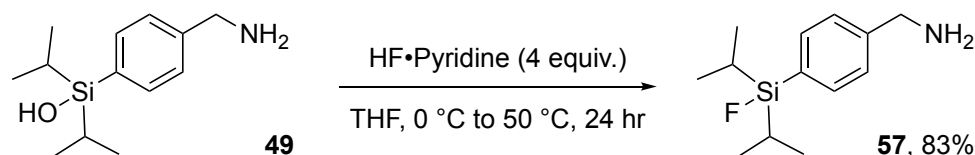


A 5M solution of NaOH (18.07 mL, 90.3 mmol) was added dropwise to a cooled, 0 °C solution of **56** (2.00 g, 9.03 mmol) in MeOH (40 mL). After complete addition of the NaOH solution the ice bath was removed, and the reaction left to come to room temperature. After stirring at room temperature for 16 hr, the methanol was removed under reduced pressure. The residue was

diluted with H₂O (10 mL) and extracted with EtOAc (3 × 30 mL). The organic phases were combined, washed with brine (40 mL), dried (Na₂SO₄), filtered and the solvent removed under reduced pressure to afford **49** as a white solid (2.08 g, 97%). Mp: 94 – 100 °C; IR (ν_{max}): 3360, 3296, 2940, 2890, 2863, 1601, 1462, 1105, 985, 885, 872, 673 cm⁻¹; ¹H NMR (600 MHz, Chloroform-*d*) δ_H 7.52 (d, *J* = 7.9 Hz, 2H, ArH), 7.30 (d, *J* = 7.6 Hz, 2H, ArH), 3.87 (s, 2H, CH₂), 1.80 (br. s, 4H), 1.22 (m, 2H, *i*PrH), 1.05 (d, *J* = 7.4 Hz, 6H, *i*PrCH₃), 0.97 (d, *J* = 7.5 Hz, 6H, *i*PrCH₃); ¹³C NMR (151 MHz, Chloroform-*d*) δ_C 144.28, 134.57, 133.99, 126.52, 46.58, 17.33, 17.08, 12.60; HRMS (ESI) calculated for [C₁₃H₂₄NSi]⁺ 238.1627; found 238.1627.

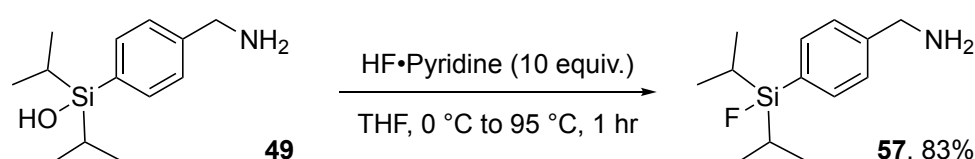
1-[(4-Diisopropylfluorosilyl)benzyl]amine (**57**)

Scheme 2.8, Entry 1



HF•Pyridine (~70% HF) (9.18 μL, 0.340 mmol) was added to a cooled, 0 °C solution of **49** (20.3 mg, 0.086 mmol) in THF (0.1 mL). After addition of the HF•Pyridine the ice bath was removed, and the reaction left to come to room temperature. The reaction then heated to 50 °C and stirred for 24 hr. At this point, the reaction was cooled to room temperature and H₂O (2 mL) was added. The reaction was quenched with NH₃ (28% aq. solution) until the reaction mixture reach a pH of 10. The organics were extracted with EtOAc (3 × 3 mL), washed with brine (5 mL), dried (Na₂SO₄), filtered and the solvent removed under reduced pressure to afford **57** (16.8 mg, 82%). ¹H NMR (600 MHz, Chloroform-*d*) δ_H 7.52 (d, *J* = 7.9 Hz, 2H, ArH), 7.35 (d, *J* = 7.6 Hz, 2H, ArH), 3.89 (s, 2H, CH₂), 1.65 (br. s, 2H, NH₂), 1.27 (m, 2H, *i*PrH), 1.08 (d, *J* = 7.5 Hz, 6H, *i*PrCH₃), 1.01 (d, *J* = 7.5 Hz, 6H, *i*PrCH₃); ¹³C NMR (151 MHz, Chloroform-*d*) δ_C 145.07, 134.30, 134.28, 131.24, 131.14, 126.70, 46.59, 16.83, 16.82, 16.67, 12.43, 12.35; ¹⁹F NMR (565 MHz, Chloroform-*d*) δ_F -187.06 (t, *J* = 6.0 Hz, SiF).

Scheme 2.8, Entry 2



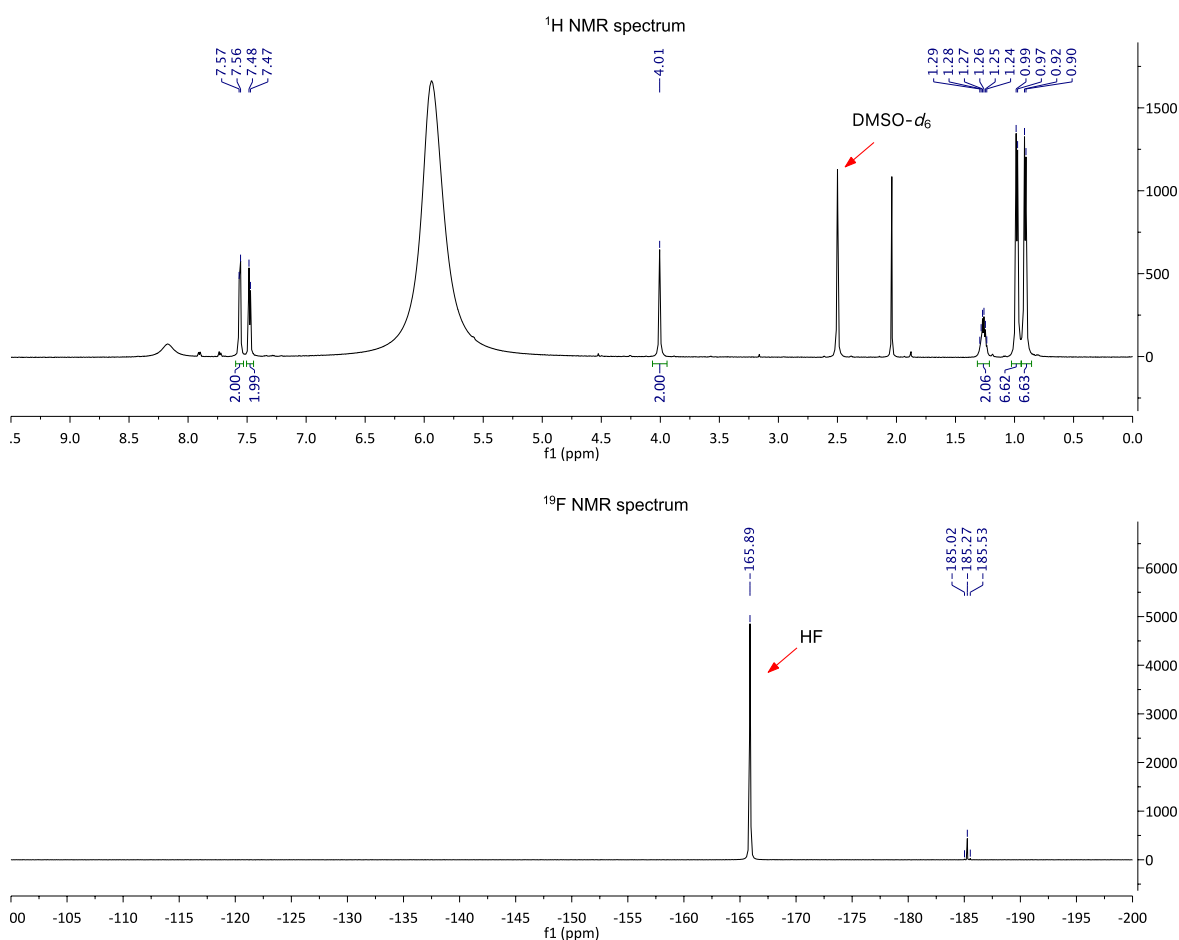
HF•Pyridine (~70% HF) (179 μ L, 4.93 mmol) was added to a cooled, 0 $^{\circ}$ C solution of **49** (117 mg, 0.493 mmol) in THF (2 mL). After addition of the HF•Pyridine the ice bath was removed, and the reaction left to come to room temperature. The reaction then heated to 95 $^{\circ}$ C and stirred for 1 hr before being cooled back to room temperature. H₂O (2 mL) was added and the reaction quenched with NH₃ (28% aq. solution) until the reaction mixture reach a pH of 10. The organics were extracted with EtOAc (3 \times 5 mL), washed with brine (10 mL), dried (Na₂SO₄), filtered and the solvent removed under reduced pressure to afford **57** (98.2 mg, 83%). Spectroscopic data was consistent with that reported for **57** above.

2.8.3 Direct aqueous fluorination of 1-[(4-diisopropylsilanol)benzyl]amine (**57**)

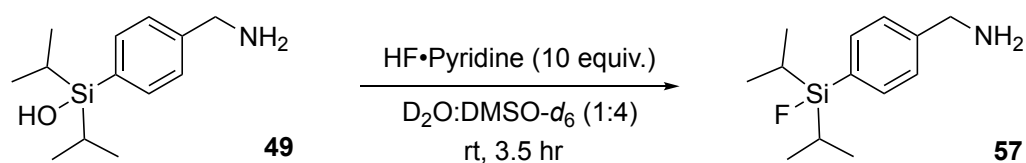
NMR data of **57** in DMSO-*d*₆:D₂O used for comparisons in Scheme 2.9

¹H NMR (600 MHz, DMSO-*d*₆) δ _H 7.56 (d, *J* = 7.4 Hz, 2H, ArH), 7.48 (d, *J* = 7.4 Hz, 2H, ArH), 4.01 (s, 2H, CH₂), 1.27 (m, 2H, *i*PrH), 0.98 (d, *J* = 7.4 Hz, 6H, *i*PrCH₃), 0.91 (d, *J* = 7.5 Hz, 6H, *i*PrCH₃);

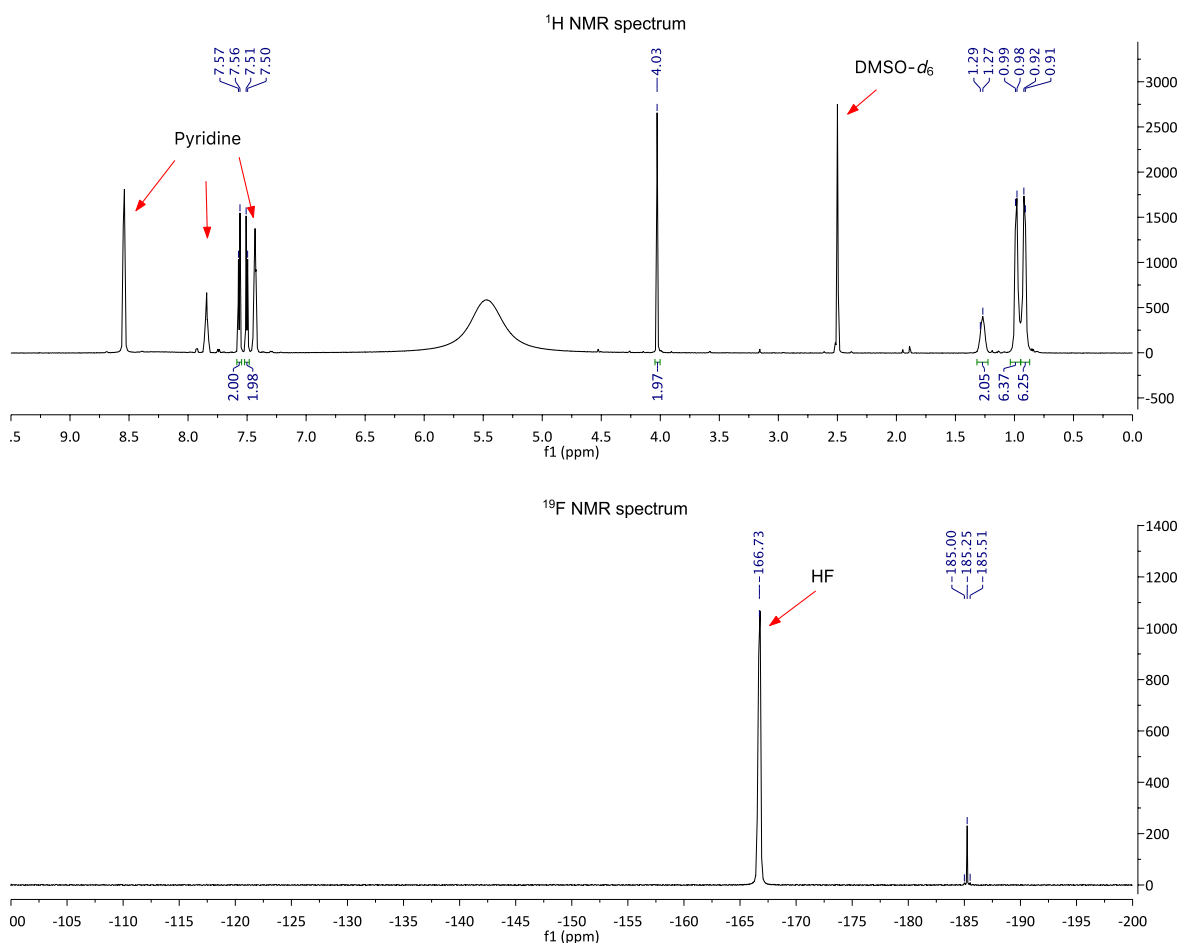
¹⁹F NMR (565 MHz, DMSO-*d*₆) δ _F -185.3.



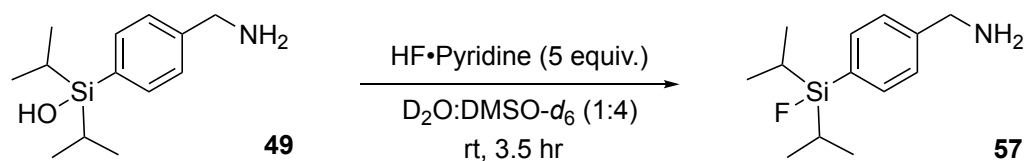
Scheme 2.9, Entry 1



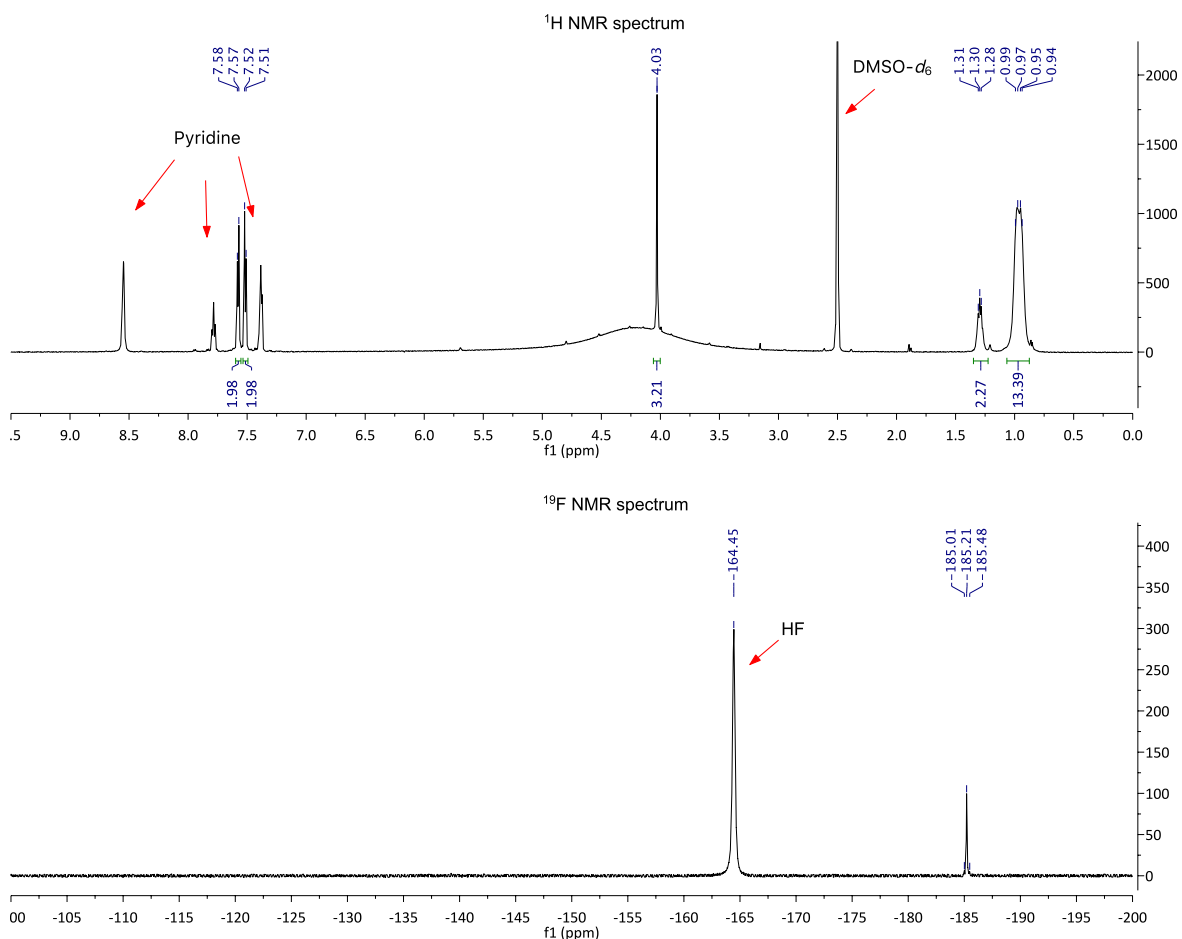
HF•Pyridine (~70% HF) (16.6 μL , 0.438 mmol) was added to a solution of **49** (10.4 mg, 0.0438 mmol) in DMSO- d_6 (100 μL) and D₂O (20 μL) in a 0.5 mL microcentrifuge Eppendorf tube. After the addition of HF•Pyridine the reaction was placed on a rotisserie (60 RPM) and allowed to react for 3.5 hr. After this time the solution was transferred to FEP liner NMR tube and analysed by NMR spectroscopy. A signal at δ_{F} -185.25 ppm, consistent with a Si-F bond, in the ¹⁹F NMR spectrum supported that fluorination had occurred. The ¹H NMR spectrum revealed 100% conversion to **57**.



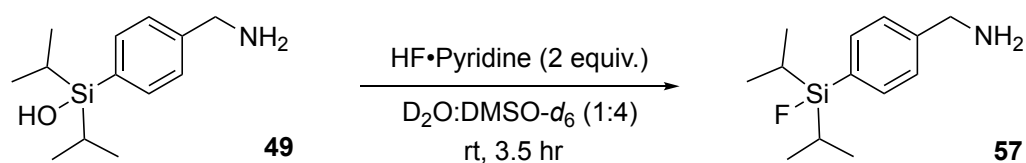
Scheme 2.9, Entry 2



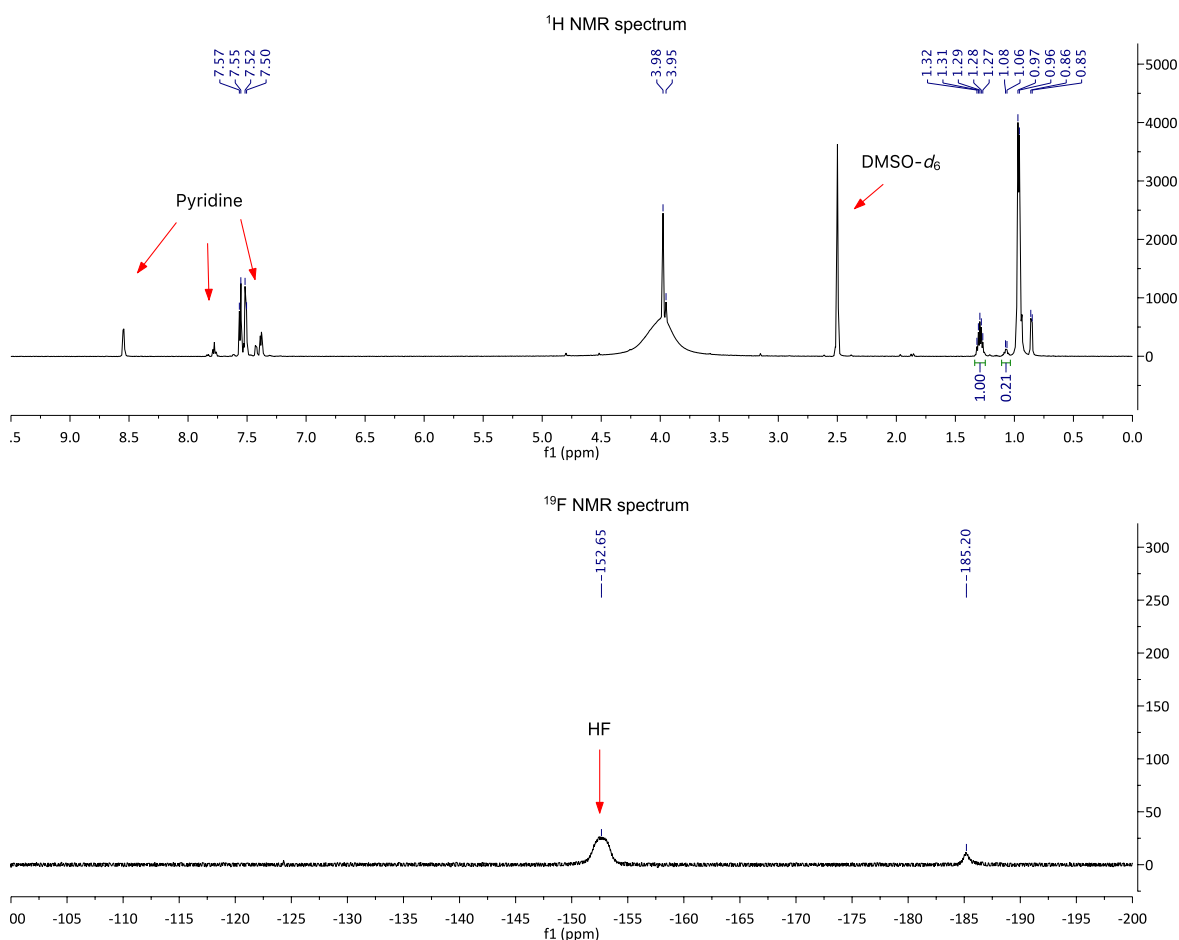
$\text{HF}\cdot\text{Pyridine}$ (~70% HF) (8.86 μL , 0.234 mmol) was added to a solution of **49** (11.1 mg, 0.0467 mmol) in $\text{DMSO-}d_6$ (100 μL) and D_2O (20 μL) in a 0.5 mL microcentrifuge Eppendorf tube. After the addition of $\text{HF}\cdot\text{Pyridine}$ the reaction was placed on a rotisserie (60 RPM) and allowed to react for 3.5 hr. After this time the solution was transferred to FEP liner NMR tube and analysed by NMR spectroscopy. A signal at δ_{F} -185.21 ppm, consistent with a Si-F bond, in the ^{19}F NMR spectrum supported that fluorination had occurred. The ^1H NMR spectrum revealed 100% conversion to **57**.



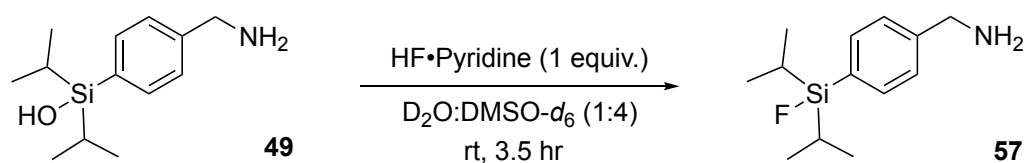
Scheme 2.9, Entry 3



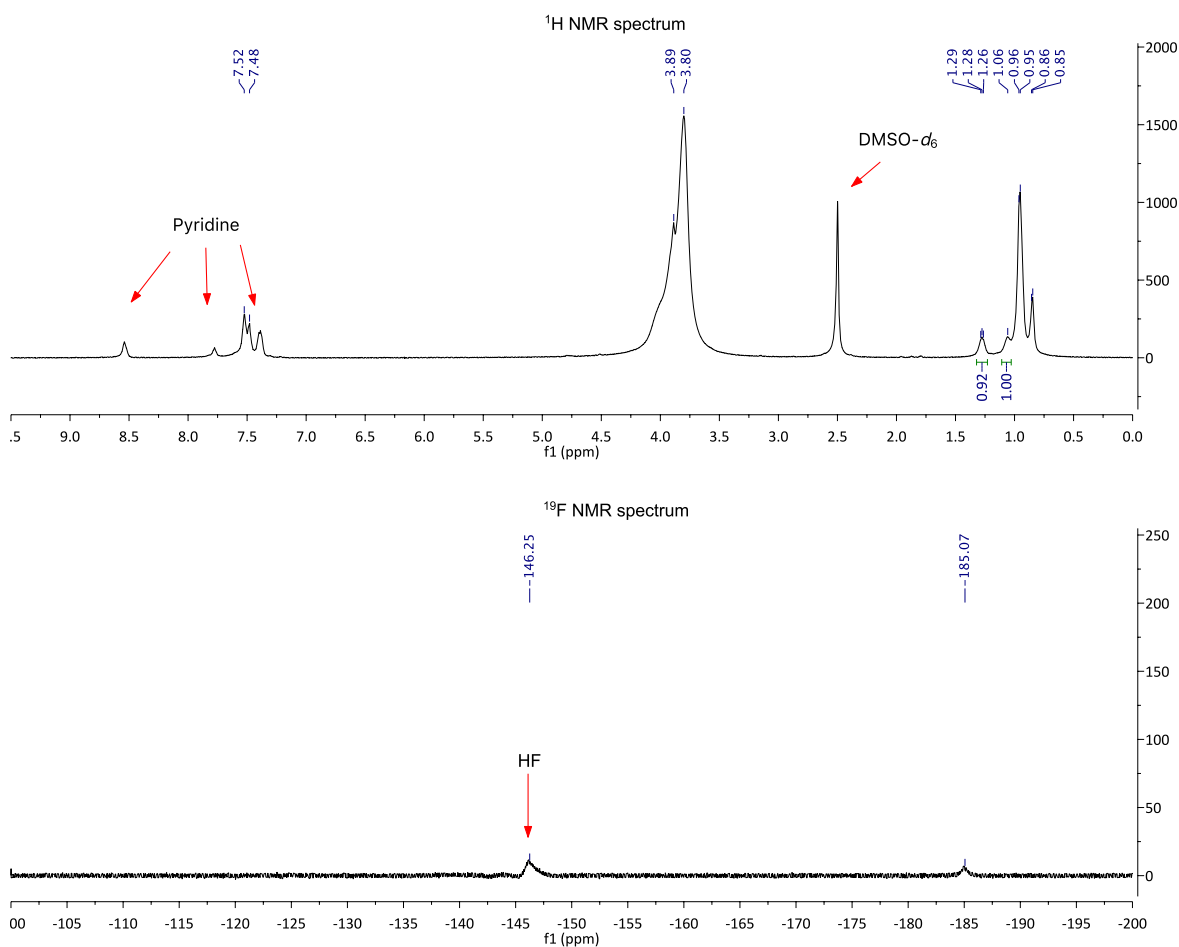
HF•Pyridine (~70% HF) (3.64 μL , 0.096 mmol) was added to a solution of **49** (11.4 mg, 0.048 mmol) in DMSO- d_6 (100 μL) and D₂O (20 μL) in a 0.5 mL microcentrifuge Eppendorf tube. After the addition of HF•Pyridine the reaction was placed on a rotisserie (60 RPM) and allowed to react for 3.5 hr. After this time the solution was transferred to FEP liner NMR tube and analysed by NMR spectroscopy. A signal at δ_{F} -185.20 ppm, consistent with a Si-F bond, in the ¹⁹F NMR spectrum supported that fluorination had occurred. Integration of the isopropyl signals in the ¹H NMR spectrum (δ_{H} 01.29 ppm for **57** and δ_{H} 1.07 ppm for **49**) revealed a 1:0.2 mixture and 83% conversion to **57**.



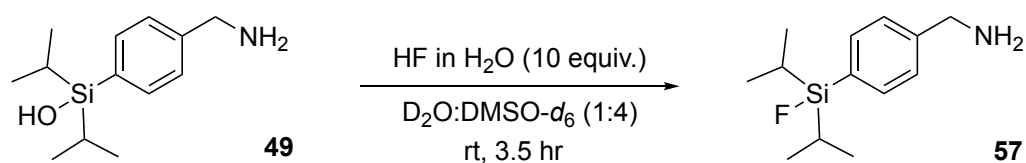
Scheme 2.9, Entry 4



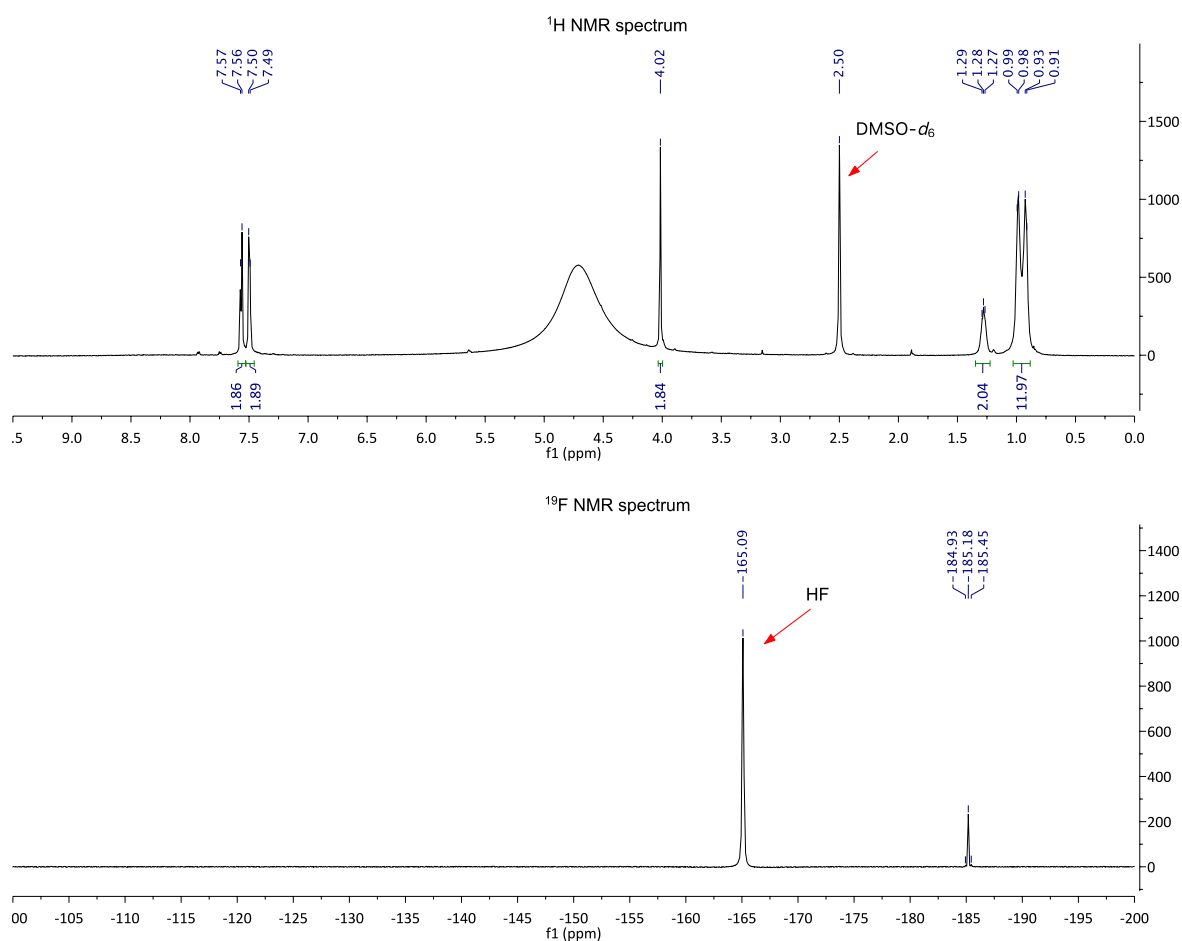
HF•Pyridine (~70% HF) (1.66 μL , 0.0438 mmol) was added to a solution of **49** (10.4 mg, 0.0438 mmol) in DMSO- d_6 (100 μL) and D₂O (20 μL) in a 0.5 mL microcentrifuge Eppendorf tube. After the addition of HF•Pyridine the reaction was placed on a rotisserie (60 RPM) and allowed to react for 3.5 hr. After this time the solution was transferred to FEP liner NMR tube and analysed by NMR spectroscopy. A signal at δ_{F} -185.07 ppm, consistent with a Si-F bond, in the ¹⁹F NMR spectrum supported that fluorination had occurred. Integration of the isopropyl signals in the ¹H NMR spectrum (δ_{H} 0.128 ppm for **57** and δ_{H} 1.06 ppm for **49**) revealed a 0.9:1 mixture and 48% conversion to **57**.



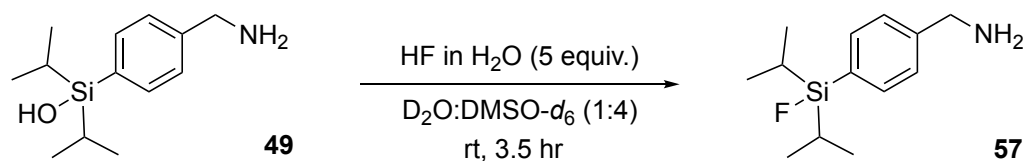
Scheme 2.9, Entry 5



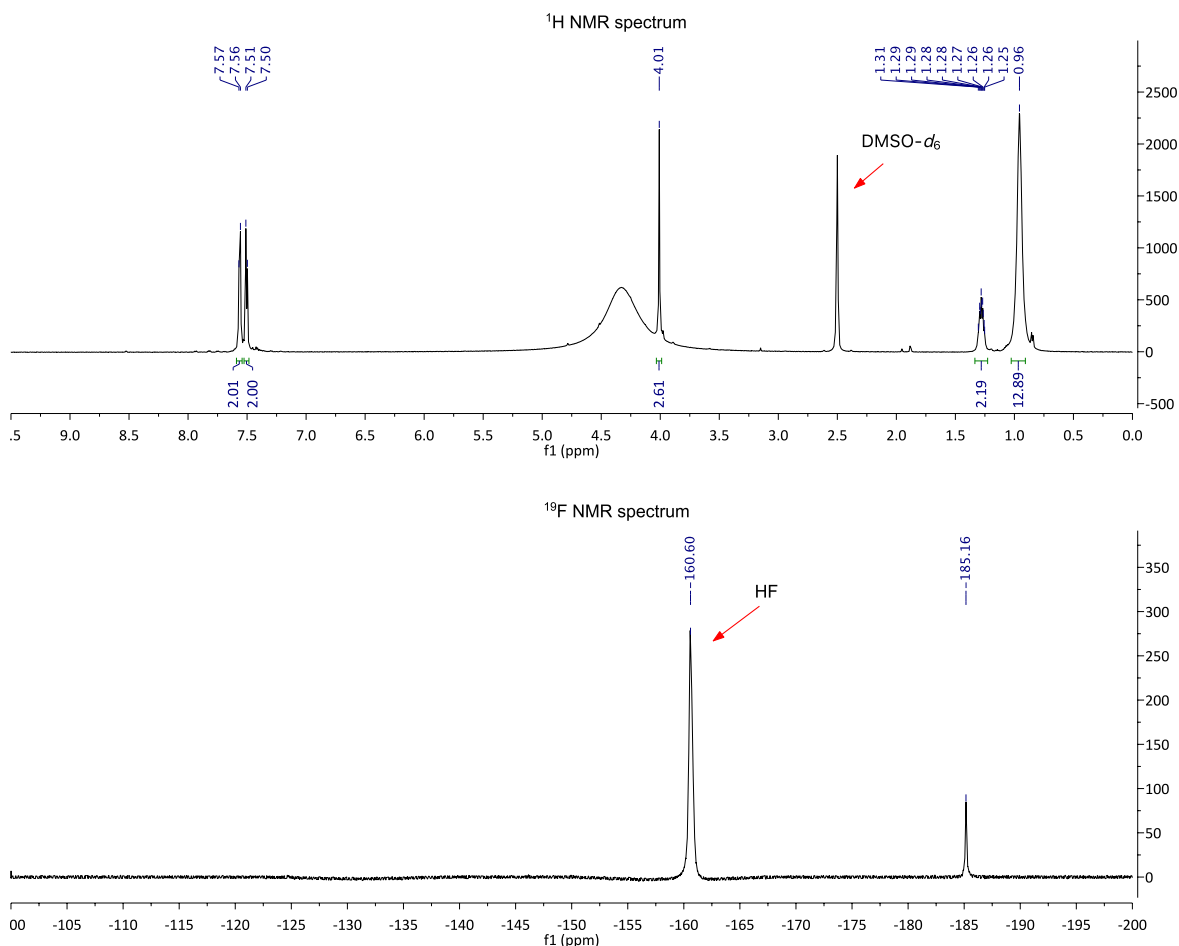
HF in H₂O (~48% HF) (15.88 μ L, 0.438 mmol) was added to a solution of **49** (10.4 mg, 0.0438 mmol) in DMSO-*d*₆ (100 μ L) and D₂O (20 μ L) in a 0.5 mL microcentrifuge Eppendorf tube. After the addition of HF•Pyridine the reaction was placed on a rotisserie (60 RPM) and allowed to react for 3.5 hr. After this time the solution was transferred to FEP liner NMR tube and analysed by NMR spectroscopy. A signal at δ_F -185.18 ppm, consistent with a Si-F bond, in the ¹⁹F NMR spectrum supported that fluorination had occurred. The ¹H NMR spectrum revealed 100% conversion to **57**.



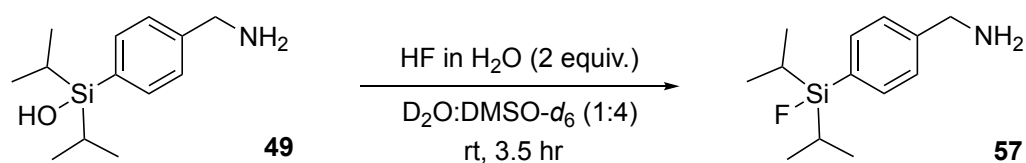
Scheme 2.9, Entry 6



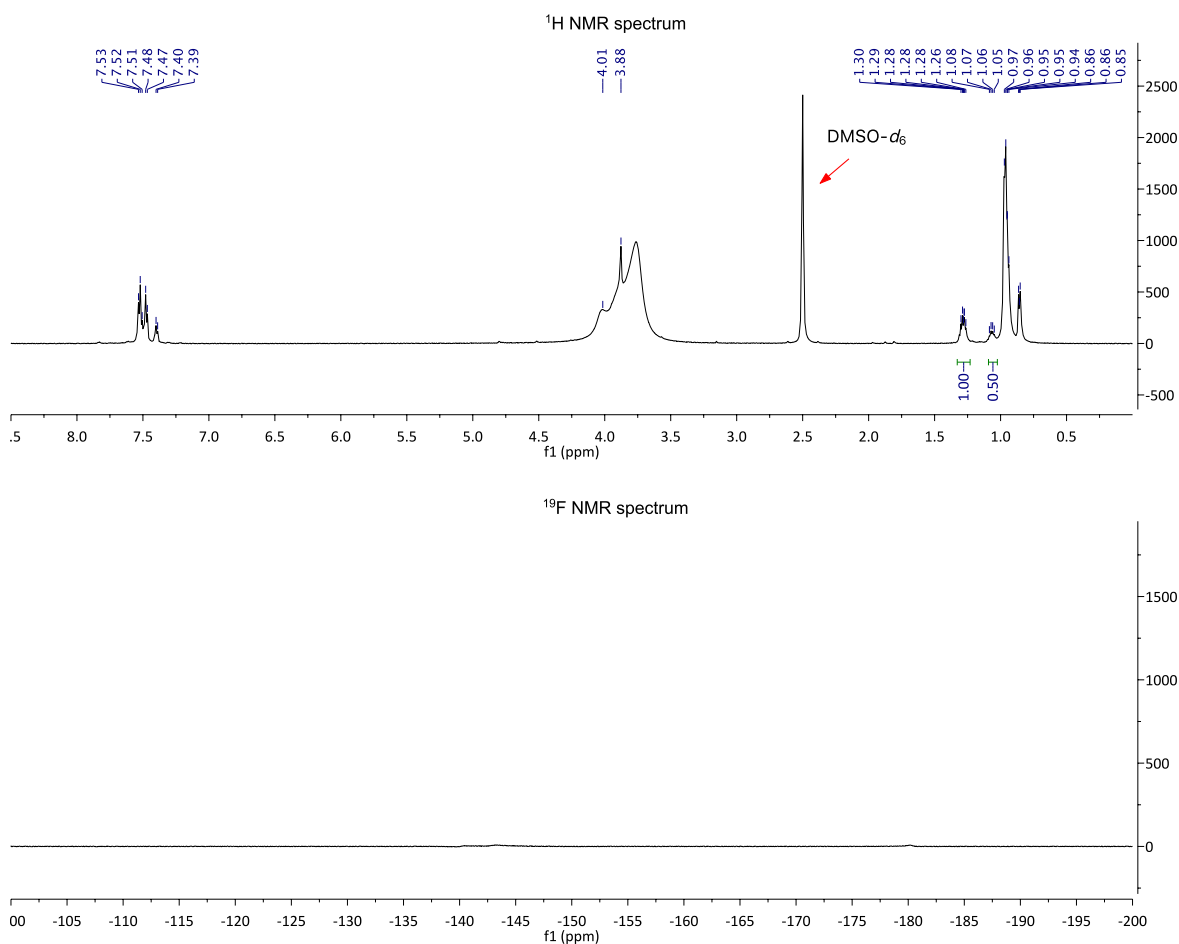
HF in H₂O (~48% HF) (7.79 μ L, 0.215 mmol) was added to a solution of **49** (10.2 mg, 0.043 mmol) in DMSO-*d*₆ (100 μ L) and D₂O (20 μ L) in a 0.5 mL microcentrifuge Eppendorf tube. After the addition of HF•Pyridine the reaction was placed on a rotisserie (60 RPM) and allowed to react for 3.5 hr. After this time the solution was transferred to FEP liner NMR tube and analysed by NMR spectroscopy. A signal at δ_F -185.16 ppm, consistent with a Si-F bond, in the ¹⁹F NMR spectrum supported that fluorination had occurred. The ¹H NMR spectrum revealed 100% conversion to **57**.



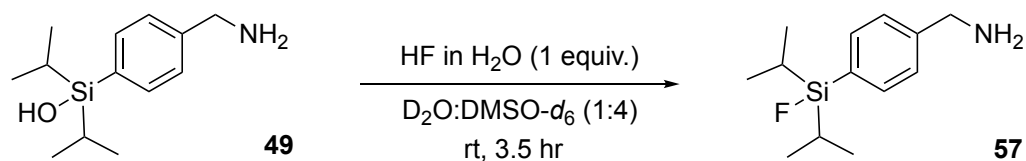
Scheme 2.9, Entry 7



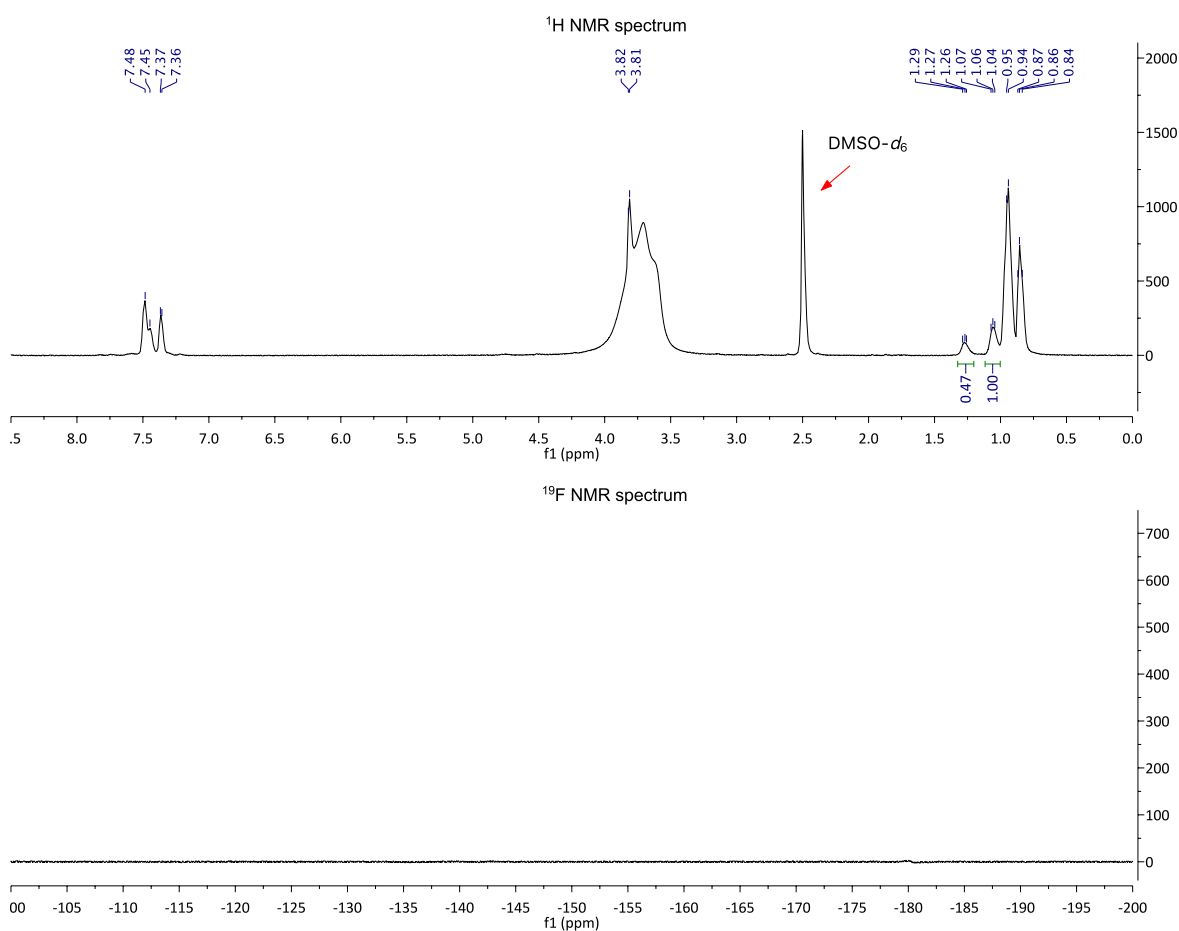
HF in H₂O (~48% HF) (2.90 μL, 0.08 mmol) was added to a solution of **49** (9.5 mg, 0.04 mmol) in DMSO-*d*₆ (100 μL) and D₂O (20 μL) in a 0.5 mL microcentrifuge Eppendorf tube. After the addition of HF•Pyridine the reaction was placed on a rotisserie (60 RPM) and allowed to react for 3.5 hr. After this time the solution was transferred to FEP liner NMR tube and analysed by NMR spectroscopy. No signals were observed in the ¹⁹F NMR spectra for the hydrogen fluoride or the product. Integration of the isopropyl signals in the ¹H NMR spectrum (δ_H 0.128 ppm for **57** and δ_H 1.06 ppm for **49**) revealed a 1:0.5 mixture and 48% conversion to **57**.



Scheme 2.9, Entry 8



HF in H₂O (~48% HF) (1.54 μL, 0.0425 mmol) was added to a solution of **49** (10.1 mg, 0.0425 mmol) in DMSO-*d*₆ (100 μL) and D₂O (20 μL) in a 0.5 mL microcentrifuge Eppendorf tube. After the addition of HF•Pyridine the reaction was placed on a rotisserie (60 RPM) and allowed to react for 3.5 hr. After this time the solution was transferred to FEP liner NMR tube and analysed by NMR spectroscopy. No signals were observed in the ¹⁹F NMR spectra for the hydrogen fluoride or the product. Integration of the isopropyl signals in the ¹H NMR spectrum (δ_{H} 0.128 ppm for **57** and δ_{H} 1.06 ppm for **49**) revealed a 0.5:1 mixture and 32% conversion to **57**.



Chapter Three

Chemical incorporation of silicon into proteins and their direct aqueous fluorination

3.1 Introduction

A novel silanol specifically designed for the incorporation of silicon into proteins via chemical modification was introduced in Chapter 2. Readily fluorinated in the presence of water and at room temperature, in sharp contrast to the dry conditions and/or high temperatures normally employed, it proved to be a viable candidate for the direct fluorination of proteins. This encouraged us to move our research forward and focus our efforts on the chemical modification of proteins with the novel silanol and the direct aqueous fluorination of these proteins at the newly incorporated silicon.

For protein radiotracers with a specific *in vivo* target, being able to site-selectively modify the protein can be essential to maintaining its affinity for its target. Chapter 3 details our attempts, the successful and the unsuccessful, to site-selectively incorporate silicon into proteins. Chemical modifications at both cysteine and lysine will be presented and discussed. This chapter concludes with reports on the direct aqueous fluorination of the chemically modified proteins.

The data and conclusions presented here in this Chapter had not been prepared for publication in any scientific journal nor had been reported elsewhere at the date of thesis submission. The data presented in this chapter on the chemical modification of lysozyme, ubiquitin(K63C), C2Am(S78C) and annexin V was collected by the candidate during research visits at The Department of Chemistry, University of Cambridge, England. The candidate planned, researched, conducted and prepared the following Chapter with full intellectual and practical contributions unless otherwise state in-text.

3.2 Incorporating silicon into proteins at cysteine

Of the natural residues, cysteine is the most convenient for the site-selective modification of proteins. Cysteine is found in a low abundance, constituting approximately only 2% of all residues present in proteins.^{131,132} This infrequency and the capability of installing cysteine at a chosen site via site-directed mutagenesis means that it is relatively easy to engineer single cysteine mutant proteins. Cysteine is also a potent nucleophile that reacts readily with a wide range of electrophiles.

Maleimides are by far the most popular electrophiles used to modify cysteine. The maleimide-thiol chemistry is particularly well suited to protein conjugation. The thioether bond formed upon reaction of the thiol with the maleimide forms in aqueous solvents, at ambient temperature and requires no additional reagents. In the literature, Michael addition with a maleimide is the only method that has been used to incorporate silicon into proteins at cysteine for either indirect or direct radiolabelling.^{64,67} However, maleimides are known to undergo retro-Michael reactions with exogenous free thiols and disulfides,¹³³ a detrimental property for their use in the synthesis of imaging agents for PET. While various efforts have been made to prevent retro-Michael reaction of maleimides,¹³⁴ we have chosen to avoid this issue entirely and explore the use of alternative methods to incorporate the silicon site-selectively at cysteine.

Proteins can be modified at cysteine using a diverse range of chemistries. In addition to maleimides, cysteine has been modified via Michael additions with other Michael acceptors, substitution reactions with α -halocarbonyls, oxidation with thiols to form disulfides and irradiation with UV to generate radicals that partake in thiol-ene and thiol-yne reactions.¹³⁵⁻¹³⁷ It has also been modified using a two-step process by which it is first converted to dehydroalanine. This method

generates a unique electrophilic site on the protein that can then be used in further modifications.¹²² In the sections that follow we report the use of a selection of those methods mentioned above to site-selectively incorporate silicon into ubiquitin, C2Am, annexin V and bovine serum albumin (BSA).

3.2.1 Ubiquitin(K63C)

Ubiquitin is a regulatory protein, named after its omnipresence in eukaryotic cells. A complex code, the post-translational modification of proteins with ubiquitin, known as ubiquitylation, is used to communicate the protein's fate within cells.^{138,139} While the native ubiquitin does not contain a cysteine residue, a single cysteine mutant, ubiquitin(K63C), had previously been engineered¹⁴⁰ that we could use to site-selectively incorporate the silanol **49**. As discussed in Chapter 2, we intended to modify ubiquitin by converting the cysteine to dehydroalanine installing a unique electrophilic site that has previously been shown to be reactive towards benzyl amines.¹²⁴

To convert cysteine to dehydroalanine in preparation for the chemical modification of ubiquitin with **49**, ubiquitin(K63C) was treated with 150 equivalents of α,α' -di-bromo-adipyl(bis)amide. The modification of cysteine to dehydroalanine on proteins can be achieved via a number of methods. We chose to use the bis-alkylation elimination method with α,α' -di-bromo-adipyl(bis)amide (**58**) as it is efficient at pH 8.0 with limited side reactions and thus is highly compatible with proteins.¹²² After 4 hours the reaction was analysed by LC-MS. Elimination was observed, though some of the monoalkylated ubiquitin still remained. An additional 12 hours was required to get full conversion to the eliminated dehydroalanine product **59** (Figure 3.1). The extended time required indicates that the rate determining step is cyclisation and subsequent elimination to dehydroalanine. That is consistent with previous studies.¹²²

With dehydroalanine installed we next explored the conjugation of **49** to the protein. First **59** was reacted with 100 equivalents of **49** at 37 °C at pH 8.0. After 24 hours there was no evidence of conjugation and only the starting material was observed in the deconvoluted mass spectrum. In an attempt to drive the conjugation, we repeated the reaction using 300, 500 and 1000 equivalents of **49** (Figure 3.2). Using greater than 1000 equivalents resulted in precipitation, presumably due to the low solubility of **49** in water. Unfortunately, all of these reactions failed to

yield any of the desired ubiquitin adduct. Not having observed any conjugation could be due to one of two factors.

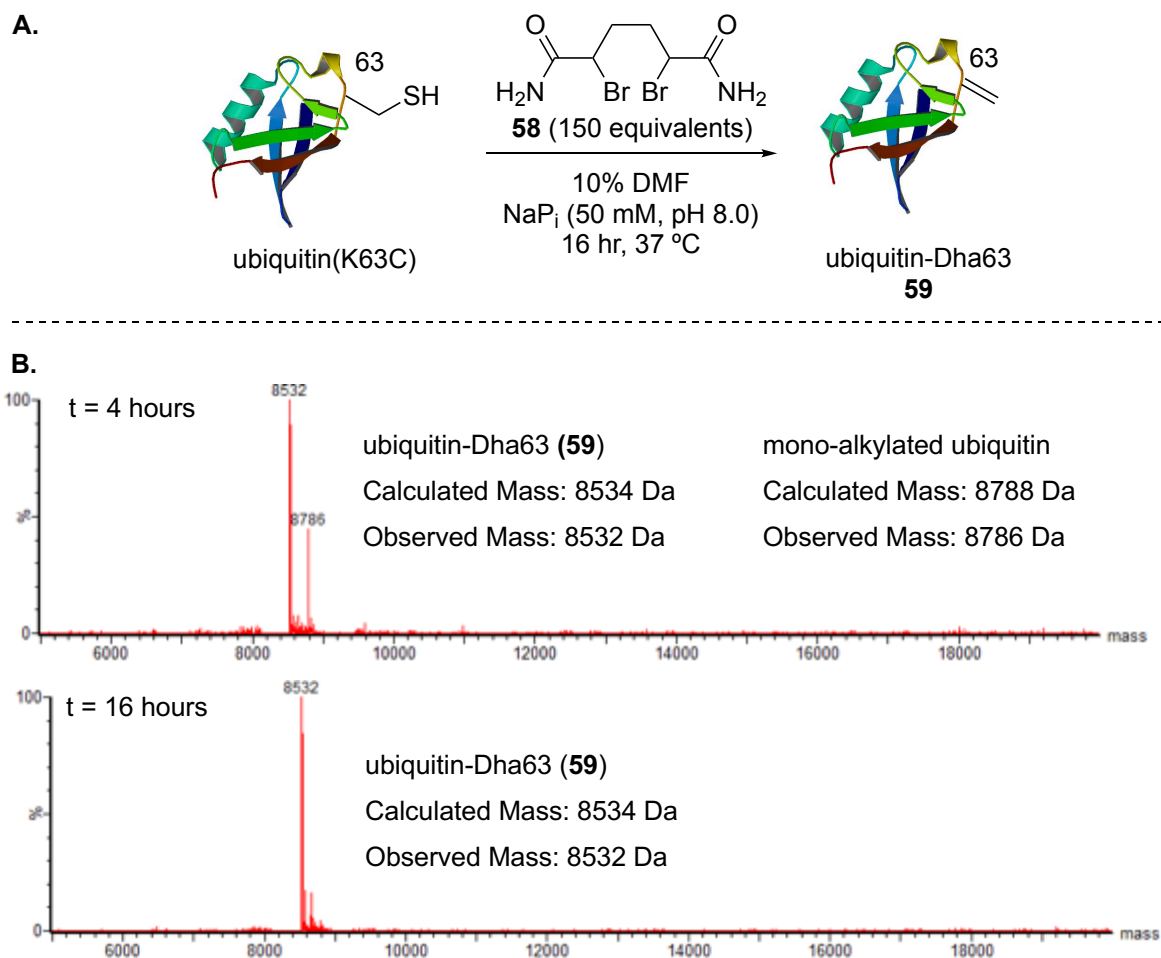


Figure 3.1 **A)** Conversion of the single cysteine in ubiquitin(K63C) to dehydroalanine. **B)** Mono-alkylated ubiquitin(K63C) still remains in the deconvoluted mass spectrum after 4 hours at 37 °C (top). Full conversion to dehydroalanine is observed in the deconvoluted mass spectrum after 16 hours at 37 °C (bottom).

Firstly, it could be that the conjugate partner is not reactive under these conditions. The most reasonable explanation for this being that at pH 8.0 the majority of **49** is in its protonated form and thus unreactive. Increasing the pH would therefore increase the amount of reactive amine in solution and increase the likelihood of conjugation. However, it would also be pushing towards the boundaries of pH that most proteins can tolerate. It seems unlikely that the amine would not be reactive at pH 8.0 however, as wide range of benzylamines that have been conjugated to dehydroalanine at pH 8.0.¹²⁴

Secondly, it could be that the site of modification is not accessible. The native ubiquitin

however, which has a lysine residue at position 63 rather than a cysteine residue, is regularly modified at this position with additional ubiquitin units creating K63 linked chains.¹³⁹ Thus it should be accessible, even to quite large molecules. We had also previously been able to access this site when the cysteine was converted to dehydroalanine as have others who have modified the cysteine of ubiquitin(K63C).¹⁴¹ Alternatively, the polarity of neighbouring residues may create a microenvironment that limits the accessibility to hydrophilic compounds, explaining why no conjugation was observed with the lipophilic **49**.

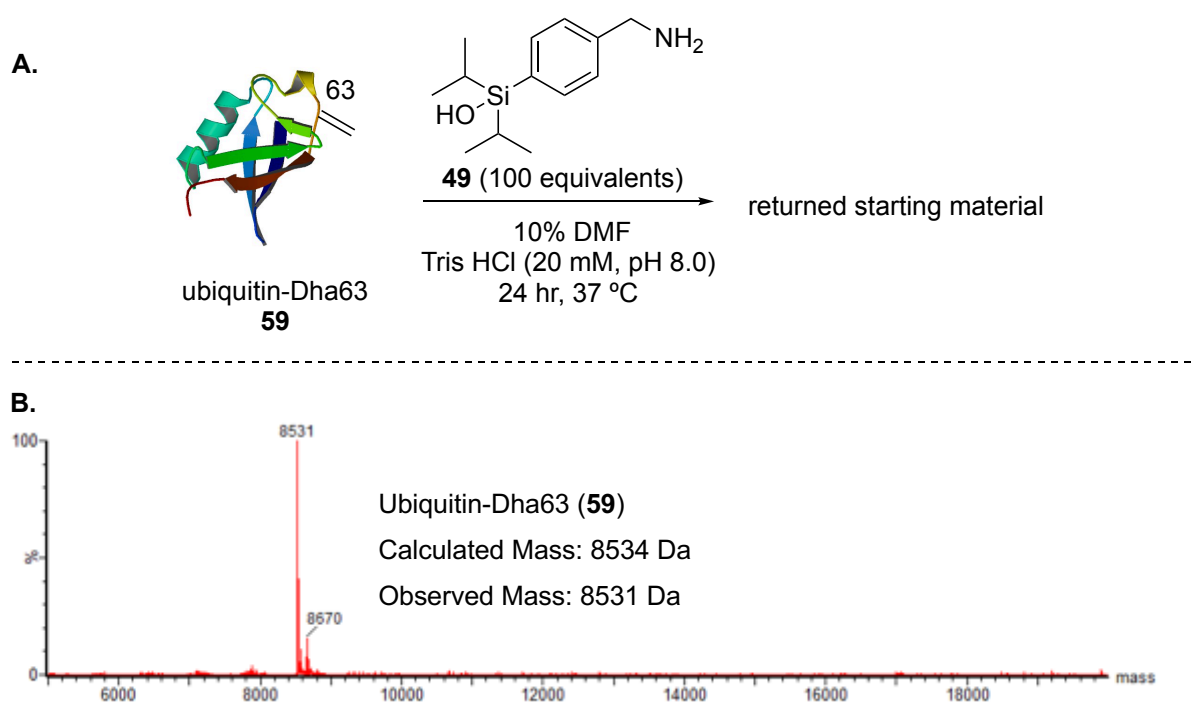


Figure 3.2 A) Attempts to conjugate **49** (100 equivalents) to **59** at pH 8.0 and 37 °C for 24 hours returned starting material when 100, 300, 500 and 1000 equivalents of **49** was used. **B)** The deconvoluted mass spectrum after 24 hours at 37 °C reveals no conversion. The same results were found with 300, 500 and 1000 equivalents of **49** were used (see Section 3.6.4).

In search of model protein to test the fluorination on, we moved on to another protein, C2Am(S78C). The single cysteine of C2Am(S78C) has previously been converted to dehydroalanine and subsequently shown to react with benzylamines at pH 8.0.¹²⁴

3.2.2 C2Am(S78C)

The C2A domain of Synaptotagmin I binds, dependant on Ca²⁺, to phosphatidylserine, a phospholipid that is externalised during apoptosis.¹⁴² To compare the ability of C2Am to

accurately image cell death with the golden standard, annexin V, Alam *et al.* developed a mutant of C2Am, C2Am(S78C). A cysteine free protein, this mutant was engineered to incorporate a single cysteine at position 78 to aid in site-selective conjugations.¹⁴³

As with ubiquitin(K63C), the cysteine of C2Am(S78C) was converted to dehydroalanine via the bis-alkylation elimination method with α,α' -di-bromo-adipyl(bis)amide. C2Am(S78C) commonly exists as a dimer, formed through an intermolecular disulfide bridge between two domains. Thus, the protein was first treated with TCEP to reduce the disulfide bridge and reform the free thiols (see Section 3.6). C2Am(S78C) was then reacted with 150 equivalents of **58** with complete conversion to dehydroalanine observed via LC-MS after 4 hours at 37 °C (Figure 3.3).

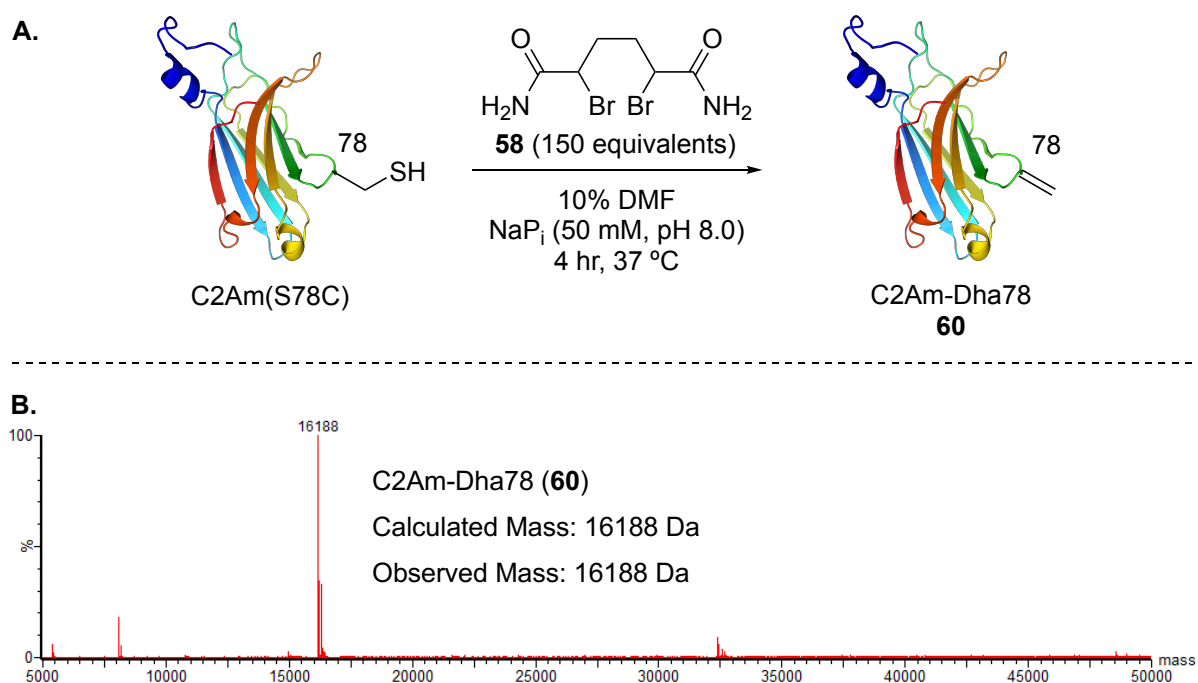


Figure 3.3 **A)** Conversion of the single cysteine in C2Am(S78C) to dehydroalanine. **B)** Full conversion to dehydroalanine is observed in the deconvoluted mass spectrum after 4 hours at 37 °C.

With dehydroalanine installed, the protein was next reacted with 1000 equivalents of **49** under identical conditions that we used for ubiquitin(K63C). Gratifyingly, full conversion was observed by LC-MS after 24 hours at 37 °C and pH 8.0 (Figure 3.4). At lower pH, the amine was found to be unreactive with no conjugation observed even after 24 hours at 37 °C (see Section 3.6.5). Juxtaposed to the unsuccessful conjugation of **49** to ubiquitin(K63C) this result indicated that at pH 8.0 **49** does react with dehydroalanine. We therefore concluded that **49** could not be

conjugated to ubiquitin(K63C) due to limited access to the site of intended modification. Whether it is due to the polarity of the neighbouring residues as previously mentioned, or some other property of the protein was not determined. No matter the cause, this method allowed for the successful incorporation of silicon into C2Am(S78C) and we continued to trial this method on other proteins.

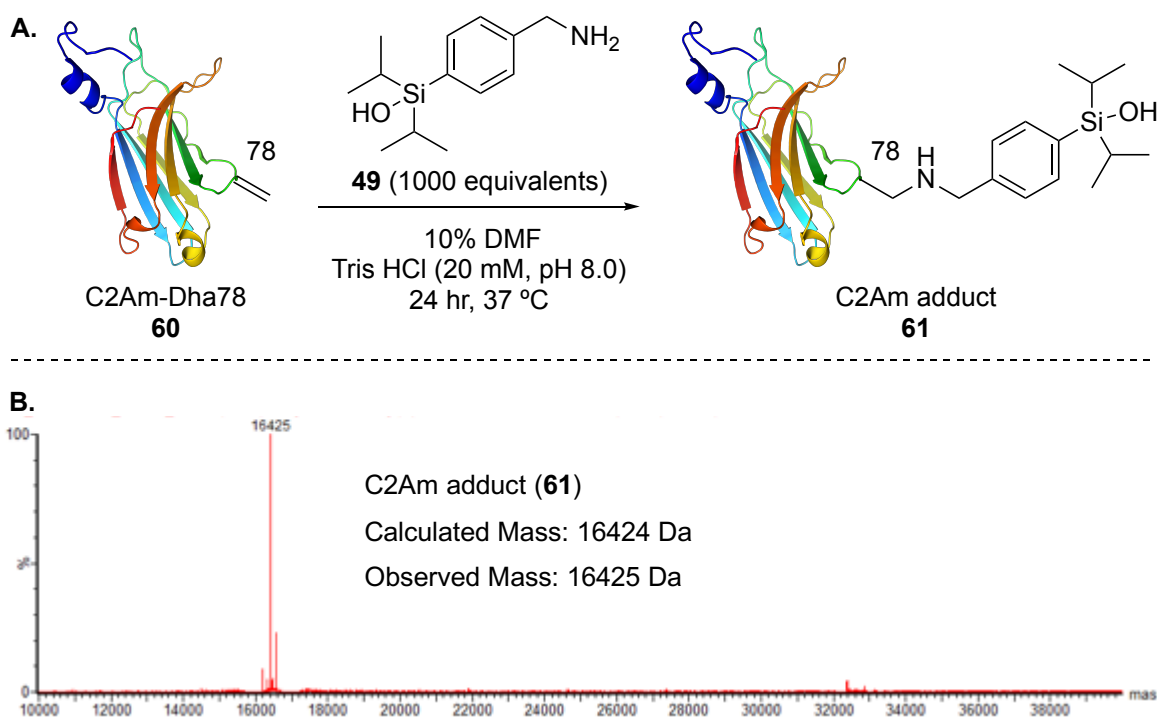


Figure 3.4 A) Conjugation of **49** to **60**. **B)** Full conversion to the C2Am adduct **61** is observed in the deconvoluted mass spectrum after 24 hours at 37 °C.

3.2.3 Annexin V

Annexin V is a phosphatidylserine binding protein and the gold standard for the detection of apoptotic cells. Similar to C2Am in the way it binds to phosphatidylserine, it is also similar in that it only contains a single cysteine residue. Annexin V has previously been site-selectively modified at the cysteine residue^{55,144} and therefore, was a promising candidate for our newly developed method to site-selectively incorporate silicon.

Using the same method to convert cysteine to dehydroalanine as we did for ubiquitin(K63C) and C2Am(S78C), annexin V was reacted with 150 equivalents of **58**. After 5 hours at 37 °C however, the deconvoluted mass spectrum revealed only starting material (Figure 3.5). Upon leaving the

reaction for a total of 24 hours, no protein was detected during LC-MS analysis, presumably a result of protein degradation and/or precipitation.

While it may be possible to optimise this reaction and convert the cysteine of annexin V to dehydroalanine, it was clear that annexin V was not stable at 37 °C over extended periods of time. Looking comparatively at the conjugation of **49** to dehydroalanine on C2Am(S78C), it took 24 hours to reach full conversion, over which time, annexin V would have conceivably degrade. Therefore, if the silanol was to be incorporated into annexin V via chemical modification, either a much faster method or one that could be conducted at lower temperatures would be needed.

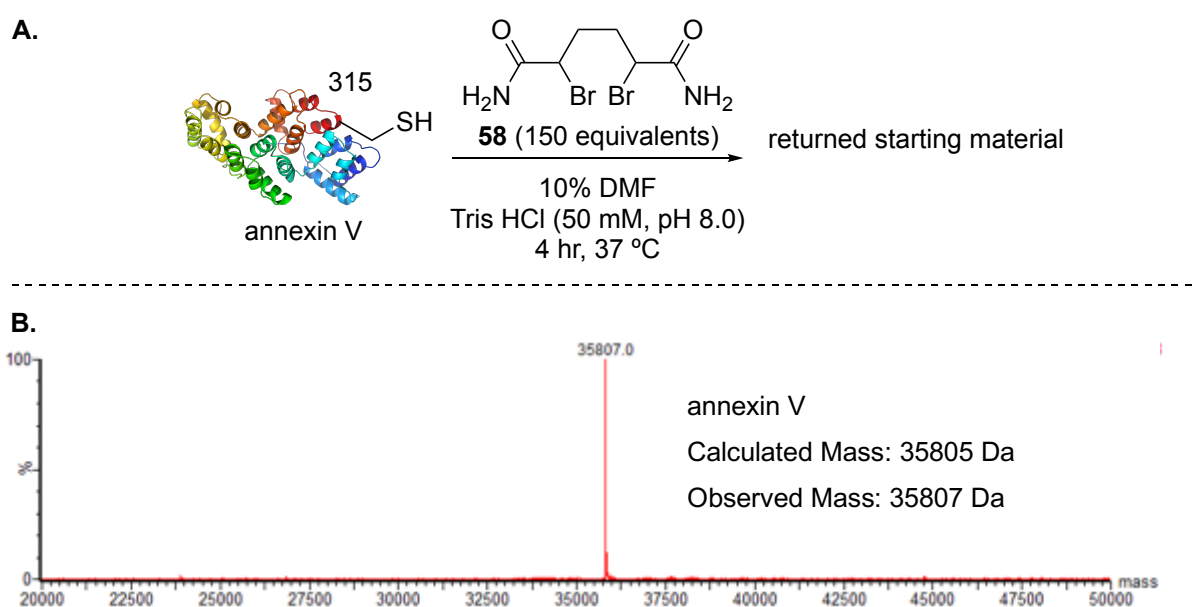
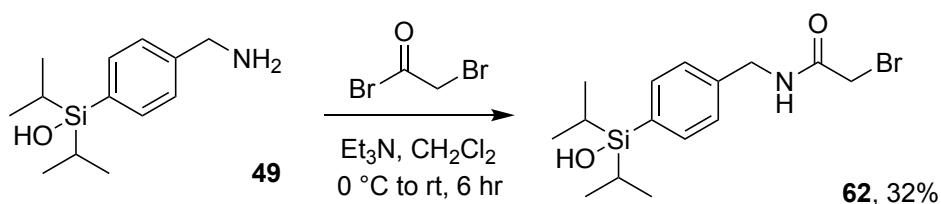


Figure 3.5 A) Attempts to convert the single cysteine in annexin V to dehydroalanine returned starting material. **B)** The deconvoluted mass spectrum at 5 hours at 37 °C reveals no conversion.

In search of a faster method for the chemical modification of annexin V, we chose to use a haloacetamide. Containing an electron deficient α carbon, haloacetamides react rapidly with the nucleophilic thiol side chain of cysteine residues. Unfortunately, they can also react with other nucleophilic side chains of amino acids and at the C- and N-termini of proteins. Given the complexity of proteins, this isn't completely surprising but thankfully, this complexity also allows for a degree of control over the site of modification. For example, conjugation at cysteine can be favoured by conducting the reaction at pH 8.0. At this pH the highly nucleophilic thiolate is formed while the majority of the other nucleophilic sites remain protonated and unreactive. Though, even at pH 8.0, iodoacetamide has been shown to react with not only cysteine but also

aspartic acid, glutamic acid, histidine, lysine, tyrosine and the C- and N-termini of proteins.¹⁴⁵ On the other hand, the less reactive bromoacetamides have been used to regioselectively modify cysteine residues and only reacts at the most nucleophilic sites.¹⁴⁶

While the site-selective modification of proteins via conjugation of electrophiles like haloacetamides can be a juggling act, this method has a number of advantages over our original method. Firstly, it is much faster. This increases the likelihood of being able to incorporate the silanol into annexin V before it degrades due to heat. Secondly, single cysteine proteins can be site-selectively modified directly without the need to first convert cysteine to dehydroalanine. Furthermore, the haloacetamide could be easily synthesised in a single step from **49**. By reacting **49** with bromoacetyl bromide in the presence of triethylamine in dichloromethane, the bromoacetamide **62** was obtained in an isolated yield of 32% after 6 hours at room temperature (Scheme 3.1).



Scheme 3.1 The bromoacetamide **62** is easily accessed from **49** via nucleophilic substitution with bromoacetyl bromide in the presence of triethylamine.

With the bromoacetamide at hand, it was reacted with annexin V. In the first attempt the protein was treated with 5 equivalents of **62**. Unfortunately, when the reaction was analysed via LC-MS after 5 hours at 37 °C no conjugation of **62** to annexin V was observed. At this stage it was unclear whether the rate of this reaction was simply slow under the chosen reaction conditions or if it would not proceed at all. Despite knowing that annexin V is not stable at 37 °C for 24 hours, in an attempt to promote conjugation and determine if this reaction would occur at all, the reaction was incubated at 37 °C for a further 19 hours. As anticipated, LC-MS analysis supported degradation and/or precipitation of the protein and the protein concentration was very low. However, the protein that remained was found to have a mass consistent with the bromoacetamide adduct **63** revealing that the reaction does in fact occur, albeit slowly (see Section 3.6).

With evidence of the bromoacetamide adduct forming, the conjugation reaction between **62** and annexin V was explored further. In order to be practical, the reaction conditions would need to be optimised to support full conversion while avoiding protein degradation and/or precipitation. Already prone to degradation and/or precipitation at 37 °C, increasing the temperature to increase the rate of the reaction would be counterproductive. So instead, we focused on increasing the rate of reaction by means of increasing the concentration of **62** in solution. Intuitively, the number of equivalents of **62** was first doubled to 10. Unfortunately, again after 5 hours at 37 °C, LC-MS analysis revealed that no conjugation had occurred (see Section 3.6). Whilst further increases in the number of equivalents were considered, the low solubility of the benzylamine in water led us to presume that the bromoacetamide would also have a low solubility in water. Thus, while increasing the number of equivalents would increase the concentration of **63** in solution it was also likely that precipitation would occur.

Alternatively, the concentration of **62** in solution could be increased and the likelihood of precipitation limited by raising the amount of organic co-solvent. Gratifyingly, annexin V was found to be stable in solutions of up to 20% DMF and at this concentration full conversion to the bromoacetamide adduct was achieved with 5 equivalents of **62** in only 4 hours (Figure 3.6). In comparison to our original method this reaction was simpler, more efficient and faster. Accordingly, we investigated the general applicability of this method to other proteins.

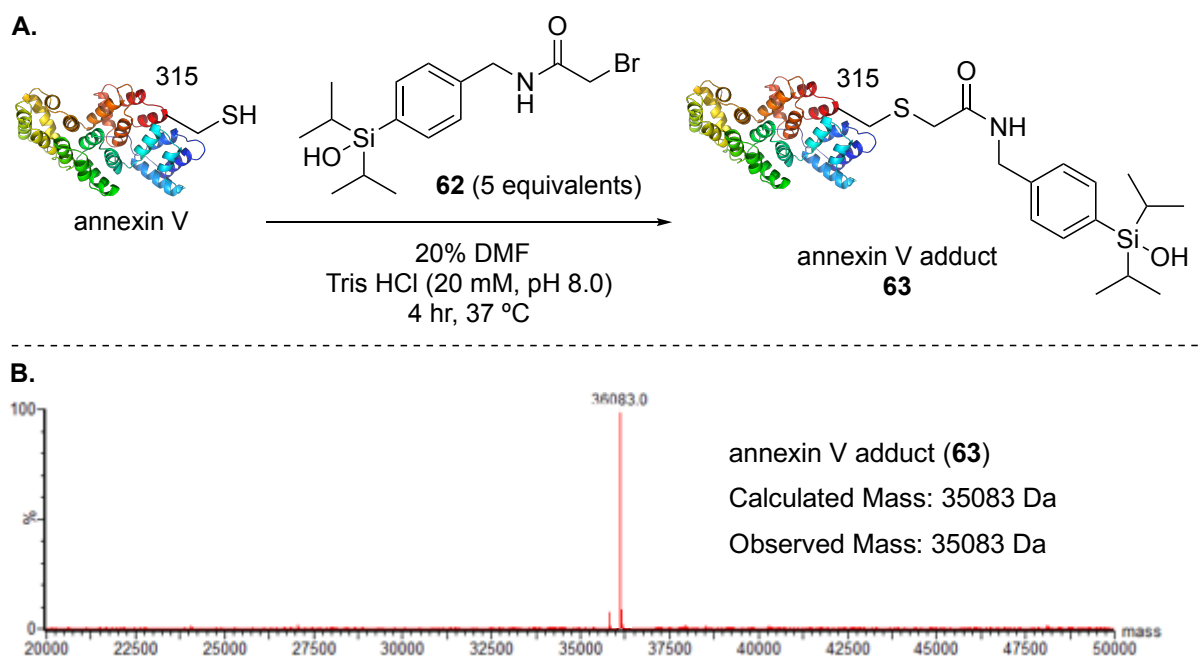


Figure 3.6 A) Conjugation of **62** to the single cysteine in annexin V. **B)** Full conversion to the annexin V adduct **63** is observed in the deconvoluted mass spectrum after 4 hours at 37 °C.

3.2.4 Bovine serum albumin (BSA)

BSA is a 66.4 kDa protein that contains in total 35 cysteine residues. Only one, however, is a cysteine in its reduced form with the other 34 forming intramolecular disulfide bridges. Therefore, the silanol could potentially be site-selectively incorporated into BSA using the same method applied to annexin V. Additionally, conjugation of **62** to BSA would give us insight into the compatibility of this method with disulfide bonds, a feature absent from annexin V.

The modification of BSA was first tested under the conditions optimised for annexin V. BSA was treated with 5 equivalents of **62** at pH 8.0 using a 20% v/v DMF co-solvent concentration. After 5 hours at 37 °C the reaction was analysed by LC-MS and unexpectedly, revealed multiple modifications (Figure 3.7B). From the conjugation of **62** to annexin V we concluded that **62** only reacts with cysteine residues as no additional modifications were detected by LC-MS. Therefore, we believed that the multiple modifications of BSA were a result of the dissociation of a disulfide bridge and subsequent conjugation of **62** to the newly formed thiols. With no disulfide bridges within the tertiary structure of annexin V, this hypothesis was also consistent with why we had not observed multiple modification during the conjugation of **62** to annexin V.

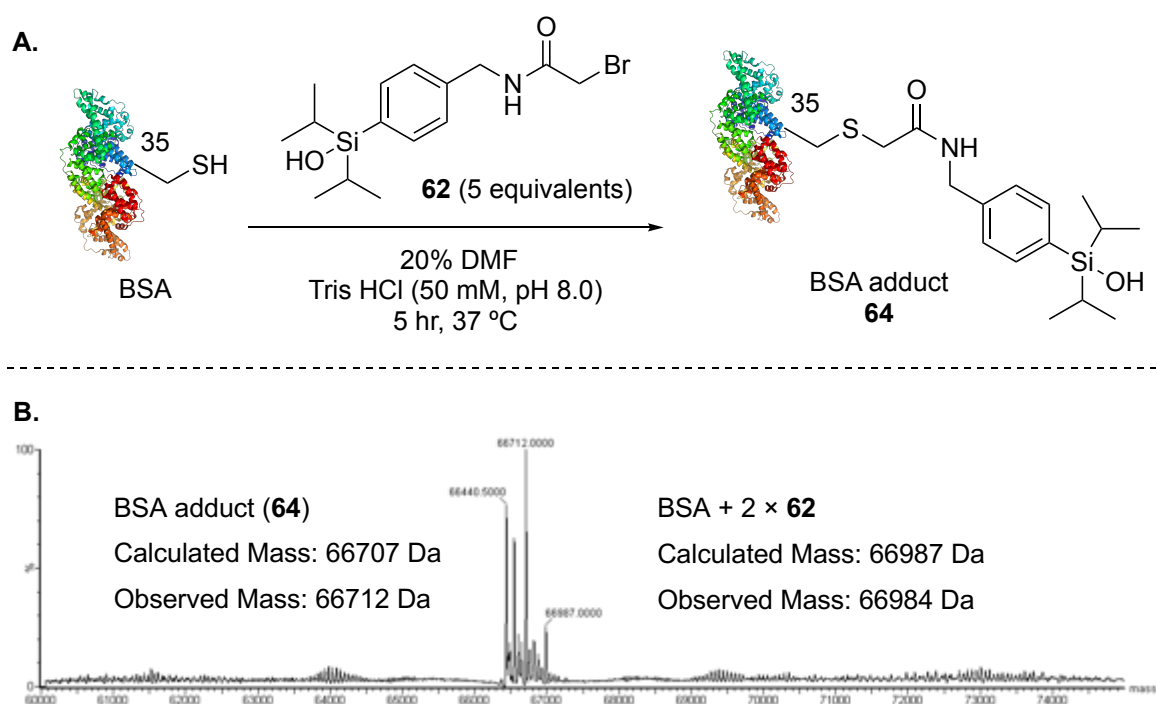


Figure 3.7 A) Conjugation of **62** to the single cysteine in BSA. **B)** Multiple additions of **62** to BSA were observed in the deconvoluted mass spectrum after 5 hours at 37 °C.

To determine if the multiple modifications of BSA were a result of disulfide dissociation we conducted several controls with Ellman's reagent. Used to quantify the thiol content of proteins, Ellman's reagent reacts rapidly with cysteine through a disulfide exchange.¹⁴⁷ If indeed BSA was being denatured, Ellman's reagent would react with any thiols resulting for the dissociation of disulfide bridges and would be evident in the deconvoluted mass spectrum. As an initial control, BSA was first treated with 2 equivalents of Ellman's at pH 8.0. Only one product was detected via LC-MS analysis and the average mass in the deconvoluted mass spectrum was consistent with the addition of Ellman's reagent to a single thiol (see Section 3.6.7). This result supported that at pH 8.0 BSA has only one reduced cysteine present. Next, we examined the influence of DMF and temperature on the thiol content of BSA. A 10% DMF solution of BSA was first treated with 2 equivalents of Ellman's at pH 8.0 and the reaction then heated to 37 °C for 2 hours. LC-MS analysis of the reaction before heating and after 2 hours at 37° C again revealed only a single reduced cysteine (see Section 3.6.7). These results provided direct evidence that BSA is not denatured at 37 °C or by the inclusion of DMF up to 10%.

Showing that at 37 °C with 10% DMF only a single reduced cysteine is present in BSA we concluded that the relatively high 20% DMF co-solvent concentration was the most likely culprit to be causing the protein to denature. Therefore, dropping it down from 20% to 10% would resolve this issue. In anticipation of a slower reaction due to a lower concentration of **62** in solution when using only 10% DMF, we also doubled the number of equivalents of the bromoacetamide to 10 before repeated the reaction. While conjugation was observed, full conversion was not achieved within 5 hours. Longer reaction times resulted in protein precipitation or degradation, as evidenced by reduced signal in the LC-MS trace (Figure 3.8). However, only a single modification was observed and thus we were encouraged to further optimise this reaction. In an attempt to reach full conversion before degradation and/or precipitation occurred the number of equivalents of **62** was increased. Under otherwise identical reaction conditions bromoacetamide equivalents of 25, 50 and 100 were tested. No starting material was detected in any of these experiments but unfortunately, they were to no avail and multiple modifications were again observed in all cases. After only 1 hour, LC-MS analysis revealed that BSA was modified twice when using 25 equivalents of the bromoacetamide. With 50 and 100 equivalents up to 5 and 8 modifications were detected respectively (see Section 3.6.7).

Eliminating any dissociation of intramolecular disulfide bridges as a result of the temperature and DMF concentrations used, it had to be considered that, at least in this case, the multiple modifications may be due to **62** reacting with other residues. While we did not observe this during any modifications of annexin V with **62**, the complexity and differing microenvironments within proteins mean that the same residue in different proteins, and even at different positions within the same protein, can have very different reactivities. To gauge the reactivity of the residues in BSA we reacted the native protein with iodoacetamide. As mentioned previously, iodoacetamide can react with a number of residues.¹⁴⁵ It is therefore expected that the multiple residues reacting with **62** would also react with iodoacetamide. Using 10 equivalents of iodoacetamide, a solution of BSA and iodoacetamide was heated at 37 °C with a 10% DMF co-solvent concentration, the same conditions that resulted in multiple modifications of BSA with **62**. After 2.5 hours the reaction was analysed via LC-MS and the deconvoluted mass spectrum revealed only a single product with an average mass of 66485 Da consistent with the conjugation of 1 equivalent of iodoacetamide to BSA (see Section 3.6.7).

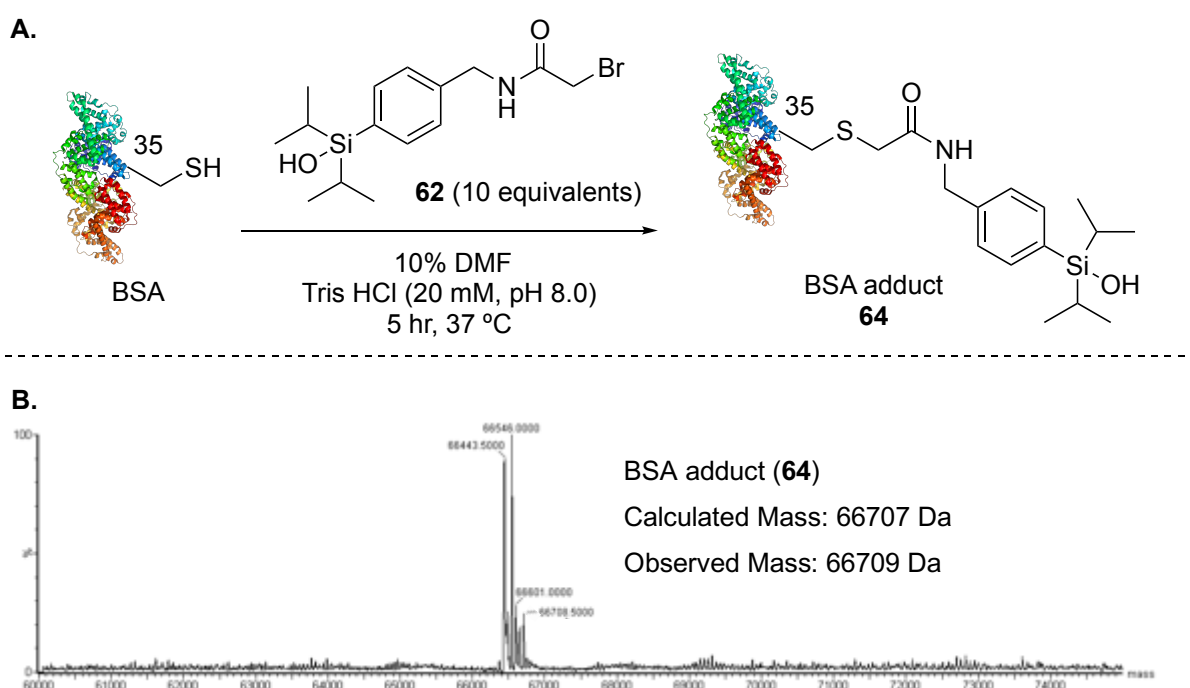


Figure 3.8 A) Conjugation of **62** to the single cysteine in BSA. **B)** Using only 10% DMF as a co-solvent and 10 equivalents of **62** only a single addition to BSA was observed but full conversion was not observed in the deconvoluted mass spectrum after 4 hours at 37 °C.

The results for the modification of BSA with iodoacetamide were very unexpected. Only a single modification indicates that the single cysteine is the only residue that should be reactive towards **62** under the conditions used. Sadly, this infers that the undesired modification must in

some way be directly related to **62** itself. With this new insight we revisited the dissociation of a disulfide bridge and considered that conjugation of **62** to the protein would create changes in the microenvironment around the modified residue and that it may be disrupting intramolecular disulfide bridges. To test this hypothesis, we again used Ellman's reagent. First BSA was treated with 10 equivalents of **62** and allowed to react for 2.5 hours at 37 °C. Then 10 equivalents of Ellman's reagent was added to the reaction and it was analysed via LC-MS. If the addition of **62** to the reduced cysteine was resulting in the dissociation of a disulfide bridge, Ellman's reagent would react with the newly formed thiols and the products detected via LC-MS.

The LC-MS analysis showed that there was both conjugation of **62** and Ellman's reagent to the protein (Figure 3.9B), but the products observed present conflicting evidence towards what is occurring. One product has an average mass of 67178 Da and is consistent with two additions of **62** and a single addition of Ellman's reagent and thus is consistent with the dissociation of a disulfide bond. In this case, after the first addition of **62** to BSA and the dissociation of a disulfide bond, **62** is able to react with BSA a second time at one of the two newly formed thiols. The final remaining thiol then reacts with Ellman's reagent upon its addition to the reaction mixture.

Another product we observed that has an average mass of 66902 Da is not consistent with dissociation of a disulfide bridge. This was evident from two observations. The first is that this product is consistent with only two modifications; one addition of **62** and one addition of Ellman's reagent. When disulfide bridges dissociate, the number of reactive thiols increases in pairs. In the presence of Ellman's reagent which reacts rapidly and reliably with thiols and taking into account the reduced cysteine, the masses of the products should be consistent with 1, 3, 5, etc modifications. Hence, if the disulfide bonds were dissociating as hypothesised, it is not expected that this product would be observed at all. Rather, it is expected that the remaining thiol would react with the excess Ellman's reagent and be observed as a product with an average mass of 67103 Da (one addition of **62** and two additions of Ellman's reagent). That it is not consistent with dissociation of a disulfide bridge was further supported by a second observation, the absence of this product.

The final product observed in the deconvoluted mass spectrum has as an average mass of 66624 Da consistent with the addition of Ellman's reagent to the single reduced cysteine of BSA. This can be explained by unreacted BSA being present at the time Ellman's reagent was added to the reaction.

With these conflicting results, we were no closer to understanding exactly how the multiple modifications of BSA observed were occurring. Future studies using the bromoacetamide method on other proteins that contain disulfide bonds may help to reveal the mechanism that led to this and whether or not this method is truly incompatible with disulfides.

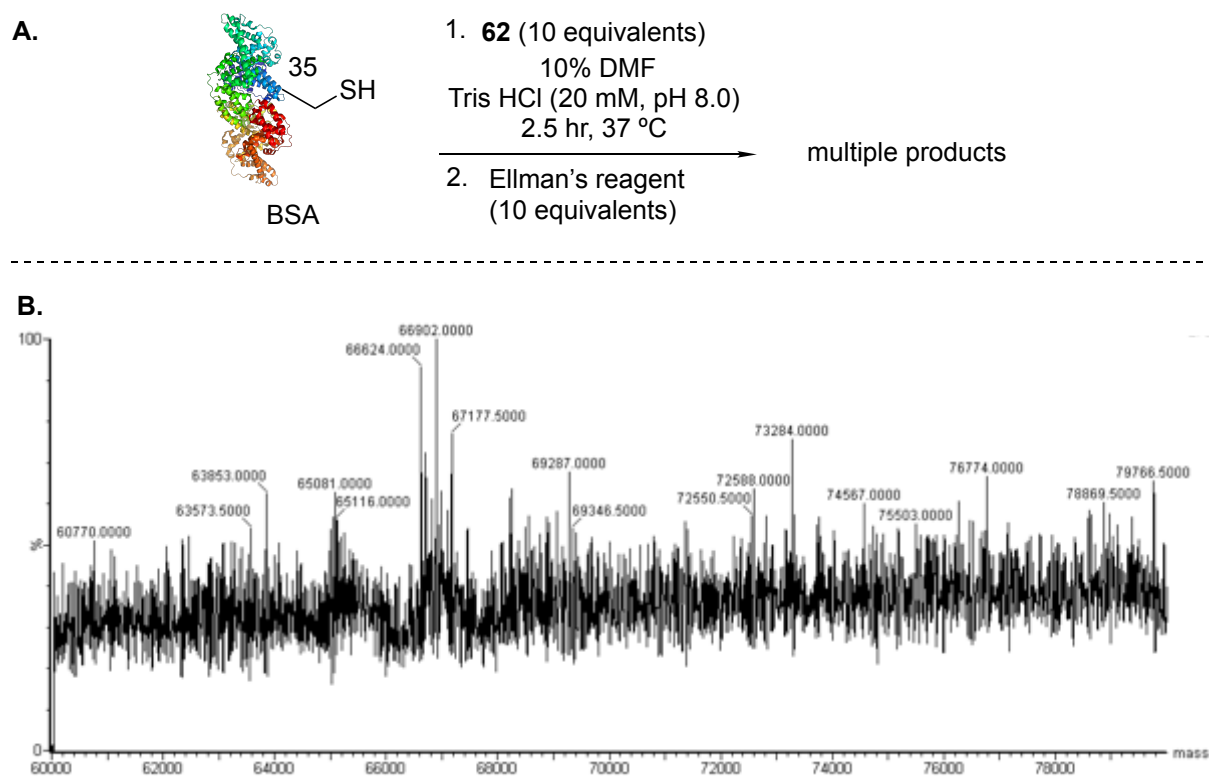


Figure 3.9 **A)** **62** was first conjugated to BSA before the addition of Ellman's reagent. **B)** The deconvoluted mass spectrum reveals multiple conflicting products.

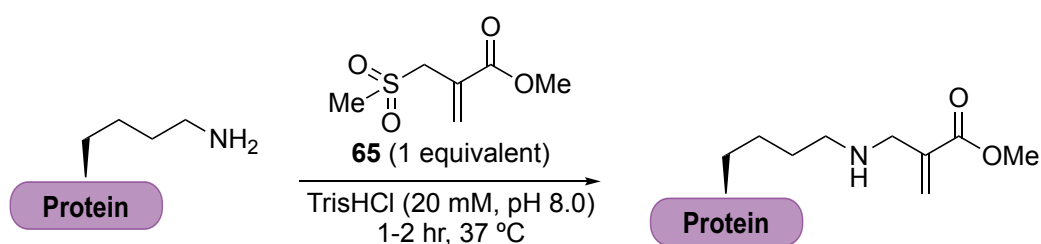
3.3 Incorporating silicon into proteins at lysine

Proteins are often modified at lysine residues though these modifications are difficult to achieve in a site-selective manner. This is not only due to lysine being relatively abundant within proteins (5.9%),¹³² but also that the reactive functional group of the lysine side chain, an amine, is also found at the N-terminus of proteins. Thus, with multiple amine groups within a protein, conjugation must not only be chemoselective but also regioselective to achieve a site-selective modification.

While this is challenging, the site-selective modification of proteins at amines has been achieved. In the literature, this generally involves the modification of N-terminal amines. With a

lower pK_a value than lysine amines, N-terminal amines can be favoured by performing reactions at a lower pH.¹³² Furthermore, site-selective modification at the N-terminus can be achieved through the unique ability of the terminal amino acid to react at both its amine and side chain. The most prominent example of this can be found in native chemical ligation whereby the side chain of a terminal cysteine first reacts with a thioester followed by a *S,N*-acyl shift lead by the lone pair of electrons on the amine.¹⁴⁸

The amines of lysine residues have also been successfully modified site-selectively. These methods primarily rely on differences in the pK_a values^{123,149,150} and microenvironments¹⁵¹ or are mediated/directed modifications.¹⁵²⁻¹⁵⁶ Of particular interest to this work is the method developed by Matos *et al.* whereby the lysine with the lowest pK_a is selectively modified with the sulfonyl acrylate **65** (Scheme 3.2). This modification results in the installation of a unique electrophilic site that could be further modified through Michael additions with benzyl amines.¹²³



Scheme 3.2 Site-selectively modification of the lysine residue with the lowest pK_a can be achieved with only 1 equivalent of **65** within 1 to 2 hours at 37 °C.

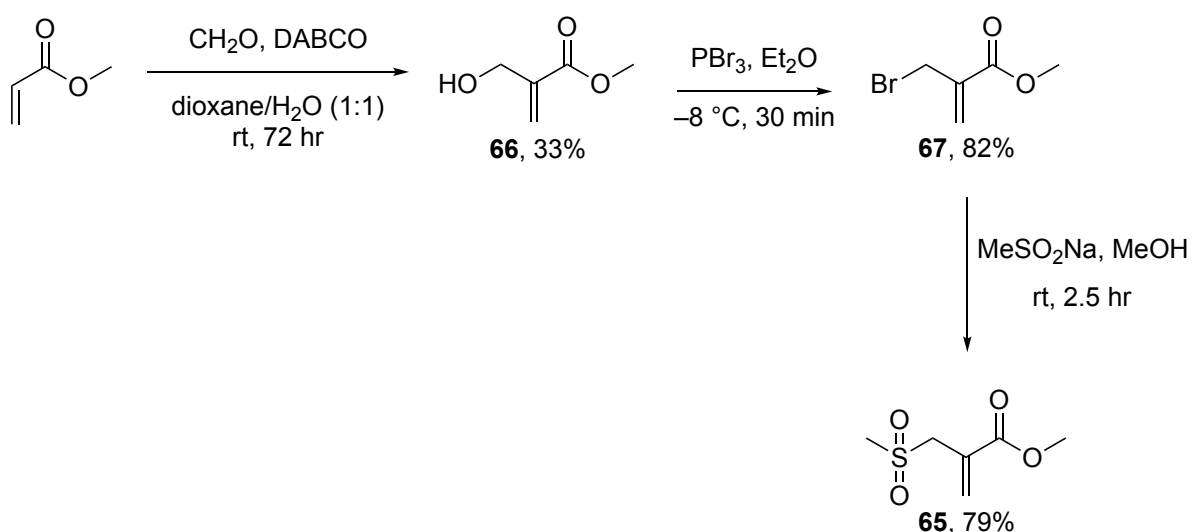
We envisioned that this method could be used to modify lysine residues in a complementary manner to the modification of cysteine residues using the dehydroalanine method we reported above. This would be particularly valuable in expanding the incorporation of the silanol into proteins with multiple or no cysteine residues. In the sections that follow, we report the use of this complimentary method to site-selectively incorporate silicon into proteins.

3.3.1 Lysozyme

Lysozyme is a relatively stable enzyme. Its resistance to heat was first noted by Alexander Fleming in his 1922 publication disclosing his discovery of lysozyme.¹⁵⁷ Owing to the thermal stability and enzymatic activity of lysozyme are its 8 cysteine residues that form 4 disulfides bridges in the protein's native structure.¹⁵⁸ With no free cysteine residues, lysozyme cannot be modified using the dehydroalanine method and is a prime candidate for the incorporation of the

silanol using the acrylate method. Furthermore, it had been shown in the original publication that lysozyme is site-selectively modified with **65** at lysine 33.¹²³

The sulfonyl acrylate **65** was synthesised from methyl acrylate. In the first step, the addition of formaldehyde in the presence of 1,4-diazabicyclo[2.2.2]octane yielded **66** after 72 hours in a 33% isolated yield. Next, using phosphorus tribromide the hydroxyl was exchanged for bromine giving **67** in an 82% yield. A better leaving group now installed the final step, a substitution reaction with sodium methanesulfinate, gave **65** in a 79% yield (Scheme 3.3). The modification of lysozyme at lysine with this acrylate was performed by Maria Matos as has previously been described.¹²³



Scheme 3.3 The sulfonyl acrylate **65** was synthesised from methyl acrylate in 3 steps.

With the electrophilic site installed onto the protein we next explore the incorporation of the silanol through conjugation of **49** to the modified protein. The modified lysozyme **68** was first treated with 1000 equivalents of **49**. Analysis via LC-MS after 3 hours at 37 °C showed partial conversion to the desired product. Alongside a mass for the desired product **69** (14639 Da) and the remaining starting material **68** (14403 Da), 2 other signals were observed in the deconvoluted mass spectrum (Figure 3.10B. Top). The first and largest signal in the spectrum had an average mass of 14626 Da consistent with the conjugate addition of **49** followed by hydrolysis of the methyl ester resulting in **70**. The hydrolysis of the methyl ester has previously been studied and was also observed in the original publication.¹²³ The second had an average mass of 14652 Da. An addition of 13 Da to the desired protein conjugate, this indicated further modification of the product, but it has not been identified.

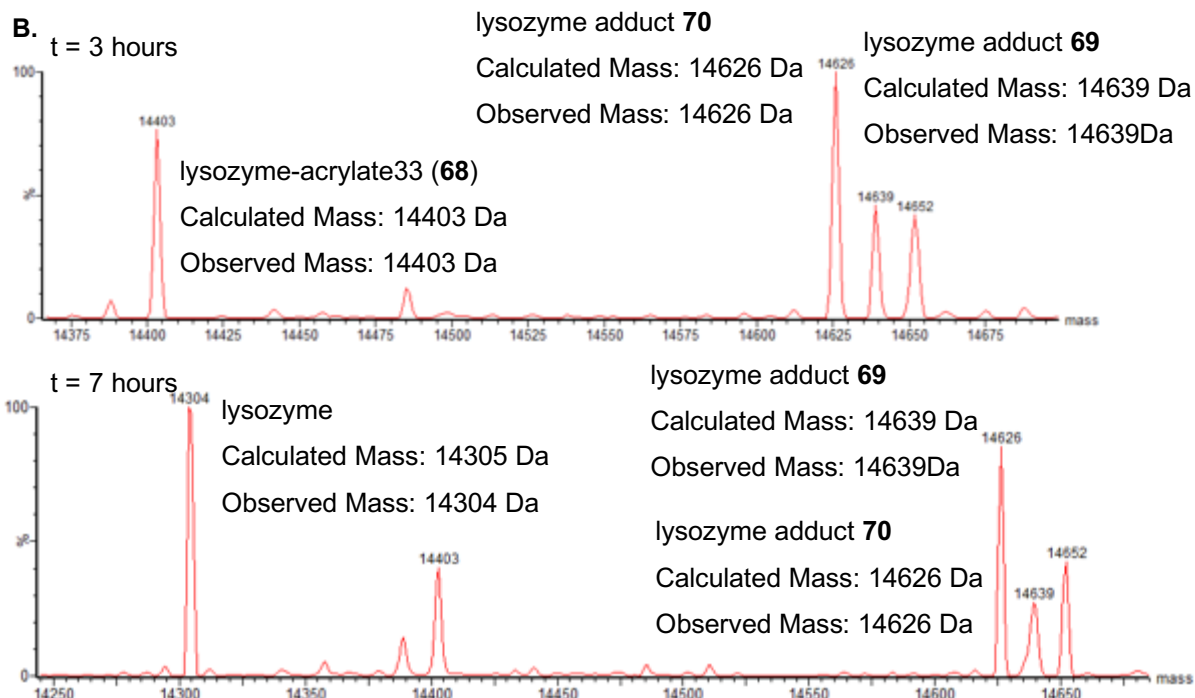
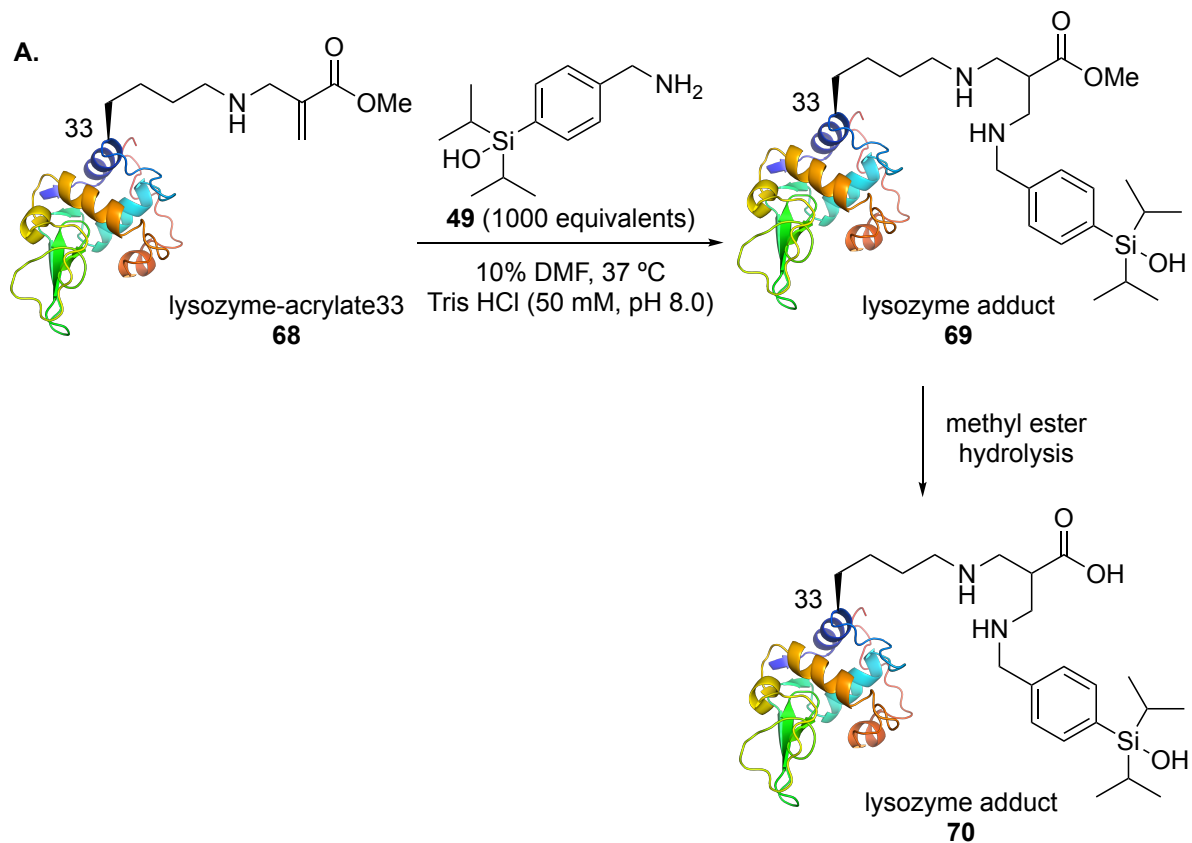


Figure 3.10 A) The reaction of **49** with **68** at pH 8.0 at 37 °C. **B)** Deconvoluted mass spectrum of the reaction shown in A above after 3 hours does not reach full conversion (top). Deconvoluted mass spectrum of the reaction shown in A above after 7 hours does not reach full conversion (bottom).

In an attempt to reach full conversion, an additional 1000 equivalents of **49** was added to the above reaction. After a further 4 hours (7 hours total) at 37 °C LC-MS analysis revealed that full conversion had still not been reached. Again, the same masses were observed in the deconvoluted spectrum with the interesting addition of a mass of 14304 Da consistent with the native lysozyme (Figure 3.10B. Bottom). Not carried through from the previous reaction this indicated that the protein conjugate may be unstable. Whether this was a result of cleavage of **69** or **70** was not determined and on no other occasion was native lysozyme observed where it could not be explained from carry through.

Due to the minimal solubility of **49** and the previous issues with precipitation when using equivalents >1000 we did not attempt to optimise this reaction by increase the number of equivalents. Serendipitously, when repeating this reaction at high protein concentration, a lower number of equivalents was found to be more optimal. This is discussed further in Section 3.4.

3.4 Direct fluorination of proteins at silicon

Having successfully incorporated the silanol into C2Am, annexin V and lysozyme, the next step was to fluorinate the proteins directly. In the small molecule aqueous fluorination studies (Chapter 2), HF•Pyridine was found to be the fluoride source that gave the highest yields of fluorination at silicon. These experiments were performed with a maximum aqueous content of 25% due to the limited solubility of the small molecules in water. Here however, the direct fluorination could be performed in 100% aqueous conditions and we would be able to determine if silanols can truly be used for the direct and aqueous fluorination of a protein.

As with the small molecules in Chapter 2, ¹⁹F NMR spectroscopy could be used to provide evidence that would support the formation of a Si-F bond and thus successful fluorination of the protein. To do this however, the concentration of protein in solution would need to be increased to allow for sufficient detection by the NMR instrument. By running ¹⁹F NMR experiments in deuterated water solutions containing differing concentrations of HF•Pyridine, it was determined that a minimum fluoride concentration of 100 μM was required for detection. Based on this, we chose to use a protein concentration of 500 μM for the fluorination experiments using the rationale that at this concentration yields of 20% and above would be detectable.

Unfortunately, obtaining the large quantities of C2Am and annexin V required for ^{19}F NMR spectroscopy was impractical and we therefore chose to only explore the direct fluorination of lysozyme. Analysing the direct fluorination of C2Am and annexin V via LC-MS was considered. However, with a mass difference of only 2 Da between the starting material and product, LC-MS analysis alone would not be enough to confidently confirm fluorination of the protein. This is only an issue for 'cold' fluorinations. When radiolabelling proteins via hydroxide displacement, fluorination can then be confidently determined via radio-HPLC.

3.4.1 Lysozyme

To obtain **69** at a concentration of 500 μM , it was necessary to adjust the conditions used for the modification of lysozyme. With the limited solubility of **49** in water and the need to keep the maximum amount of dimethylformamide to 10% v/v so as not to denature the protein, the addition of 1000 equivalents of **49** all at once was no longer feasible. In an attempt to avoid the precipitation, we therefore chose to add the solution of **49** in dimethylformamide in 5 μL aliquots (equal to 64 equivalents of **49**) at 35 minute intervals. Gratifyingly, we found that after the addition of only 6 aliquots (a total of 380 equivalents of **49**) complete conversion to **70** was observed via LC-MS analysis (Figure 3.11). This result was exceptional considering that at lower concentrations even with 1000 equivalents of **49** only partial conversion was achieved. A small amount of lysozyme was also detected, a carry through from the previous modification of lysozyme with the sulfonyl acrylate. Another, lower intensity mass at 14710 Da was also detected though this remains unidentified.

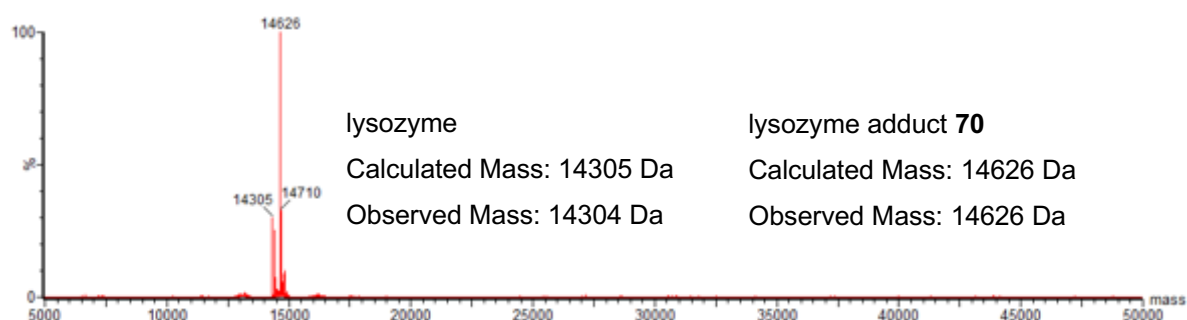


Figure 3.11 Deconvoluted mass spectrum reveals that at 37 °C and pH 8.0, the addition of 6 aliquots of **49** to **68** in 35 minute intervals results in full conversion to protein adduct **70** (total reaction time 3.5 hours, total equivalents of **49** was 380).

With a sample of **70** at an adequate concentration we next moved on to the direct fluorination of lysozyme. As an initial control we treated lysozyme with HF•Pyridine to determine if the protein reacts with the fluoride source in any way. After 4 hours at 37 °C no changes in the mass were observed by LC-MS (see Section 3.6). With this confirmation, we next treated the modified protein with HF•Pyridine. In line with Glaser *et al.* who directly fluorinated a protein through $^{19}\text{F}/^{18}\text{F}$ isotopic exchange at pH 4.0⁶⁴ and Mu *et al.* who showed that the addition of acid increases the fluorination yields of silanols in DMSO,⁶⁰ we performed the direct fluorination of lysozyme at a low pH of 3.4. The modified protein was purified with a size exclusion spin column (Zeba 5 kDa MWCO) to remove any remaining **49** and resuspended in NaP_i buffer (pH 3.4). Ten equivalents of HF•Pyridine were then added, and the reaction heated at 37 °C. The reaction was limited to only 2 hours, as were the conditions we used in the small molecule fluorination studies. After 2 hours the reaction was analysed via ^{19}F NMR spectroscopy. Gratifyingly, we observed a signal at $\delta_{\text{F}} -184.98$ ppm consistent with Si-F bond formation indicating the successful fluorination of lysozyme at the silicon atom via hydroxide displacement (Figure 3.12).

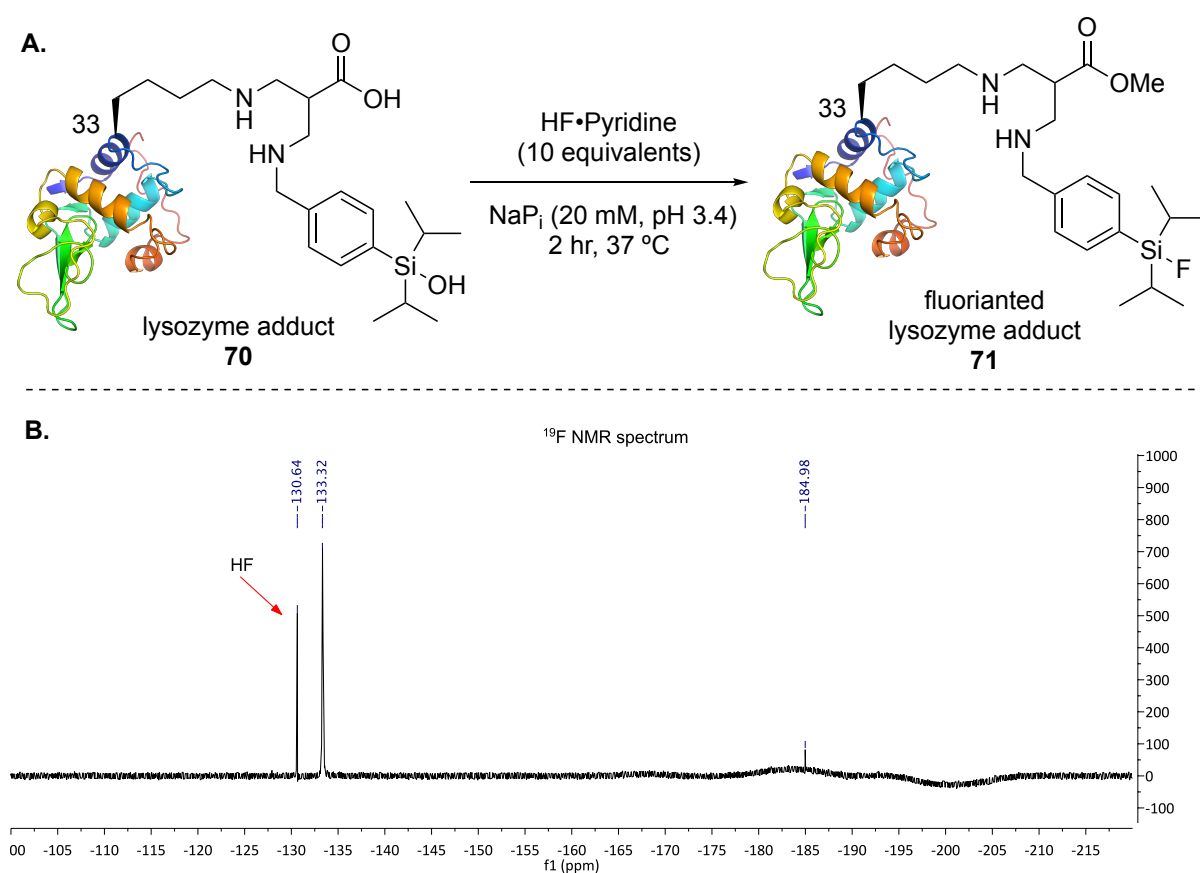


Figure 3.12 A) Fluorination of **70** **B)** ^{19}F NMR spectrum reveals the direct fluorination of lysozyme at silicon evident from a signal consistent with the formation of a Si-F bond at $\delta_{\text{F}} -184.98$ ppm.

A lower pH proved to be critical in achieving the direct fluorination of lysozyme. When the reaction was repeated at a pH of 8.0 there was no evidence of Si-F bond formation in the ^{19}F NMR spectrum (see Section 3.6). Likely, this is due to the protonation of the hydroxide leaving group at the lower pH creating a better leaving group. A signal in the ^{19}F NMR spectrum at -130.6 ppm which is unidentified was also observed for the fluorination performed at pH 3.4. The same signal was not observed in the fluorination at pH 8.0 and it was not determined whether or not this was also present when the native lysozyme treated with $\text{HF}\cdot\text{Pyridine}$.

3.5 Concluding remarks and chapter summary

C2Am was site-selectively modified at the single cysteine residue via first converting it to dehydroalanine before conjugation of **49**. Using this same method however, **49** could not be incorporated into ubiquitin and this method has a limited applicability to a wide range of proteins. Similarly, annexin V could be site-selectively modified with bromoacetamide **62** with complete conversion within 5 hours. For BSA, however, this chemical modification method resulted in multiple modifications. Attempts to understand the cause of this created more questions than it did answers. Future work to determine the sites in which BSA via tryptic digestion and MS-MS analysis would provide unambiguous confirmation of what sites of BSA are being modified and help to build a greater understanding of how this occurs. While we are confident that C2Am and annexin V were modified at cysteine, a tryptic digestion and MS-MS analysis would also be required to unambiguously confirm that this is the case.

Lysozyme was site-selectively modified at lysine 33 by first conjugating it to sulfonyl acrylate and then reacting with **65**. Again, this method was not generally applicable with no conjugation observed when it was used in attempts to modify C2Am at a lysine residue (results not shown). In future studies, the site of modification needs to be unambiguously confirmed via tryptic digestion and MS-MS analysis.

These chemical modification experiments gave us access to proteins containing a silanol that could be used to study the direct fluorination of proteins. Using ^{19}F NMR spectroscopy it was shown that proteins can be directly fluorinated at silicon atoms via hydroxide displacement. The modified lysozyme successfully underwent fluorination in aqueous media at pH 3.4 and at room temperature with no addition of an organic co-solvent. At pH 8.0 no reaction occurred

highlighting that the pH at which the reaction is performed is integral to successful fluorination. Requiring a low pH certainly limits the proteins that can be directly fluorinated in this way without affecting their structure. Furthermore, in this reaction the fluoride was in excess. When radiolabelling with fluoride-18, however, the protein will generally be in excess. Future studies into the radiolabelling of the protein and radio-HPLC analysis will be required to determine if fluorination still occurs at lower concentration.

Overall the evidence presented in this Chapter established strong leads and provides preliminary evidence for the direct fluorination of proteins with fluorine-18 via hydroxide substitution. This encourages further investigation into a more general method for the incorporation of silanols into proteins.

3.6 Experimental procedures

3.6.1 General experimental details

All reactions requiring anhydrous conditions were performed under a nitrogen atmosphere in flame-dried glassware. Dichloromethane and triethylamine were distilled over calcium hydride, tetrahydrofuran and diethyl ether were distilled over sodium and benzophenone. All other solvents and reagents were used as supplied from commercial suppliers without further purification. All fluorination reactions were conducted using plastic reaction vessels to avoid etching of glass with HF. Fluorination NMR experiments were conducted with a fluorinated ethylene polypropylene (FEP) copolymer NMR tube liner. All fluorination reactions that were heated were carried out on a Grant Bio PMHT Thermoshaker.

Analytical thin layer chromatography was performed on aluminium sheets coated with silica gel containing a fluorescent indicator (0.15-0.2mm thickness, 8 μm granularity) and were visualised using UV light or developed in a potassium permanganate or ninhydrin dip. Thin layer chromatography sheets used to analyse amines were pre-treated with 0.1% Et_3N in the required solvent system. Column chromatography was performed using silica gel (230–400 mesh, 60 \AA pore diameter).

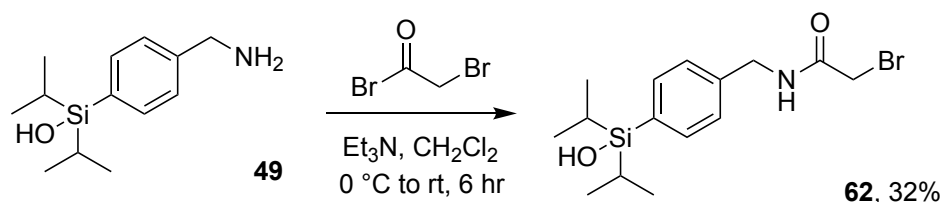
All NMR spectra were recorded using a Bruker Ultrashield 400 or a Bruker Ultrashield 600. Deuterated chloroform (CDCl_3) or deuterated water (D_2O) were used as the solvent and for

internal locking. ^1H NMR chemical shifts were referenced to δ 7.26 ppm (CDCl_3) or δ 4.79 ppm (D_2O) and ^{13}C NMR chemical shifts to δ 77.16 ppm. Chemical shifts (δ) were measured in parts per million (ppm) and coupling constants (J) in hertz (Hz). Multiplicity is reported as s = singlet, d = doublet, m = multiplet, br. s = broad singlet. Infrared spectra were recorded on an FTIR spectrometer with the absorptions reported in wavenumbers (cm^{-1}). High resolution mass spectrometry was recorded using a Perkin Elmer AxION connected to a DSA-ToF using atmospheric pressure chemical ionization (APCI) or on a Waters Synapt HDMS using electrospray ionisation (ESI). All HRMS data is reported as the observed molecular ion unless otherwise stated. Melting points were recorded on a Gallenkamp melting point apparatus.

At the University of Cambridge LC-MS characterisation of proteins was recorded using a Xevo G2S-ToF mass spectrometer coupled to an Acquity UPLC system or an Agilent 6230 ToF LC/MS using an Acquity UPLC BEH C4 column (1.7 μm particle size, 300 \AA pore diameter, 2.1 \times 50 mm). At Flinders University LC-MS characterisation of protein was recorded using a Waters Synapt high definition mass spectrometer (HDMS) coupled to an Acquity UPLC system using an Acquity UPLC BEH C4 column (1.7 μm particle size, 300 \AA pore diameter, 2.1 \times 50 mm). In all LC-MS characterisation experiments of proteins a standard injection volume of 5 μL was used. The mobile phases used were water containing 0.1% formic acid (solvent A) and acetonitrile (solvent B) at a flow rate of 0.2 mL/min. The gradient was programmed as follows: 95-5% A over 15, 18 or 20 min, hold for 5 min, then 5-95% A over 5 min. Eluting ions were measured with an ESI ion source in positive mode and scanned from 500-3200 m/z. Ion series were deconvoluted using the MaxEnt algorithm preinstalled on MassLynx software (Waters).

3.6.2 Synthetic procedures and analytical data

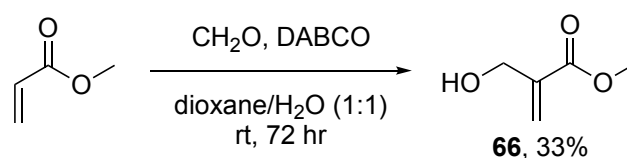
1-[(4-Diisopropylsilylanol)benzyl]bromoacetamide (**62**)



At 0 °C bromoacetyl bromide (211 μL , 1.06 mmol, 1.2 eq.) was added to a solution of **49** (0.209 g, 0.88 mmol) and Et₃N (148 μL , 1.06 mmol, 1.2 eq.) in CH₂Cl₂ (2 mL). The reaction was stirred at 0 °C for 5 min before the ice bath was removed, and the reaction left to come to room

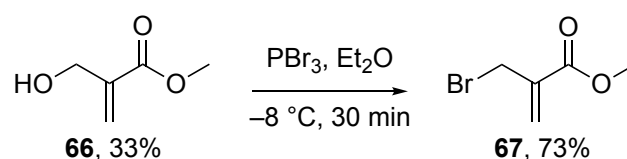
temperature. After stirring at room temperature for 6 hr, the solvent was removed under reduced pressure. The residue was purified by column chromatography (40% EtOAc in hexanes) to afford **62** ($R_f=0.68$) as a brown solid (100 mg, 32%). Mp: 98 – 100 °C; IR (ν_{\max}): 3402, 2943, 2891, 2864, 1655, 1462, 1361, 1107, 993, 882, 675 cm^{-1} ; ^1H NMR (600 MHz, Chloroform- d) δ 7.55 (d, $J = 8.0$ Hz, 2H, ArH), 7.29 (d, $J = 7.6$ Hz, 2H, ArH), 6.77 (s, 1H, NH), 4.50 (d, $J = 5.8$ Hz, 2H, ArCH₂), 3.95 (s, 2H, CH₂Br), 1.75 (s, 1H, OH), 1.22 (m, 2H, *i*PrH), 1.05 (d, $J = 7.4$ Hz, 6H, *i*PrCH₃), 0.97 (d, $J = 7.5$ Hz, 6H, *i*PrCH₃); ^{13}C NMR (151 MHz, Chloroform- d) δ 165.46, 138.41, 135.19, 134.78, 127.06, 44.32, 29.32, 17.29, 17.03, 12.57; HRMS (APCI) calculated for $[\text{C}_{15}\text{H}_{25}\text{BrNO}_2\text{Si}]^+$ 358.0838; found 358.0832.

Methyl-2-(hydroxymethyl)acrylate (**66**)



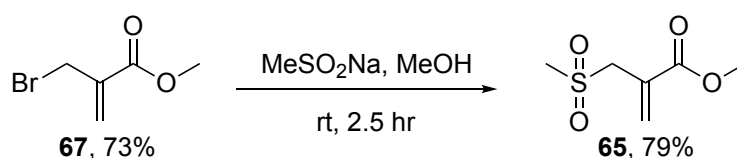
DABCO (2.17 g, 19.4 mmol) was added to a solution of methyl acrylate (5.23 ml, 58.1 mmol) in H₂O and 1,4-dioxane (1:1, 10 ml). Once the DABCO was fully dissolved formaldehyde (37 % wt. in H₂O, 9.43 ml, 116 mmol) was added dropwise. The reaction was stirred for 72 hr before the mixture was partitioned between H₂O (10 ml) and EtOAc (10 ml) and the aqueous phase extracted with EtOAc (3 × 10 ml). The combined organic fractions were washed with brine (20 ml), dried (Na₂SO₄), filtered and the solvent removed under reduced pressure. Purification by column chromatography with a gradient solvent system of 25% to 50% EtOAc in hexanes yielded **66** ($R_f = 0.26$, 25% EtOAc in hexanes) as a colourless liquid (2.25 g, 33 %). IR (ν_{\max}): 3422, 2955, 1717, 1636, 1440, 1201, 1057 cm^{-1} ; ^1H NMR (600 MHz, Chloroform- d) δ 6.26 (q, $J = 1.0$ Hz, 1H, C=CH_A), 5.84 (q, $J = 1.4$ Hz, 1H, C=CH_B), 4.33 (s, 2H, CH₂), 3.79 (s, 3H, OCH₃), 2.33 (br. s, 1H, OH); ^{13}C NMR (151 MHz, Chloroform- d) δ 166.91, 139.40, 126.06, 62.69, 52.08; HRMS (APCI) calculated for $[\text{C}_5\text{H}_9\text{O}_3]^+$ 117.0546; found 117.0548.

Methyl-2-(bromomethyl)acrylate (**67**)



At $-8\text{ }^{\circ}\text{C}$ PBr_3 (0.405 ml, 4.3 mmol) was dropwise to a solution of **66** (0.221 ml, 2.16 mmol) in Et_2O . The reaction was maintained at this temperature with stirring for 30 min before being quenched with saturated aqueous NaHCO_3 (3 ml). The aqueous layer was extracted with EtOAc (3×2 ml). The combined organic layers were then washed with brine (5 ml), dried (Na_2SO_4), filtered and the solvent removed under reduced pressure to afford **67** (0.31 g, 82%). Spectroscopic data was consistent with that previously reported.¹⁵⁹ IR (ν_{max}): 2953, 1728, 1440, 1336, 1224, 1200, 1174 cm^{-1} ; ^1H NMR (600 MHz, Chloroform-*d*) δ 6.34 (s, 1H, $\text{C}=\text{CH}_A$), 5.96 (s, 1H, $\text{C}=\text{CH}_B$), 4.18 (s, 2H, CH_2), 3.82 (s, 3H, OCH_3); ^{13}C NMR (151 MHz, Chloroform-*d*) δ 165.48, 137.45, 129.39, 52.47, 29.41.

Methyl-2-(sulfonylmethyl) acrylate (**65**)



To a solution of **67** in MeOH (5 ml) was added MeSO_2Na (0.143 g, 1.40 mmol) in portions. The reaction was stirred for 1.5 hr before a further 0.5 equivalents of MeSO_2Na (0.067g, 0.652 mmol) was added. After 1 hr the reaction TLC indicated complete consumption of the starting material and the solvent was removed under reduced pressure. The residue was diluted in H_2O (5 ml), extracted with EtOAc (3×3 ml), washed with brine (5 ml), dried (Na_2SO_4), filtered and the solvent removed under reduce pressure to afford **65** as a colourless oil that solidified upon cooling (0.19 g, 79%). IR (ν_{max}): 2933, 1721, 1630, 1441, 1303, 1206, 1138 cm^{-1} ; ^1H NMR (600 MHz, Chloroform-*d*) δ 6.64 (s, 1H, $\text{C}=\text{CH}_A$), 6.17 (s, 1H, $\text{C}=\text{CH}_B$), 4.06 (s, 2H, CH_2), 3.84 (s, 3H, OCH_3), 2.90 (s, 3H, SO_2CH_3); ^{13}C NMR (151 MHz, Chloroform-*d*) δ 165.97, 134.38, 128.91, 56.65, 52.90, 40.72; HRMS (APCI) calculated for $[\text{C}_6\text{H}_{11}\text{O}_4\text{S}]^+$ 179.0373; found 179.0364.

3.6.3 Proteins used in this study

C2Am(S78C) was kindly provided by Dr. André and Professor Kevin Brindle.¹⁴³ Lysozyme and bovine serum albumin were purchased from Sigma-Aldrich. Annexin V¹⁶⁰ and ubiquitin (K63C)¹⁴¹ were expressed and purified as previously described.

Ubiquitin(K63C)

Sequence: SAQIFVKLTLT GKTITLEVEP SDTIENVKAK IQDKEGIPPD QQRLLFAGKQ 50
LEDGRTLSDY NIQC~~EST~~LHL VLRLRGG 77

Isotopically Averaged Molecular Weight = 8568 Da

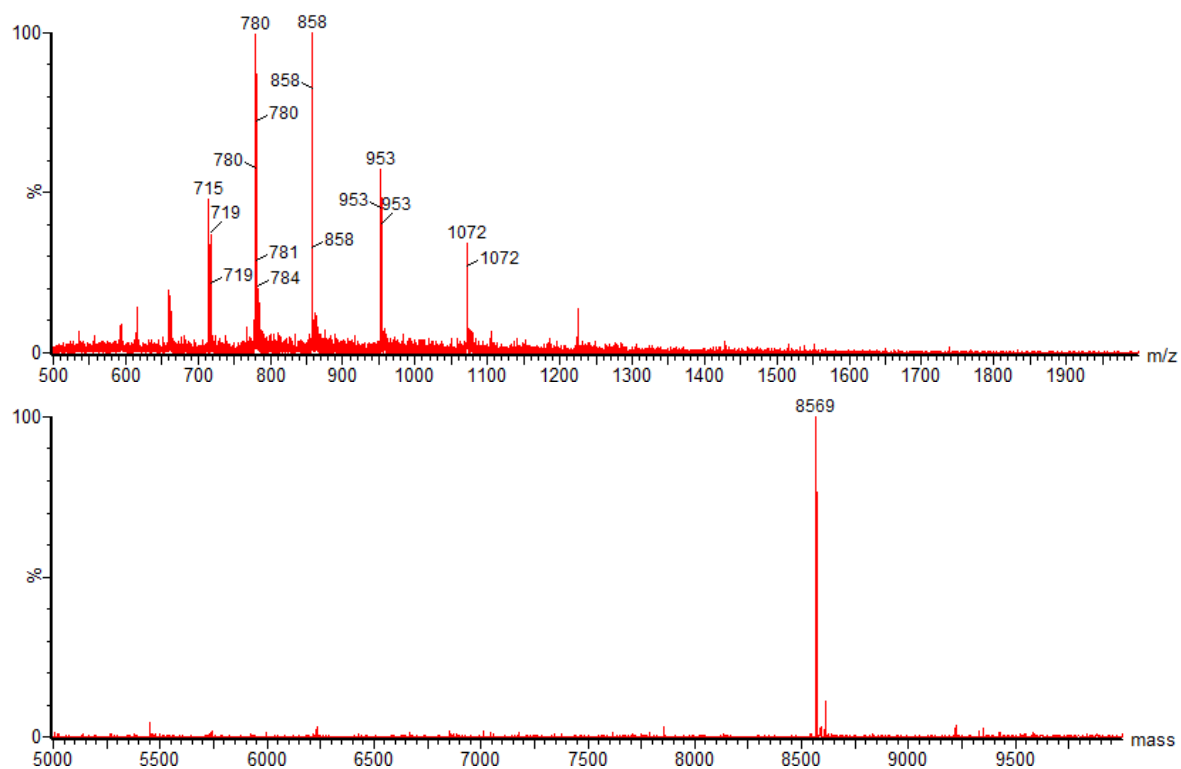


Figure S3.1 Ion series (top) and the deconvoluted mass spectrum (bottom) obtained by LC-MS for ubiquitin(K63C).

C2Am(S78C)

Sequence: GSPGISGGGG GILDSMVEKL GKLOYSLDYD FQNNQLLVGI IQAAELPALD 50
MGGTSDPYVK VLLPDKKKK FETKVHRKTL NPFVNEQFTF KVPYCELGGK 100 TLVMAVYDFD
RFSKHDIIGE FKVPMNTVDF GHVTEEWRDL QSAEK 145

Isotopically Averaged Molecular Weight = 16222 Da; when present as a dimer 32444 Da

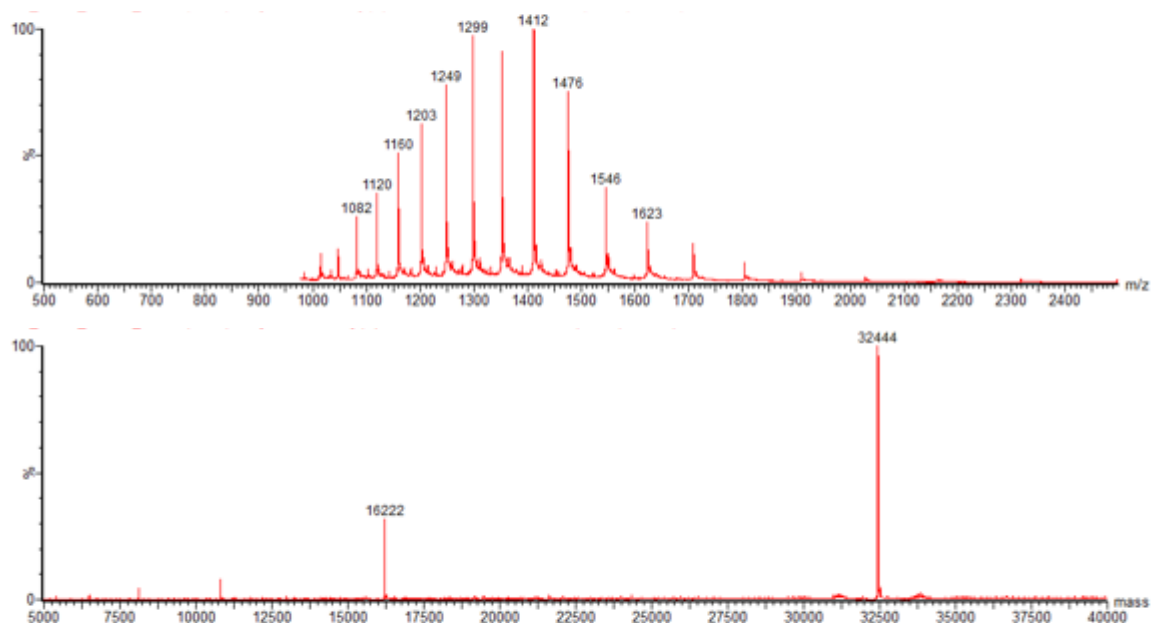


Figure S3.2 Ion series (top) and the deconvoluted mass spectrum (bottom) obtained by LC-MS for C2Am(S78C).

Annexin V

Sequence: AQVLRGTVTD FPGFDERADA ETLRKAMKGL GTDEESILTL LTRSNAQRQ 50
EISAAFKTLF GRDLLDDLKS ELTGKFEKLI VALMKPSRLY DAYELKHALK 100
GAGTNEKVL T EIISRTPEE LRAIKQVYEE EYSSLEDDV VGDTSGYYQR 150
MLVLLQANR DPDAGIDEAQ VEQDAQALFQ AGELKWTGDE EKFITIFGTR 200
SVSHLRKVF D KYMTISGFQI EETIDRETSG NLEQLLAW KSIRSIPAYL 250
AETLYYAMKG AGTDDHTLIR VMVSRSEIDL FNIRKEFRKN FATSLSYMIK 300
GDTSGDYKKA LLLLCGEDD 319

Isotopically Averaged Molecular Weight = 35805 Da

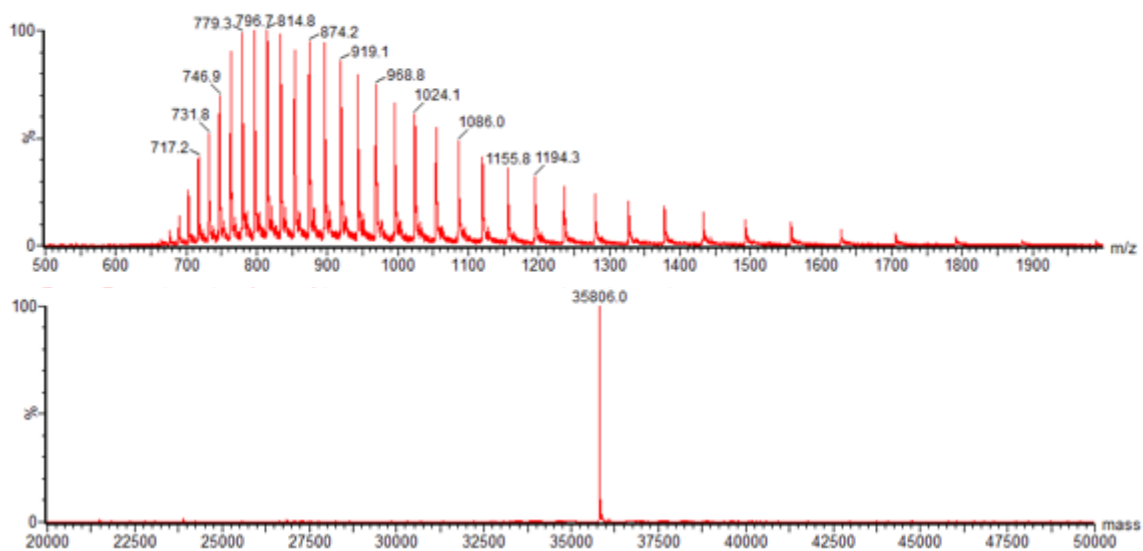


Figure S3.3 Ion series (top) and the deconvoluted mass spectrum (bottom) obtained by LC-MS for annexin V.

Bovine serum albumin (BSA)

Sequence: DTHKSEIAHR FKDLGEEHFK GLVLIAFSQY LQQCPFDEHV KLVNELTEFA 50
KTCVADESHA GCEKSLHTLF GELCKVASL RETYGDMA DC CEKQEPERNE 100
CFLSHKDDSP DLPKLPDPN TLCDEFKADE KKFWDGKLYE IARRHPYFYA 150
PELLYANKY NGVFOECCQA EDKGACLLPK IETMREKVL A SSARQRLRCA 200
SIQKFGERAL KAWSVARLSQ KFPKAEFVEV TKLVTDLTKV HKECCHGDL L 250
ECADDRADLA KYICDNQDTI SSKLKECCDK PLLEKSHCIA EVEKDAIPEN 300
LPPLTADFAE DKDVCKNYQE AKDAFLGSFL YEYSRRHPEY AVSVLLRLAK 350
EYEATLEEC AKDDPHACYS TVFDKLGHLV DEPQNLIKQN CDQFEKLG EY 400
GFQNALIVRY TRKVPQVSTP TLVEVSRSLG KVGTRCCTK P ESERMPCTED 450
YLSLILNRLC VLHEKTPVSE KVTKCCTESL VNRRPCFSAL TPDETYVPKA 500
FDEKLFTFHA DICTLPDTEK QIKKQ TALVE LLKHKPKATE EQLKTMENF 550
VAFVDKCCAA DDKEACFAVE GPKLVSTQT ALA 583

Isotopically Averaged Molecular Weight = 66430 Da

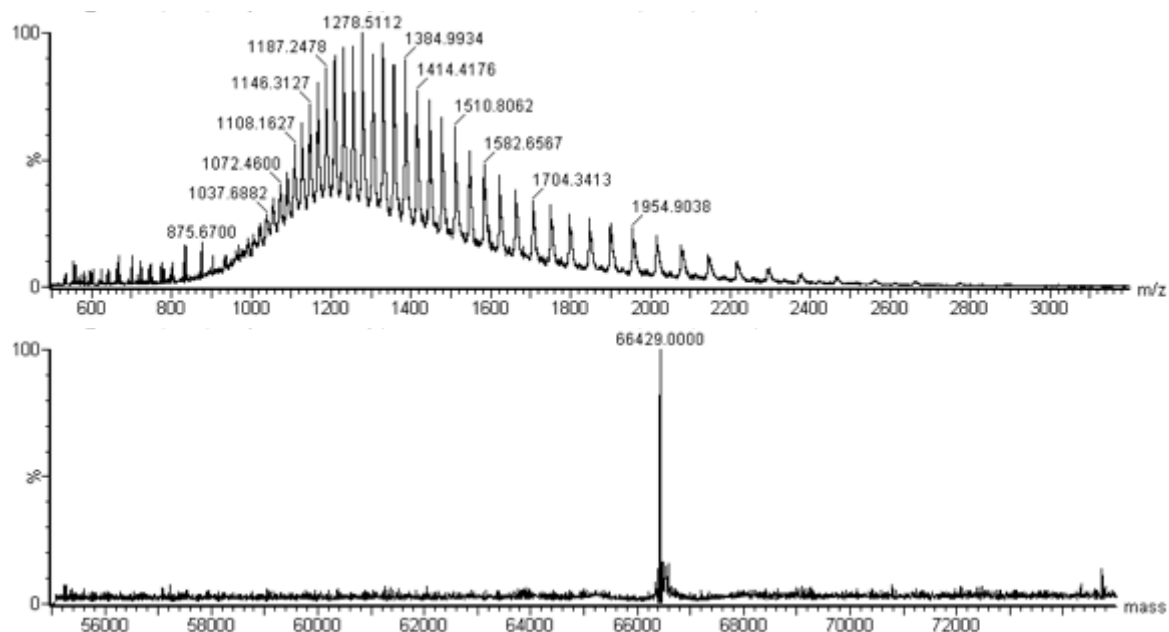


Figure S3.4 Ion series (top) and the deconvoluted mass spectrum (bottom) obtained by LC-MS for BSA.

Lysozyme

Sequence: KVFGRCLEAA AMKRHGLDNY RGYSLGNWVC AAKFESNFNT QATNRNTDGS 50
TDYGILQINS RWWCNDGRTP GSRNLCNIPC SALLSSDITA SVNCAKKIVS 100
DGNGMNAWVA WRNRCKGTDV QAWIRGCRL 129

Isotopically Averaged Molecular Weight = 14313 Da; with 4 internal disulfides: 14305 Da

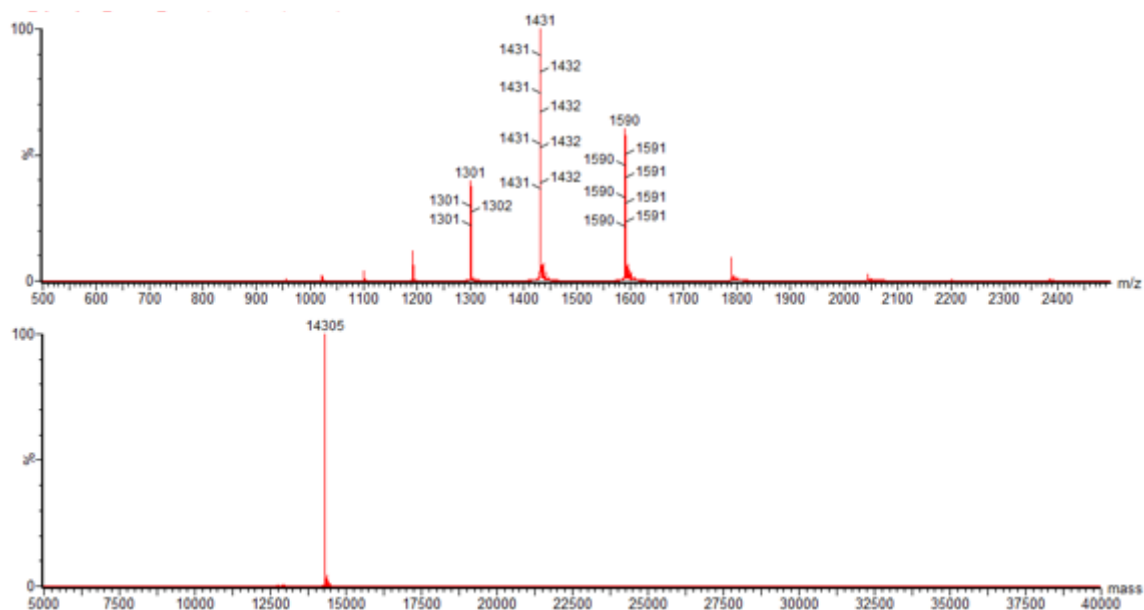
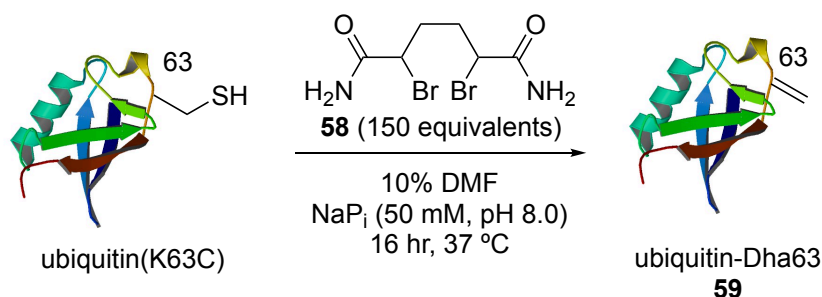


Figure S3.5 Ion series (top) and the deconvoluted mass spectrum (bottom) obtained by LC-MS for lysozyme.

3.6.4 Chemical modifications of ubiquitin(K63C)

Addition of **58** to ubiquitin(K63C)



To a solution of ubiquitin(K63C) (100 μ L, 100 μ M) in a 0.5 mL Eppendorf tube was added a solution of **58** (7.8 μ L, 192 μ M) in DMF. The solution was vortexed and left to react at 37 °C with shaking. A 2 μ L aliquot was diluted to 10 μ L with NaPi buffer (50 mM, pH 8.0) and analysed directly by LC-MS at time points 4 and 16 hr. After 16 hr full conversion to **59** (calculated mass: 8534 Da,

observed mass: 8532 Da) was observed. The remaining small molecules were removed via sample purification with a Zeba size exclusion spin column (3 kDa MWCO). The protein samples were flash frozen with liquid nitrogen and stored at $-20\text{ }^{\circ}\text{C}$.

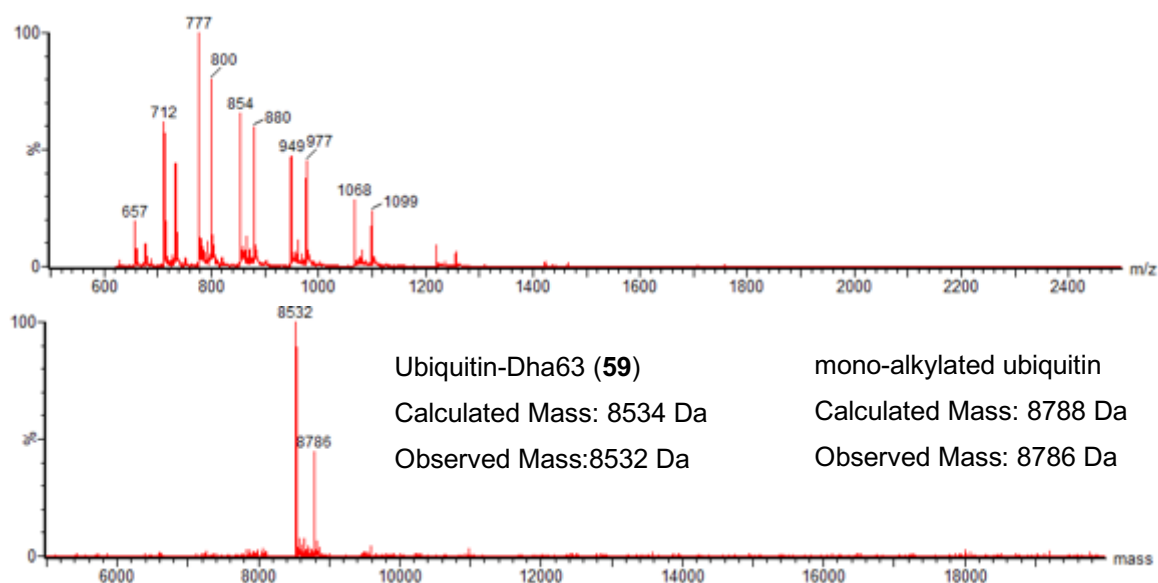


Figure S3.6 Ion series (top) and the deconvoluted mass spectrum (bottom) obtained from LC-MS analysis at 4 hr.

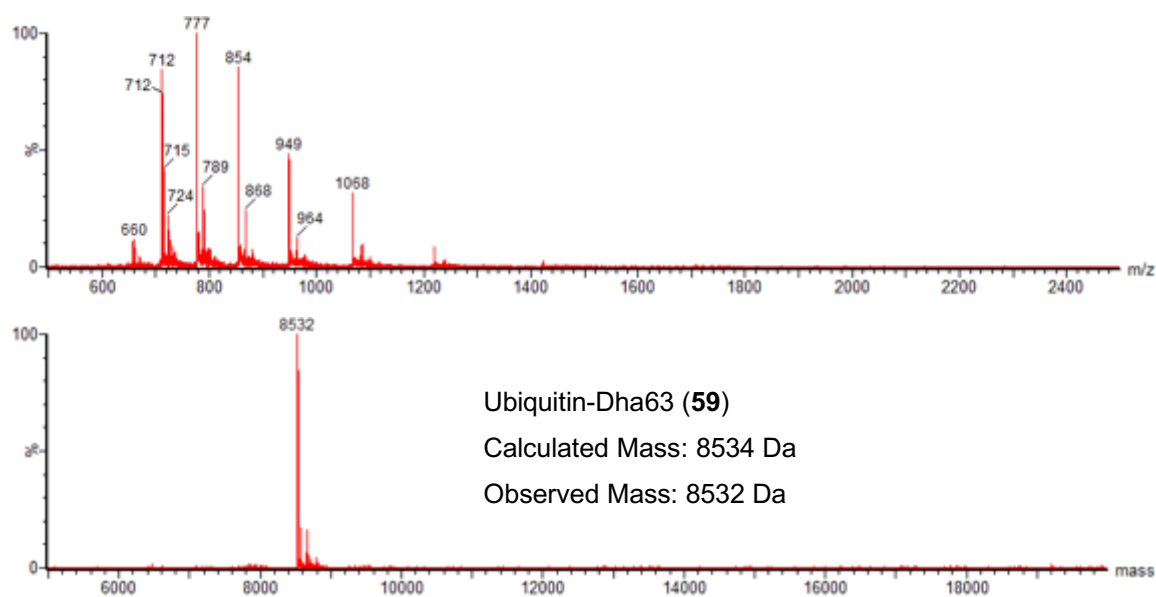
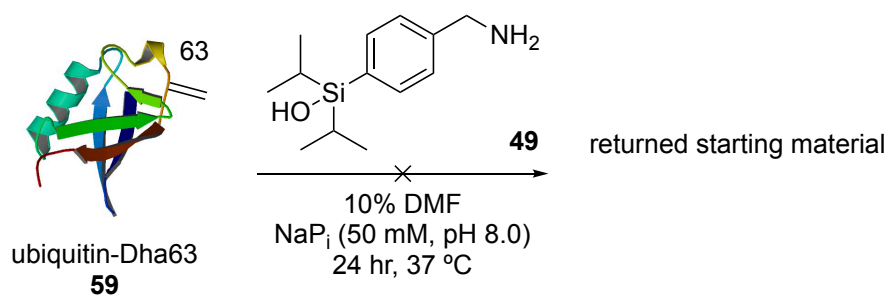


Figure S3.7 Ion series (top) and the deconvoluted mass spectrum (bottom) obtained from LC-MS analysis at 16 hr.

Addition of **49** to ubiquitin-Dha63 (**59**)



1000 equivalents of **49**

A solution of **59** (8 μ L, 100 μ M) was diluted with NaP_i buffer (28 μ L, 50 mM, pH 8.0) in a 0.5 mL Eppendorf tube to a final protein concentration of 20 μ M. A solution of **49** (3.8 μ L, 211 mM) in DMF was added. The solution was vortexed and left to react at 37 °C with shaking. A 10 μ L aliquot was analysed directly by LC-MS after 24 hr showed returned starting material (calculated mass: 8534 Da, observed mass: 8531 Da).

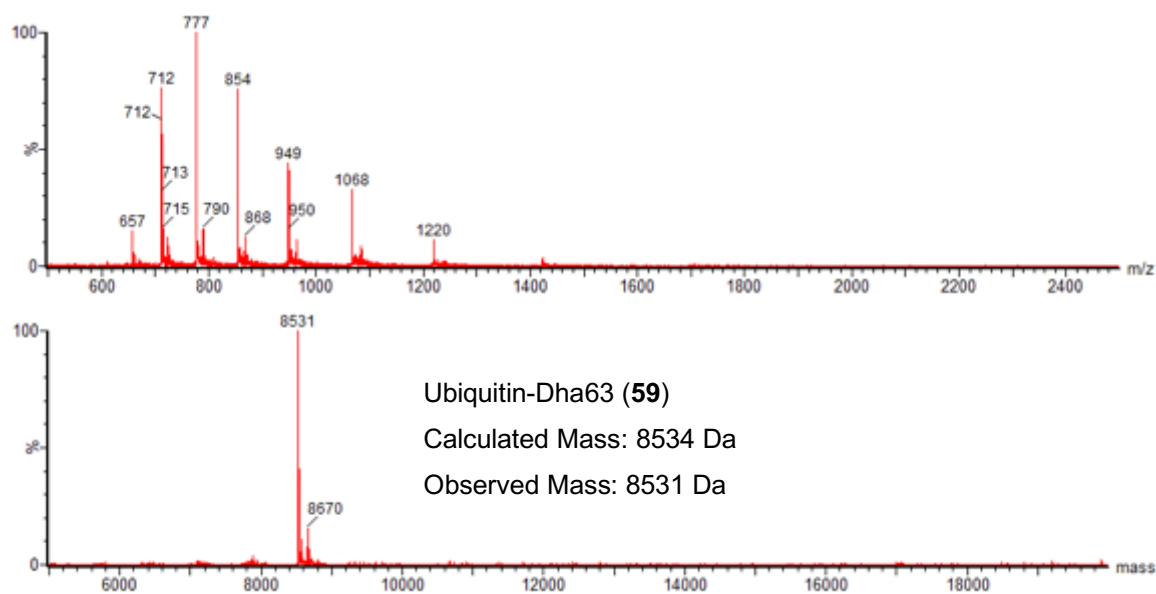


Figure S3.8 Ion series (top) and the deconvoluted mass spectrum (bottom) obtained from LC-MS analysis at 24 hr.

500 equivalents of **49**

A solution of **59** (8 μ L, 100 μ M) was diluted with NaP_i buffer (29 μ L, 50 mM, pH 8.0) in a 0.5 mL Eppendorf tube to a final protein concentration of 20 μ M. A solution of **49** (3.17 μ L, 126 mM) in DMF was added. The solution was vortexed and left to react at 37 °C with shaking. A 10 μ L aliquot was analysed directly by LC-MS after 24 hr showed returned starting material (calculated mass: 8534 Da, observed mass: 8531 Da).

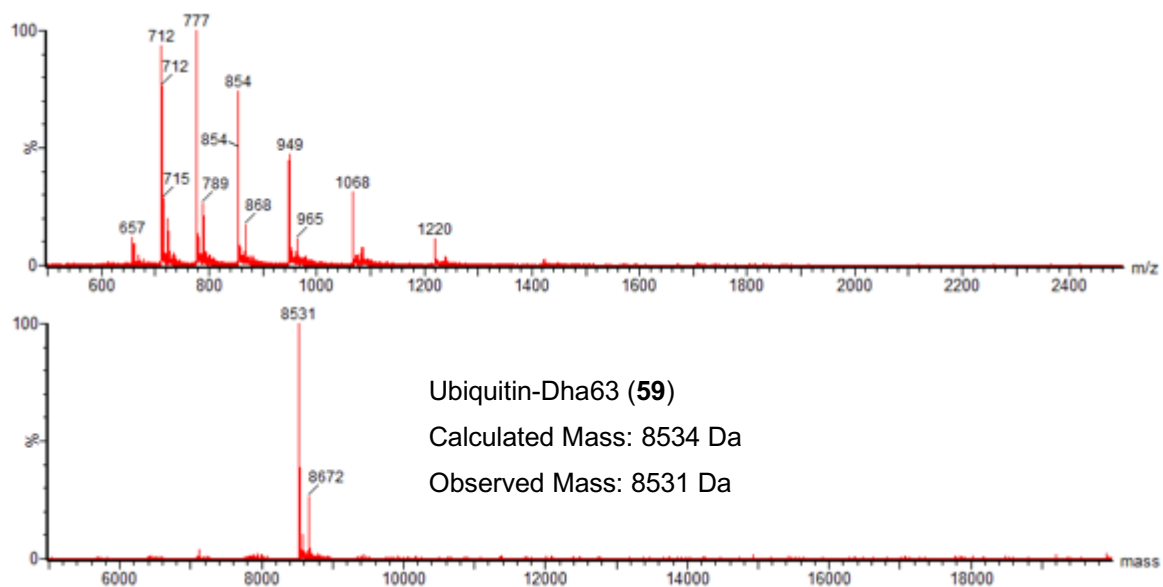


Figure S3.9 Ion series (top) and the deconvoluted mass spectrum (bottom) obtained from LC-MS analysis at 24 hr.

300 equivalents of **49**

A solution of **59** (8 μ L, 100 μ M) was diluted with NaP_i buffer (30 μ L, 50 mM, pH 8.0) in a 0.5 mL Eppendorf tube to a final protein concentration of 20 μ M. A solution of **49** (1.90 μ L, 126 mM) in DMF was added. The solution was vortexed and left to react at 37 °C with shaking. A 10 μ L aliquot was analysed directly by LC-MS after 24 hr showed returned starting material (calculated mass: 8534 Da, observed mass: 8532 Da).

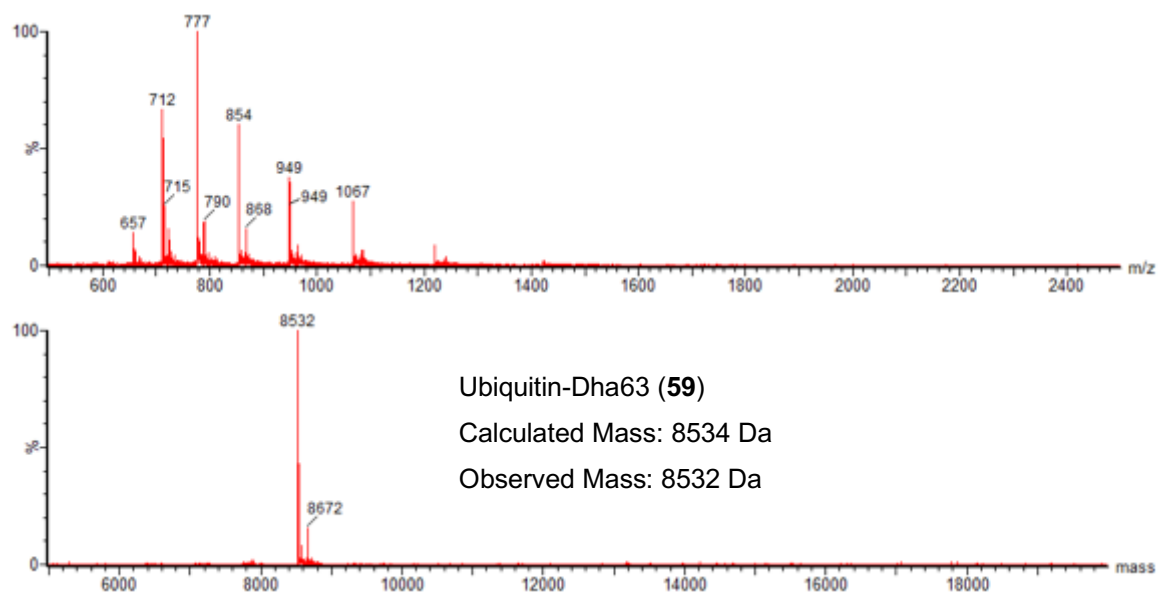


Figure S3.10 Ion series (top) and the deconvoluted mass spectrum (bottom) obtained from LC-MS analysis at 24 hr.

150 equivalents **49**

A solution of **59** (8 μ L, 100 μ M) was diluted with NaP_i buffer (31 μ L, 50 mM, pH 8.0) in a 0.5 mL Eppendorf tube to a final protein concentration of 20 μ M. A solution of **49** (0.95 μ L, 126 mM) in DMF was added. The solution was vortexed and left to react at 37 °C with shaking. A 10 μ L aliquot was analysed directly by LC-MS after 24 hr showed returned starting material (calculated mass: 8534 Da, observed mass: 8531 Da).

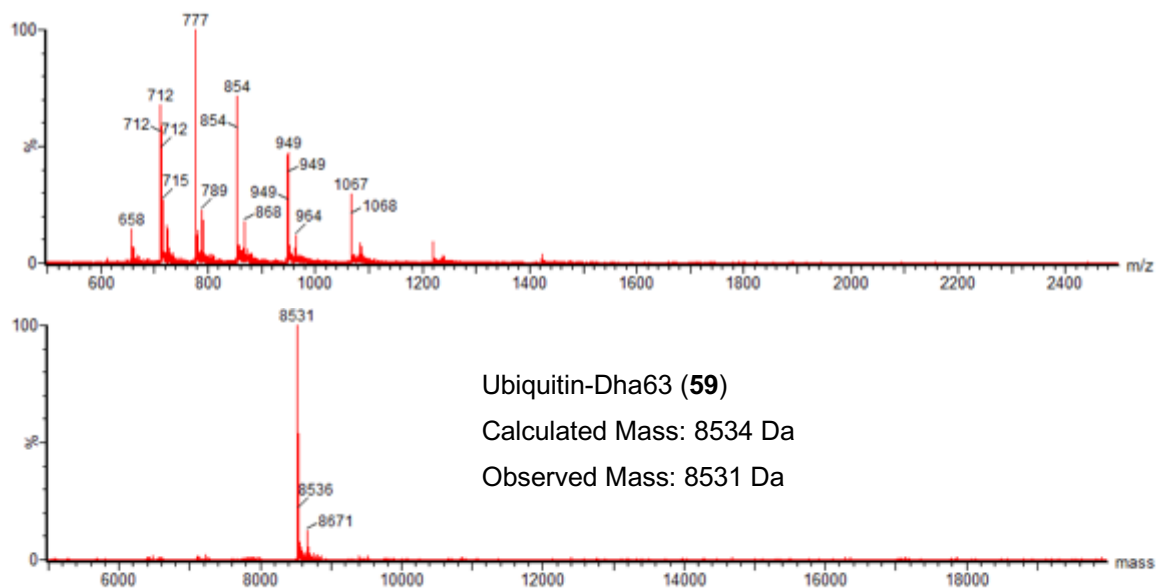
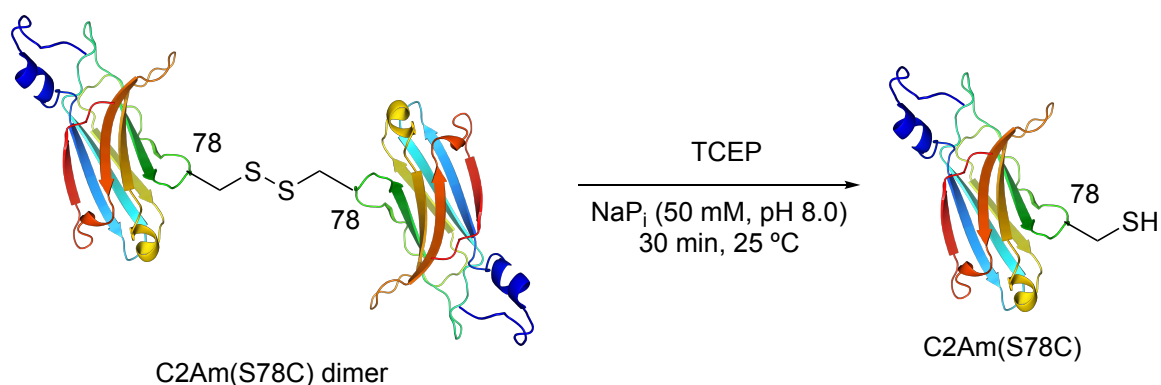


Figure S3.11 Ion series (top) and the deconvoluted mass spectrum (bottom) obtained from LC-MS analysis at 24 hr.

3.6.5 Chemical modifications of C2Am(S78C)

C2Am(S78C) disulfide reduction



A solution of C2Am(S78C) (40 μ L, 100 μ M) was diluted in NaP_i buffer (40 μ L, 50 mM, pH 8.0) in a 0.5 mL Eppendorf tube to a final protein concentration of 50 μ M. A solution of TCEP (2 μ L, 20 mM) in sodium phosphate buffer (pH 8.0) was added. The solution was vortexed and left to react at 25 °C with shaking. After 30 min a 10 μ L aliquot was analysed directly by LC-MS with full reduction of the disulfide observed (calculated mass: 16222 Da, observed mass 16222 Da). The reduced C2A(S78C) was used without further purification.

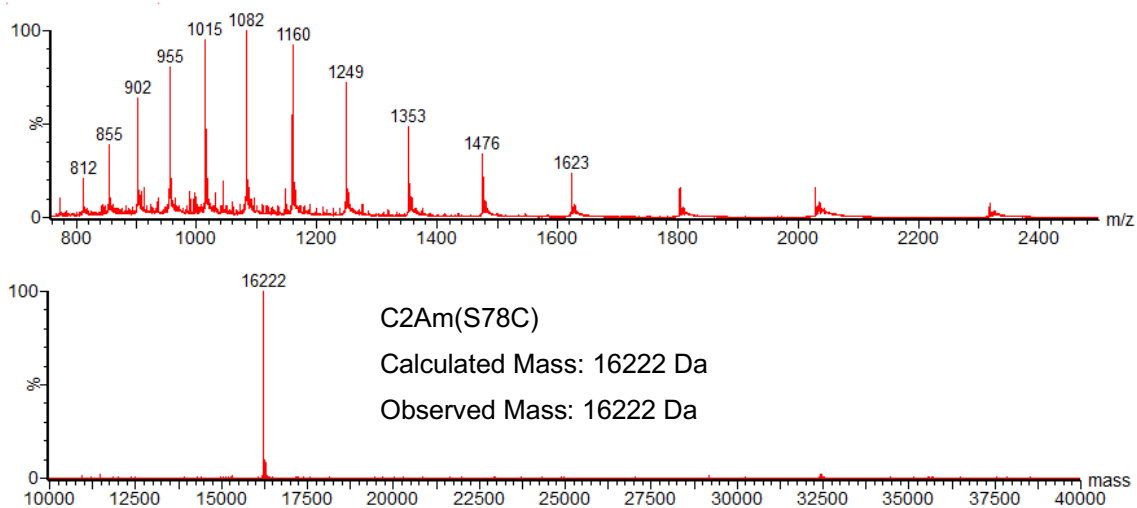
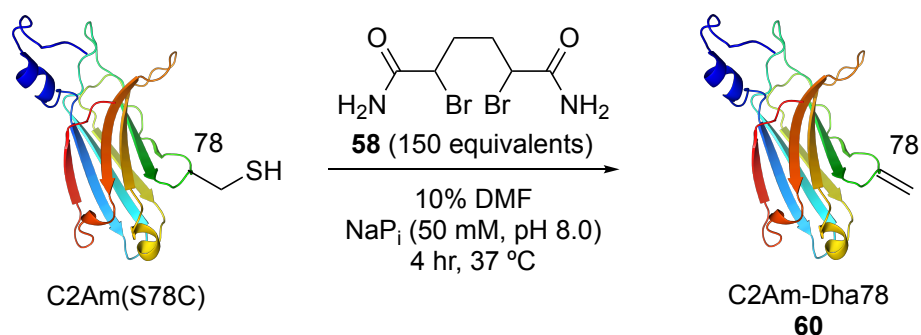


Figure S3.12 Ion series (top) and the deconvoluted mass spectrum (bottom) obtained from LC-MS analysis at 30 min.

Addition of **58** to C2Am(S78C)



A solution of C2Am(S78C) (25 μ L, 100 μ M) was diluted with NaPi buffer (50 μ L, 50 mM, pH 8.0) in a 0.5 mL Eppendorf tube to a final protein concentration of 50 μ M. A solution of **58** (2.54 μ L, 192 μ M) in DMF was added. The solution was vortexed and left to react at 37 °C with shaking. After 4 hr a 5 μ L aliquot was diluted to 10 μ L with sodium phosphate buffer (50 mM, pH 8.0) and analysed directly by LC-MS with full conversion to **60** (calculated mass: 16188 Da, observed mass: 16188 Da). The remaining small molecules were removed via sample purification with a Zeba size exclusion spin column (5 kDa MWCO). The protein samples were flash frozen with liquid nitrogen and stored at -20 °C.

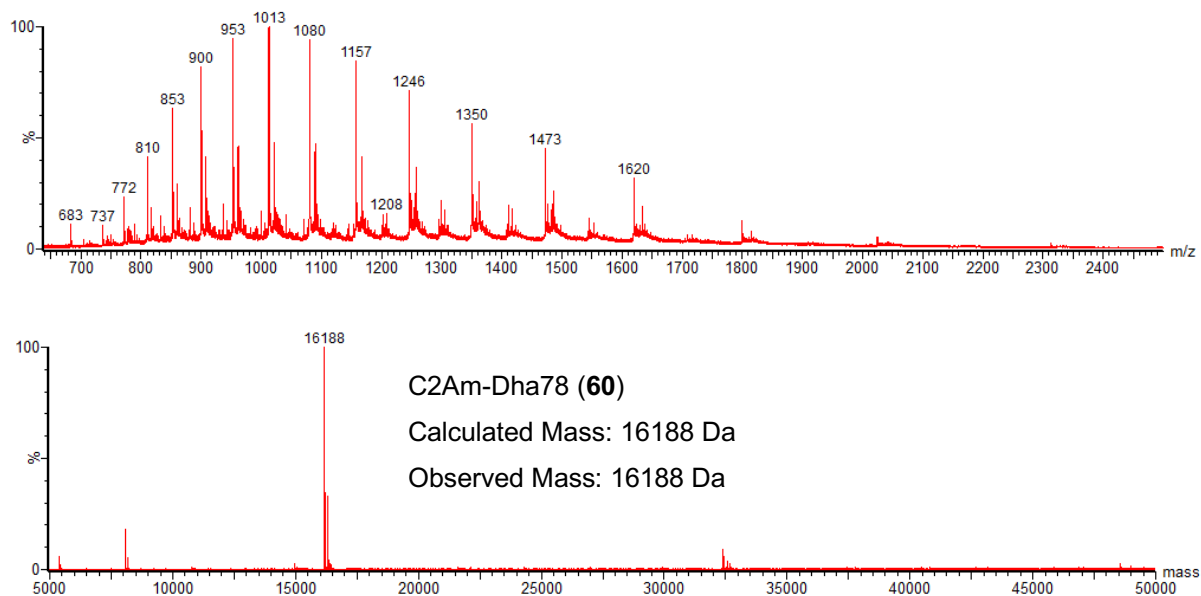
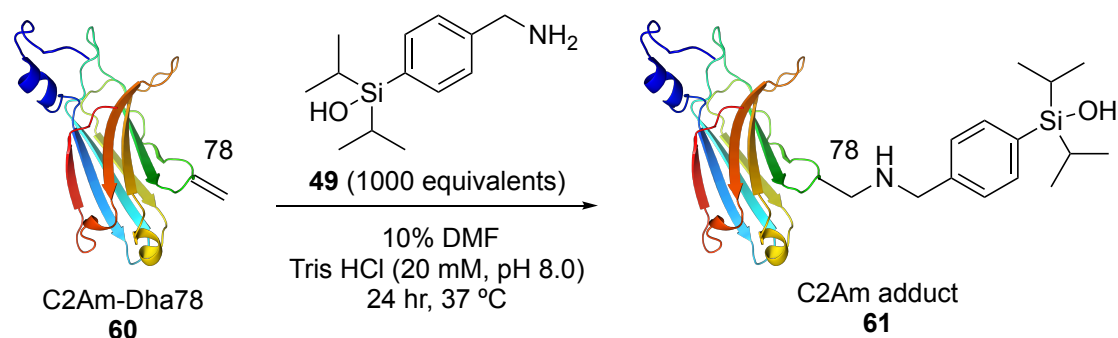


Figure S3.13 Ion series (top) and the deconvoluted mass spectrum (bottom) obtained from LC-MS analysis at 4 hr.

Addition of **49** to C2Am-Dha78

1000 equivalents at pH 8.0



A solution of **60** (20 μ L, 10 μ M) was diluted with Tris HCl buffer (20 μ L, 20 mM, pH 8.0) in a 0.5 mL Eppendorf tube to a final protein concentration of 5 μ M. A solution of **49** (4.75 μ L, 84.2 mM) in DMF was added. The solution was vortexed and left to react at 37 °C with shaking. The reaction was monitored at time points by direct analysis by LC-MS of a 10 μ L aliquot. Full conversion to **61** (calculated mass: 16424 Da, observed mass: 16425 Da) was observed after 24 hr. The remaining small molecules were removed via sample purification with a Zeba size exclusion spin column (5 kDa MWCO). The protein samples were flash frozen with liquid nitrogen and stored at -20 °C.

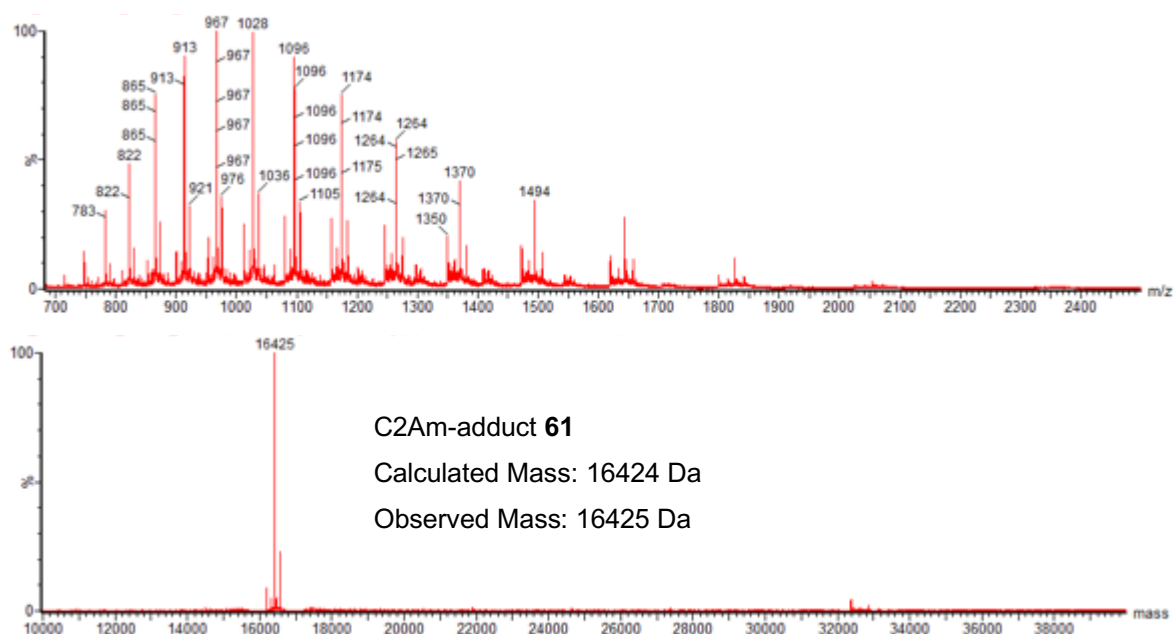
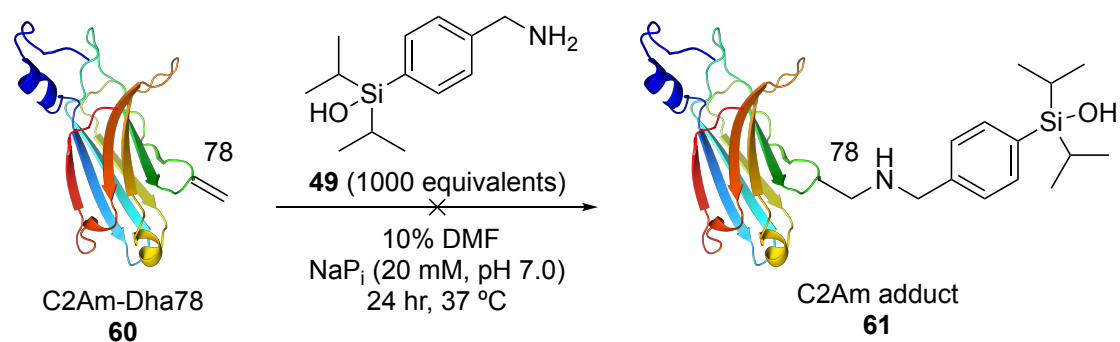


Figure S3.14 Ion series (top) and the deconvoluted mass spectrum (bottom) obtained from LC-MS analysis at 24 hr.

1000 equivalents at pH 7.0



A solution **60** (20 μ L, 10 μ M) was diluted with NaP_i buffer (20 μ L, 50 mM, pH 7.0) in a 0.5 mL Eppendorf tube to a final protein concentration of 5 μ M. A solution of **49** (4.75 μ L, 84.2 mM) in DMF was added. The solution was vortexed and left to react at 37 °C with shaking for 24 hr. A 10 μ L aliquot was analysed directly by LC-MS. Only starting material (calculated mass: 16188 Da, observed mass 16188 Da) and an unknown impurity at 15690 Da were observed.

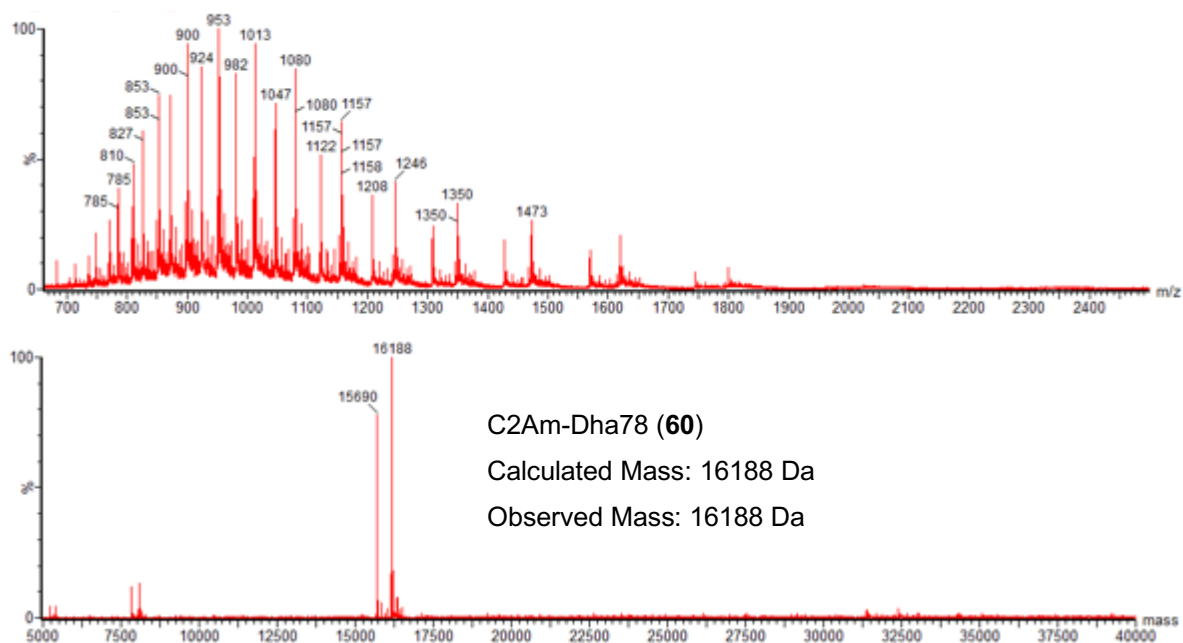
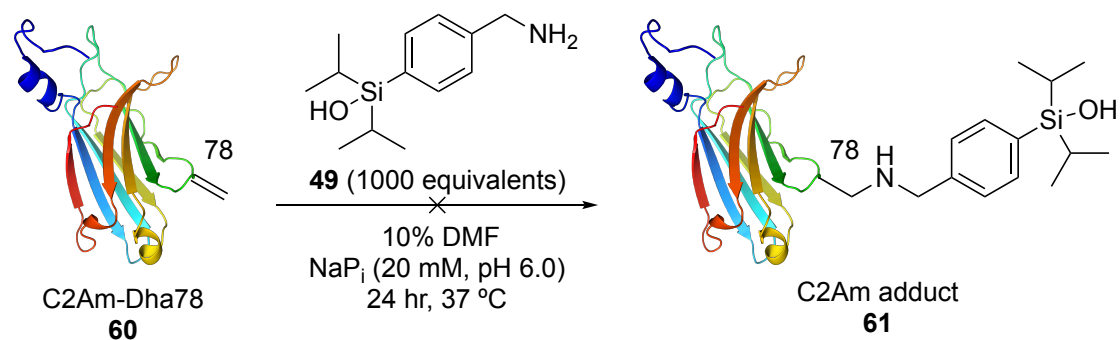


Figure S3.15 Ion series (top) and the deconvoluted mass spectrum (bottom) obtained from LC-MS analysis at 24 hr.

1000 equivalents at pH 6.0



A solution of **60** (20 μ L, 10 μ M) was diluted with NaPi buffer (20 μ L, 50 mM, pH 6.0) in a 0.5 mL Eppendorf tube to a final protein concentration of 5 μ M. A solution of **49** (4.75 μ L, 84.2 mM) in DMF was added. The solution was vortexed and left to react at 37 °C with shaking for 24 hr. A 10 μ L aliquot was analysed directly by LC-MS. Only starting material (calculated mass: 16188 Da, observed mass: 16188 Da) and an unknown impurity at 15690 Da were observed.

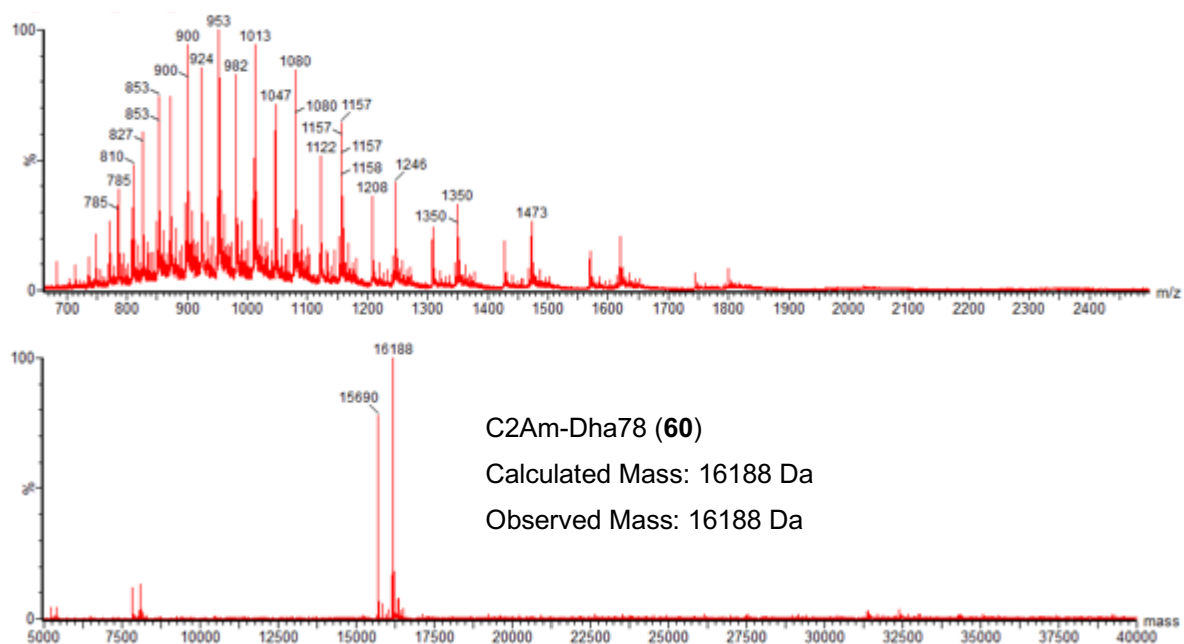
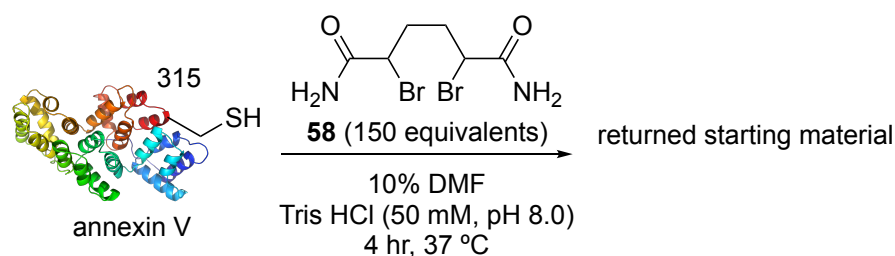


Figure S3.16 Ion series (top) and the deconvoluted mass spectrum (bottom) obtained from LC-MS analysis at 24 hr.

3.6.6 Chemical modifications of annexin V

Addition of **58** to annexin V



To a solution of annexin V (20 μ L, 27 μ M) in a 0.5 mL Eppendorf tube was added a solution of **58** (2 μ L, 40 μ M) in DMF. The solution was vortexed and left to react at 37 °C with shaking. After 4 hr, a 10 μ L aliquot was analysed directly by LC-MS. Only returned starting material was observed (calculated mass: 35805 Da, observed mass: 35807 Da).

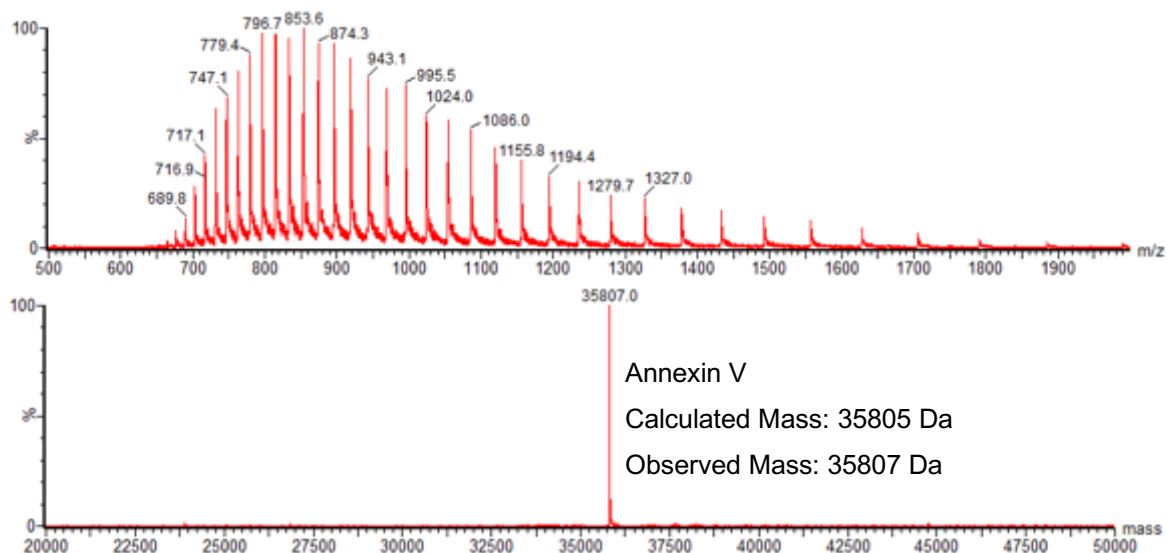
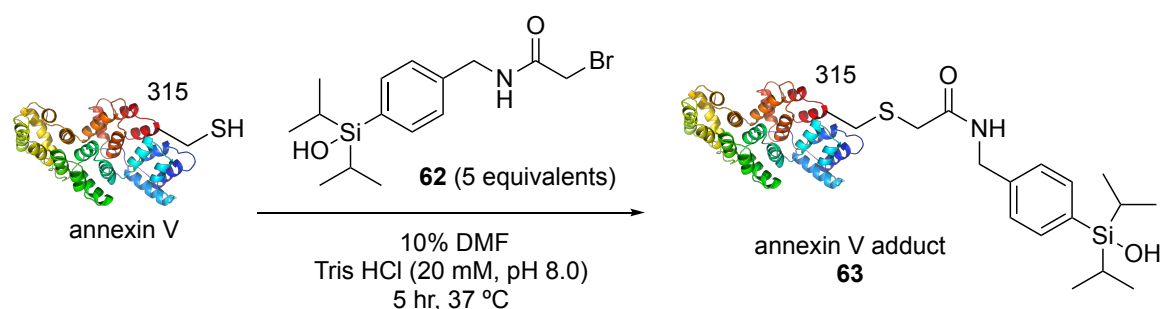


Figure S3.17 Ion series (top) and the deconvoluted mass spectrum (bottom) obtained from LC-MS analysis at 4 hr.

Addition of **62** to annexin V

5 equivalents of **62**, 10 % DMF



To a solution of annexin V (20 μ L, 27 μ M) in a 0.5 mL Eppendorf tube was added a solution of **62** (2 μ L, 1.35 mM) in DMF, final protein concentration 24.5 μ M. The solution was vortexed and left to react at 37 °C with shaking. After 5 hr, a 10 μ L aliquot was analysed directly by LC-MS and returned starting material was observed (calculated mass: 35805 Da, observed mass: 35806 Da).

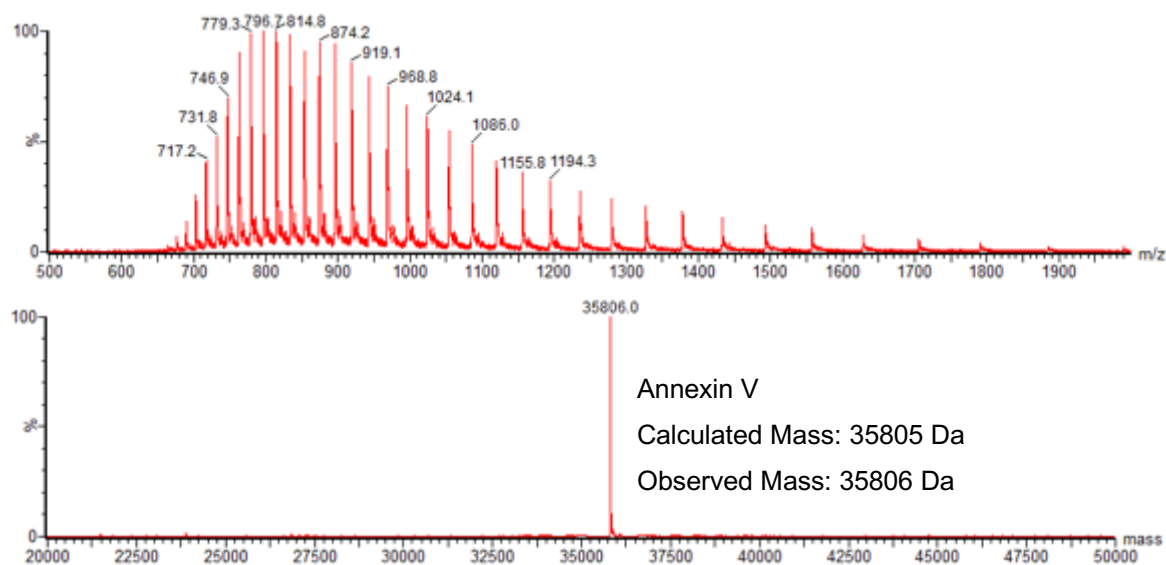
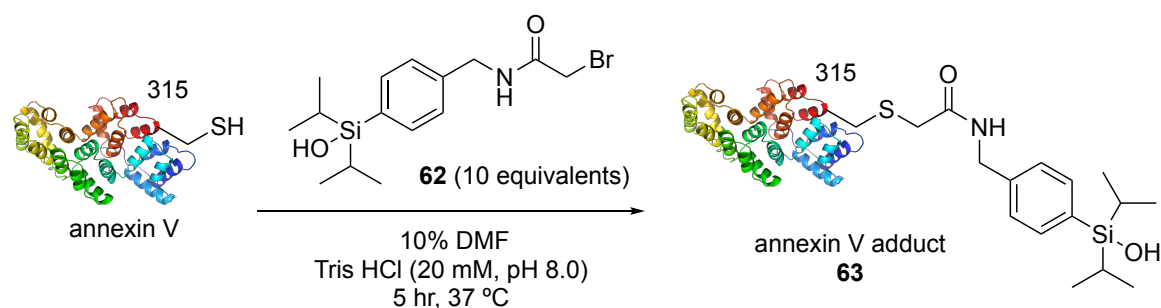


Figure S3.18 Ion series (top) and the deconvoluted mass spectrum (bottom) obtained from LC-MS analysis at 5 hr.

10 equivalents of **62**, 10 % DMF



To a solution of annexin V (20 μ L, 27 μ M) in a 0.5 mL Eppendorf tube was added a solution of **62** (2 μ L, 2.71 mM) in DMF, final protein concentration 24.5 μ M. The solution was vortexed and left to react at 37 °C with shaking. After 5 hr, a 10 μ L aliquot was analysed directly by LC-MS and returned starting material was observed (calculated mass: 35805 Da, observed mass: 35805 Da).

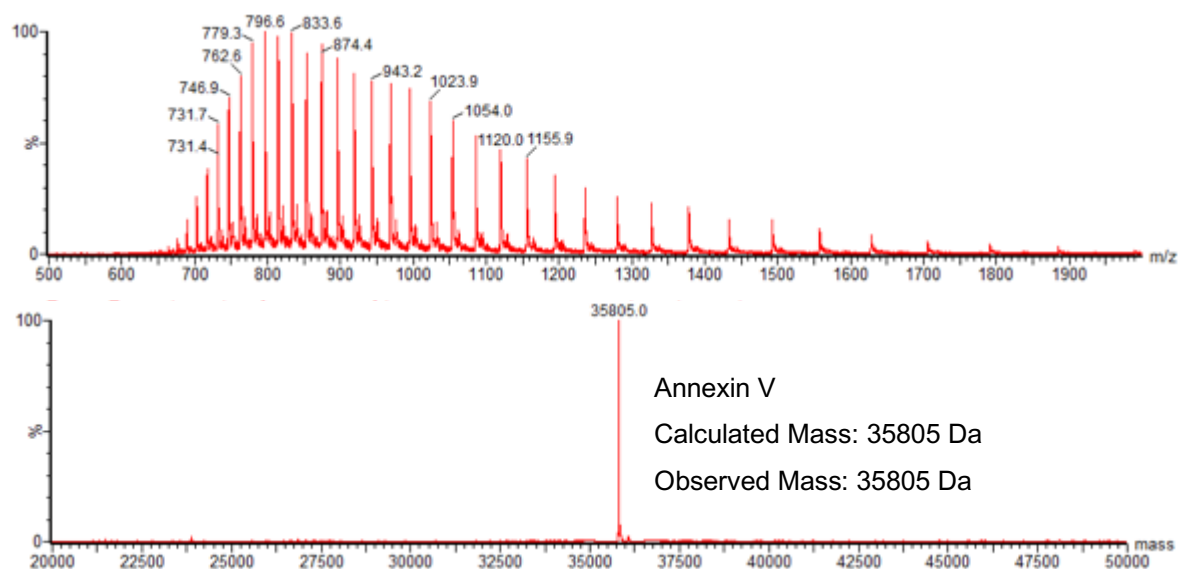
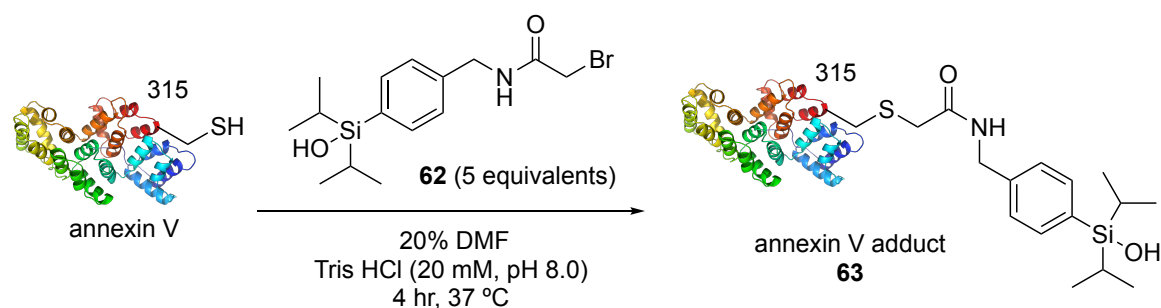


Figure S3.19 Ion series (top) and the deconvoluted mass spectrum (bottom) obtained from LC-MS analysis at 5 hr.

5 equivalents of **62**, 20 % DMF



To a solution of annexin V (20 μ L, 27 μ M) in a 0.5 mL Eppendorf tube was added a solution of **62** (4 μ L, 0.73 mM) in DMF, final protein concentration 22.5 μ M. The solution was vortexed and left to react at 37 °C with shaking. After 4 hr, a 10 μ L aliquot was analysed directly by LC-MS and the expected annexin V adduct, **63** was observed (calculated mass: 35083 Da, observed mass: 35083 Da).

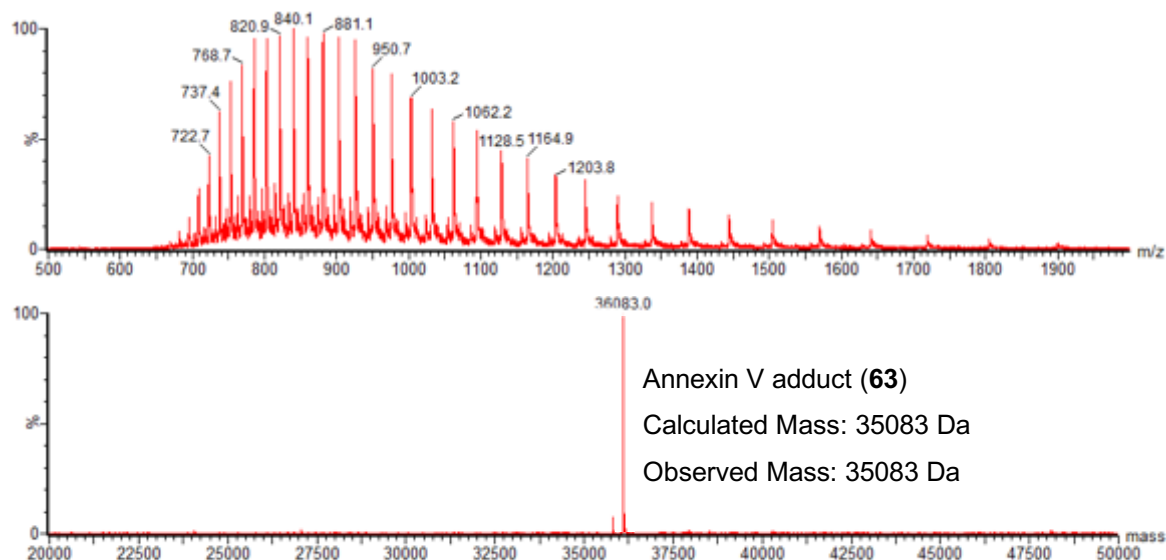
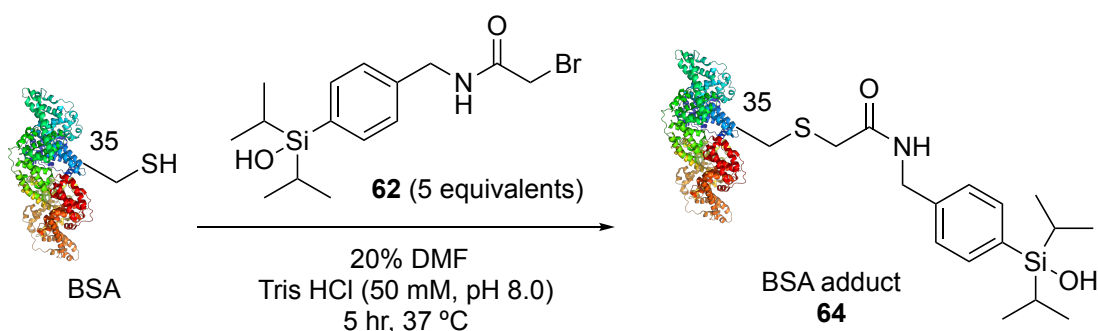


Figure S3.20 Ion series (top) and the deconvoluted mass spectrum (bottom) obtained from LC-MS analysis at 4 hr.

3.6.7 Chemical modifications of BSA

Addition of 5 equivalents of **62**, 20 % DMF



A solution of BSA (8 μ L, 30 μ M) was diluted with Tris HCl buffer (13.6 μ L, 50 mM, pH 8.0) in a 0.5 mL Eppendorf tube to a final protein concentration of 10 μ M. A solution of **62** (1 μ L, 0.2 mM) in DMF was added. The solution was vortexed and left to react at 37 $^{\circ}$ C with shaking. After 5 hr, a 10 μ L aliquot was analysed directly by LC-MS with multiple modifications observed.

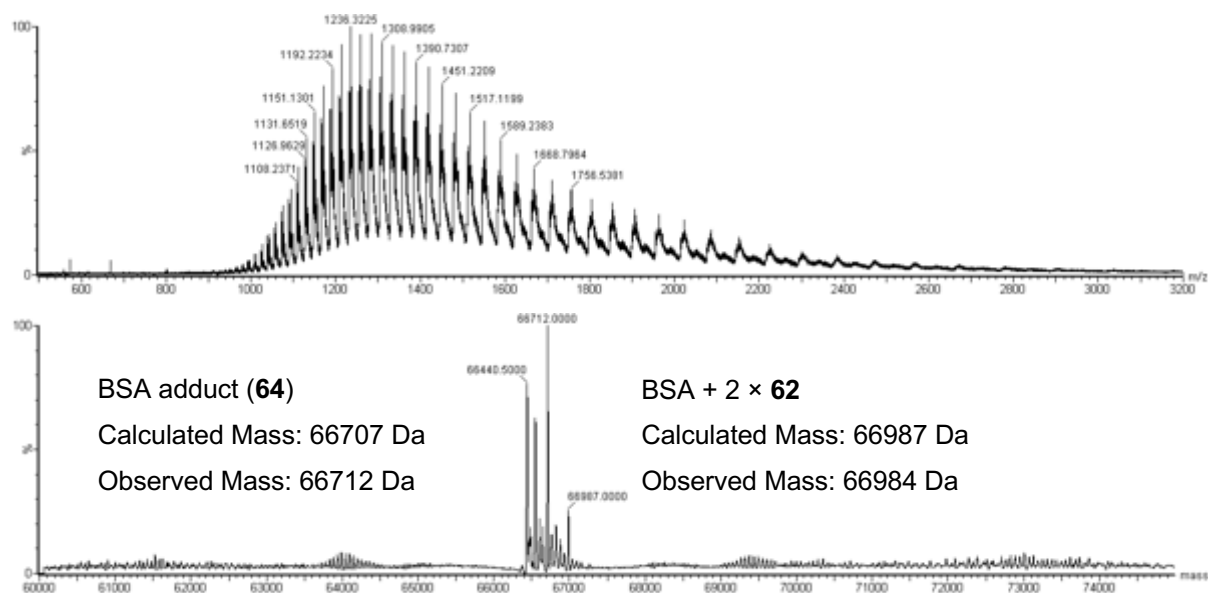
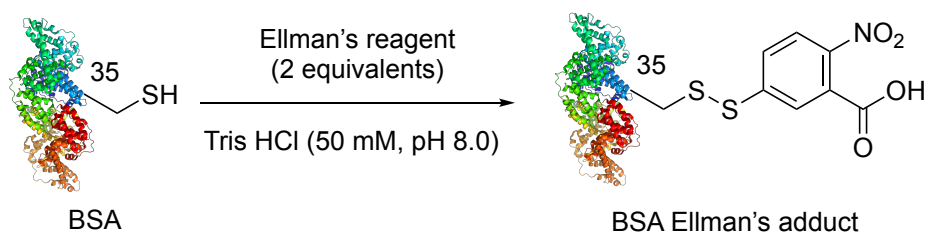


Figure S3.21 Ion series (top) and the deconvoluted mass spectrum (bottom) obtained from LC-MS analysis at 5 hr.

Addition of 2 equivalents of Ellman's reagent, no DMF



A solution of BSA (5 μ L, 30 μ M) was diluted with Tris HCl buffer (44.8 μ L, 50 mM, pH 8.0) in a 0.5 mL Eppendorf tube to a final protein concentration of 3 μ M. A solution of Ellman's reagent (0.12 μ L, 2.5 mM) in DMF was added. A 10 μ L aliquot was analysed directly by LC-MS with a single addition of Ellman's to BSA was observed (calculated mass: 66626 Da, observed mass: 66626 Da).

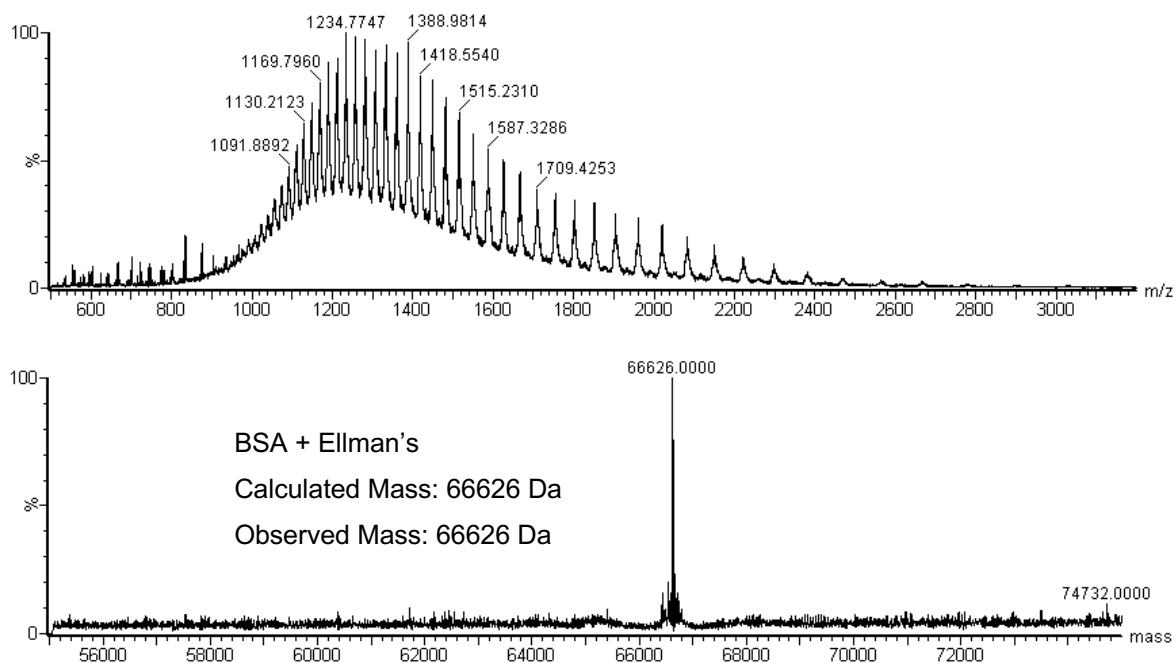
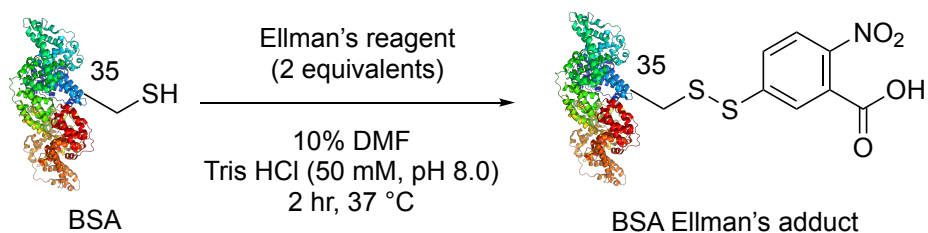


Figure S3.22 Ion series (top) and the deconvoluted mass spectrum (bottom) obtained from LC-MS analysis.

Addition of 2 equivalents of Ellman's reagent, 10% DMF



A solution of BSA (5 μ L, 30 μ M) was diluted with Tris HCl buffer (39.8 μ L, 50 mM, pH 8.0) and DMF (5 μ L) in a 0.5 mL Eppendorf tube to a final protein concentration of 3 μ M. A solution of Ellman's reagent (0.12 μ L, 2.5 mM) in DMF was added. The solution was vortexed and left to react at 37 °C with shaking. After 2 hr, a 10 μ L aliquot was analysed directly by LC-MS with a single addition of Ellman's to BSA observed (calculated mass: 66626 Da, observed mass: 66625 Da).

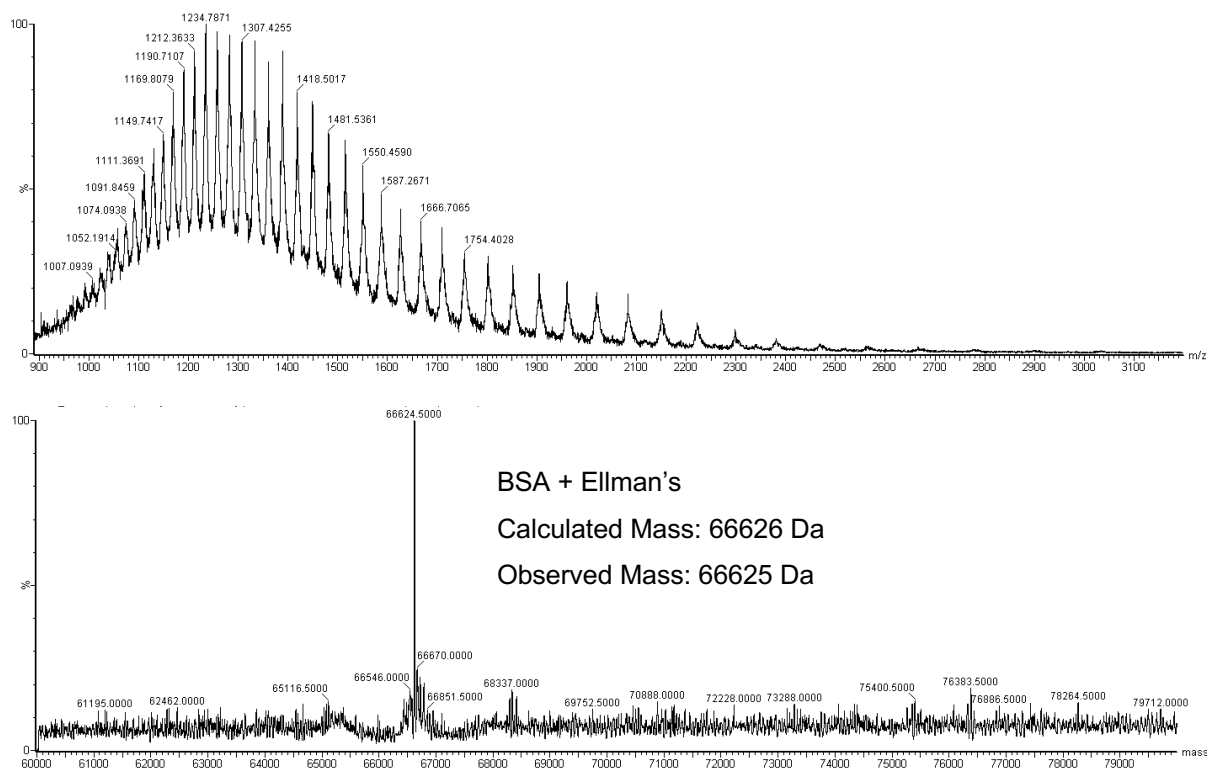
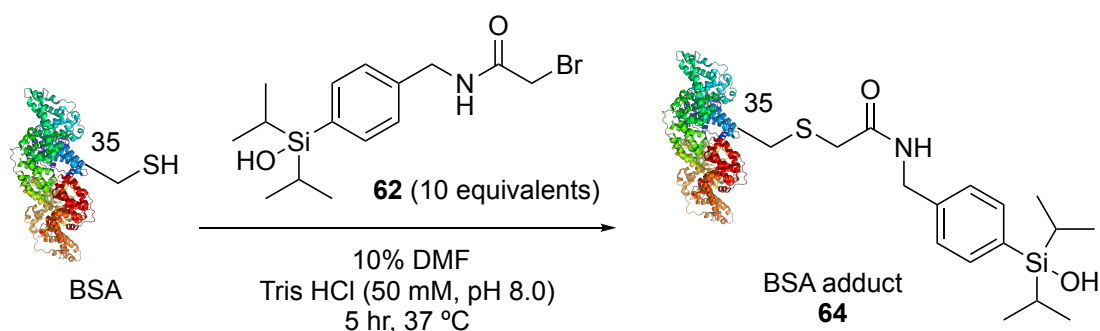


Figure S3.23 Ion series (top) and the deconvoluted mass spectrum (bottom) obtained from LC-MS analysis at 2 hr.

Addition of 10 equivalents of **62**, 10 % DMF



A solution of BSA (8 μ L, 30 μ M) was diluted with Tris HCl buffer (13.6 μ L, 50 mM, pH 8.0) and DMF (3.8 μ L) in a 0.5 mL Eppendorf tube to a final protein concentration of 10 μ M. A solution of **62** (2 μ L, 0.2 mM) in DMF was added. The solution was vortexed and left to react at 37 °C with shaking. After 5 hr, a 10 μ L aliquot was analysed directly by LC-MS. Partial conversion was observed (**64** calculated mass: 66707 Da, observed mass: 66709 Da.) as well as two unknown impurities at 66546 Da and 66601 Da.

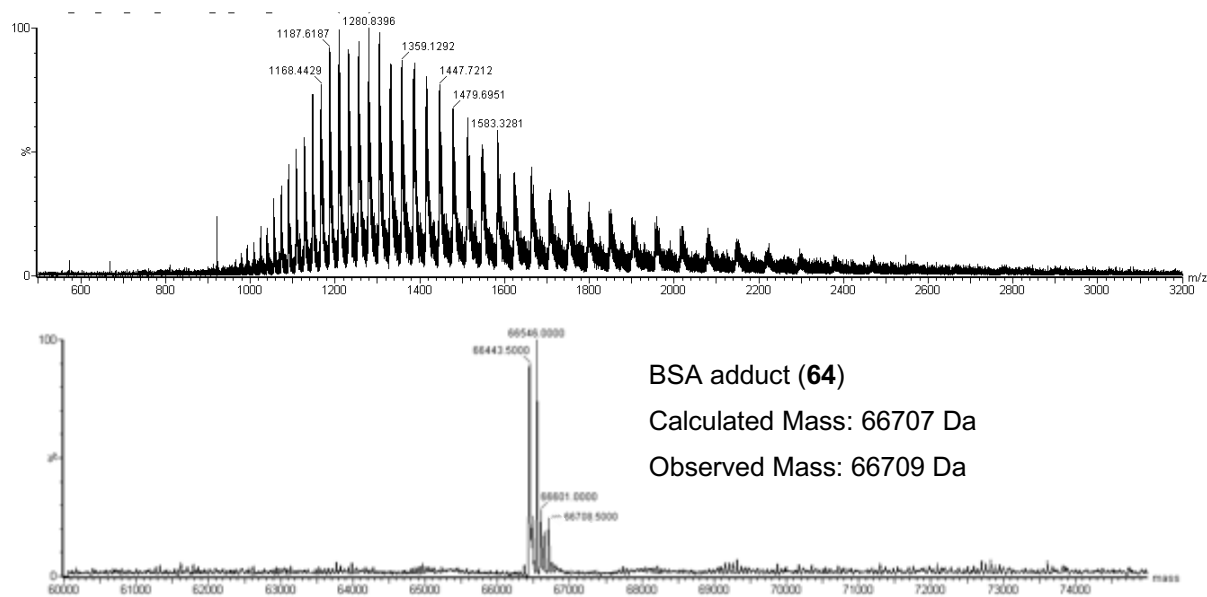
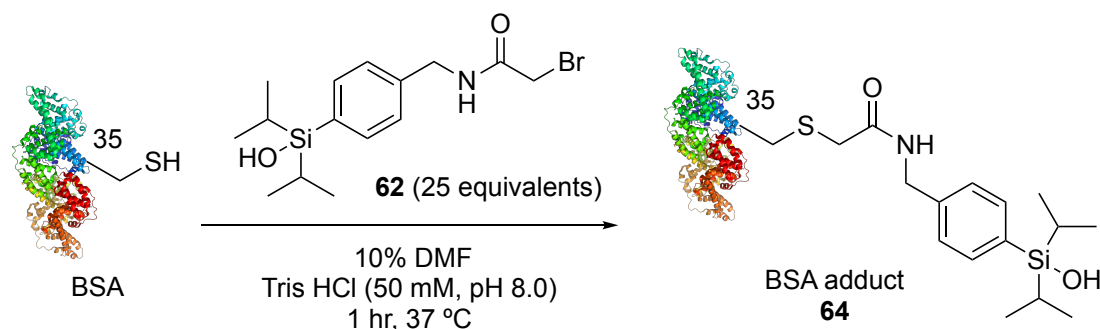


Figure S3.24 Ion series (top) and the deconvoluted mass spectrum (bottom) obtained from LC-MS analysis at 5 hr.

Addition of 25 equivalents of **62**, 10 % DMF



A solution of BSA (33.3 μ L, 30 μ M) was diluted with Tris HCl buffer (56.7 μ L, 50 mM, pH 8.0) and DMF (7.5 μ L) in a 0.5 mL Eppendorf tube to a final protein concentration of 10 μ M. A solution of **62** (2.5 μ L, 10 mM) in DMF was added. The solution was vortexed and left to react at 37 °C with shaking. After 1 hr, a 10 μ L aliquot was analysed directly by LC-MS. Multiple modifications were observed; BSA adduct **64** (calculated mass: 66707 Da, observed mass: 66719 Da), BSA + 2 \times **62** (calculated mass: 66987 Da, observed mass: 66996 Da).

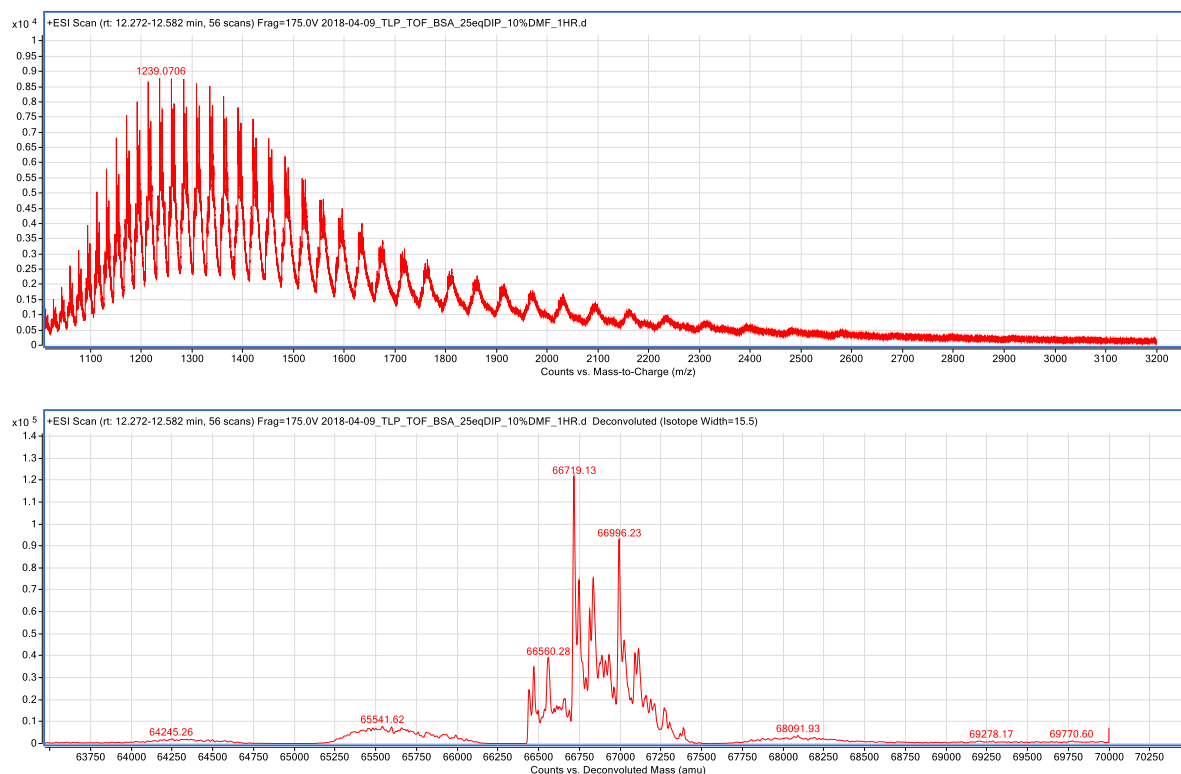
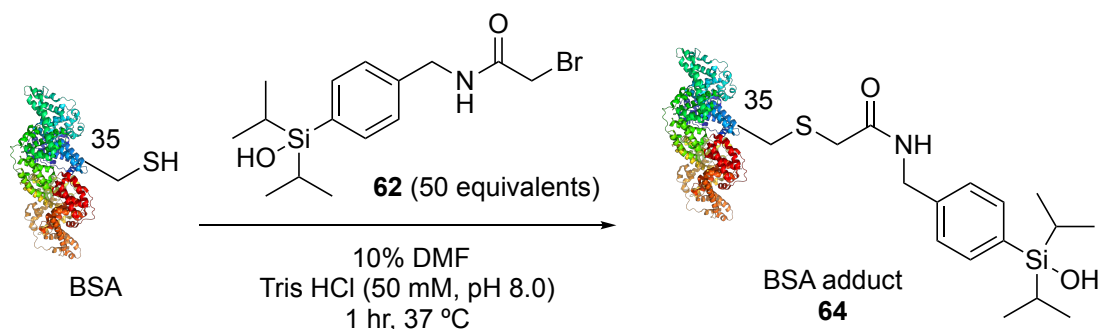


Figure S3.25 Ion series (top) and the deconvoluted mass spectrum (bottom) obtained from LC-MS analysis at 1 hr.

Addition of 50 equivalents of **62**, 10 % DMF



A solution of BSA (33.3 μ L, 30 μ M) was diluted with Tris HCl buffer (56.7 μ L, 50 mM, pH 8.0) and DMF (5 μ L) in a 0.5 mL Eppendorf tube to a final protein concentration of 10 μ M. A solution of **62** (5 μ L, 10 mM) in DMF was added. The solution was vortexed and left to react at 37 °C with shaking. After 1 hr, a 10 μ L aliquot was analysed directly by LC-MS. Multiple modifications were observed; BSA adduct **64** (calculated mass: 66707 Da, observed mass: 66720 Da), BSA + 2 \times **62** (calculated mass: 66987 Da, observed mass: 66996 Da), BSA + 3 \times **62** (calculated mass: 67264 Da, observed mass: 67273 Da), BSA + 4 \times **62** (calculated mass: 67543 Da, observed mass: 67551 Da) and BSA + 5 \times **62** (calculated mass: 67820 Da, observed mass: 67828 Da).

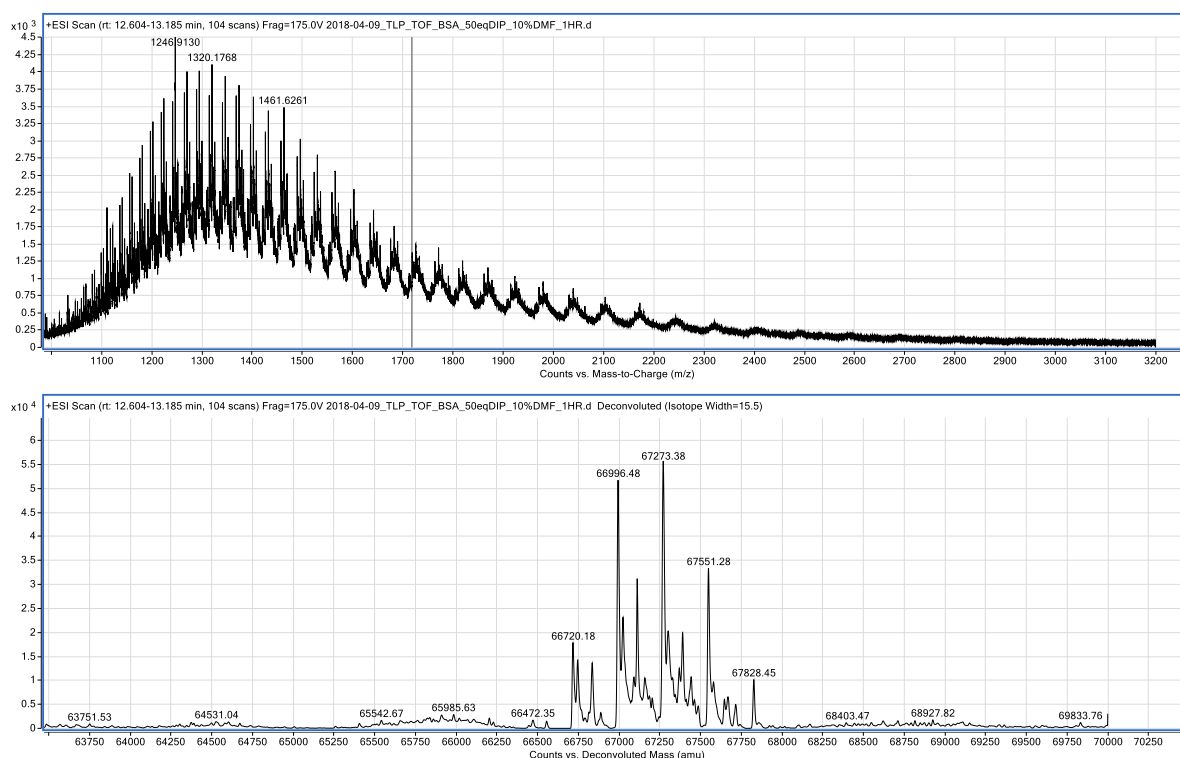
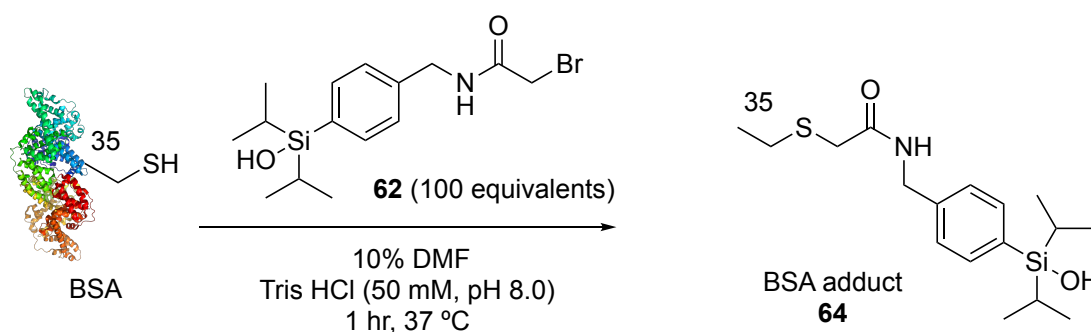


Figure S3.26 Ion series (top) and the deconvoluted mass spectrum (bottom) obtained from LC-MS analysis at 1 hr.

Addition of 100 equivalents of **62**, 10 % DMF



A solution of BSA (33.3 μ L, 30 μ M) was diluted with Tris HCl buffer (56.7 μ L, 50 mM, pH 8.0) in a 0.5 mL Eppendorf tube to a final protein concentration of 10 μ M. A solution of **62** (10 μ L, 10 mM) in DMF was added. The solution was vortexed and left to react at 37 °C with shaking. After 1 hr, a 10 μ L aliquot was analysed directly by LC-MS. Multiple modifications were observed; BSA + 2 \times **62** (calculated mass: 66987 Da, observed mass: 66997 Da), BSA + 3 \times **62** (calculated mass: 67264 Da, observed mass: 67274 Da), BSA + 4 \times **62** (calculated mass: 67543 Da, observed mass: 67551 Da), BSA + 5 \times **62** (calculated mass: 67820 Da, observed mass: 67828 Da), BSA + 6 \times **62** (calculated mass: 68099 Da, observed mass: 68105 Da), BSA + 7 \times **62** (calculated mass: 68376 Da, observed mass: 68385 Da) and BSA + 8 \times **62** (calculated mass: 68655 Da, observed mass: 68662 Da).

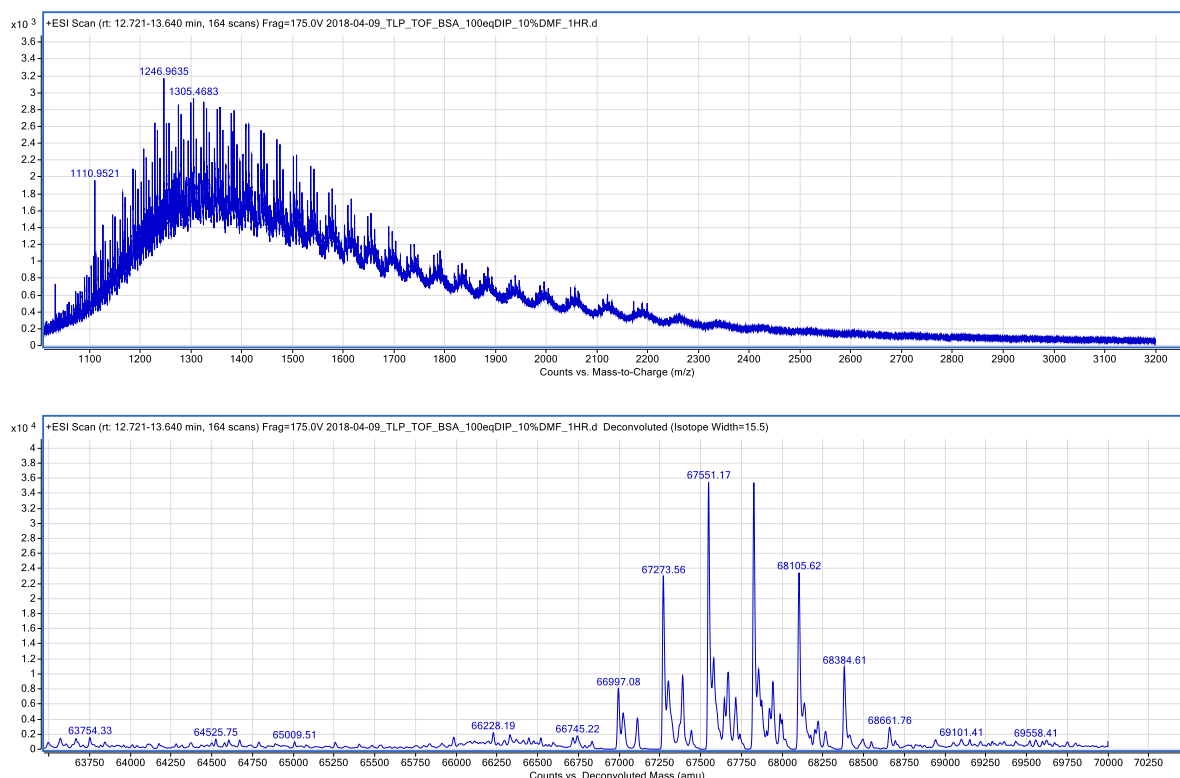
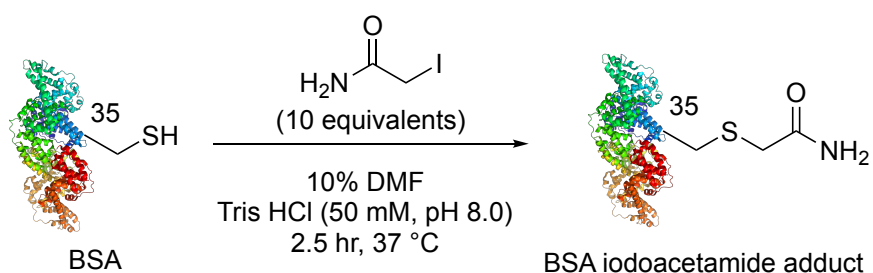


Figure S3.27 Ion series (top) and the deconvoluted mass spectrum (bottom) obtained from LC-MS analysis at 1 hr.

Addition of iodoacetamide, 10% DMF



A solution of BSA (5 μ L, 30 μ M) was diluted with Tris HCl buffer (39.8 μ L, 50 mM, pH 8.0) and DMF (5 μ L) in a 0.5 mL Eppendorf tube to a final protein concentration of 3 μ M. A solution of Ellman's reagent (0.12 μ L, 2.5 mM) in DMF was added. The solution was vortexed and left to react at 37 $^{\circ}$ C with shaking. After 2.5 hr, a 10 μ L aliquot was analysed directly by LC-MS with a single addition of iodoacetamide to BSA observed (calculated mass: 66487 Da, observed mass: 66485 Da).

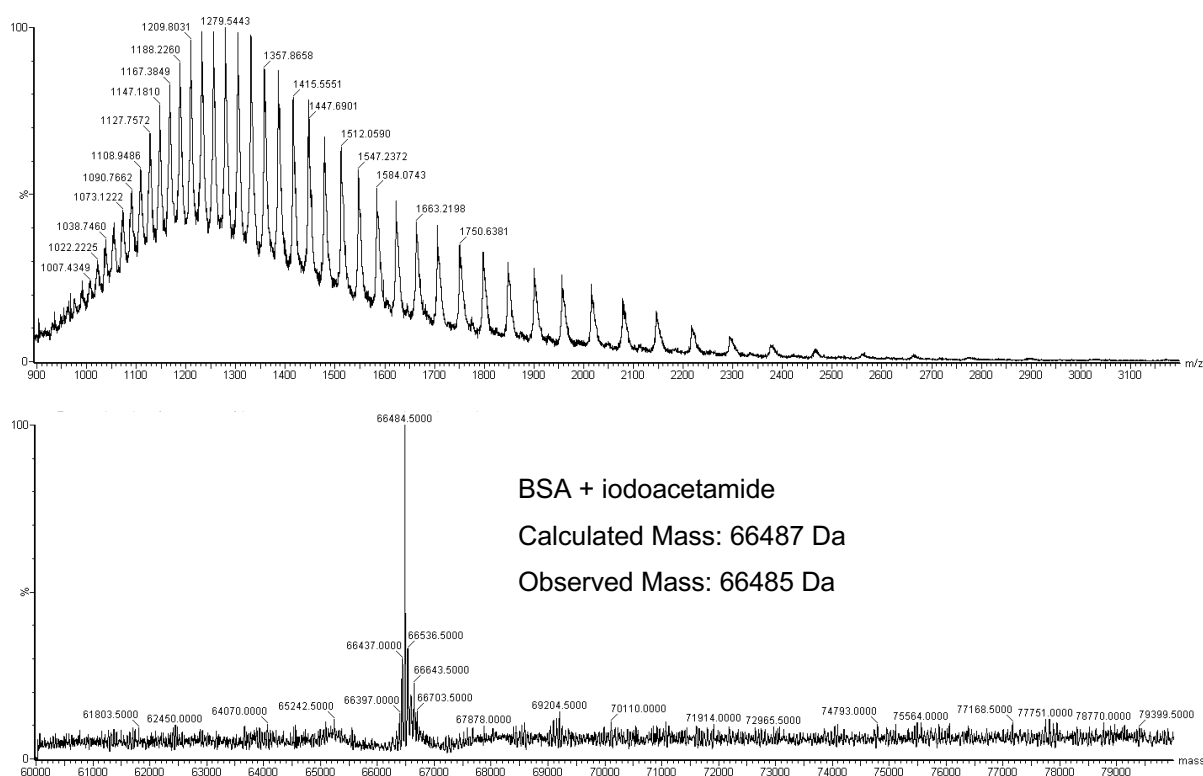
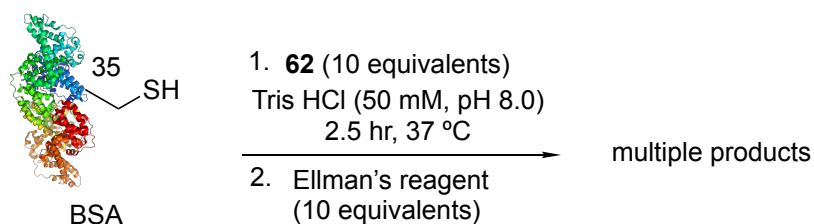


Figure S3.28 Ion series (top) and the deconvoluted mass spectrum (bottom) obtained from LC-MS analysis at 2.5 hr.

Addition of **62** followed by Ellman's reagent



A solution of BSA (5 μ L, 30 μ M) was diluted with Tris HCl buffer (43.8 μ L, 50 mM, pH 8.0) in a 0.5 mL Eppendorf tube to a final protein concentration of 3 μ M. A solution of **62** (0.6 μ L, 2.5 mM) in DMF was added and the solution vortexed and left to react at 37 °C with shaking. After 2.5 hr, a solution of Ellman's reagent (0.6 μ L, 2.5 mM) in DMF. The solution was vortexed and a 10 μ L aliquot was analysed directly by LC-MS with multiple products observed; BSA + Ellman's (calculated mass: 66626 Da, observed mass: 66624 Da), BSA + **62** + Ellman's (calculated mass: 67905 Da, observed mass: 66902 Da) and BSA + 2 \times **62** + Ellman's (calculated mass: 67178 Da, observed mass: 67178 Da).

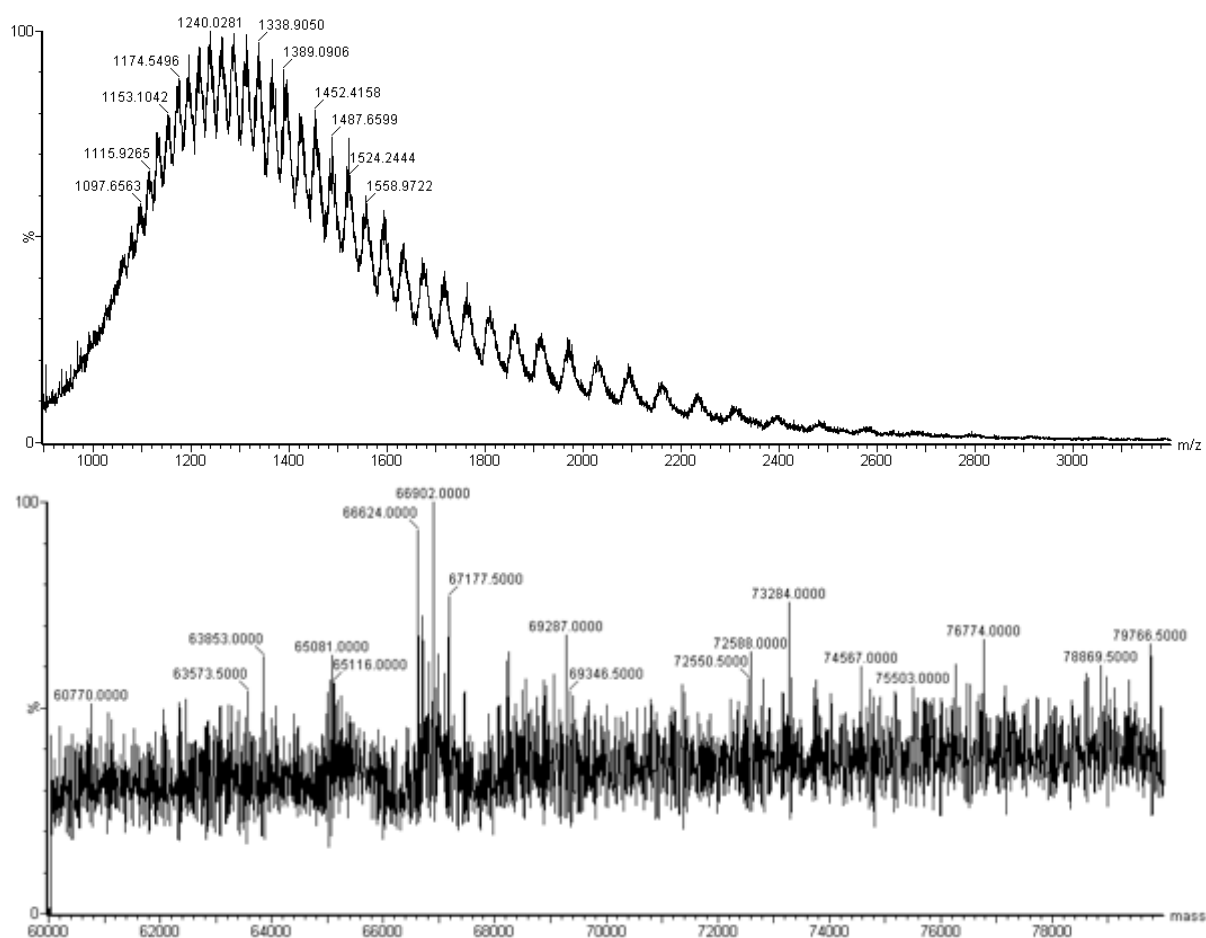
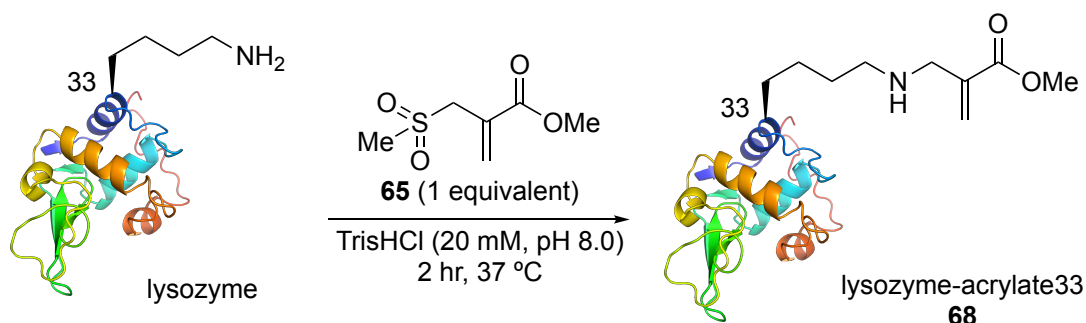


Figure S3.29 Ion series (top) and the deconvoluted mass spectrum (bottom) obtained from LC-MS analysis at 2.5 hr.

3.6.8 Chemical modifications of lysozyme

Addition of **65** to lysozyme



Lower concentration for LC-MS analysis

A solution of lysozyme (5.7 μL , 69.93 μM) was diluted with Tris HCl buffer (30.3 μL , 20 mM, pH 8.0) was in a 0.5 mL Eppendorf tube to a final protein concentration of 9.97 μM . To the solution **65** (0.7 μL , 0.560 mM) in DMF was added. The solution was vortexed and left to react at 37 °C. The reaction was monitored at time points by direct analysis by LC-MS of a 10 μL aliquot. After 2 hr, full conversion to lysozyme-acrylate33 (**68**, calculated mass: 14403 Da, observed mass: 14403 Da) was observed. This experiment was performed by Maria Matos.

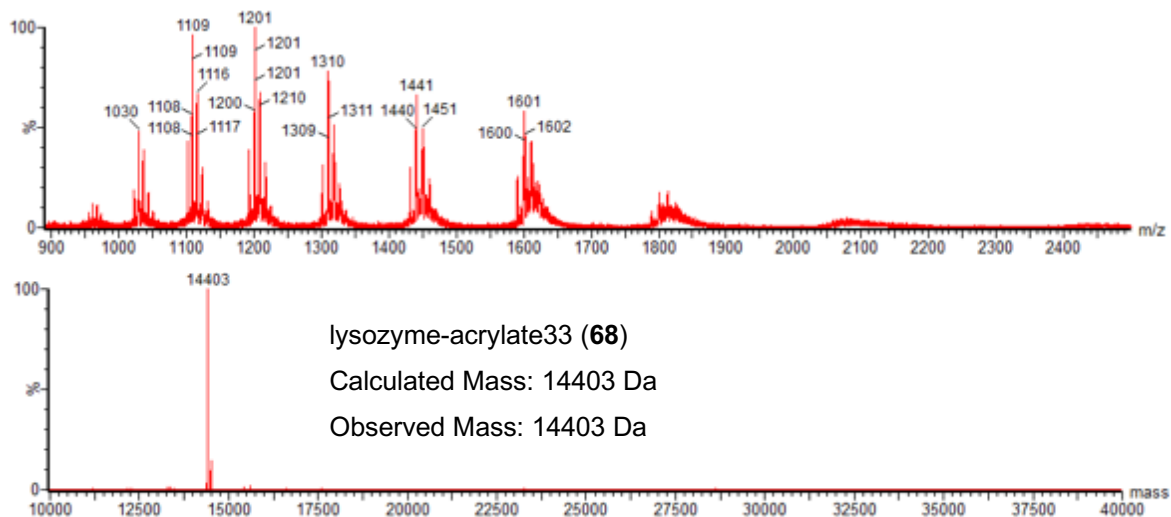
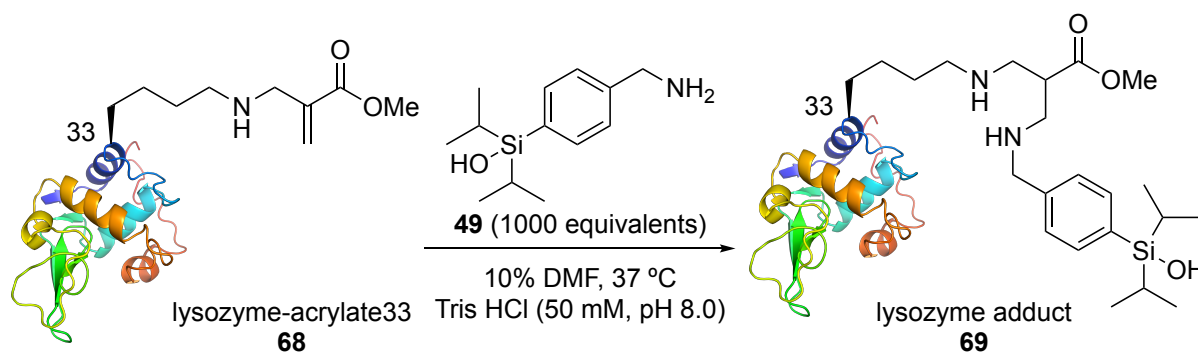


Figure S3.30 Ion series (top) and the deconvoluted mass spectrum (bottom) obtained from LC-MS analysis at 2 hr.

Higher concentration for NMR analysis

A solution of lysozyme (215 μL , 699 μM) was diluted with Tris HCl buffer (32 μL , 20 mM, pH 8.0) was in a 1.5 mL Eppendorf tube to a final protein concentration of 9.97 μM . To the solution, **65** (53.5 μL) was added. The mixture was vortexed and left to react at 37 $^{\circ}\text{C}$ for 6 hr. The resulting product was used in the next step without purification nor was it analysed by LC-MS.

Addition of **49** to lysozyme-acrylate33



Lower concentration for LC-MS analysis

To a solution of **68** (100 μL , 10 μM) in a 0.5 mL Eppendorf tube was added a solution of **49** (2.37 μL , 421 mM) in DMF. The solution was vortexed and left to react at 37 $^{\circ}\text{C}$ with shaking. After 3 hr a 10 μL aliquot was analysed directly by LC-MS. The masses observed corresponded to unreacted **48** (calculated mass: 14403 Da, observed mass: 14403 Da), the expected benzylamine adduct **69** (calculated mass: 14639 Da, observed mass: 14639 Da), **69** – 13 Da (**70**) likely due to demethylation of the methyl acrylate. The peak at 14652 was unidentified. A further 1000 equivalents of **49** (2.37 μL , 421 mM) was added to the reaction which was again vortexed and left at 37 $^{\circ}\text{C}$ with shaking. LC-MS analysis after a further 4 hr (7 hr total reaction time) showed the same peaks and an additional mass at 14304 Da corresponding to lysozyme.

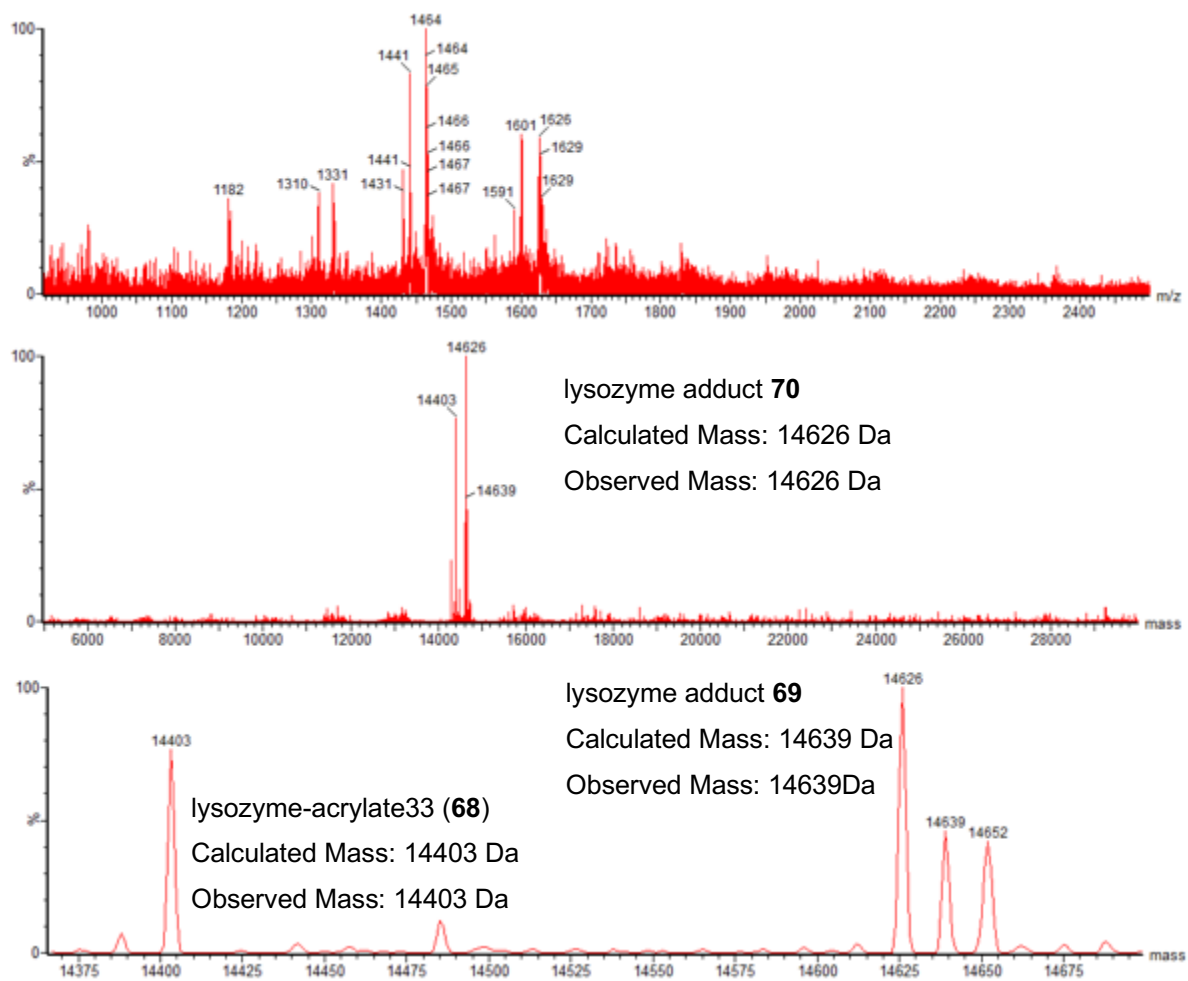


Figure S3.31 Ion series (top) and the deconvoluted mass spectrum (bottom) obtained from LC-MS analysis at 3 hr.

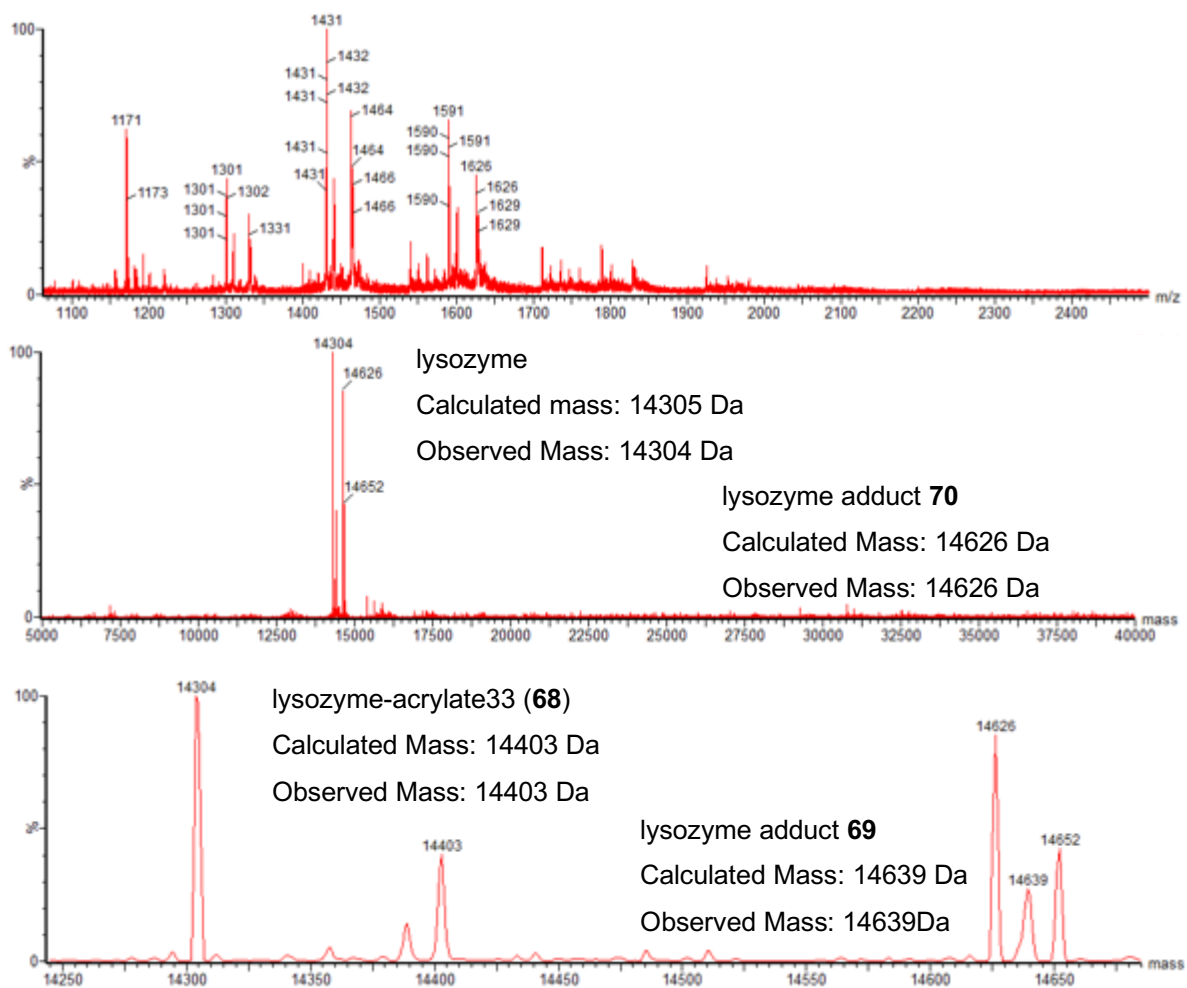


Figure S3.32 Ion series (top) and the deconvoluted mass spectrum (bottom) obtained from LC-MS analysis at 7 hr.

High concentration for NMR spectroscopy analysis

To a solution of **68** (300 μ L, 500 μ M) in a 1.5 mL Eppendorf tube was added a solution of **49** (30 μ L, 1.90 M, 380 eq.) in DMF as 5 μ L aliquots. The reaction was vortexed and left to react at 37 $^{\circ}$ C with shaking between additions for 35 min. Precipitation occurred from the first aliquot. After a total of 3.5 hr, a 2 μ L aliquot was diluted with 8 μ L of Tris HCl (20 mM, pH 8.0) and analysed by LC-MS. Full conversion to the lysozyme adduct **69** was observed with the product present as the carboxylate anion **70** (calculated mass: 16426 Da, observed mass: 16426 Da). A small amount of lysozyme was also present (calculated mass: 14403 Da, observed mass: 14403 Da) along with an unidentified peak at 14710 Da. The remaining small molecules were removed via sample purification with a Zeba size exclusion spin column (10 kDa MWCO).

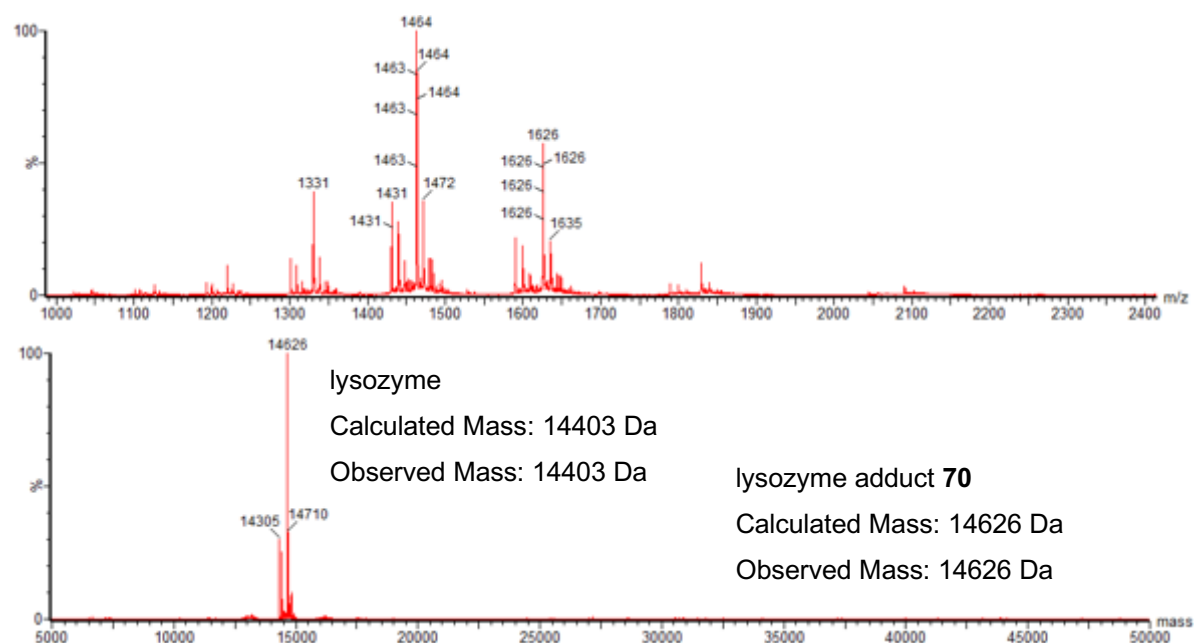


Figure S3.33 Ion series (top) and the deconvoluted mass spectrum (bottom) obtained from LC-MS analysis at 3.5 hr.

3.6.9 Direct fluorination of lysozyme

Fluorination control

A solution of lysozyme (10 μL , 69 μM) was diluted with Tris HCl (20 μL , 20 mM, pH 8.0) in a 0.5 mL Eppendorf tube to a final protein concentration of 23 μM . A solution of HF•Pyridine (0.2 μL , 10 mM, 10 eq.) in Tris HCl (20 mM, pH 8.0) was added. The solution was vortexed and left to react at 37 $^{\circ}\text{C}$. After 4 hr a 10 μL aliquot was analysed directly by LC-MS. No changes in the mass were observed.

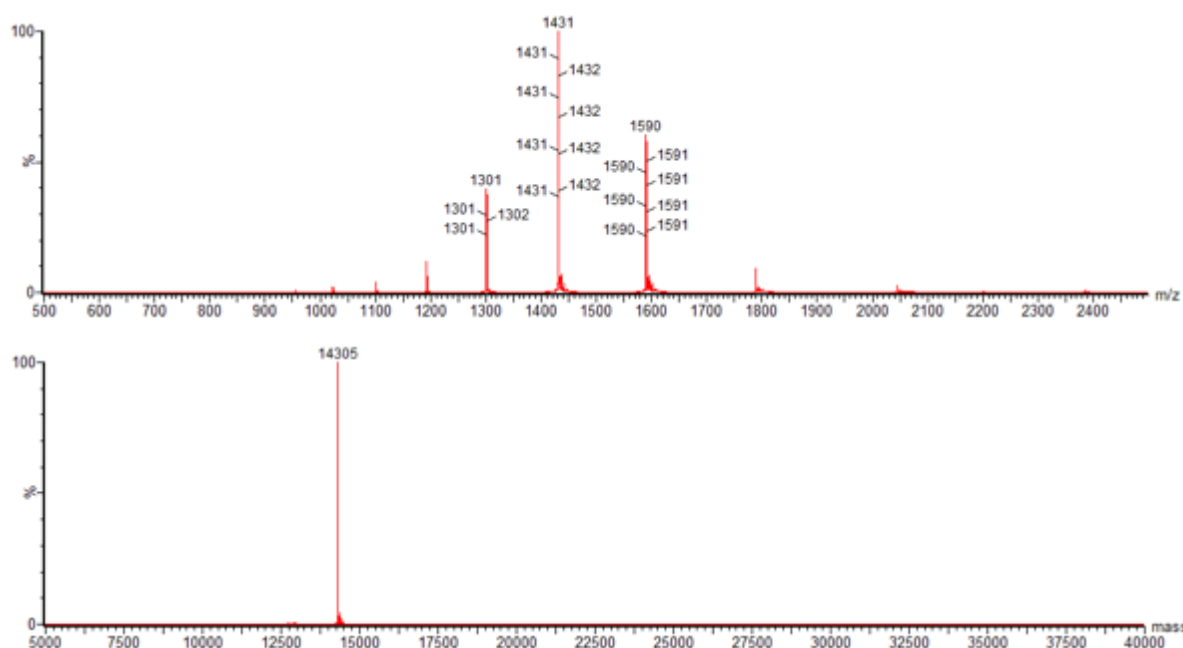
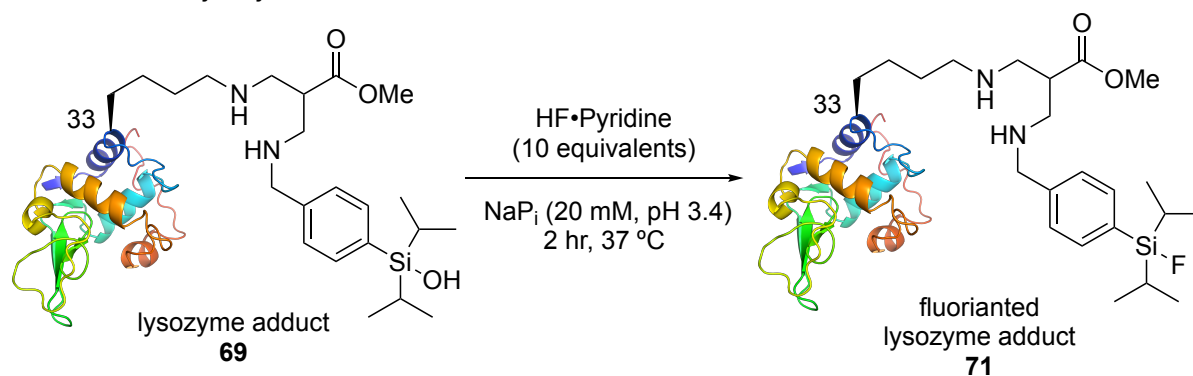


Figure S3.34 Ion series (top) and the deconvoluted mass spectrum (bottom) obtained from LC-MS analysis at 4 hr.

A solution of **68** (10 μL , 69 μM) was diluted with Tris HCl (20 μL , 20 mM, pH 8.0) in a 0.5 mL Eppendorf tube to a final protein concentration of 23 μM . A solution of HF•Pyridine (0.2 μL , 10 mM, 10 eq.) in Tris HCl (20 mM, pH 8.0) was added. The solution was vortexed and left to react at 37 $^{\circ}\text{C}$. After 4 hr a 10 μL aliquot was analysed directly by LC-MS. No changes in the mass were observed.

Fluorination of lysozyme adduct **69**



To a solution of **69** (270 μL , 417 μM) in NaP_i buffer (20 mM, pH 3.4) in a 1.5 mL Eppendorf tube was added a solution of $\text{HF}\cdot\text{Pyridine}$ (12.5 μL , 100 mM) in Tris HCl (20 mM, pH 8.0). The solution was vortexed and left to react at 37 $^\circ\text{C}$. After 2 hr the solution was transferred to FEP liner NMR tube and analysed by NMR spectroscopy. The ^{19}F NMR spectrum revealed the direct fluorination of lysozyme at silicon evident from a signal consistent with the formation of a Si-F bond at $\delta_{\text{F}} -184.98$ ppm.

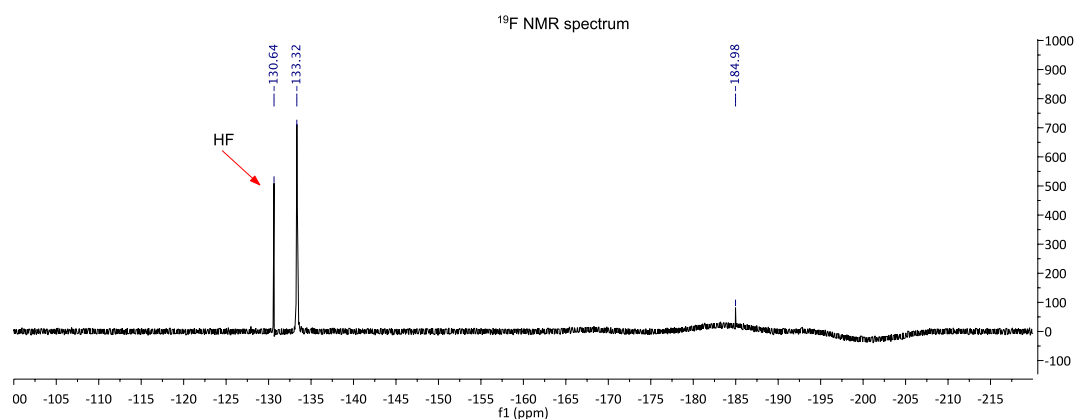


Figure S3.35 ^{19}F NMR spectrum after 2 hr at 37 $^\circ\text{C}$ pH 3.4.

The fluorination of **69** was repeated in Tris HCl (20 mM, pH 8.0). No signal consistent with Si-F bond formation was observed in the ^{19}F NMR spectrum.

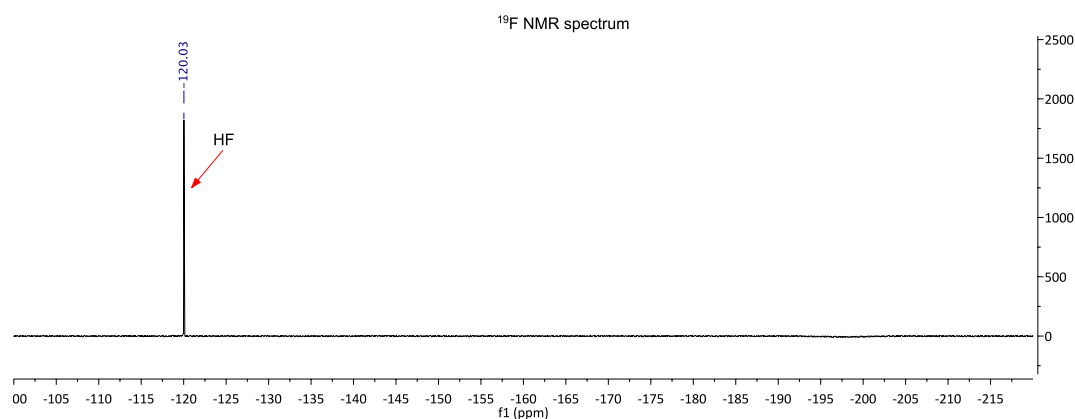


Figure S3.36 ^{19}F NMR spectrum after 2 hr at 37 $^\circ\text{C}$ pH 8.0.

Chapter Four

Design, synthesis and direct aqueous fluorination of a silanol-based amino acid

4.1 Introduction

In Chapter 3, a novel silanol was chemically incorporated into proteins site-selectively at both cysteine and lysine and it was shown that these modified proteins can be directly fluorinated under aqueous conditions. These results were reassuring, supporting our hypothesis that silanols could be used for the radiolabelling of proteins with fluorine-18. Issues arose however, with the general applicability of the modification methods to different proteins. To facilitate further studies into the direct fluorination of proteins through Si-F bond formation, a general method for the incorporation of the silanol is required.

Chapter 4 details the design and synthesis of a silanol-based amino acid for genetic incorporation into proteins. With a greater solubility in water, the fluorination of silanols in solution of up to 90% water was explored. Incorporation of this silanol-based amino acid into a protein is the topic of Chapter 5. Additionally, this Chapter reports an unexpected oxidative cleavage of a key aldehyde intermediate during the synthesis of the amino acid which resulted in the discovery of a novel reaction.

The candidate planned, researched, conducted and prepared the following Chapter with full intellectual and practical contributions unless otherwise stated in-text. Components of the work detailed in this Chapter, including the synthesis and fluorination of 2-amino[3-(4-diisopropylsilanol)phenyl]propanoic acid and the studies into the oxidative cleavage of homobenzyl alcohols, has previously been published in the peer reviewed journal *Peptide Science*, Wiley. This article was published on 13 March 2018 under the title 'A silicon-labelled amino acid suitable for late-stage fluorination and unexpected oxidative cleavage reactions in the preparation of a key intermediate in the Strecker synthesis' (DOI: 10.1002/pep.2.24069). The candidate is listed as the lead author of this publication.

4.2 Genetic incorporation of unnatural amino acids

Conserved across all organisms is the same genetic code that encodes the same 20 amino acids. Remarkably, these 20 amino acids have formed the basis of all life, however we now have the ability to expand this genetic code. By hijacking the translational machinery, unnatural amino acids that contain unique chemical handles can be incorporated into proteins produced *in vivo*. Over 200 unnatural amino acids have now been incorporated into proteins facilitating many new biological insights.¹²¹

A common method for the incorporation of unnatural amino acids *in vivo* involves the reassignment and suppression of the amber stop codon (TAG).¹⁶¹ This method requires a transfer RNA (tRNA) that recognises the amber codon and an aminoacyl-tRNA synthetase (aaRS) that can charge the tRNA with the unnatural amino acid. To guarantee that it is the unnatural amino acid and not one of the 20 endogenous amino acids that is incorporated in response to the amber codon; 1) the tRNA must not be aminoacylated by any of the endogenous aaRSs, 2) the aaRS must not aminoacylate any of the endogenous tRNAs and 3) the aaRS must only aminoacylate the tRNA with the unnatural amino acid and not any of the endogenous amino acids.¹⁶² That is to say that the tRNA/aaRS pair must be orthogonal.

One such pair that is orthogonal in *E.coli* is derived from the tyrosyl tRNA/aaRS pair of *Methanocaldococcus jannaschii* (*M.jannaschii*). Xie *et al.* evolved the amber suppressant tRNA_{CUA} from the wild type *M. jannaschii* tyrosyl tRNA which paired with the wild type *M. jannaschii* tyrosyl aaRS was found to be orthogonal and able to suppress the amber codon incorporating tyrosine.¹⁶³

This orthogonal tRNA_{CUA} has since been optimised to increase its efficiency in the production of proteins in bacteria¹⁶⁴ and a number of aaRS that charge this optimised orthogonal tRNA_{CUA} with different unnatural amino acids have been evolved from the libraries derived from the wild type *M. jannaschii* tyrosyl aaRS.¹⁶⁵⁻¹⁷¹

In the sections that follow, we present the synthesis of a silanol-based amino acid for incorporation into proteins using a *M. jannaschii* derived tRNA/aaRS pair. The evolution of an aaRS specifically for this unnatural amino acid and its incorporation into proteins is presented in Chapter 5.

4.3 Designing a silanol-based amino acid for genetic incorporation into proteins

In general, the greater the similarity between the unnatural amino acid and the endogenous amino acid that the wild type synthetase charges the tRNA with, the greater the chance of it being incorporated by a mutant aminoacyl-tRNA synthetase. Most established methods make use of the *M.jannaschii* tyrosyl-tRNA synthetases. Therefore, we proposed the tyrosine-like amino acid **72** (Figure 4.1).

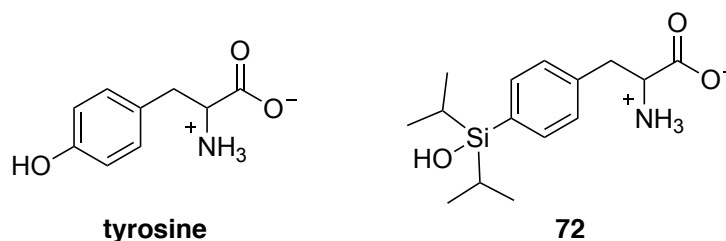
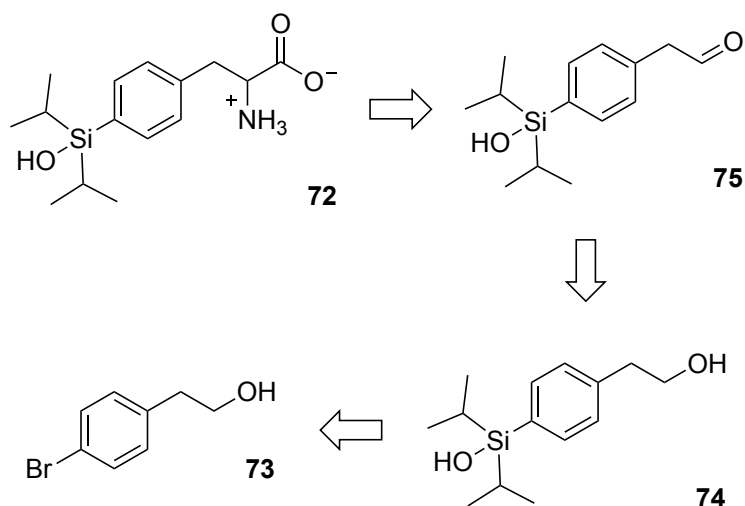


Figure 4.1 The unnatural amino acid **72** is based on the natural amino acid tyrosine in which the hydroxyl group on the aromatic ring is replaced with a silanol group.

We envisioned that the silicon core of the amino acid could be built using the same robust and high yielding synthesis route used for the benzylamine **49**; lithium halogen exchange and silylation followed oxidation of the silane to the silanol. Starting for the homobenzylic alcohol **73** this would lead to the intermediate **74**. At this point oxidation of the homobenzylic alcohol would yield the key aldehyde **75** which could be converted to the amino acid using the Strecker synthesis (Scheme 4.1). We had confidence in this retrosynthesis as the oxidation of a homobenzylic alcohol to an aldehyde and conversion to the corresponding amino acid via the Strecker synthesis had previously been successfully used in the synthesis of a similar amino acid.¹⁷²



Scheme 4.1 Retrosynthetic analysis of the silanol-based amino acid **72**.

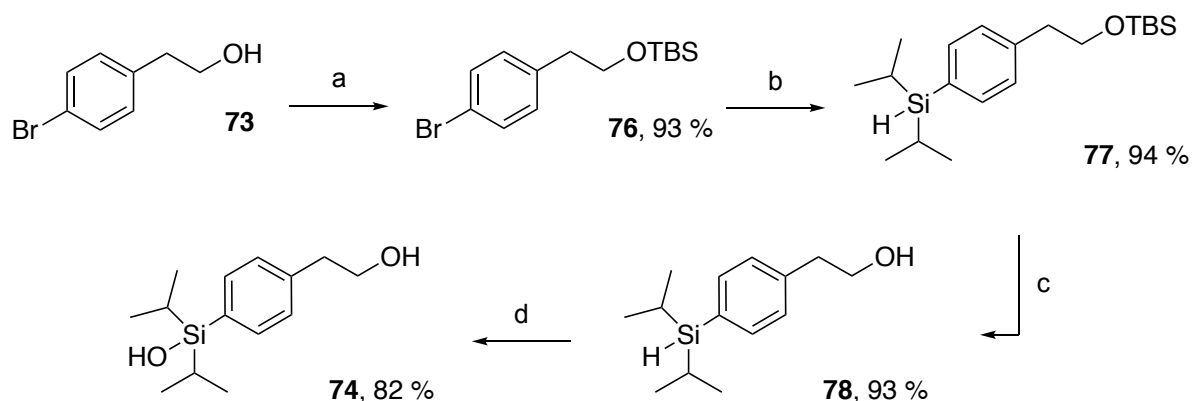
4.4 Synthesis of 2-amino[3-(4-diisopropylsilanol)phenyl]propanoic acid (**72**)

4.4.1 Installing the silicon core

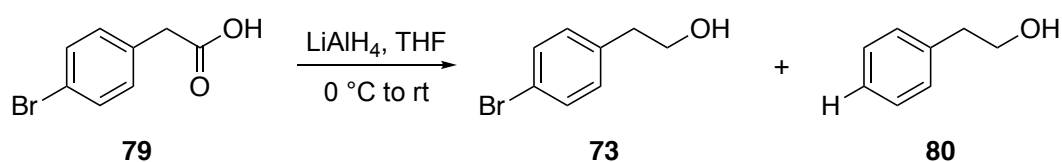
The synthesis began with protection of the primary alcohol, converting **73** to the silyl ether **76** by reacting the starting material with *tert*-butyldimethylsilyl chloride in dichloromethane overnight at ambient temperature. Using imidazole as the base and catalyst, **76** was isolated in 93% yield (Scheme 4.2). With the alcohol protected, next the silicon core was installed via a two-step procedure. First, the aryllithium was formed through lithium halogen exchange with *n*-BuLi at -78 °C. This was followed by silylation with diisopropylchlorosilane and **77** was isolated in 94% yield. The *tert*-butyldimethylsilyl protecting group was then removed under acidic conditions and the primary alcohol **78** was reformed in a 93% yield. Finally, the silane was oxidised to the silanol with methanol in a basic solution of water. The silanol **74** was obtained in an 82% yield.

While **73** is the desired starting material for the synthesis of **74**, it was financially advantageous to begin with the carboxylic acid **79**. The carboxylic acid derivative is commercially available at a tenth of the price of the alcohol and can be reduced using two equivalents of a reducing agent to give the desired starting material **73**. When we used LiAlH_4 as the reducing agent, the desired reduction to the alcohol occurred alongside halogen hydride exchange (Scheme 4.3). In all attempts no remaining carboxylic acid were observed. This indicates that halogen hydride exchange may be occurring in a second step when there is an excess of the

hydride used. Reducing the equivalents of LiAlH_4 to 1.2 and a shorter reaction time did not, however, reduce the extent to which **80** was forming.



Scheme 4.2 Synthesis of the silanol **74**. a) TBS-Cl, imidazole, CH_2Cl_2 , rt, 20 hr; b) *n*-BuLi in hexanes, THF, $-78\text{ }^\circ\text{C}$, 1 hr, then $i\text{Pr}_2\text{SiHCl}$, $-78\text{ }^\circ\text{C}$ to rt, 20 hr; c) HCl, H_2O , MeOH, rt, 16 hr; d) NaOH, H_2O , MeOH, $0\text{ }^\circ\text{C}$ to rt, 20 hr.



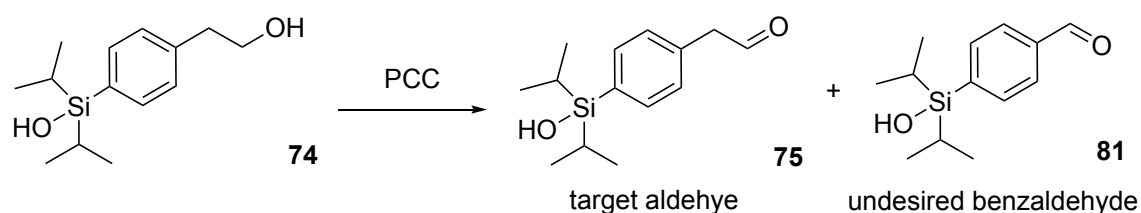
Scheme 4.3 Reduction of 4-bromophenylacetic acid with LiAlH_4 results in reduction of the carboxylic acid and halogen hydride exchange.

Unfortunately, **73** and **80** were found to be inseparable by column chromatography. When we took the mixture of **73** and **80** through the proceeding steps in the synthesis as described above (Scheme 4.2) we did find that **73** could be separated from **74** by column chromatography using 20% ethyl acetate in hexanes. Despite the formation of **80**, we found that it had minimal interference in the synthesis of **74**. As such, starting from the carboxylic acid is still financially favourable despite the occurrence of halogen hydride exchange. This was particularly true for the upscale of this synthesis to gram scale.

4.4.2 Oxidation studies of homobenzylic alcohols

With **74** in hand we next explored the oxidation of this homobenzylic alcohol to the key aldehyde **75**. Following work by Iovkova,¹⁷² we first attempted to oxidise the homobenzylic alcohol to the aldehyde using pyridinium chlorochromate (PCC). Using thin layer chromatography to track the reaction, complete conversion of the starting material was observed in 3 hours using

two equivalents of PCC. As expected, this led the conversion of **74** to the aldehyde **75**. Surprisingly however, oxidative C-C bond cleavage was also observed with the undesired benzaldehyde **81** formed alongside the expected aldehyde (Scheme 4.4).



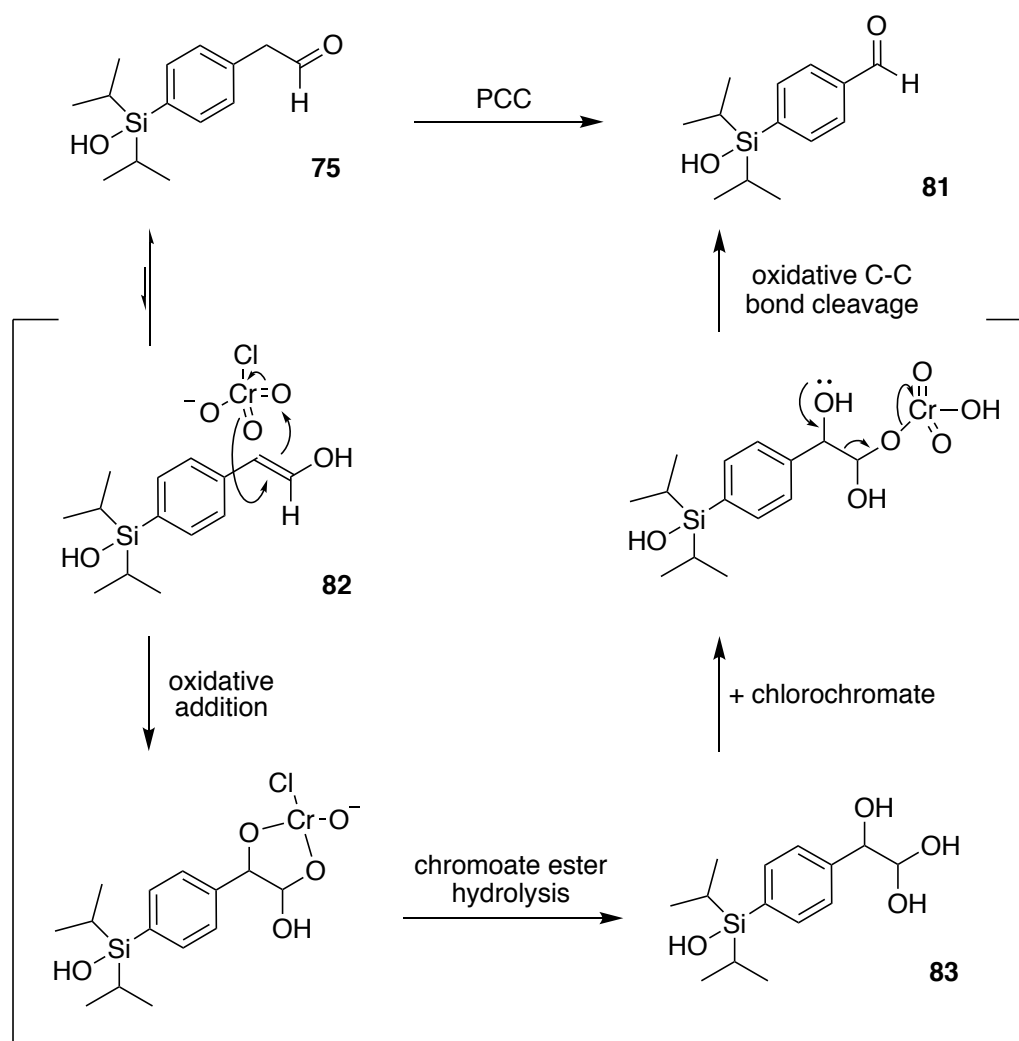
Scheme 4.4 PCC oxidation of **74** resulting in the expected oxidation to aldehyde **75** and the unexpected oxidative C-C cleavage to the benzaldehyde.

In attempts to avoid the benzaldehyde we tried this oxidation using only a single equivalent of PCC. In this case, the reaction gave the desired product **75** in good yields but conversion to the undesired benzaldehyde still occurred (Scheme 4.7, Entry 4). This result indicated that the benzaldehyde must form before complete consumption of the starting material. Noteworthy of this reaction was the high levels of conversion to the benzaldehyde that could be achieved. When using 2 equivalents of PCC, 27% was converted to **81** (Scheme 4.7, Entry 1). Increase the number of equivalents of PCC to 4, the conversion increased to 64% (Scheme 4.7, Entry 2). Further, doubling the reaction time to 6 hours resulted in 91% conversion (Scheme 4.7, Entry 3). Not unexpectedly, these high conversions were also seen with the less acidic pyridinium dichromate (PDC) (Scheme 4.7, Entry 5).

Whilst the formation of a benzaldehyde was not noted by Iovkova, despite very similar conditions and reactants, there is precedence for chromium-based oxidative C-C bond cleavage of homobenzylic alcohols.¹⁷³ The mechanism by which this occurs for homobenzylic alcohols has not been studied^{173,174} although, mechanistic studies of C-C bond cleavage with chromium(VI) reagents on other substrates have been published.¹⁷⁵⁻¹⁸¹

In accordance with literature, we suspected that the homobenzylic aldehyde **75** may be an intermediate in the conversion to **81**. As depicted in Scheme 4.5, it is presumed that the formation of **81** occurs through the oxidative addition of PCC across the C=C of the enol tautomer **82**. Oxidative fragmentation of the unstable chromate ester would then yield the benzaldehyde **81** releasing formic acid as a by-product.^{177,178} Alternatively, hydrolysis of the chromate ester

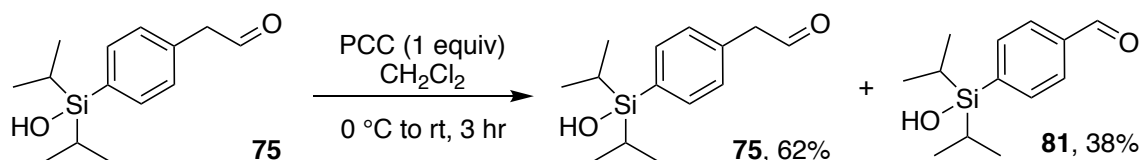
would yield the 1,1,2-triol **83**. Treatment with another equivalent of PCC would result in C–C bond cleavage also yielding the benzaldehyde and formic acid.^{182,183}



Scheme 4.5 Proposed mechanism for PCC mediated C–C oxidative cleavage of the homobenzyl aldehyde **75**.

In an attempt to elucidate more information about the mechanism, we first treated **75** with PCC and observed for the formation of **81**. With a single equivalent of PCC 38% of **75** was converted to the benzaldehyde **81** after 3 hours (Scheme 4.6) indicating that indeed, **75** acts as an intermediate. With a conservative conversion rate of only 38% it may be plausible that more than one equivalent is used in the reaction mechanism indicating chromoate ester hydrolysis. We next ran the same experiment in deuterated dichloromethane (CD_2Cl_2) and followed the reaction via ^1H NMR looking for evidence towards the formation of formic acid and/or **83**. Neither were detected in the ^1H NMR spectra collected at intervals of 60 seconds over 1.5 hours. The absence

of formic acid is most likely due to its decomposition to H₂ and CO₂ as has been identified in oxidative C-C bond cleavage using alternative oxidants.^{184,185} No testing to identify H₂ or CO₂ was performed. No evidence of **83** in the ¹H NMR spectra alludes to oxidative fragmentation rather than chromate ester hydrolysis. With two opposing results, further analysis would be required to completely eliminate either of the proposed mechanistic pathways.



Scheme 4.6 Treatment of the homobenzyl aldehyde **75** with PCC results in oxidative C-C cleavage.

Similar retention factors for **75** and **81** made separation via column chromatography difficult and even a slight amount of **81** proved problematic. Aldehyde **75** is key to the Strecker reaction proposed for this synthesis thus, other oxidants were explored in hopes to avoid the unwanted benzaldehyde. Trying to move away from the chromium-based oxidants, we also tested Uemura's aerobic oxidation.¹⁸⁶ In this oxidation, alcohols are oxidised to the aldehyde or ketone in the presence of catalytic palladium and molecular oxygen. Intriguingly, this oxidation also resulted in C-C oxidative cleavage was observed yielding **75:81** in a 2:1 ratio (Scheme 4.7, entry 6). Although remaining starting material was the predominant compound in the ¹H NMR spectrum of the reaction mixture, this was the first report, to our knowledge, of C-C oxidative cleavage when performing Uemura's aerobic oxidation on a homobenzyl alcohol. It is noted that when using 2-phenylethanol as the substrate oxidative cleavage again occurred indicating that the C-C oxidative cleavage it is not substrate dependant. Alternatively, it may be specific to the catalytic system. At the time this result was published in *Peptide Science*, other studies of palladium catalysed aerobic oxidations of homobenzyl alcohols did not report C-C oxidative cleavage. Since, C-C oxidative cleavage using a dual catalytic system of PdCl₂ and CuCl has been published¹⁸⁵ although this remains the only other example.

Efforts to oxidise **74** to **75** using DMSO and oxalyl chloride under standard Swern oxidation conditions¹⁸⁷ failed while use of *N*-methylmorpholine-*N*-oxide and catalytic tetrapropylammonium perruthenate (TPAP)¹⁸⁸ returned the starting material. Satisfyingly, **75** was finally obtained without any unwanted **81** using Dess-Martin periodinane (DMP). Initial attempts at this reaction using 1.5 equivalents of DMP yielded the desired aldehyde along with returned

starting material after 18 hours (Scheme 4.7, Entry 7). Using 4 equivalents allowed for complete consumption of starting material and **75** was isolated in a 70% yield after purification by column chromatography (Scheme 4.7, Entry 8). Decreasing the reaction time to one and a half hours slightly reduced the yield (Scheme 4.7, Entry 9).

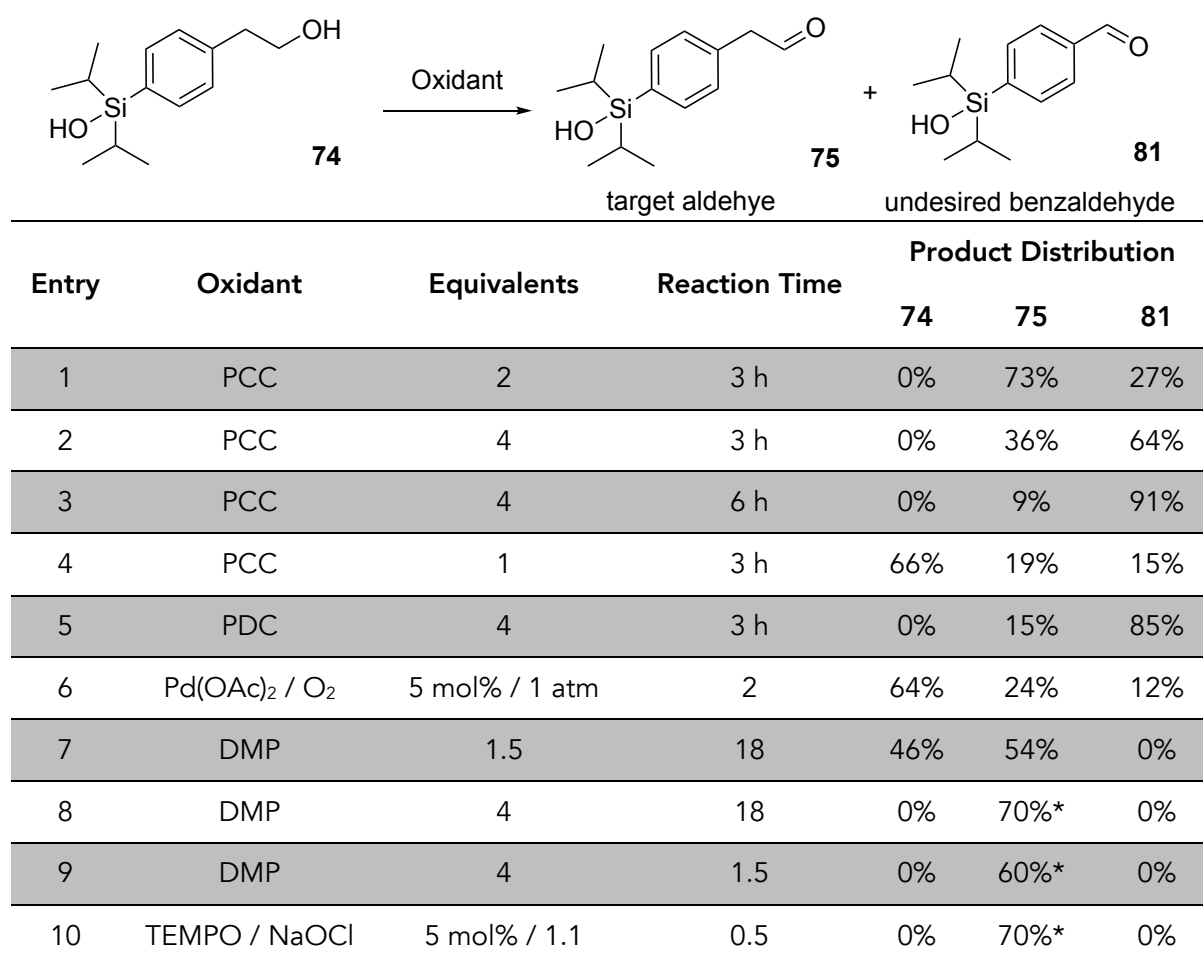
The large excess of DMP required and the low atom efficiency of this reaction, however, is not ideal when up-scaling. Therefore, we also tested the oxidation of **74** using Anelli's sodium hypochlorite and catalytic TEMPO.¹⁸⁹ Although this protocol is relatively easy to execute, there are multiple factors of this oxidation reaction that can affect the yield and must be carefully controlled.

Firstly, the oxoammonium salt that acts as the primary oxidant is catalytic and can further oxidise the aldehyde to the carboxylic acid.¹⁸⁹ Relatively slow compared to the oxidation of alcohols, oxidation can generally be stopped at the aldehyde. Secondly, the oxoammonium salt is unstable in water (used as a co-solvent) rapidly decomposing at 25 °C.¹⁸⁹ With TEMPO used only catalytically, maintaining a reaction temperature between 0–10 °C is important to ensure sufficient amounts of the oxidant are present to reach full conversion. Finally, the reaction rate is dependent on the presence of KBr or NaBr and therefore the pH is also important.¹⁹⁰ Addition of these bromide salts generates HOBr, a better oxidant than HOCl which is generated in their absence. Under the highly basic pH of bleach (the origin of sodium hypochlorite) HOBr predominately exists as its conjugate base ^-OBr and regeneration of the oxoammonium salt becomes the rate-determining step. Ideal for Anelli's oxidation is a pH range ca. 8.6–10. Commonly a $NaHCO_3$ buffered system and adjustments with NaOH or HCl are used to fine tune the pH.¹⁹¹

Taking these factors into account we attempted to oxidise **74** using TEMPO (5 mol%) and NaOCl along with an equivalent of KBr. In the first instance, this oxidation gave the expected aldehyde after only 25 minutes. No over oxidation to the carboxylic acid was observed nor the C-C oxidation cleavage previously described. Further, the desired aldehyde was isolated in a 70% yield (Scheme 4.7, Entry 10) and could be used without the need for purification by column chromatography. When repeating this reaction, the isolated yield and purity of **75** was inconsistent with yields ranging from 40% to 70% and purification required on almost every occasion. On one occasion, over oxidation to the carboxylic acid was also observed. The oxidation itself occurs in the organic phase and formation of the carboxylic acid may be due to the lack of

solubility of **74** in toluene. With regeneration of the oxoammonium salt by the secondary oxidant formation of the carboxylic acid may be occurring before all the substrate is present in the organic phase. It is expected that the use of a solvent where solubility is not an issue such as CH₂Cl₂ should overcome this issue.

With the inconsistencies in the TEMPO/sodium hypochlorite oxidation and the ease of oxidation with DMP, all future instances of this reaction were performed using the DMP method. It is noted that *o*-iodoxybenzoic acid (IBX) was not tested in this oxidation study as loss of the carbon along with over oxidation to the carboxylic acid has previously been reported for primary alcohols.¹⁹²



Scheme 4.7 Oxidation of **74** using a range of oxidants and condition and the product distribution of **75** and **81** as determined by integration of the ¹H NMR spectra. *Isolated yield

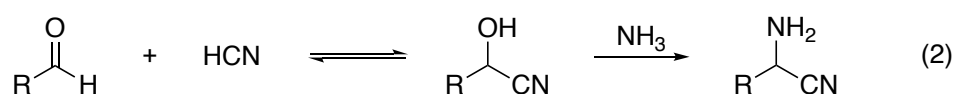
4.4.3 Strecker synthesis

With an oxidation method to produce **75** we turned our attention to the final step in the synthesis, the Strecker reaction. A powerful and simple method for synthesising amino acids from aldehydes over two-steps described for the first time by Adolf Strecker in 1850.¹⁹³ The first step involves the formation of an aminonitrile by treatment with HCN. In the second step the aminonitrile is hydrolysed to the corresponding amino acid. HCN can either be added to the reaction or generation in situ from ammonium chloride and a cyanide salt such as sodium cyanide, as shown in equation (1). The aminonitrile can then be formed through a cyanohydrin intermediate where ^-CN adds to the aldehyde as shown in equation (2) and/or the aldehyde first reacts with ammonium, forming an imine intermediate which then forms the aminonitrile on addition of HCN, shown in equation (3).¹⁹⁴ Finally acid or base catalysed hydrolysis of the aminonitrile yields the amino acid, equation (4).

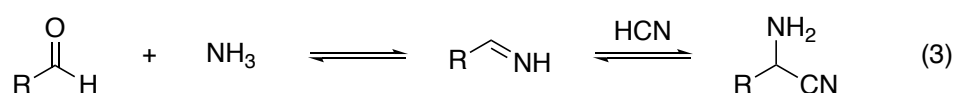
Generation of HCN



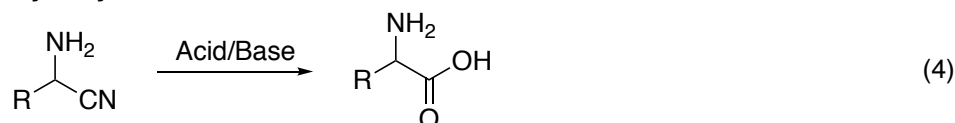
Pathway 2a



Pathway 2b



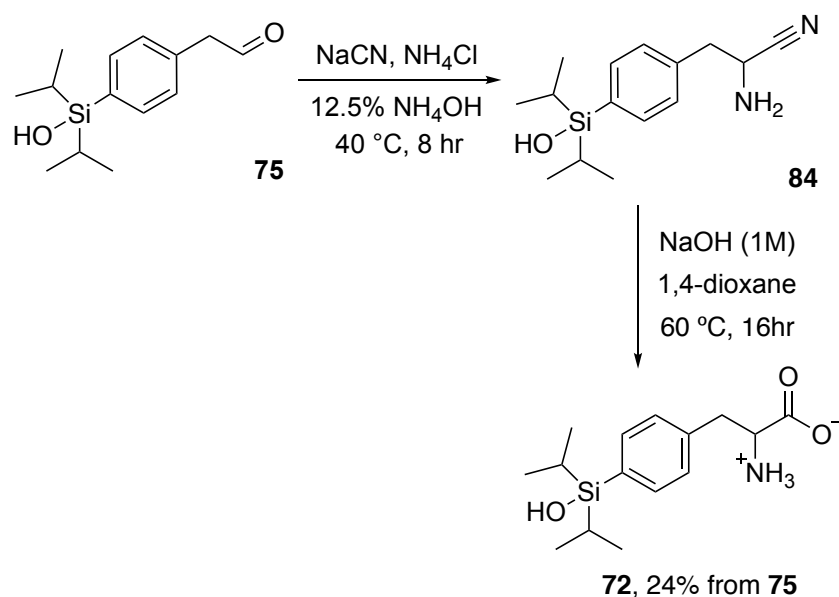
Hydrolysis



Scheme 4.8 Steps of the Strecker synthesis.

In the interest of safety, HCN was generated in situ and the aldehyde added to a solution of ammonium chloride and sodium cyanide in a 12% aqueous solution of ammonium hydroxide that had been stirred for an hour. Monitoring the reaction by TLC indicated that heating to 40 °C for 2 hours after the addition of a solution of aldehyde **75** in MeOH was sufficient for complete consumption of the starting material but an intermediate cyanohydrin was isolated along with the desired aminonitrile **84**. Complete conversion required 8 hours at 40 °C and **84** was isolated via

liquid-liquid extraction and used without further purification. Basic catalysed hydrolysis in 1,4-dioxane and purification via ion exchange chromatography gave the desired amino acid **72**

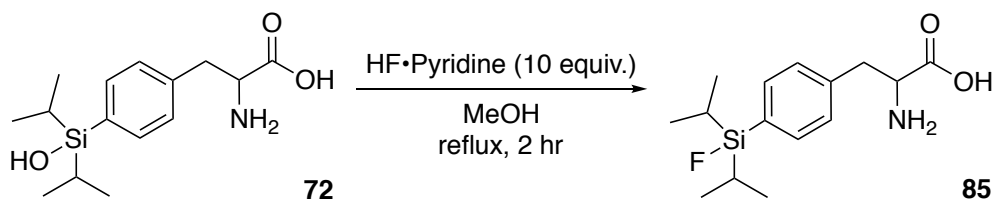


in a 24% yield from the starting aldehyde **75**. With the amino acid in hand, fluorination conditions were explored.

Scheme 4.9 The Strecker reaction provided the target amino acid **72** in a 24% yield from the key aldehyde **75**.

4.5 Aqueous fluorination of 2-amino[3-(4-diisopropylsilanol)phenyl]propanoic acid (**72**)

As in Chapter 2 fluorination studies were first investigated with organic solvents and high temperatures to support complete conversion. Due to low solubility of the amino acid in many organic solvents, fluorination was performed with HF•Pyridine in MeOH at reflux. Full conversion was observed after only 2 hours at reflux.

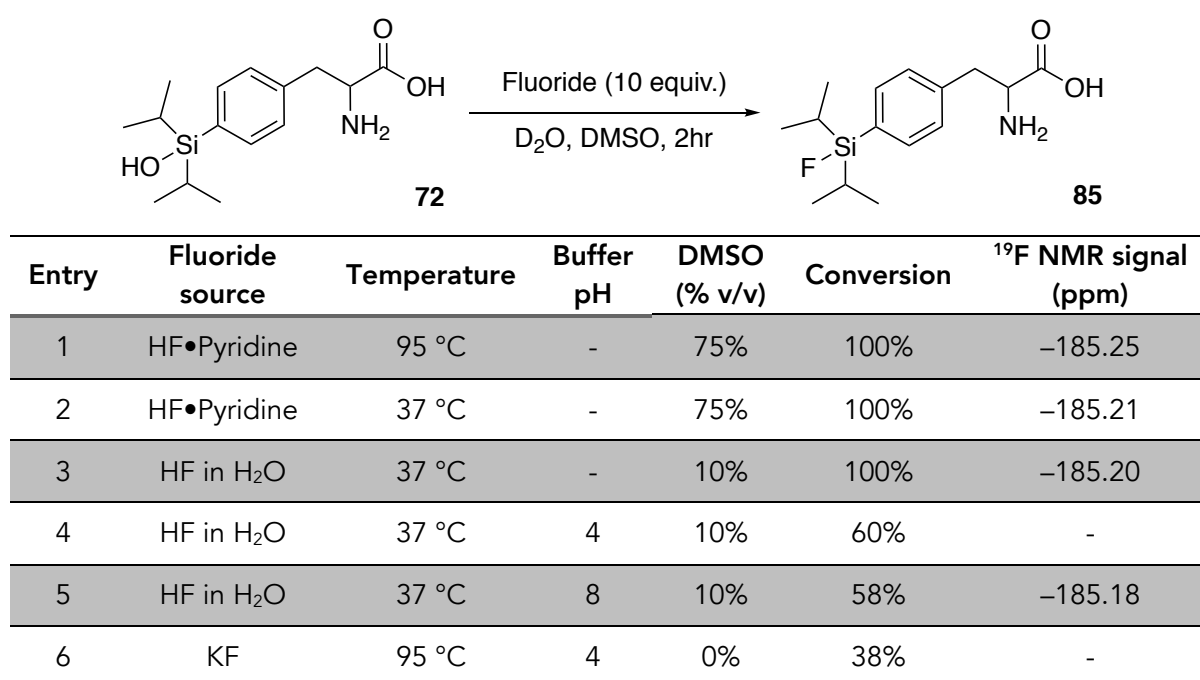


Scheme 4.10 Fluorination of **72** in protic solvents still gives full conversion.

Encouraged by the results of fluorination of **72** that gave high conversions to the fluorosilane under aqueous conditions (discussed in Chapter 2), fluorination of **72** was also tested

in the presence of water. Fortunately, significant differences in the ^1H NMR chemical shifts of **72** and **85** allowed for the conversion to be determined by integration of the ^1H NMR spectra of the reaction mixture and fluorination reactions were conducted in deuterated solvents and analysed directly. ^{19}F NMR spectroscopy was also used to support the presence of the Si-F bond. Furthermore, the limitation on the aqueous content of solvent systems due to solubility issues were not a factor for the amino acid and fluorination was tested in solvent systems with a higher aqueous content.

Fluorination was first tested using HF•Pyridine in DMSO with a 25% water content. At 95 °C for 2 hours, full conversion to **85** was observed (Scheme 4.11, Entry 1). Reducing the temperature to 37 °C again gave full conversion in 2 hours (Scheme 4.11, Entry 2). Promisingly, when switching to HF in H_2O as the fluoride source and increasing the aqueous content to 90%, full conversions were still achievable (Scheme 4.11, Entry 3). Taking into consideration that fluorination of this amino acid when incorporated into a protein would be performed under buffered conditions, fluorination at pH 4.0 and pH 8.0 were also tested. A drop in the conversion was observed in both cases (Scheme 4.11, Entries 4 and 5) however these conversions were still very encouraging reaching above 50%. It is also noted that in the buffered systems precipitation was observed and this may account for the lower conversions recorded. Finally, KF was also tested as a potential fluoride source (Scheme 4.11, Entry 6).



Scheme 4.11 Fluorination of **72** in aqueous solvents.

For entries 4 and 6 no signals were observed in the ^{19}F NMR spectra for the hydrogen fluoride or the product. Presumably, this is due to the lower sensitivity of ^{19}F relative to ^1H , the small (10 mg) reaction scale and the lower yields of these experiments. With sufficient evidence in the ^1H NMR spectra that fluorination was successful these reactions were not repeated on a larger scale.

4.6 Concluding remarks and chapter summary

The successful fluorination under slightly acidic buffered aqueous condition of lysozyme chemical modified with the silanol benzylamine (Chapter 3) further inspired the synthesis of an unnatural silicon based amino acids useful for amber codon suppression. Chapter 4 details the synthesis of the unnatural silicon based amino acid **72** suitable for late-stage fluorination on a protein. The unnatural amino acid was synthesised using the conventional Strecker route through a key aldehyde intermediate. Oxidative cleavage reactions in the preparation of the key aldehyde intermediate in the Strecker synthesis resulted in oxidative C-C bond cleavage. Literature revealed that when using chromium-based agents this reaction is not unknown, however, using Uemura's aerobic oxidation with palladium acetate and molecular oxygen a novel oxidative C-C bond cleavage was observed. This undesired oxidative C-C bond cleavage was avoided using DMP or TMEPO/NaOCl. Overall this synthesis is robust and can be performed on multigram scales.

Pleasingly, fluorination of **72** under aqueous conditions was successful, even when using 100% buffered water. With these exciting and encouraging results the project moved forward and the genetic incorporation of **72** using amber codon suppression was explored. This amber codon suppression and incorporation of **72** into a protein is the focus of the next chapter.

4. Experimental procedures

4.7.1 General experimental details

All reactions requiring anhydrous conditions were performed under a nitrogen atmosphere in flame-dried glassware. CH_2Cl_2 and Et_3N were distilled over calcium hydride, THF and Et_2O was distilled over sodium and benzophenone. Toluene were distilled over calcium hydride. All other solvents and reagents were used as supplied from commercial suppliers without

further purification. All fluorination reactions were conducted using plastic reaction vessels to avoid etching of glass with HF. Fluorination NMR experiments were conducted with a fluorinated ethylene polypropylene (FEP) copolymer NMR tube liner. All fluorination reactions that were heated were carried out on a Grant Bio PMHT Thermoshaker.

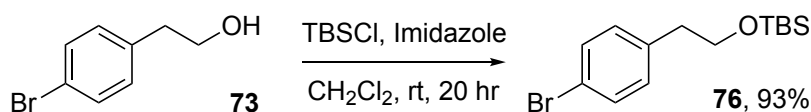
DOWEX H+ was prepared by washing 10 g of the resin in a sintered funnel connected to a diaphragm pump with acetone (25 mL) followed by methanol (25 mL). The resin was then washed with 1M HCl (15 mL), 1M NaOH (15 mL), 1M HCl (25 mL) and finally with water until the filtrate was neutral (~ pH 6-7).

Analytical thin layer chromatography was performed on aluminium sheets coated with silica gel containing a fluorescent indicator (0.15-0.2mm thickness, 8 μm granularity) and were visualised using UV light or developed in a potassium permanganate or ninhydrin dip. Thin layer chromatography sheets used to analyse amines were pre-treated with 0.1% Et₃N in the required solvent system. Column chromatography was performed using silica gel (230–400 mesh, 60 Å pore diameter).

All NMR data were recorded using a Bruker Ultrashield 400 or a Bruker Ultrashield 600. Deuterated chloroform (CDCl₃), deuterated water (D₂O) or deuterated dichloromethane (CD₂Cl₂) were used as the solvent and for internal locking. ¹H NMR chemical shifts were referenced to δ_{H} 7.26 ppm (CDCl₃), δ_{H} 4.79 ppm (D₂O) or δ_{H} 5.30 ppm (CD₂Cl₂) and ¹³C NMR chemical shifts to δ_{C} 77.16 ppm. Chemical shifts (δ) were measured in parts per million (ppm) and coupling constants (J) in hertz (Hz). Multiplicity is reported as s = singlet, d = doublet, q = quartet, dd = doublet of doublets, m = multiplet and br. s = broad singlet. Infrared spectra were recorded on an FTIR spectrometer with the absorptions reported in wavenumbers (cm⁻¹). High resolution mass spectrometry was recorded using atmospheric pressure chemical ionization (APCI) on a Perkin Elmer AxION connected to a DSA-ToF or using electrospray ionisation (ESI) on a Waters Synapt HDMS. All HRMS data is reported as the observed molecular ion unless otherwise stated. Melting points were recorded on a Gallenkamp melting point apparatus.

4.7.2 Synthetic procedures and analytical data

[2-(4-bromophenyl)ethoxy](tert-butyl)dimethylsilane (**76**)



TBSCl (7.492 g, 49.76 mmol, 1.3 eq) was added to a solution of **73** (7.697 g, 38.27 mmol) and imidazole (3.384 g, 49.76 mmol, 1.3 eq.) in CH₂Cl₂ (150 mL). The reaction was stirred for 20 hr before being diluted with H₂O (50 mL). The aqueous layer was extracted with CH₂Cl₂ (3 × 50 mL). The combined organic layers were washed with brine (70 mL), dried (Na₂SO₄), and filtered before the solvent was removed under reduced pressure. The resulting residue was purified by column chromatography (10% EtOAc in hexanes) to afford **76** (R_f = 0.73) as a yellow oil (11.264 g, 93%). IR (ν_{max}): 2953, 2929, 1895, 1857, 1489, 1472, 1256, 1099, 1073, 1012, 832, 776 cm⁻¹; ¹H NMR (600 MHz, Chloroform-*d*) δ_H 7.39 (d, J = 8.3 Hz, 2H, ArH), 7.08 (d, J = 8.3 Hz, 2H, ArH), 3.78 (t, J = 6.8 Hz, 2H, CH₂CH₂OTBS), 2.76 (t, J = 6.8 Hz, 2H, CH₂CH₂OTBS), 0.86 (s, 9H, (CH₃)₃), -0.03 (s, 6H, CH₃); ¹³C NMR (151 MHz, Chloroform-*d*) δ_C 138.47, 131.36, 131.07, 120.05, 64.22, 39.07, 26.04, 18.46, -5.28; HRMS (APCI) calculated for [C₁₄H₂₄BrSiO]⁺ 315.0774; found 315.0771.

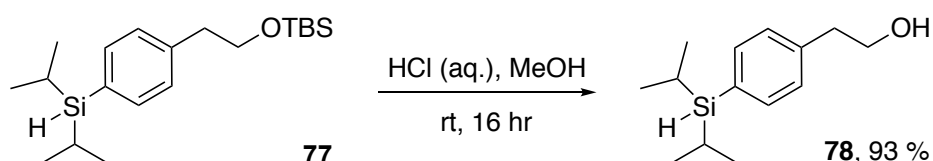
[2-(4-diisopropylsilylphenyl)ethoxy](tert-butyl)dimethylsilane (**77**)



At -78 °C, *n*-Buli in cyclohexane (2 M, 13.34 mL, 26.68 mmol, 1.2 eq.) was added to a solution of **76** (7.012 g, 22.24 mmol) in THF (150 mL). After 1 hr, diisopropylchlorosilane (4.745 mL, 27.8 mmol, 1.25 eq.) was added. The cooling bath was then removed, and the reaction was left to warm to room temperature. After 20 hr of total reaction time, the reaction was quenched with a saturated aqueous solution of NaHCO₃ (50 mL) and the aqueous layer was extracted with EtOAc (3 × 50 mL). The combined organic layers were washed with brine (100 mL), dried (Na₂SO₄), filtered and the solvent removed under reduced pressure. The resulting residue was purified by column chromatography (2% EtOAc in hexanes) to afford **77** (R_f = 0.73) as a clear oil (7.331 g, 94%). IR (ν_{max}): 2939, 2892, 2863, 2100, 1462, 1383, 1255, 1105, 1001, 880, 830, 776 cm⁻¹; ¹H NMR (600 MHz, Chloroform-*d*) δ_H 7.42 (d, J = 7.8 Hz, 2H, ArH), 7.19 (d, J = 7.8 Hz, 2H, ArH), 3.92

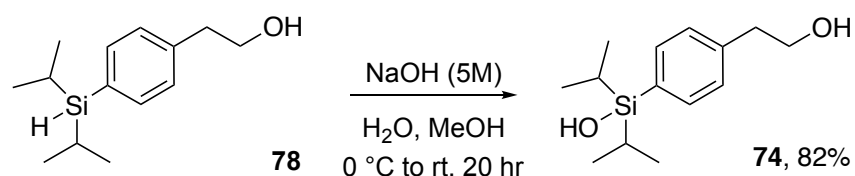
(t, $J = 3.1$ Hz, 1H, SiH), 3.82 (t, $J = 7.0$ Hz, 2H, CH₂CH₂OTBS), 2.82 (t, $J = 7.0$ Hz, 2H, CH₂CH₂OTBS), 1.21 (m, 2H, iPrH), 1.06 (d, $J = 7.4$ Hz, 6H, iPrCH₃), 0.98 (d, $J = 7.4$ Hz, 6H, iPrCH₃), 0.85 (s, 9H, (CH₃)₃), -0.05 (s, 6H, CH₃); ¹³C NMR (151 MHz, Chloroform-*d*) δ_c 140.34, 135.58, 131.42, 128.76, 64.61, 39.77, 26.07, 18.82, 18.61, 18.50, 10.87, -5.30; HRMS (APCI) calculated for [C₂₀H₃₉OSi₂]⁺ 351.2534; found 351.2545.

1-[4-(diisopropylsilyl)phenyl]ethanol (**78**)



HCl (1.5 mL 37%) was added to a solution of **77** (7.331 g, 20.9 mmol) in MeOH (75 mL). The reaction was stirred for 16 hr and then the solvent was removed under reduced pressure. The resulting residue was diluted with EtOAc (100 mL), washed with a saturated aqueous solution of NaHCO₃ (100 mL), dried (Na₂SO₄), filtered and the solvent removed under reduced pressure. The resulting residue was purified by column chromatography (40% EtOAc in hexanes) to afford **78** ($R_f = 0.56$) as a clear liquid (4.591 g, 93%). IR (ν_{max}): 3303, 2939, 2889, 2862, 2098, 1600, 1461, 1045, 1000, 880, 796, 783 cm⁻¹; ¹H NMR (600 MHz, Chloroform-*d*) δ_H 7.46 (d, $J = 7.5$ Hz, 2H, ArH), 7.22 (d, $J = 7.5$ Hz, 2H, ArH), 3.93 (t, $J = 3.2$ Hz, 1H, SiH), 3.88 (t, $J = 6.6$ Hz, 2H, ArCH₂CH₂OH), 2.87 (t, $J = 6.6$ Hz, 2H, ArCH₂CH₂OH), 1.40 (br. s, 1H, OH), 1.22 (m, 2H, iPrH), 1.06 (d, $J = 7.3$ Hz, 6H, iPrCH₃), 0.99 (d, $J = 7.4$ Hz, 6H, iPrCH₃); ¹³C NMR (151 MHz, Chloroform-*d*) δ_c 139.47, 135.96, 132.08, 128.54, 63.71, 39.39, 18.82, 18.66, 10.88; HRMS (APCI) calculated for [C₁₄H₂₅OSi]⁺ 237.1669; found 237.1678.

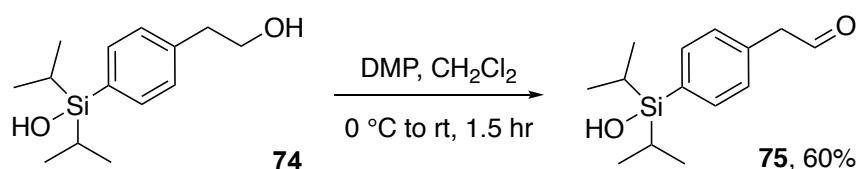
1-[4-(diisopropylsilyl)phenyl]ethanol (**74**)



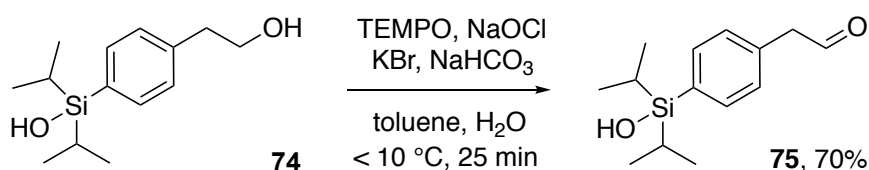
A 5M aqueous solution of NaOH (38.84 mL, 0.194 mol, 10 eq.) was added to a solution of **78** (4.591 g, 19.42 mmol) in MeOH (45 mL) at 0 °C. The reaction was stirred for 10 min and then the ice bath was removed, and the reaction allowed to warm to room temperature. After 20 hr, the methanol was removed under reduced pressure. H₂O (50 mL) was added to the residue before extraction with EtOAc (3 × 50 mL). The organic phase were combined, washed with brine

(100 mL), dried (Na_2SO_4), and filtered, before concentrating under reduced pressure. The resulting residue was purified by column chromatography (20% EtOAc in hexanes) to afford **74** as a white solid (4.037 g, 82%). Mp: 74-76 °C; IR (ν_{max}): 3332, 2942, 2891, 2865, 1602, 1463, 1109, 883, 835, 809, 679 cm^{-1} ; ^1H NMR (600 MHz, Chloroform-*d*) δ_{H} 7.51 (d, $J = 7.6$ Hz, 2H, ArH), 7.25 (d, $J = 7.6$ Hz, 2H, ArH), 3.89 (q, $J = 6.2$ Hz, 2H, ArCH₂CH₂OH), 2.88 (t, $J = 6.5$ Hz, 2H, ArCH₂CH₂OH), 1.68 (s, 1H, SiOH), 1.38 (t, $J = 6.0$ Hz, 1H, CH₂OH), 1.21 (m, 2H, *i*PrH), 1.05 (d, $J = 7.4$ Hz, 6H, *i*PrCH₃), 0.98 (d, $J = 7.5$ Hz, 6H, *i*PrCH₃); ^{13}C NMR (151 MHz, Chloroform-*d*) δ_{C} 139.78, 134.58, 133.36, 128.55, 63.70, 39.41, 17.33, 17.08, 12.60; HRMS (ESI) calculated for $[\text{C}_{14}\text{H}_{24}\text{O}_2\text{SiNa}]^+$ 275.1438; found 275.1434.

1-[4-(diisopropylsilanol)phenyl]ethanal (**75**)



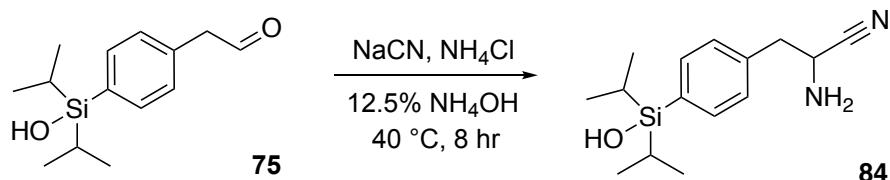
[1-(4-(diisopropylsilanol)phenyl)ethanol (**74**) (0.851 g, 3.03 mmol) was added to a suspension of DMP (2.94 g, 12.1 mmol) in CH_2Cl_2 (10 mL) at 0 °C. The ice bath was removed after 10 min and the reaction was allowed to warm to room temperature. After 1.5 hr total reaction time, the reaction was quenched with a 30 mL 1:1 saturated aqueous solution of $\text{Na}_2\text{S}_2\text{O}_3$ and NaHCO_3 . The aqueous phase was extracted with CH_2Cl_2 (3×10 mL). The organic fractions were combined, washed with brine (20 mL), dried (Na_2SO_4), filtered and concentrated under reduced pressure. The residue was purified by column chromatography (40% EtOAc in hexanes) to afford **75** ($R_f = 0.62$) as a white solid (0.507 g, 60%). Mp: 125 – 128°C; IR (ν_{max}): 3430, 2943, 2865, 1720,



1463, 1107, 882, 814, 670 cm^{-1} ; ^1H NMR (400 MHz, Chloroform-*d*) δ_{H} 9.76 (t, $J = 2.4$ Hz, 1H, HC=O), 7.56 (d, $J = 8.0$ Hz, 2H, ArH), 7.24 (d, $J = 8.0$ Hz, 2H, ArH), 3.69 (d, $J = 2.4$ Hz, 2H, CH₂), 1.22 (m, 2H, *i*PrH), 1.06 (d, $J = 7.3$ Hz, 6H, *i*PrCH₃), 0.98 (d, $J = 7.4$ Hz, 6H, *i*PrCH₃); ^{13}C NMR (101 MHz, Chloroform-*d*) δ_{C} 199.53, 134.92, 134.67, 133.06, 129.06, 50.77, 17.29, 17.03, 12.57; HRMS (ESI) calculated for $[\text{C}_{14}\text{H}_{22}\text{O}_2\text{SiNa}]^+$ 273.1281; found 273.1288.

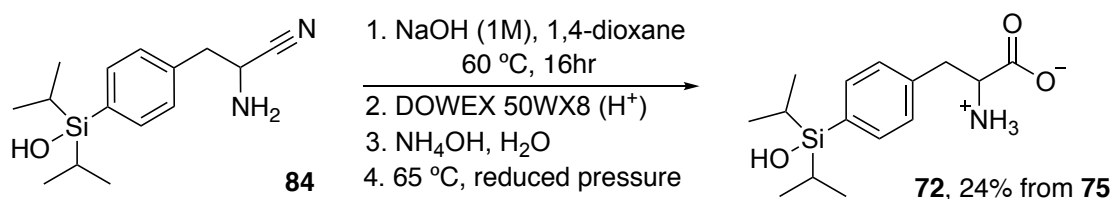
[1-(4-diisopropylsilyl)phenyl]ethanol (**74**) (116 mg, 0.459 mmol) was added to a round bottom flask and suspended in toluene (5 mL). The mixture was sonicated for 3 min to help partially dissolve **74**. Next, a saturated aqueous solution of NaHCO₃ (2.1 mL) was added to the reaction vessel followed by KBr (60 mg, 0.504 mmol) and then TEMPO (6.1 mg, 0.052 mmol). The solution was cooled to below 10 °C (internal temperature) using an ice bath and aqueous NaOCl (4 wt %, 1.475 mL, 0.79 mmol) was added dropwise. The reaction stirred for 25 min, maintaining an internal reaction temperature < 10 °C. After 25 min total reaction time, the organic phase was separated and then washed with H₂O (2 × 10 mL), dried (NaSO₄), filtered, and solvent removed under reduced pressure to afford **75** as a yellow oil (80 mg, 70%). **75** was used without further purification and spectroscopic data was consistent with **75** prepared using DMP as the oxidant.

2-amino[3-(4-diisopropylsilyl)phenyl]propane nitrile (**84**)



NaCN (1.215 g, 24.75 mmol) was added to NH₄Cl (1.325 g, 24.75 mmol) in 25 mL of a 12.5 % NH₄OH aqueous solution. After 1 hr stirring at room temperature, aldehyde **75** (3.645 g, 14.56 mmol) was dissolved in MeOH (12 mL) and then added to the reaction. The reaction was then heated to 40 °C and stirred for 8 hr. After this time, the reaction was cooled to room temperature and extracted with CH₂Cl₂ (3 × 50 mL). The organic phases were combined, washed with brine (100 mL), dried (Na₂SO₄), filtered and the solvent removed under reduced pressure. The amino nitrile **84** was sufficiently pure to carry on to the next step and was not purified further. IR (ν_{max}): 3365, 3070, 2943, 2865, 2242, 1602, 1463, 1108, 994, 883, 848, 681 cm⁻¹; ¹H NMR (600 MHz, Chloroform-*d*) δ_H 7.54 (d, J = 7.7 Hz, 2H, ArH), 7.28 (d, J = 7.7 Hz, 2H, ArH), 3.94 (t, J = 6.5 Hz, 1H, ArCH₂CH), 3.06 – 2.97 (m, 2H, ArCH₂CH), 2.25 (s, 2H, NH₂), 1.27 – 1.16 (m, 2H, *i*PrH), 1.04 (d, J = 7.4 Hz, 6H, *i*PrCH₃), 0.96 (d, J = 7.5 Hz, 6H, *i*PrCH₃); ¹³C NMR (151 MHz, Chloroform-*d*) δ_C 135.22, 134.99, 134.86, 129.13, 119.40, 62.17, 41.61, 17.29, 17.03, 12.56.

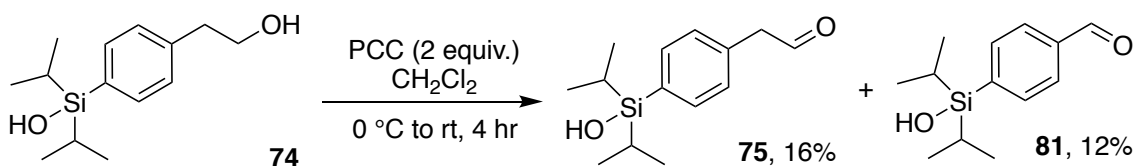
2-amino[3-(4-diisopropylsilylanol)phenyl]propanoic acid ((±)-**72**)



The crude amino nitrile **84** was dissolved in 1,4-dioxane (20 mL). Aqueous NaOH (1M, 20mL) was added and the reaction was heated at 60 °C for 16 hr. The reaction was then cooled to room temperature and DOWEX H⁺ added to the flask until the pH was ~5 (for DOWEX H⁺ preparation see Section 4.7.1). The DOWEX was collected in a sintered funnel and washed with H₂O (200 mL) and then acetone (200 mL) before eluting the target compound with 5% NH₄OH (300 mL). The solvent was removed under reduced pressure (bath temp. 65 °C) to afford (±)-**72** as a yellow solid (1.025 g, 24% from aldehyde **75**). IR (ν_{max}): 3449, 2943, 2865, 2556, 1578, 1436, 880 cm⁻¹; ¹H NMR (600 MHz, Deuterium Oxide) δ_H 7.64 (d, J = 7.6 Hz, 2H, ArH), 7.37 (d, J = 7.6 Hz, 2H, ArH), 3.76 (dd, J = 7.8, 5.2 Hz, 1H, CH_AH_B), 3.18 (dd, J = 14.0, 5.2 Hz, 1H, CH_AH_B), 2.99 (dd, J = 14.0, 7.9 Hz, 1H, CH_AH_B), 1.27 (m, 2H, iPrH), 1.04 (dd, J = 7.4, 1.4 Hz, 6H, iPrCH₃), 0.97 (d, J = 7.4 Hz, 6H, iPrCH₃); ¹³C NMR (151 MHz, Deuterium Oxide) δ_C 178.27, 138.31, 134.69, 133.96, 128.85, 56.70, 38.65, 16.38, 16.12, 16.11, 11.77, 11.75; HRMS (ESI) calculated for [C₁₅H₂₄O₃SiN]⁻ 294.1531; found 294.1519.

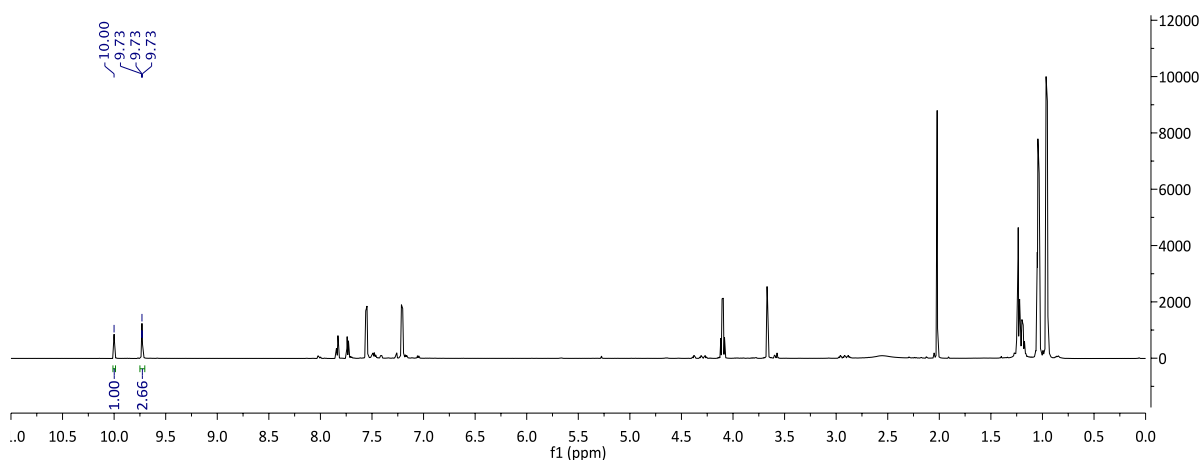
4.7.3 Oxidative cleavage studies

Pyridinium chlorochromate (PCC)



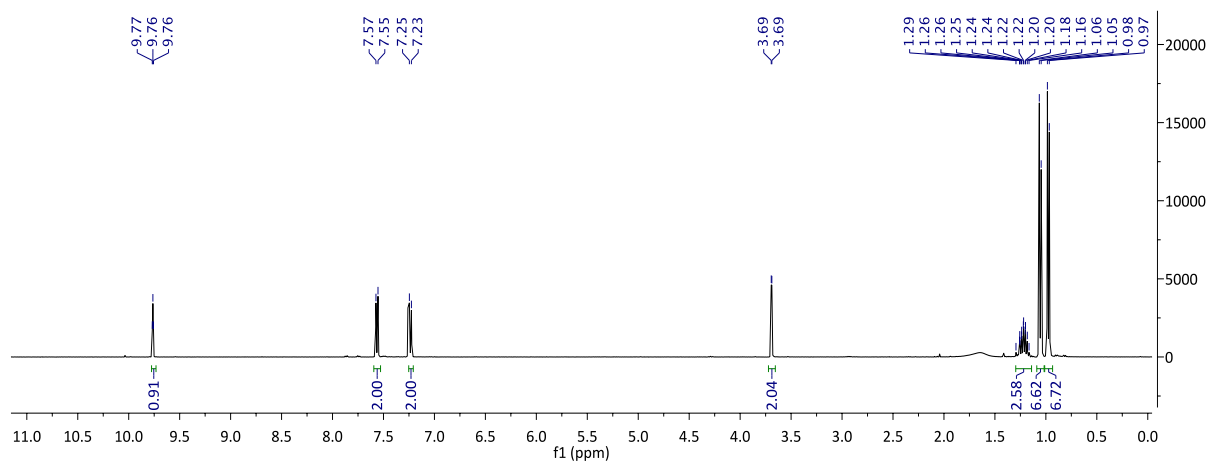
[1-(4-diisopropylsilylanol)phenyl]ethanol (**74**) (102 mg, 0.404 mmol) was added to a suspension of PCC (171 mg, 0.808 mmol) and silica (191 mg) in CH₂Cl₂ (5 mL) at 0 °C. The reaction was removed from the ice bath and then allowed to warm to room temperature. After 4 hr total reaction time, the mixture was passed through a column of silica topped with a bed of celite, eluting first with CH₂Cl₂ and then 40% EtOAc in hexane to yield a 2.7:1 mixture of **75** and **81**, as determined by ¹H NMR spectroscopy. The ratio of aldehyde to benzaldehyde products was

determined by integration of the proton signals at δ_{H} 9.7 and δ_{H} 10.0 ppm, respectively. These two compounds were separated by a second round of column chromatography eluting with 5% EtOAc in hexanes, providing **75** in a 16% yield and **81** in a 12% yield.



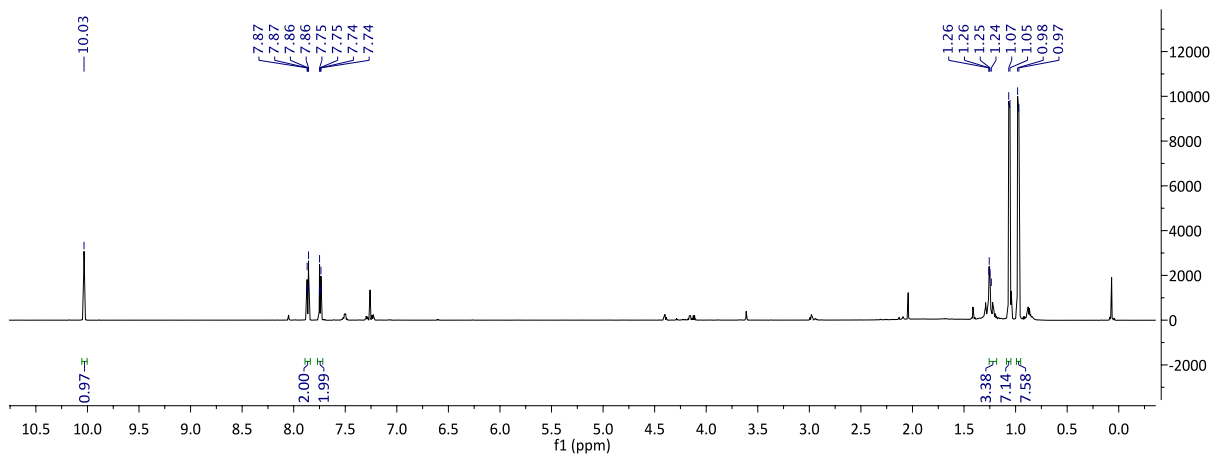
[1-(4-diisopropylsilyl)phenyl]ethanal (**75**)

16.4 mg (16 %), IR (ν_{max}): 3430, 2943, 2865, 1720, 1463, 1107, 882, 814, 670 cm^{-1} ; ^1H NMR (400 MHz, Chloroform-*d*) δ_{H} 9.76 (t, $J = 2.4$ Hz, 1H, COH), 7.56 (d, $J = 8.0$ Hz, 2H, ArH), 7.24 (d, $J = 8.0$ Hz, 2H, ArH), 3.69 (d, $J = 2.4$ Hz, 2H, CH₂), 1.22 (m, 2H, iPrH), 1.06 (d, $J = 7.3$ Hz, 6H, iPrCH₃), 0.98 (d, $J = 7.4$ Hz, 6H, iPrCH₃); ^{13}C NMR (101 MHz, Chloroform-*d*) δ_{C} 199.53, 134.92, 134.67, 133.06, 129.06, 50.77, 17.29, 17.03, 12.57; HRMS (ESI) calculated for [C₁₄H₂₂O₂SiNa]⁺ 273.1281; found 273.1288.

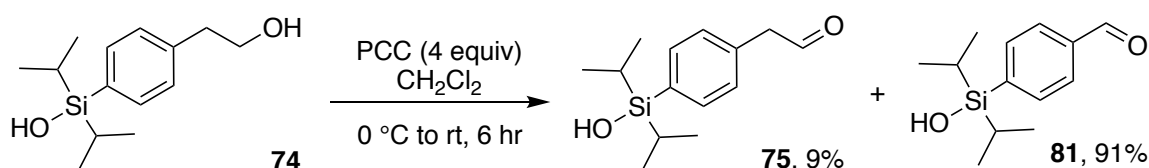


1-(4-diisopropylsilyl)benzaldehyde (**81**)

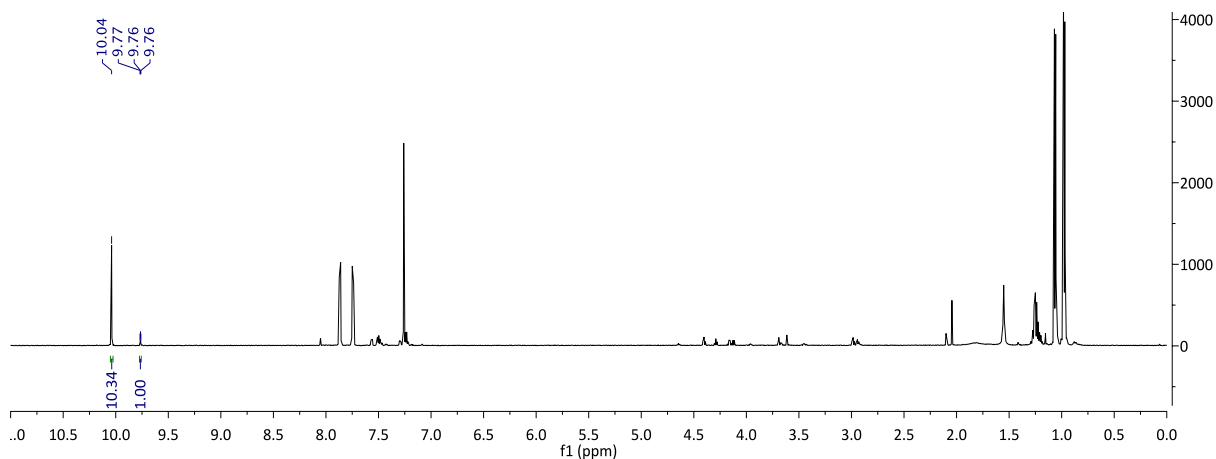
11.5 mg, (12 %), IR(ν_{\max}): 3433, 2944, 2866, 1701, 1464, 1214, 883, 833, 814, 696 cm^{-1} ; ^1H NMR (600 MHz, Chloroform-*d*) δ_{H} 10.03 (s, 1H, COH), 7.89 – 7.84 (m, 2H, ArH), 7.77 – 7.72 (m, 2H, ArH), 1.26 (m, 2H, *i*PrH), 1.06 (d, $J = 7.3$ Hz, 6H, *i*PrCH₃), 0.98 (d, $J = 7.5$ Hz, 6H, *i*PrCH₃); ^{13}C NMR (151 MHz, Chloroform-*d*) δ_{C} 192.76, 144.26, 136.86, 134.62, 128.52, 17.09, 16.83, 12.42; HRMS (EI) calculated for [C₁₃H₁₉O₂Si]⁺ 235.1160; found 235.1161.



Scheme 4.7, Entry 1

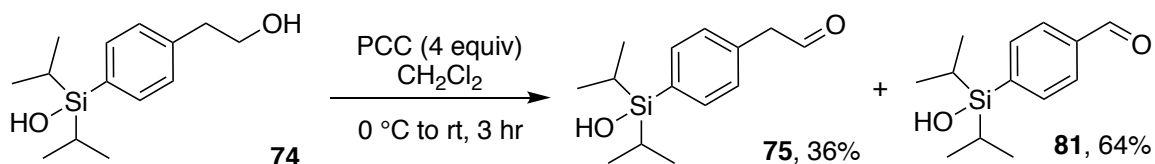


[1-(4-diisopropylsilyl)phenyl]ethanol (**74**) (100 mg, 0.396 mmol) was added to a suspension of PCC (345 mg, 1.60 mmol) and silica (351 mg) in CH₂Cl₂ (5 mL) at 0 °C. The reaction was removed from the ice bath and then allowed to warm to room temperature. After 6 hr total reaction time, the mixture was passed through a column of silica topped with a bed of celite, eluting first with CH₂Cl₂ and then 40 % EtOAc in hexane to yield a 1:10.34 mixture of **75** (9%) and **81** (91%), as determined by ^1H NMR spectroscopy. The ratio of aldehyde to benzaldehyde products was determined by integration of the proton signals at δ_{H} 9.7 and δ_{H} 10.0 ppm, respectively.

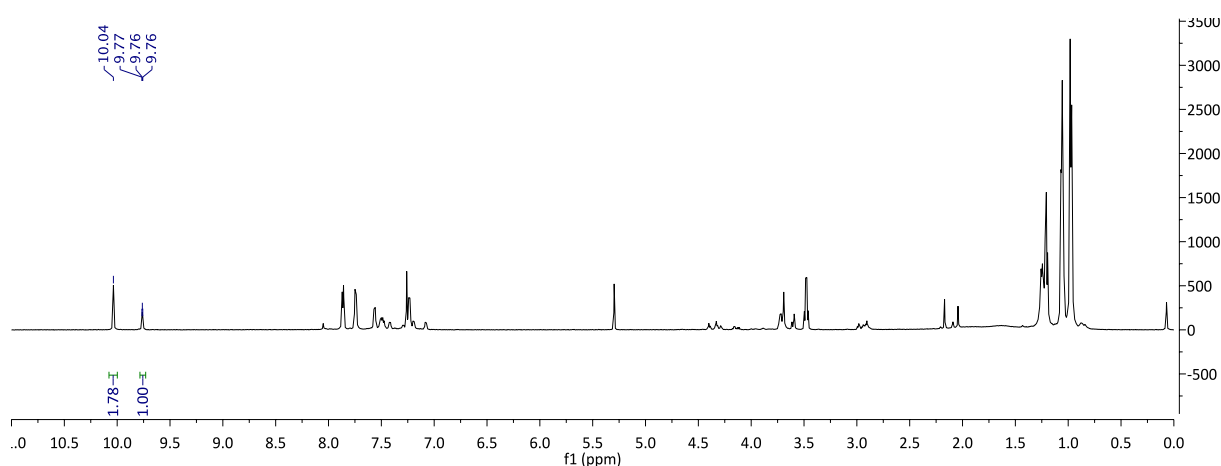


Scheme 4.7, Entry 2

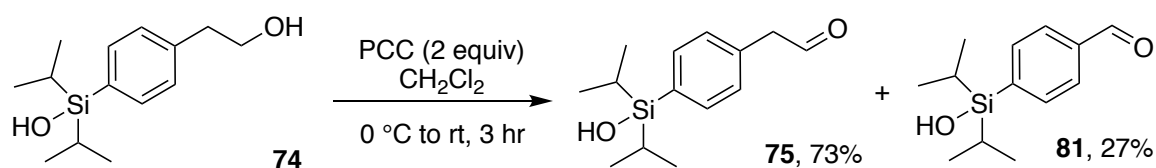
[1-(4-diisopropylsilyl)phenyl]ethanol (**74**) (19.9 mg, 0.0788 mmol) was added to a



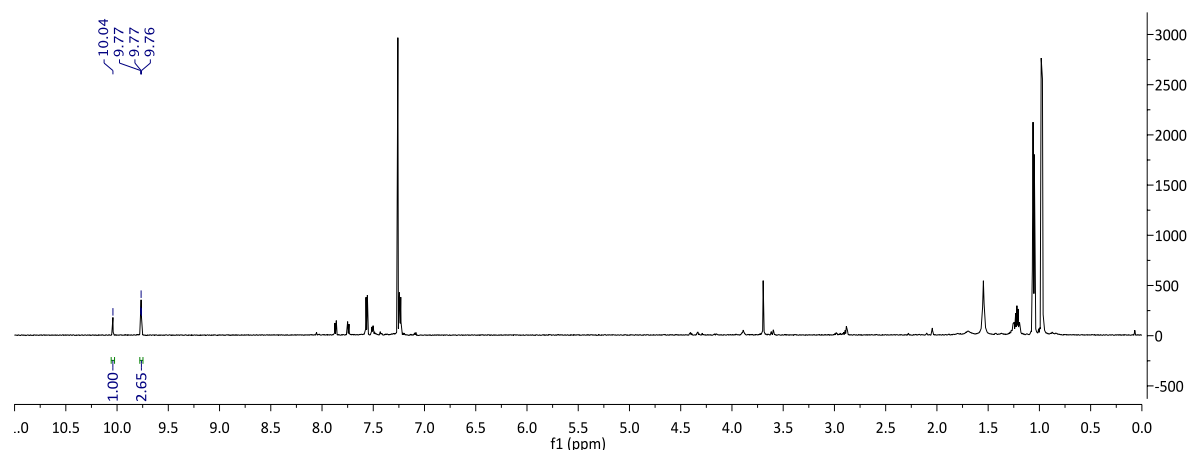
suspension of PCC (70.0 mg, 0.315 mmol) and silica (70.6 mg) in CH_2Cl_2 (0.5 mL) at 0 °C. The reaction was removed from the ice bath after 5 min and then allowed to warm to room temperature. After 3 hr total reaction time, the mixture was passed through a column of silica topped with a bed of celite, eluting with CH_2Cl_2 to yield a 1:1.78 mixture of **75** (36%) and **81** (64%), as determined by ^1H NMR spectroscopy. The ratio of aldehyde to benzaldehyde products was determined by integration of the proton signals at δ_{H} 9.7 and δ_{H} 10.0 ppm, respectively.



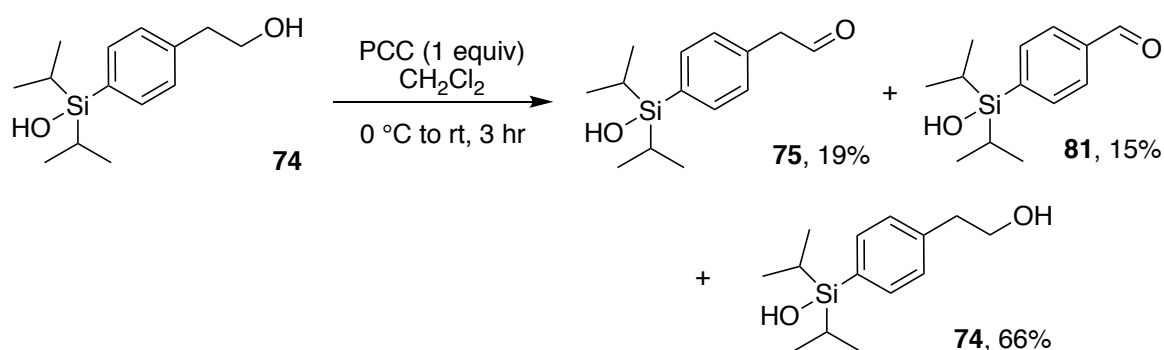
Scheme 4.7, Entry 3



[1-(4-diisopropylsilyl)phenyl]ethanol (**74**) (20.1 mg, 0.0796 mmol) was added to a suspension of PCC (34.3 mg, 0.159 mmol) and silica (35.5 mg) in CH_2Cl_2 (0.5 mL) at 0 °C. The reaction was removed from the ice bath after 5 min and then allowed to warm to room temperature. After 3 hr total reaction time, the mixture was passed through a column of silica topped with a bed of celite, eluting with CH_2Cl_2 to yield a 2.65:1 mixture of **75** (73%) and **81** (27%), as determined by ^1H NMR spectroscopy. The ratio of aldehyde to benzaldehyde products was determined by integration of the proton signals at δ_{H} 9.7 and δ_{H} 10.0 ppm, respectively.

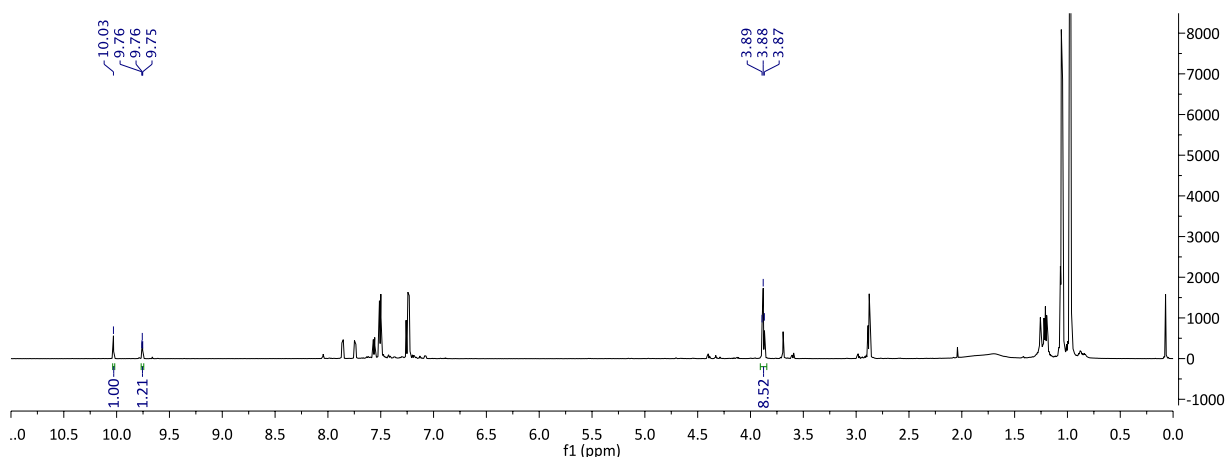


Scheme 4.7, Entry 4



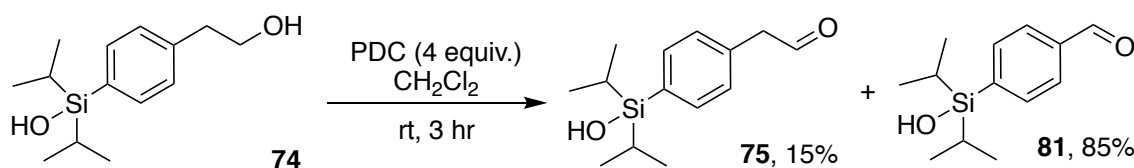
[1-(4-diisopropylsilyl)phenyl]ethanol (**74**) (20.1 mg, 0.0796 mmol) was added to a suspension of PCC (34.3 mg, 0.159 mmol) and silica (35.5 mg) in CH_2Cl_2 (0.5 mL) at 0 °C. The reaction was removed from the ice bath after 5 min and then allowed to warm to room temperature. After 3 hr total reaction time, the mixture was passed through a column of silica topped with a bed of celite, eluting with CH_2Cl_2 to yield a 1.21:1:4.26 mixture of **75** (19%) and **81**

(15%) and unreacted **74** (66%), as determined by ^1H NMR spectroscopy. The ratio of aldehyde and benzaldehyde products and starting material was determined by integration of the proton signals at δ_{H} 9.7, δ_{H} 10.0 and δ_{H} 3.8 ppm, respectively.

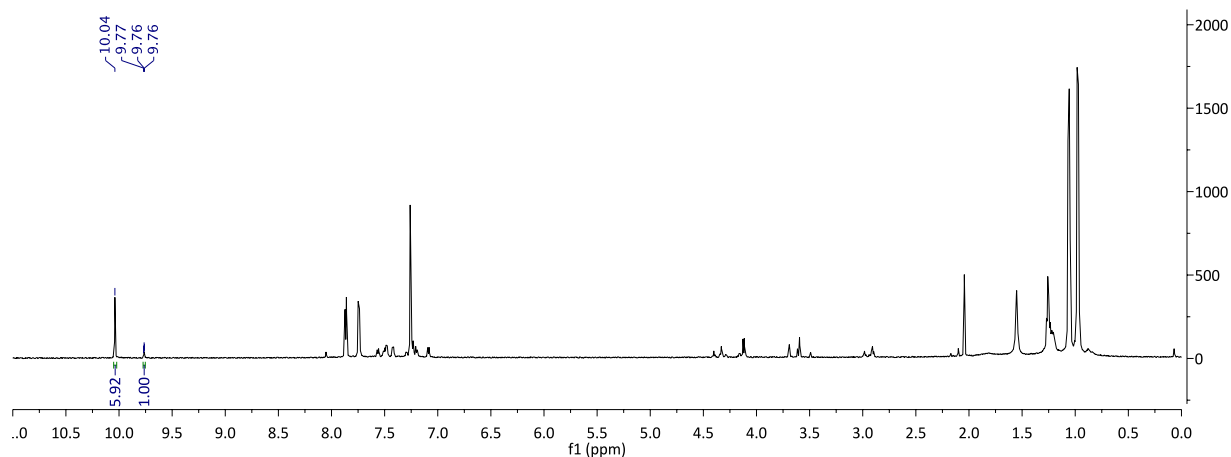


Pyridinium dichromate (PDC)

Scheme 4.7, Entry 5

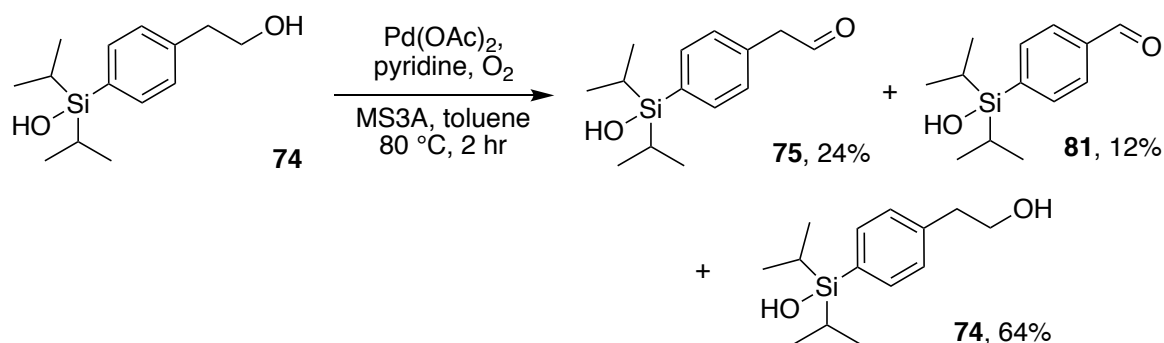


[1-(4-diisopropylsilyloxy)phenyl]ethanol (**74**) (102 mg, 0.404 mmol) was added to a suspension of PDC (610 mg, 1.62 mmol) and silica (630 mg) in CH_2Cl_2 (2 mL). The reaction was stirred for 3 hr. The reaction mixture was passed through a column of silica topped with a bed of celite, eluting first with CH_2Cl_2 and then 40 % EtOAc in hexane to yield a 1:5.92 mixture of **75** (15%) and **81** (85%), as determined by ^1H NMR spectroscopy. The ratio of aldehyde to benzaldehyde products was determined by integration of the proton signals at δ_{H} 9.7 and δ_{H} 10.0 ppm, respectively.

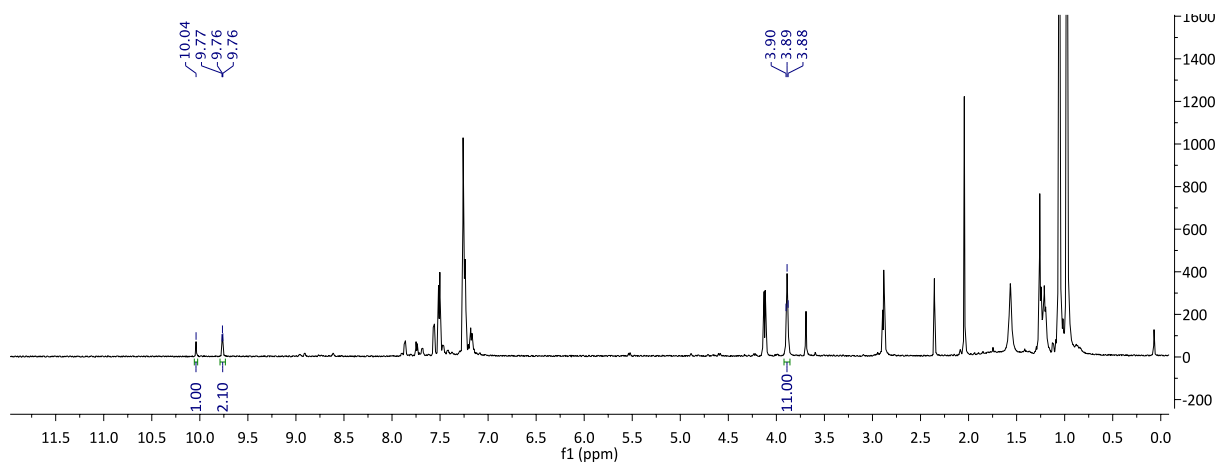


Palladium catalysed aerobic oxidation ($\text{Pd}(\text{OAc})_2/\text{O}_2$)

Scheme 4.7, Entry 6

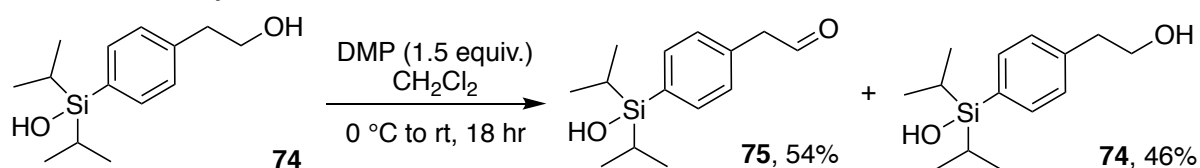


Pyridine (6 μL , 20 mol %) and molecular sieves (3 \AA , 284 mg) were added to a suspension of $\text{Pd}(\text{OAc})_2$ (5 mg, 5 mol %) in toluene (3 mL). Oxygen was bubbled through the solution (2 balloon volumes) before the reaction was heated to 80°C and maintained under 1 atmosphere of oxygen (balloon). Once the temperature had stabilised a solution of [1-(4-diisopropylsilyl)phenyl]ethanol (**74**) (103 mg, 0.410 mmol) in toluene (2 mL) was added and the reaction stirred for 2 hr. The reaction mixture was filtered over a bed of celite and the solvent removed to afford a mixture of **75** (24%), **81** (12%) and unreacted **74** (64%), as determined by ^1H NMR spectroscopy. The ratio of aldehyde to benzaldehyde to starting material was determined by integration of the proton signals at δ_{H} 9.7, δ_{H} 10.0 and δ_{H} 3.89 ppm, respectively.

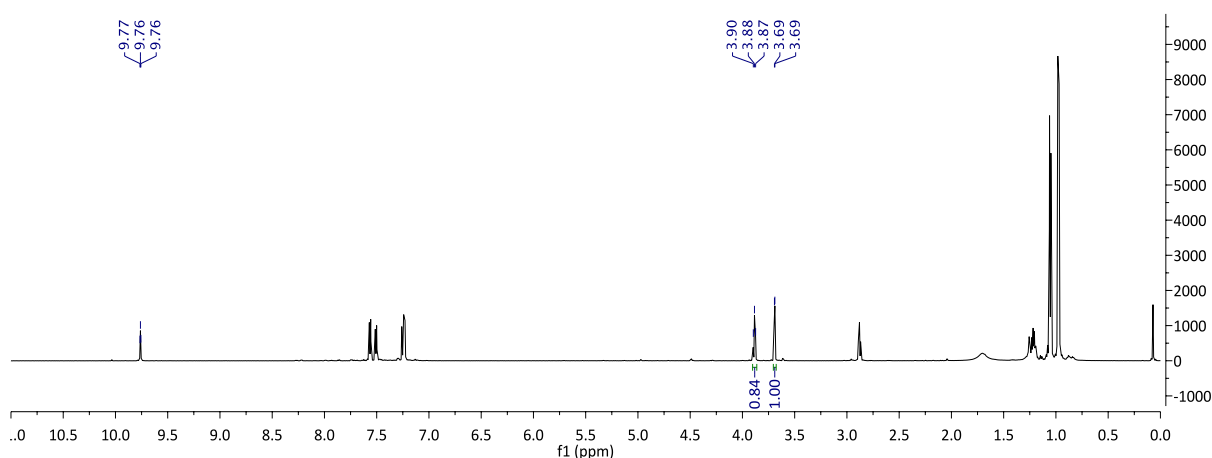


Dess–Martin periodinane (DMP)

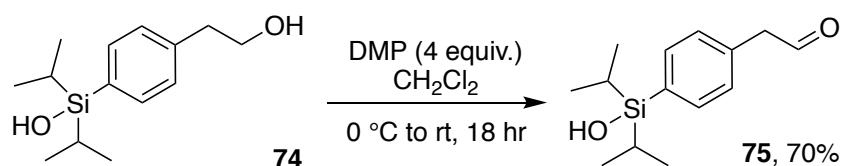
Scheme 4.7, Entry 7



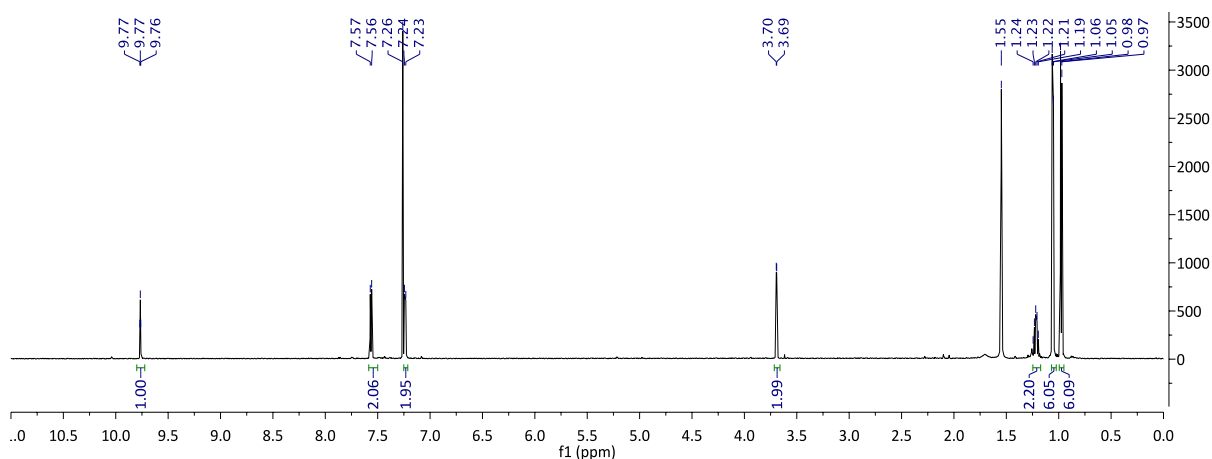
[1-(4-diisopropylsilylanol)phenyl]ethanol (**74**) (20.3 mg, 0.080 mmol) was added to a suspension of DMP (29.1 mg, 0.121 mmol) in CH₂Cl₂ (1 mL) at 0 °C. The ice bath was removed after 5 min and the reaction was allowed to warm to room temperature. After 18 hr total reaction time, the reaction was quenched with a 2 mL 1:1 saturated aqueous solution of Na₂S₂O₃ and NaHCO₃. The aqueous phase was extracted with CH₂Cl₂ (3 × 3 mL). The organic fractions were combined, washed with brine (5 mL), dried (Na₂SO₄), filtered and the solvent removed under reduced pressure to yield a 1:0.84 mixture of **75** (54%) and unreacted **74** (46%), as determined by ¹H NMR spectroscopy. The ratio of aldehyde to benzaldehyde was determined by integration of the proton signals at δ_H 3.8 and δ_H 3.7 ppm, respectively.



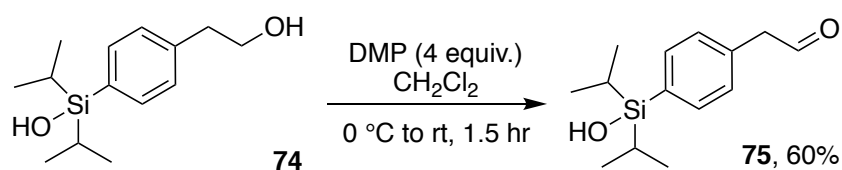
Scheme 4.7, Entry 8



[1-(4-diisopropylsilylanol)phenyl]ethanol (**74**) (50.0 mg, 0.198 mmol) was added to a suspension of DMP (192 mg, 0.792 mmol) in CH₂Cl₂ (5 mL) at 0 °C. The ice bath was removed after 5 min and the reaction was allowed to warm to room temperature. After 18 hr total reaction time, the reaction was quenched with a 16 mL 1:1 saturated aqueous solution of Na₂S₂O₃ and NaHCO₃. The aqueous phase was extracted with CH₂Cl₂ (3 × 5 mL). The organic fractions were combined, washed with brine (10 mL), dried (Na₂SO₄), filtered and the solvent removed under reduced pressure. The residue was purified by column chromatography (40% EtOAc in hexanes) to afford **75** (R_f = 0.62) as a clear liquid (34.8 mg, 70 %).



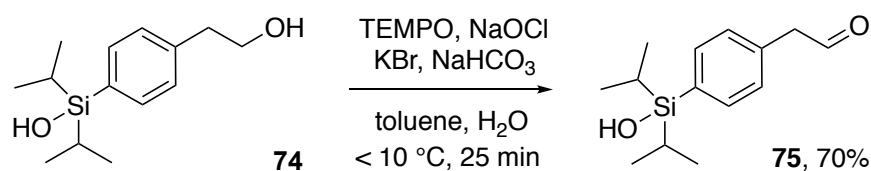
Scheme 4.7, Entry 9



[1-(4-diisopropylsilyl)phenyl]ethanol (**74**) (851 mg, 3.03 mmol) was added to a suspension of DMP (2.94 g, 0.792 mmol) in CH_2Cl_2 (10 mL) at 0 °C. The ice bath was removed after 15 min and the reaction was allowed to warm to room temperature. After 1.5 hr total reaction time, the reaction was quenched with a 30 mL 1:1 saturated aqueous solution of $\text{Na}_2\text{S}_2\text{O}_3$ and NaHCO_3 . The aqueous phase was extracted with CH_2Cl_2 (3 \times 10 mL). The organic fractions were combined, washed with brine (20 mL), dried (Na_2SO_4), filtered and the solvent removed under reduced pressure. The residue was purified by column chromatography (40% EtOAc in hexanes) to afford **75** ($R_f = 0.62$) as a clear liquid (507 mg, 60 %).

TEMPO/sodium hypochlorite oxidation (TEMPO/NaOCl)

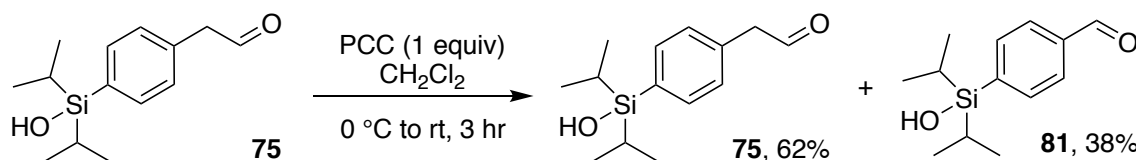
Scheme 4.7, Entry 10



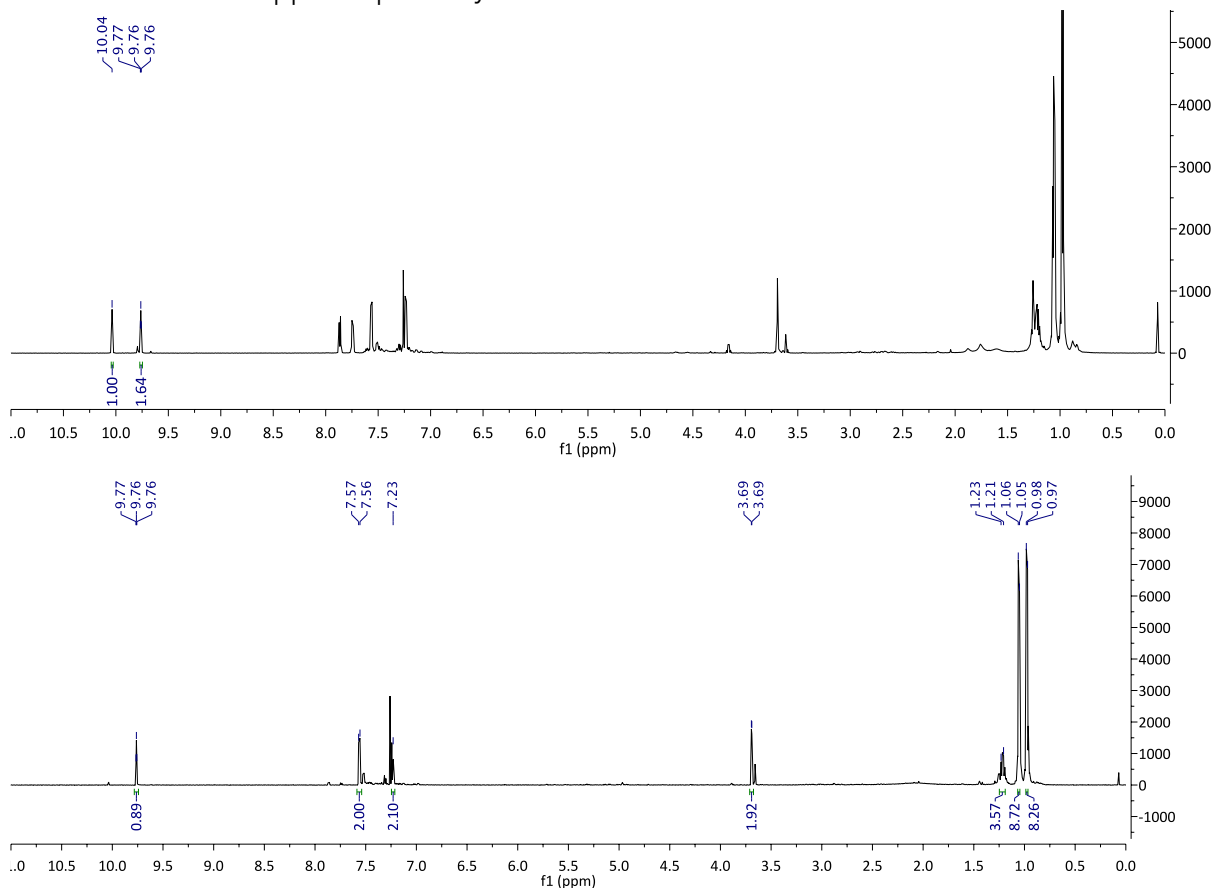
[1-(4-diisopropylsilyl)phenyl]ethanol **74** (116 mg, 0.459 mmol) was added to a round bottom flask and suspended in toluene (5 mL). The mixture was sonicated for 3 min to help partially dissolve **74**. Next, a saturated aqueous solution of NaHCO_3 (2.1 mL) was added to the reaction vessel followed by KBr (60 mg, 0.504 mmol) and then TEMPO (6.1 mg, 0.052 mmol). The solution was cooled to below 10 °C (internal temperature) using an ice bath and aqueous NaOCl

(4 wt%, 1.475 mL, 0.79 mmol) was added dropwise. The reaction stirred for 25 min, maintaining an internal reaction temperature < 10 °C. After 25 min total reaction time, the organic phase was separated and then washed with H₂O (2 × 10 mL), dried (NaSO₄), filtered, and the solvent removed under reduced pressure to afford **75** as a yellow oil (80 mg, 70%).

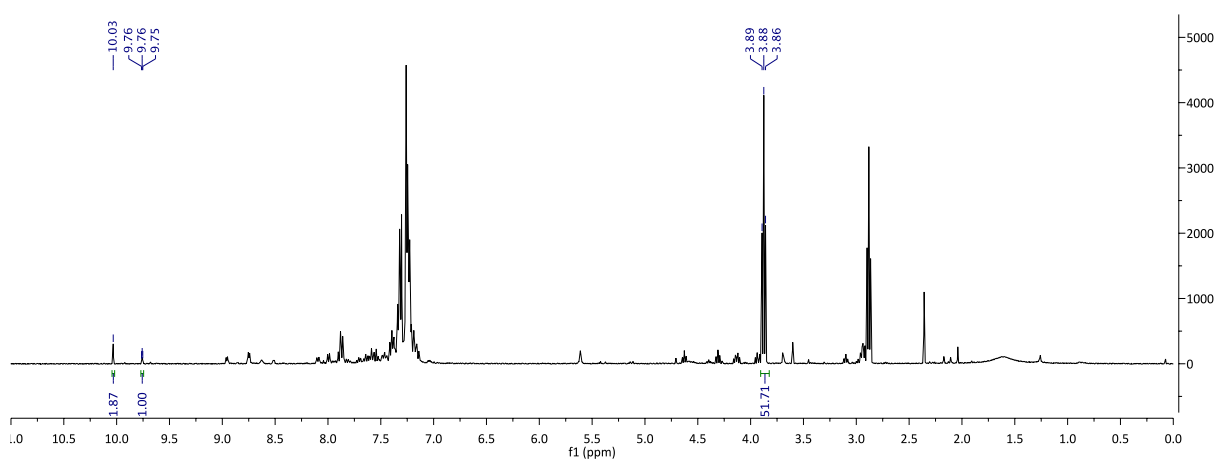
Pyridinium chlorochromate (PCC) oxidation of aldehyde 75



[1-(4-diisopropylsilyl)phenyl]ethanal (**75**) (19.9 mg, 0.0392 mmol) was added to a suspension of PCC (17.2 mg, 0.0795 mmol) and silica (22.1 mg) in CH₂Cl₂ (0.5 mL) at 0 °C. The reaction was removed from the ice bath after 5 min and then allowed to warm to room temperature. After 3 hr total reaction time, the mixture was passed through a column of silica topped with a bed of celite, eluting with CH₂Cl₂ to yield a 1:1.64 mixture of **81** (38%) and unreacted **75** (62%), as determined by ¹H NMR spectroscopy. The ratio of aldehyde and benzaldehyde products and starting material was determined by integration of the proton signals at δ_H 9.7 and δ_H 10.0 ppm respectively.

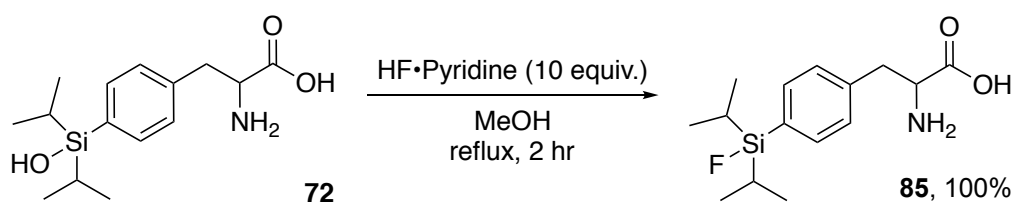


balloon volume) before the reaction was heated to 80 °C and maintained under 1 atmosphere of oxygen (balloon). Once the temperature had stabilised 2-phenylethanol (98 μL , 0.892 mmol) was added and the reaction stirred for 6 hr. The reaction mixture was filtered over a bed of celite and the solvent removed to afford a mixture of unreacted starting material (95%), 2-phenylethanal (2%) and benzaldehyde (3%), as determined by ^1H NMR spectroscopy. The ratio of aldehydes to benzaldehyde to starting material was determined by integration of the proton signals at δ_{H} 9.76, δ_{H} 10.03 and δ_{H} 3.88 ppm, respectively.



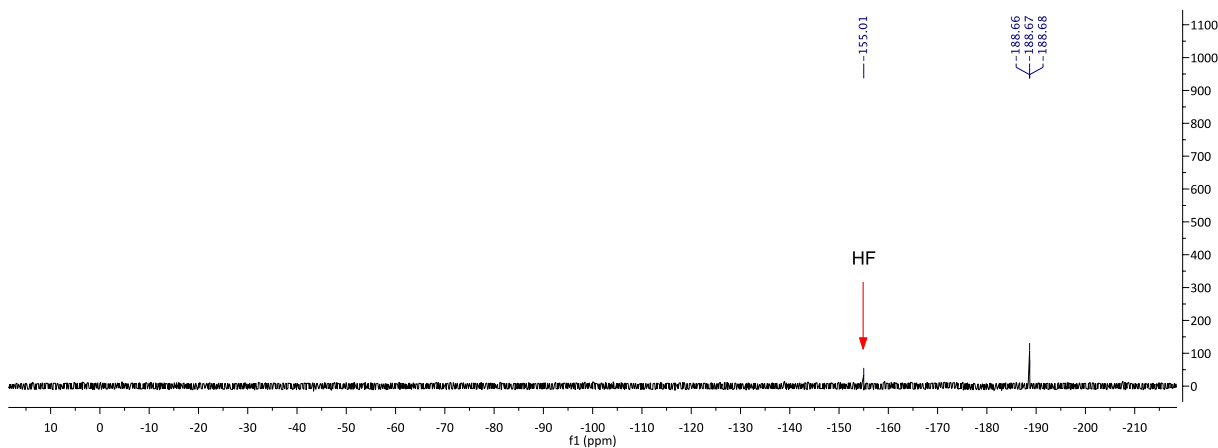
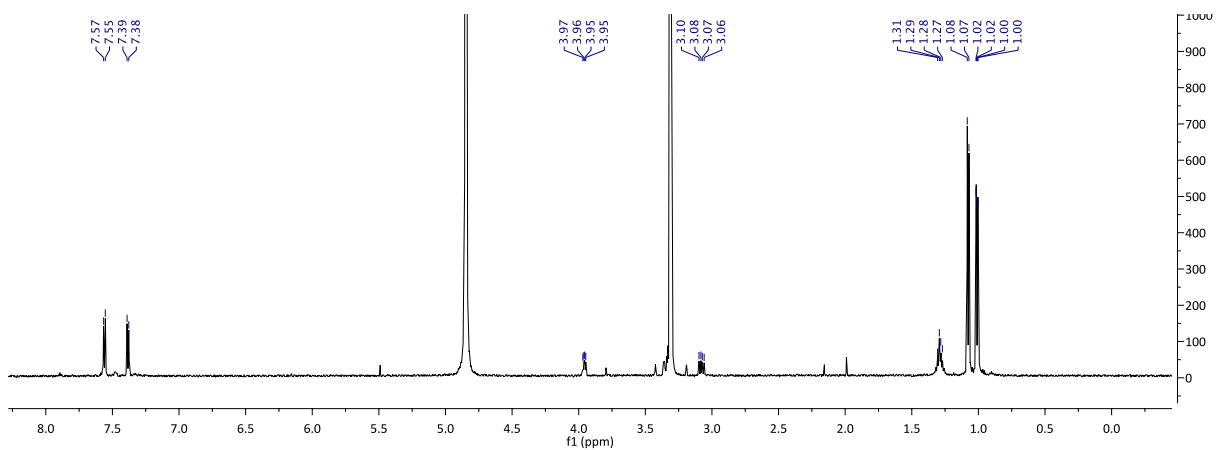
4.7.4 Aqueous fluorination studies of 2-amino[3-(4-diisopropylfluorosilyl)phenyl]propanoic acid (**72**)

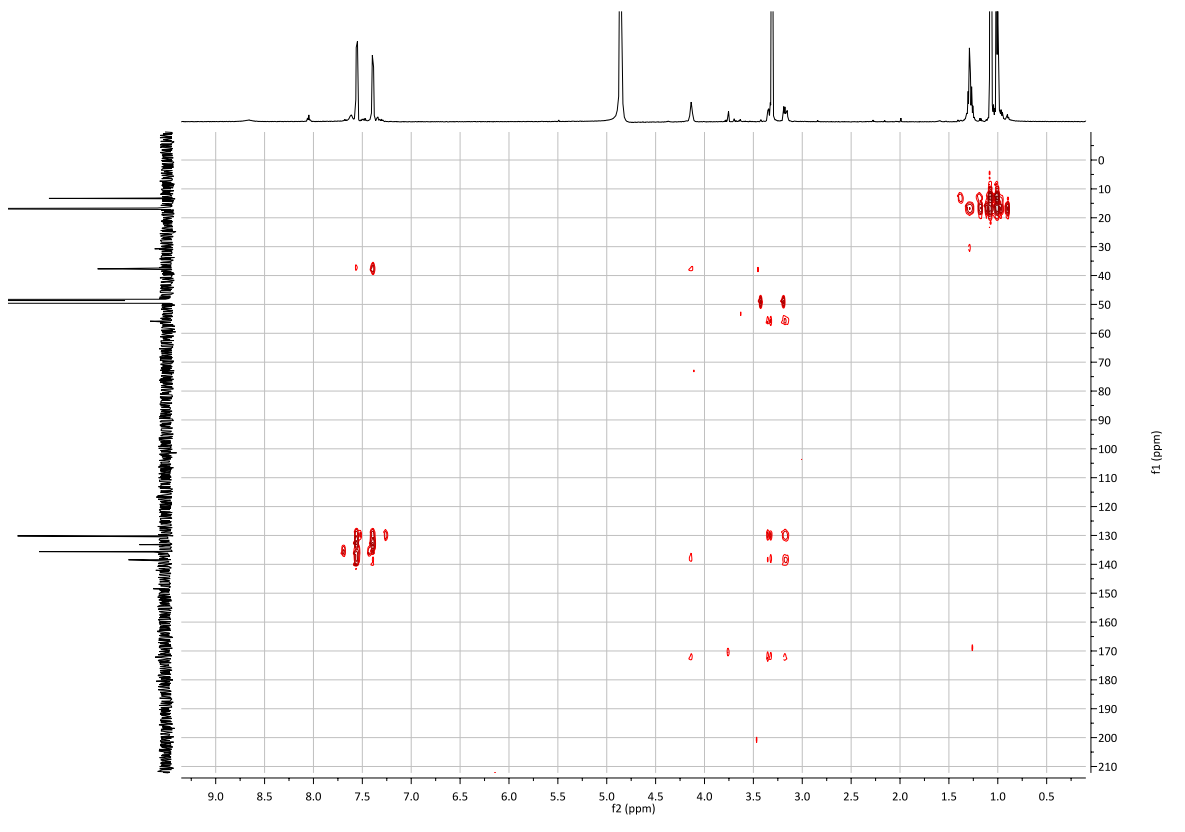
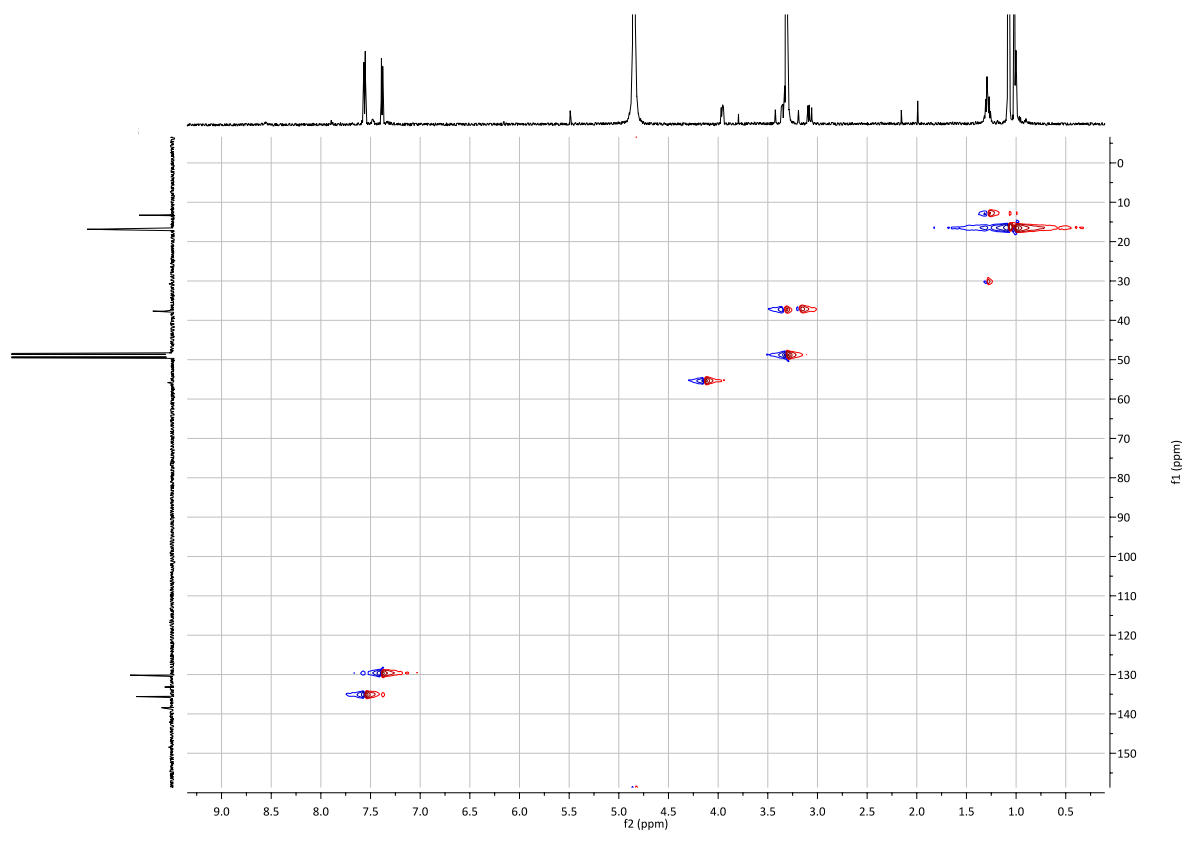
2-amino[3-(4-diisopropylfluorosilyl)phenyl]propanoic acid ((\pm)-**72**)



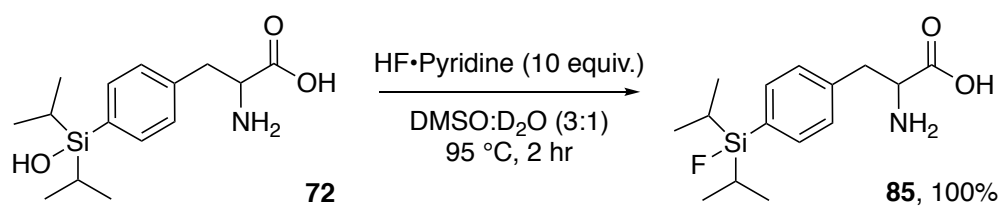
HF•Pyridine (43 μL , 1.73 mmol) was then added to (\pm)-**72** (51.2 mg, 0.173 mM, 0.016 mmol) in MeOH (2 mL) in a round bottom flask fitted with a reflux condenser. The reaction was heated at reflux. After 2 hr stirring at reflux, the reaction was cooled and the solvent removed under reduced pressure. The residue was triturated with minimal water to remove the pyridine and the resulting white solid, was dried under vacuum. Full conversion to the fluorinated derivative (\pm)-**85** was observed by NMR spectroscopy. ^1H NMR (600 MHz, Methanol- d_4) δ_{H} 7.56 (d, $J = 7.7$ Hz, 2H, ArH), 7.38 (d, $J = 7.7$ Hz, 2H, ArH), 3.96 (dd, $J = 8.4, 4.7$ Hz, 1H, CH α), one of the CH β signals is masked by MeOD, an HSQC experiment shows the correlation of CH β and CH β' to the same carbon, 3.08 (dd, $J = 14.7, 8.4$ Hz, 1H, CH β'), 1.29 (m, 2H, *i*PrH), 1.08 (d, $J =$

7.4 Hz, 6H, *iPrCH*₃), 1.01 (d, J = 7.5 Hz, 6H, *iPrCH*); ¹³C NMR (151 MHz, Methanol-*d*₄) δ_C 170.87, 137.14, 134.17, 134.15, 131.70, 131.60, 128.76, 54.58, 36.32, 15.63, 15.62, 15.46, 11.98, 11.89; ¹⁹F NMR (565 MHz, Methanol-*d*₄) δ_F -188.67 (t, J = 6.0 Hz, SiE); HRMS (ESI) calculated for [C₁₅H₂₃O₂NSiF]⁻ 296.1488; found 296.1487.

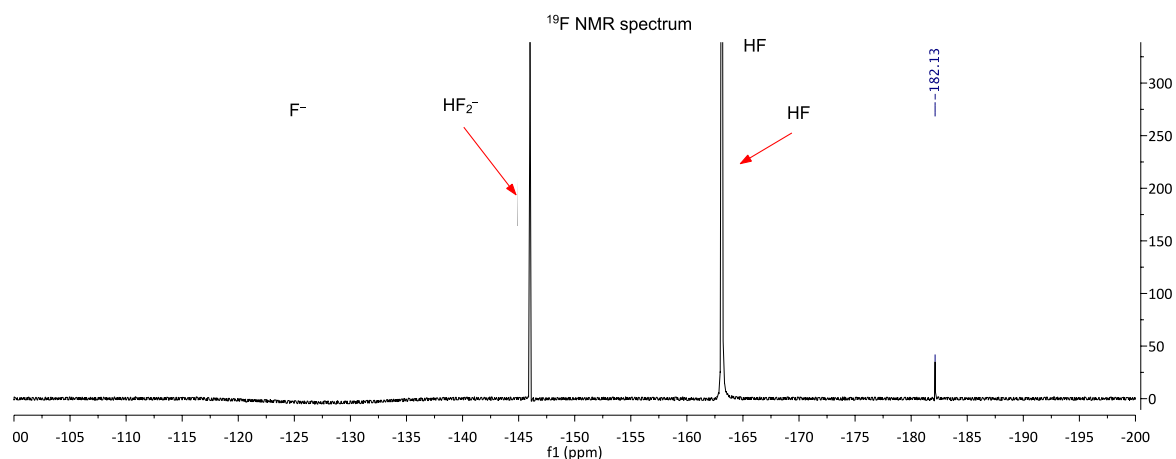
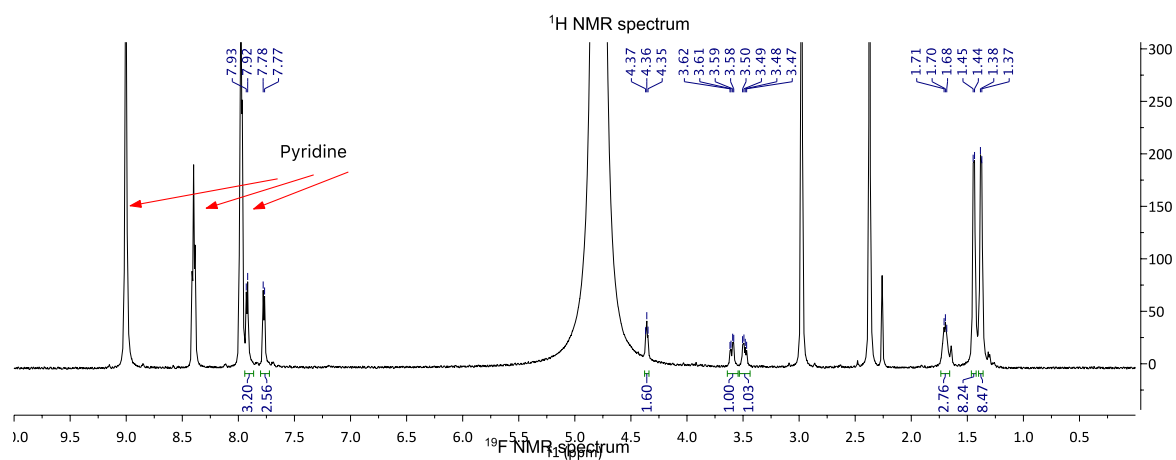




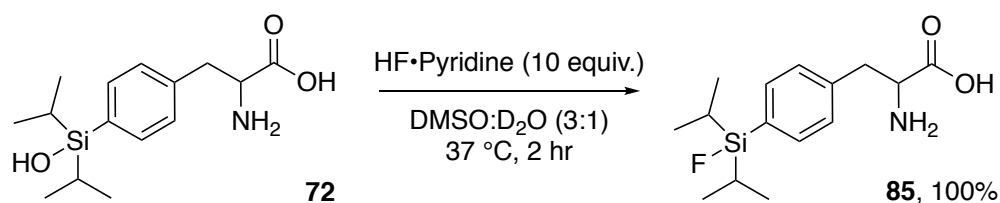
Scheme 4.11, Entry 1



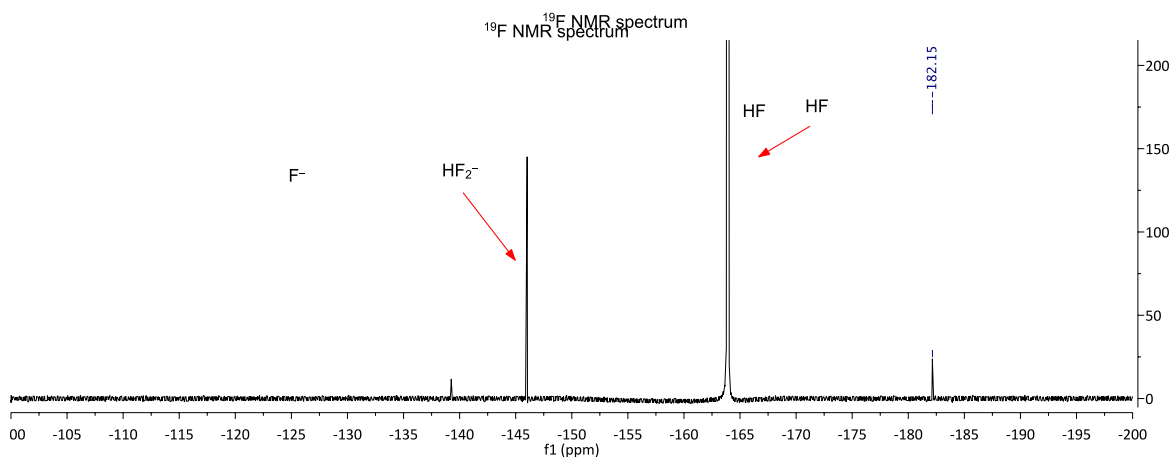
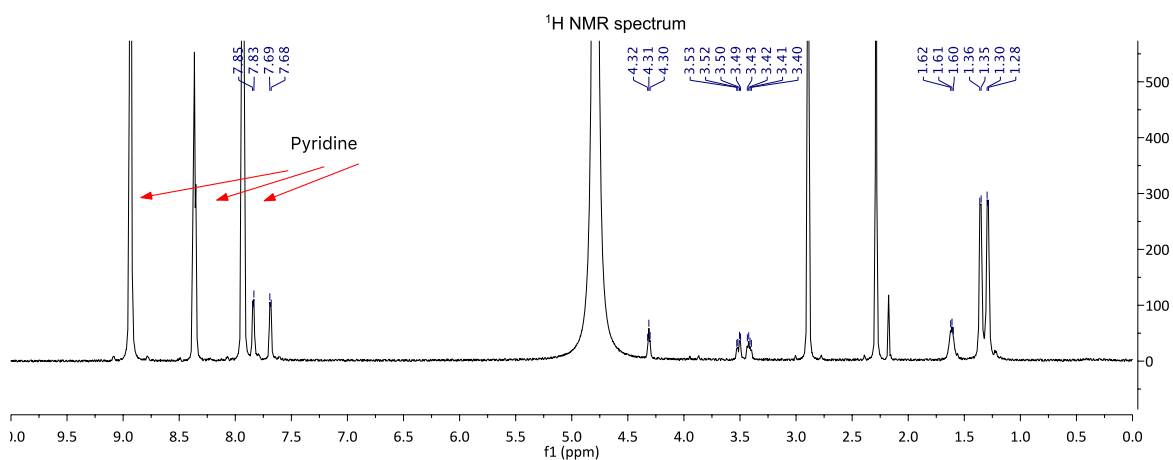
DMSO- d_6 (300 μL) was added to a solution of (\pm)-**72** (100 μL , 1.69 mM, 0.0169 mmol) in D_2O in a 1.5 mL plastic microcentrifuge tube. $\text{HF}\cdot\text{Pyridine}$ (4.4 μL , 0.169 mmol) was then added and the tube was shaken at 95 $^\circ\text{C}$ for 2 hr. After this time the solution was transferred to FEP liner NMR tube and analysed by NMR spectroscopy. A signal at $\delta_{\text{F}} -182.13$ ppm, consistent with a Si-F bond, in the ^{19}F NMR spectrum supported that fluorination had occurred. The ^1H NMR spectrum showed 100% conversion to (\pm)-**85**. ^1H NMR (600 MHz, Deuterium Oxide) δ_{H} 7.92 (d, $J = 7.6$ Hz, 2H), 7.77 (d, $J = 7.5$ Hz, 2H), 4.36 (t, $J = 6.6$ Hz, 1H), 3.60 (dd, $J = 14.4, 5.6$ Hz, 1H), 3.49 (dd, $J = 14.4, 7.3$ Hz, 1H), 1.74 – 1.66 (m, 2H), 1.44 (d, $J = 7.5$ Hz, 6H), 1.38 (d, $J = 7.5$ Hz, 6H); ^{19}F NMR (565 MHz, Deuterium Oxide) $\delta_{\text{F}} -182.13$.



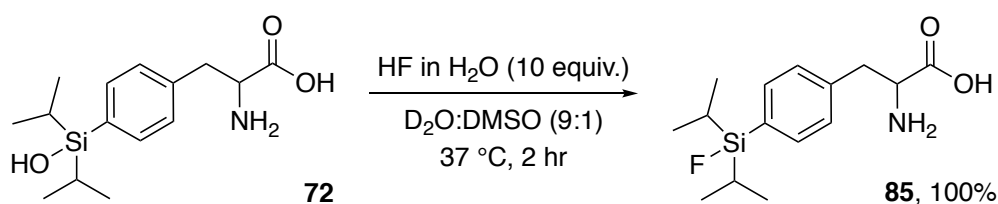
Scheme 4.11, Entry 2



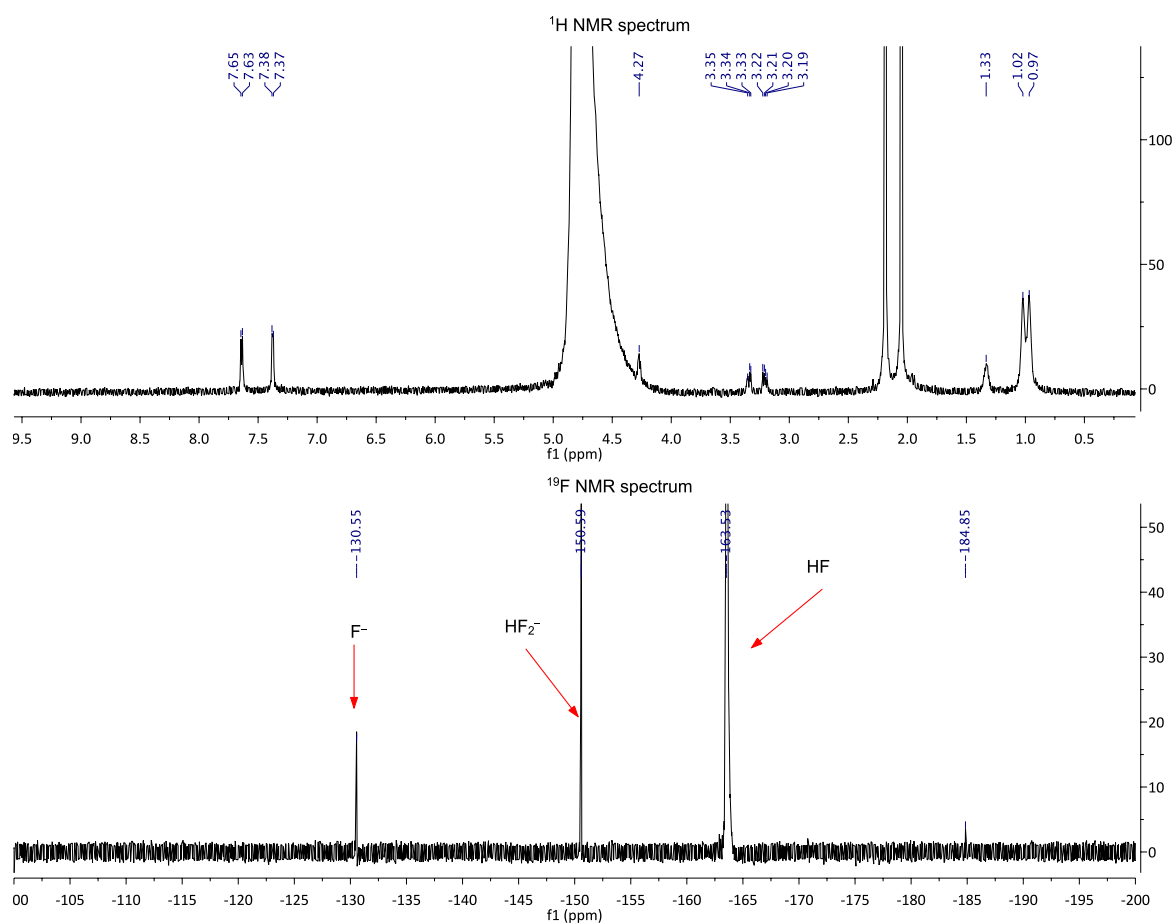
DMSO- d_6 (30 μL) was added to a solution of (\pm)-**72** (100 μL , 1.69 mM, 0.0169 mmol) in D_2O in a 1.5 mL plastic microcentrifuge tube. HF \cdot Pyridine (4.4 μL , 0.169 mmol, 10 equiv.) was then added and the tube was shaken at 37 $^\circ\text{C}$ for 2 hr. After this time the solution was transferred to FEP liner NMR tube and analysed by NMR. A signal at δ_{F} -182.15 ppm, consistent with a Si-F bond, in the ^{19}F NMR spectrum supported that fluorination had occurred. The ^1H NMR spectrum showed 100% conversion to (\pm)-**85**. ^1H NMR (600 MHz, Deuterium Oxide) δ_{H} 7.84 (d, J = 7.5 Hz, 2H), 7.69 (d, J = 7.4 Hz, 2H), 4.31 (t, J = 6.5 Hz, 1H), 3.51 (dd, J = 14.5, 5.7 Hz, 1H), 3.42 (dd, J = 14.3, 7.2 Hz, 1H), 1.66 – 1.54 (m, 2H), 1.36 (d, J = 7.4 Hz, 6H), 1.29 (d, J = 7.5 Hz, 6H); ^{19}F NMR (565 MHz, Deuterium Oxide) δ_{F} -182.15.



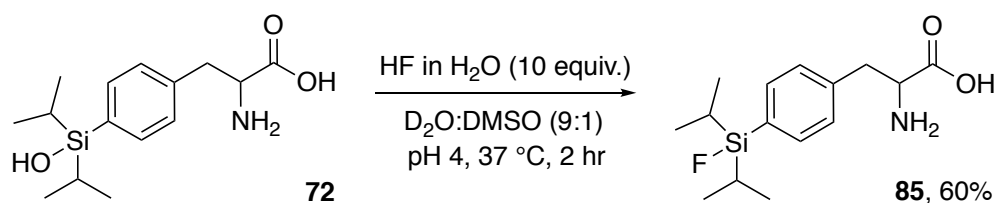
Scheme 4.11, Entry 3



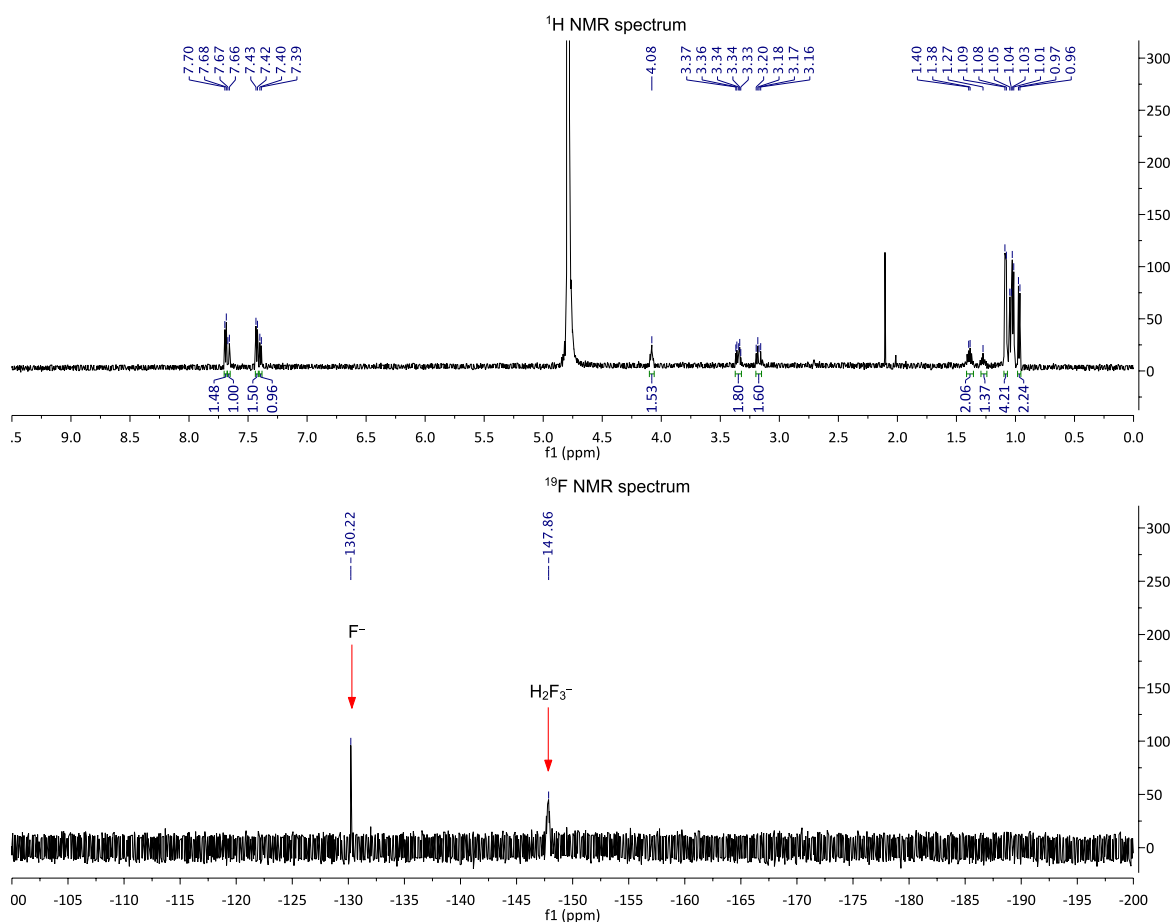
D₂O (165.6 μL) and DMSO-d₆ (30 μL, 10 %) were added to a solution of (±)-**72** (100 μL, 1.69 mM, 0.0169 mmol) in D₂O in a 1.5 mL plastic microcentrifuge tube. A solution of HF in H₂O (48 %, 6.13 μL, 0.169 mmol) was added and the tube was shaken at 37 °C for 2 hr. During the course of the reaction a precipitate formed which was found to be (±)-**85** (no unreacted starting material was detected). The supernatant was removed by pipette and the precipitated product was re-dissolved in D₂O. A signal at δ_F –184.84 ppm, consistent with a Si-F bond, in the ¹⁹F NMR spectrum supported that fluorination had occurred. The signals at δ_F –130 and –150 ppm are from that of F[–] and HF₂[–] respectively, species known to form in aqueous solutions of hydrogen fluoride.¹⁹⁵ The ¹H NMR spectrum showed 100% conversion to (±)-**85**. ¹H NMR (600 MHz, Deuterium Oxide) δ_H 7.64 (d, J = 7.6 Hz, 2H), 7.38 (d, J = 7.4 Hz, 2H), 4.27 (t, 2H), 3.34 (dd, 1H), 3.21 (dd, J = 14.4, 7.9 Hz, 1H), 1.33 (s, 3H), 1.02 (s, 6H), 0.97 (s, 6H); ¹⁹F NMR (565 MHz, Deuterium Oxide) δ_F –184.84.



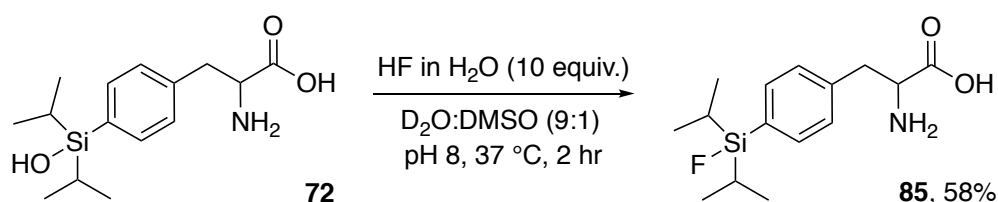
Scheme 4.11, Entry 4



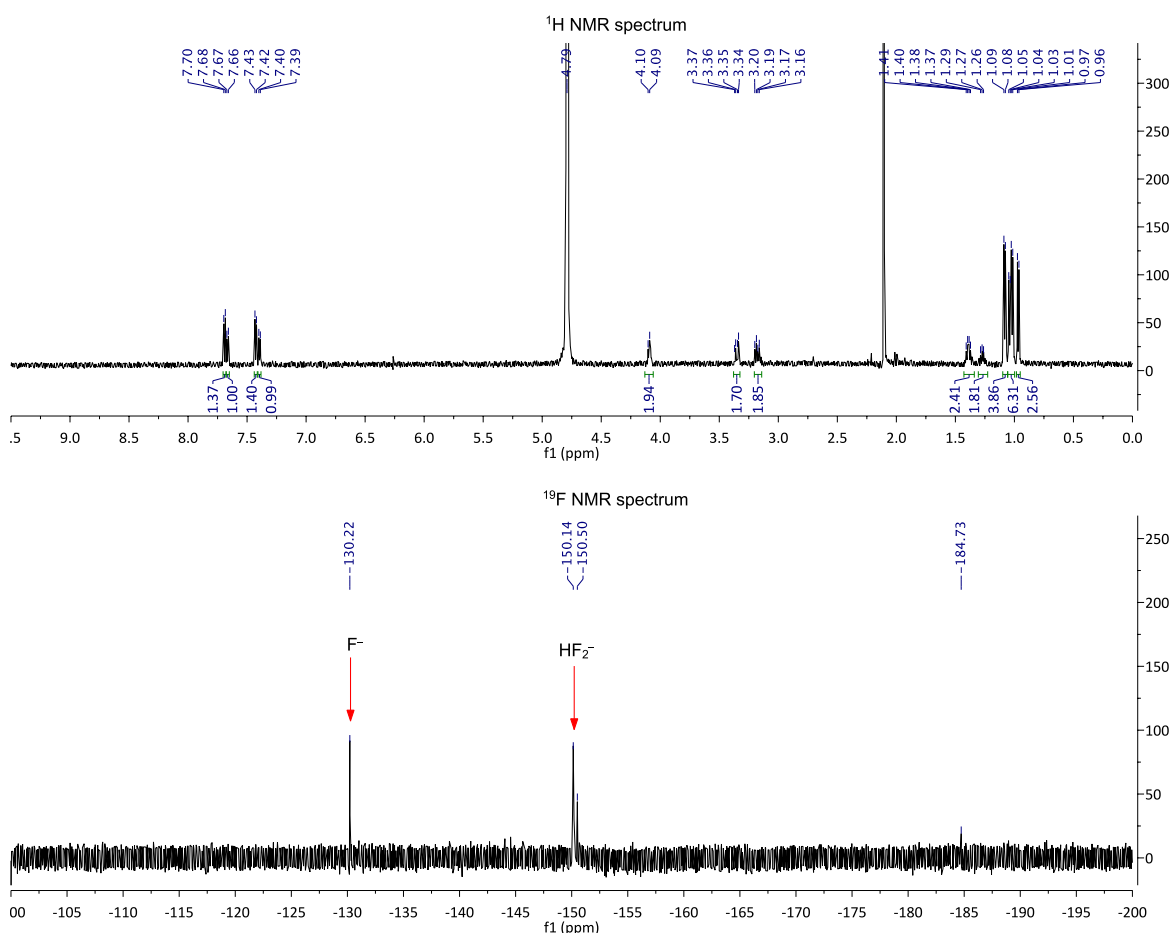
A sodium acetate buffer in D₂O (20 mM, 165.6 μL, pH 4) and DMSO-d₆ (30 μL, 10 %) were added to a solution of (±)-**72** (100 μL, 1.69 mM, 0.0169 mmol) in a 1.5 mL plastic microcentrifuge tube. A solution of HF in H₂O (48 %, 6.13 μL, 0.169 mmol) was added and the tube was shaken at 37 °C for 2 hr. During the course of the reaction a precipitate formed which was found to be a mixture of (±)-**72** and (±)-**85**. The supernatant was removed by pipette and the precipitate was dissolved in D₂O to yield a 1.5:1 mixture of (±)-**85** (60%) and (±)-**72** (40%), as determined by ¹H NMR spectroscopy. The conversion of **72** to **85** was determined by integration of the proton signals at δ_H 7.67 and δ_H 7.70 ppm, respectively. No signal for the product was observed in the ¹⁹F NMR spectra presumably due to the low yield and concentration. The signals at δ_F -130 and -147 ppm are from that of F⁻ and H₂F₃⁻ respectively, species known to form in aqueous solutions of hydrogen fluoride.¹⁹⁵



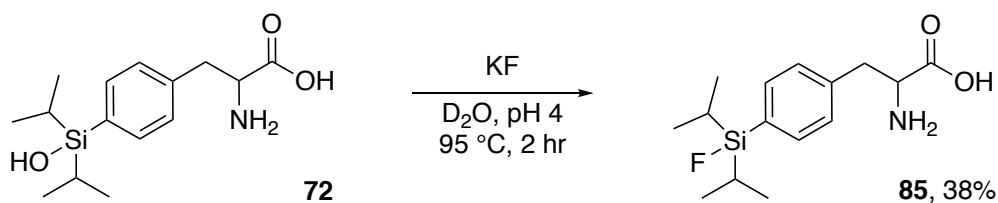
Scheme 4.11, Entry 5



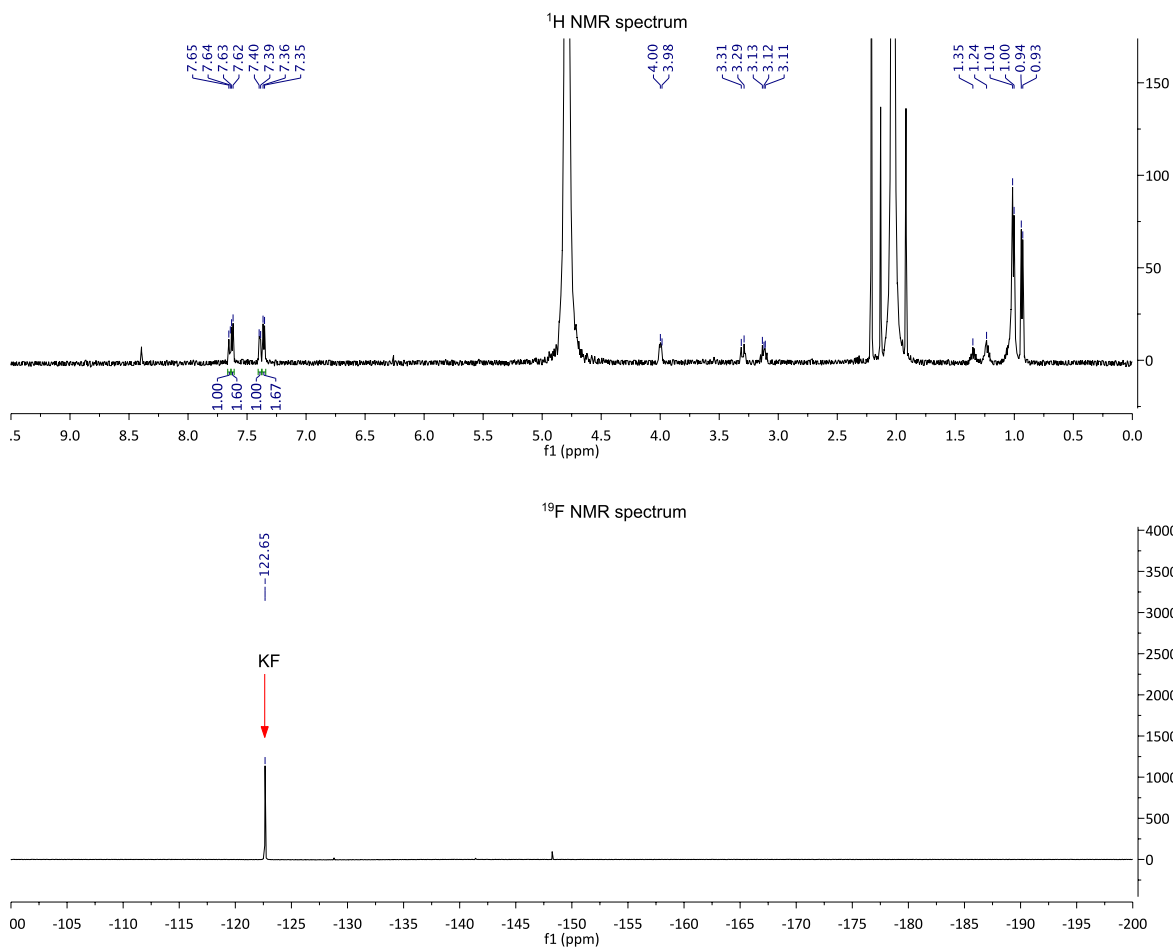
A phosphate buffer in D₂O (20 mM, 165.6 μL, pH 8) and DMSO-d₆ (30 μL, 10 %) were added to a solution of (±)-**72** (100 μL, 1.69 mM, 0.0169 mmol) in a 1.5 mL plastic microcentrifuge tube. A solution of HF in H₂O (48 %, 6.13 μL, 0.169 mmol) was added and the tube was shaken at 37 °C for 2 hr. During the course of the reaction a precipitate formed which was found to be a mixture of (±)-**72** and (±)-**85**. The supernatant was removed by pipette and the precipitate was dissolved in D₂O to yield a 1.4:1 mixture of (±)-**85** (58%) and (±)-**72** (42%), as determined by ¹H NMR spectroscopy. ¹⁹F NMR spectroscopy indicated successful fluorination with a signal at δ_F –184.84 ppm. The signals at δ_F –130 and –150 ppm are from that of F⁻ and HF₂⁻ respectively, species known to form in aqueous solutions of hydrogen fluoride.¹⁹⁵ The conversion of **72** to **85** was determined by integration of the proton signals at δ_H 7.67 and δ_H 7.70 ppm, respectively.



Scheme 4.11, Entry 6



A sodium acetate buffer in D₂O (20 mM, 500 μ L, pH 4) was added to a solution of (\pm)-**72** (100 μ L, 1.69 mM, 0.0169 mmol) in D₂O in a 1.5 mL plastic microcentrifuge tube. KF (9.8 mg, 0.169 mmol) was added and the tube was shaken at 95 $^{\circ}$ C for 2 hr. During the course of the reaction a precipitate formed which was found to be a mixture of (\pm)-**72** and (\pm)-**85**. The supernatant was removed by pipette and the precipitate was dissolved in D₂O to yield a 1:1.60 mixture of (\pm)-**85** (38%) and (\pm)-**72** (62%), as determined by ¹H NMR spectroscopy. The conversion of **72** to **85** was determined by integration of the proton signals at δ_{H} 7.63 and δ_{H} 7.65 ppm, respectively. No signal for the product was observed in the ¹⁹F NMR spectra presumable due to the low yield and concentration.



Chapter Five

Genetic incorporation of a silicon-based amino acid

5.1 Introduction

The design and synthesis of an unnatural amino acid for genetic incorporation into proteins was presented in Chapter 4. The unnatural amino acid could be fluorinated with excellent conversions in up to 90% aqueous solution and at different pH. Thus, we were encouraged to continue our research and explore the genetic incorporation of this unnatural amino acid into proteins.

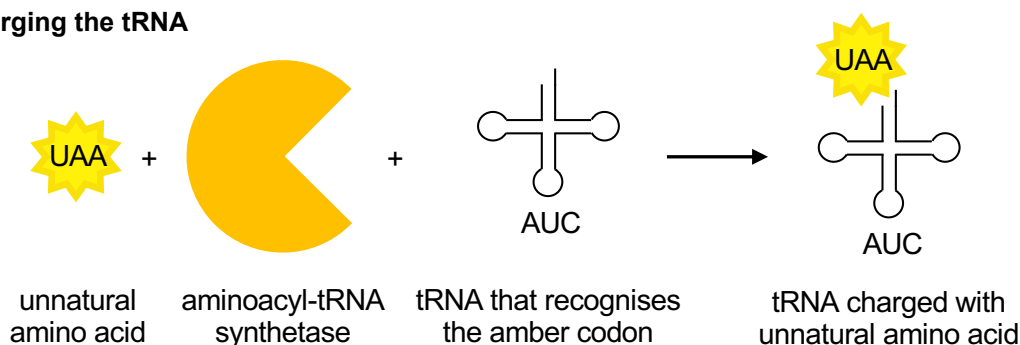
One such way to do this is through amber codon suppression whereby a mutant tRNA that recognises the amber codon allows for translation to continue therefore 'suppressing' the amber codon. With an aminoacyl-tRNA synthetase that can charge the mutant tRNA with an unnatural amino acid, it can be incorporated into the protein during translation. A depiction of amber codon suppression is shown in Scheme 5.1.

Chapter 5 details the expansion of the genetic code to incorporate this silanol-based amino acid into green fluorescent protein using amber codon suppression. The work in this

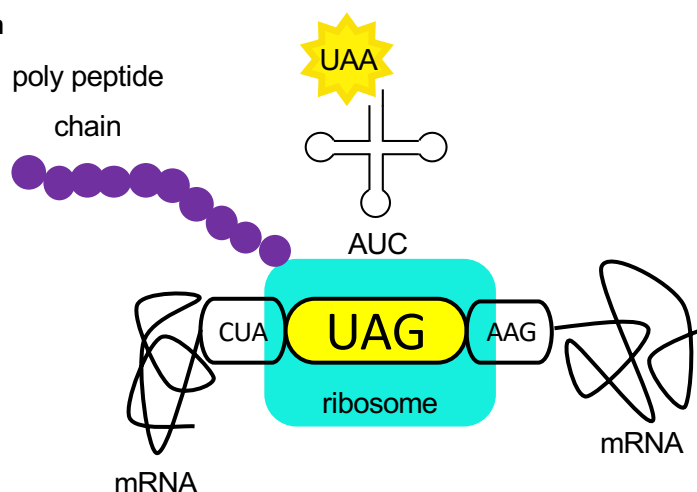
Chapter represents only one example of the numerous proteins that could be site-selectively modified to incorporate a silanol using this method.

The data and conclusions presented here in this Chapter have not been prepared for publication in any scientific journal nor have they been reported anywhere else at the date of thesis submission. The experiments and data presented in this Chapter on the genetic incorporation of an unnatural amino acid into green fluorescent protein (GFP) were conducted and collected by the candidate during a research visit to the School of Medicine, University of Virginia, USA. This research was funded in part by The Australian Federation of University Women – South Australia Graduate Centenary Scholarship. The candidate planned, researched, conducted and prepared the following Chapter with full intellectual and practical contributions unless otherwise stated in-text.

A. Charging the tRNA



B. Protein translation



Scheme 5.1 Amber codon suppression

5.2 C321.ΔA *E.coli* cells

Having synthesised a silanol-based amino acid that can be fluorinated under protein compatible conditions, we next sought to incorporate it into proteins using amber codon suppression. As the amber codon is also recognised by release factor 1 (RF1) there is a continual competition during translation between unnatural amino acid incorporation and termination by release factor 1 (RF1). To eliminate this competition at amber codons, protein expression was performed using C321.ΔA *E.coli* cells. C321.ΔA *E.coli* cells are a genomically recoded organism where all 321 amber stop codons in the original genome have been reassigned to ochre stop codons. This reassignment allows for the deletion of the *prfA* gene that encodes RF1 with all the stop codons now being recognised by RF2. The removal of all the amber codons and RF1 appears not to impair fitness and allows for the dedicated use of amber codons as sense codons for the incorporation of unnatural amino acid.^{196,197}

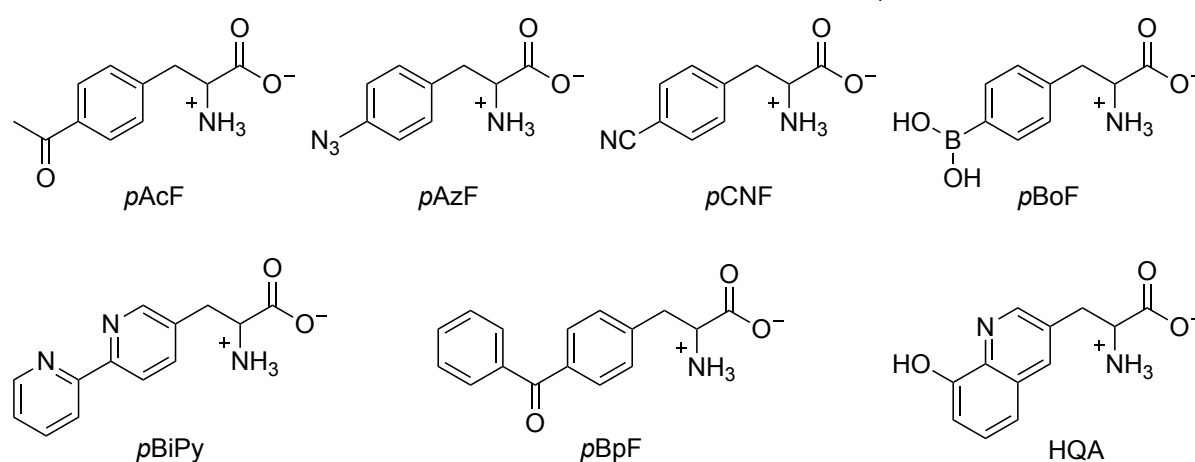
5.2.1 Incorporation using existing aminoacyl-tRNA synthetase and tRNA pairs

Before setting out to evolve a new aaRS/tRNA pair specifically for **72**, we assessed the ability of existing pairs to incorporate **72** into proteins. A number of existing *M.jannaschii* aaRS/tRNA pairs have been found to incorporate substrates other than those that they were specifically designed for. For example, the aaRS/tRNA pair designed to encode *p*-cyanophenylalanine (pCNF) has been used to incorporate 18 different unnatural amino acids and the pairs encoding *p*-acetylphenylalanine (pAcF) and *p*-azidophenylalanine (pAzF) are permissive of several other para substituted phenylalanine derivatives.¹⁹⁸ Other studies have also found aaRS/tRNA pairs to be permissive of multiple structurally similar unnatural amino acids.^{199,200} Therefore, it might be that an existing aaRS/tRNA pair can incorporate our unnatural amino acid.

We tested 7 aaRS/tRNA pairs using the pEVOL system to see if they could incorporate **72** in response to an amber codon. The pEVOL system encodes two copies of the *M.jannaschii* aaRS, one copy of the optimised *M.jannaschii* tyrosine-tRNA mutant amber suppressor and a chloramphenicol resistant gene. This system has been shown to offer increased versatility, yields and vector stability.²⁰¹ The 7 aaRS/tRNA pairs tested were originally evolved for the incorporation of *p*CNF, *p*AzF, *p*AcF, *p*-borophenylalanine (pBoF), *p*-bipyridylalanine (pBiPy), *p*-benzoylphenylalanine (pBpF) and 8-(hydroxyquinolin-3-yl)alanine (HQA) (Figure 5.1). We

assessed their ability to insert **72** into super folded green fluorescence protein (sfGFP) using a sfGFP gene disrupted with an amber codon at position 39. If the pair incorporates **72** in response to the amber codon, the full-length protein is expressed resulting in observable fluorescence. On the other hand, an inability to suppress the amber codon results in a truncated protein and no observable fluorescence. This method developed by Miyake-Stoner *et al.* is advantageous as protein expression can be qualitatively and quantitatively identified *in vivo* if required.¹⁹⁹

Figure 5.1 The amino acids that the aminoacyl-tRNA synthetase/tRNA pairs tested were originally



evolved to incorporate.

To confirm the viability of this method, we first tested the ability of each of the aaRS/tRNA pairs to incorporate the unnatural amino acid they were specifically designed for or one they are known to incorporate efficiently. Each of the aaRS/tRNA pairs in the pEVOL plasmid were co-transformed with the pBAD plasmid encoding the amber disrupted sfGFP into C321.ΔA *E. coli* cells via electroporation. The cells were plated on agar plates supplemented with carbenicillin and chloramphenicol to maintain only those cells that contained both plasmids. After being grown overnight at 37 °C, a single colony was used to inoculate a solution of 2×YT media (again supplemented with the appropriate antibiotics) and grown to saturation overnight. Next, the cell culture was diluted to an OD₆₀₀ of approximately 0.2 and a total volume of 1 mL. An OD₆₀₀ of 0.2 was used as this is approximately the beginning of the exponential growth phase. The cells were diluted with a solution of liquid 2×YT supplemented with the chloramphenicol and carbenicillin, 0.2% L-arabinose and 2 mM of either *p*-iodophenylalanine (*p*IF), *pAzF* or *pAcF*. L-arabinose was used to induce protein expression with 0.2% found to be optimal for sfGFP expression (Section 5.6). The cells were allowed to express the protein for 20 hours at 37 °C, 250 RPM after which time the cells were pelleted via centrifugation. The ability of the system to suppress the amber

codon was determined qualitative through the visualisation of fluorescence under ultraviolet light. In all cases tested, fluorescence was observed. The results are displayed in Table 5.1 below.

Table 5.1 The 7 aaRS/tRNA pairs are able to suppress amber codons and thus express sfGFP when in the presence of pIF, pAzF and/or pAcF.

Unnatural amino acid	pEVOL plasmid						HQA
	pAcF	pAzF	pBpF	pCNF	pBoF	pBiPy	
pIF	–	–	✓	✓	✓	✓	✓
pAzF	–	✓	✓	✓	✓	✓	✓
pAcF	✓	–	–	✓	–	–	–

✓ fluorescence observed, – not tested, X fluorescence not observed.

With confirmation that this system can be used for the incorporation of an unnatural amino acid, we next repeated these experiments replacing the unnatural amino acids with our own. This time protein expression was monitored in both the presence and absence of 2 mM **72**. This was to allow for any fluorescence that was a result of endogenous amino acid incorporation to be accounted for. Fresh colonies containing the pEVOL and pBAD plasmids were grown for each aaRS/tRNA pair and a single colony used to inoculate liquid 2×YT supplemented with chloramphenicol and carbenicillin. This was repeated in triplicate for each aaRS/tRNA pair and all 21 cultures were grown to saturation at 37 °C, 250 RPM. Once all samples had reached saturation, two aliquots of cells from each sample were diluted to an OD₆₀₀ of 0.2 bringing them back to beginning of the exponential growth phase in preparation for protein expression with a total volume of 1 mL. The first aliquot was diluted with a solution of liquid 2×YT supplemented with the chloramphenicol and carbenicillin and 0.2% L-arabinose. This aliquot served as the control (–UAA). The second aliquot was diluted with a solution of liquid 2×YT supplemented with the chloramphenicol and carbenicillin, 0.2% L-arabinose and 2 mM of **72** (+UAA). The 42 samples were allowed to express the protein for 48 hours at 30 °C, 250 RPM. To allow for comparisons between fluorescence a sample from each experiment was diluted with liquid 2×YT to an OD₆₀₀ of 1 with a total volume of 350 µL. The cells were then harvested via centrifugation, resuspended in phosphate buffered saline, lysed by sonication (60% amplification for 10 sec) and any solids removed via centrifugation. The ability of the pairs to incorporated **72** was determined by analysis of the supernatant using fluorescence spectroscopy. Fluorescence was recorded with excitation

at 470 nm with an emission range of 490-650 nm. The results below in Figure 5.2 are reported as the average of the triplicates performed.

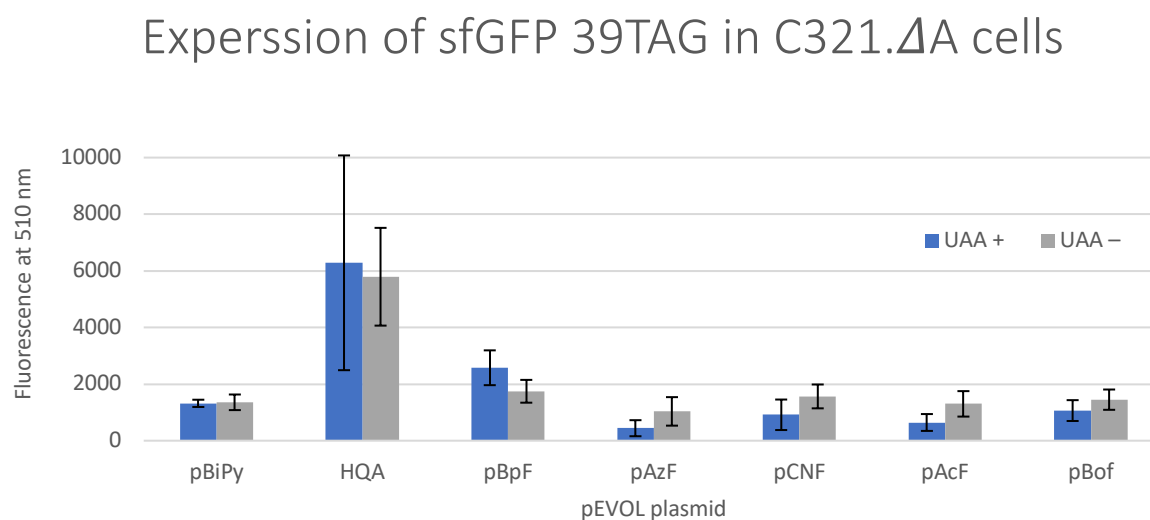


Figure 5.2 Fluorescence emitted at 510 nm with excitation at 470 nm after 48 hours of sfGFP expression at 30 °C, 250 RPM in C321.ΔA *E.coli* cells. The ability of existing aaRS/tRNA pairs to incorporate **72** into sfGFP was determined by monitoring expression in both the presence (blue) and absence (grey) of **72** (n=3).

Of the seven experiments conducted, increases in the fluorescence were observed in the presence of **72** for the pEVOL plasmids encoding for the HQA aaRS and pBpF aaRS. The HQA aaRS gave the highest level of protein expression but the incorporation of **72** was not statistically significant ($p=0.424$, $n=3$). The pBpF aaRS offered a greater ability to differentiate between **72** and endogenous amino acids but again it was not statistically significant ($p=0.061$, $n=3$). Furthermore, the total amount of protein expressed was very minimal, less than half of that when using the HQA aaRS. The relatively low expression levels observed are somewhat expected given these have not been specifically designed to incorporate **72**. It would have been extraordinary if any of them were able to incorporate **72** at high sfGFP expression levels.

In the cases of the pAzF, pCNF, pAcF and pBoF aaRSs, we found that the protein was expressed at lower levels when **72** was present versus when it was absent. This result is interesting as it suggests that **72** adversely affects protein expression, though, why we did not see it in all cases where **72** was included is unclear. Given that each experiment differs only in the aaRS used, it is reasonable to conclude that it must be related in some way. One possibility being that **72**

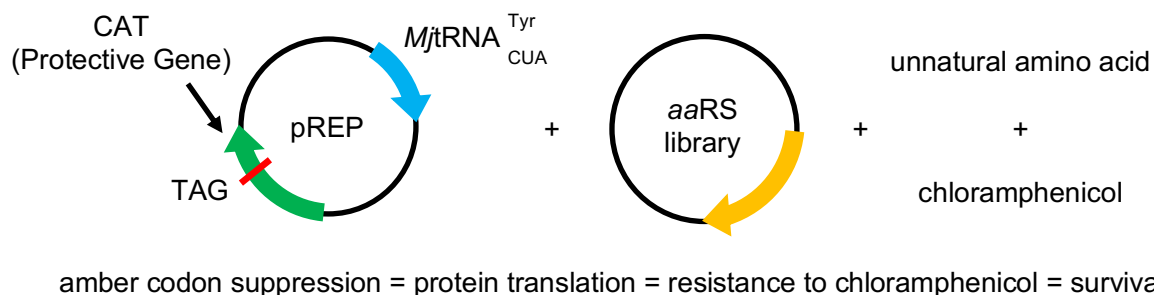
interacts with the aaRS in a way that inhibits its ability to charge the tRNA. With only a limited number of aaRS expressed from the plasmid, this would reduce the number available for the competitive incorporation of endogenous amino acids explaining why the fluorescence levels are lower than that of the controls. Of course, this negative effect on protein expression was not ideal. However, moving forward with the directed evolution of an aaRS/tRNA pair specific for **72**, it was not foreseeable that it would be an issue as any aaRS that suffered this effect would be selectively removed.

For the pBiPy aaRS we observed no difference in fluorescence with and without **72**. While pBiPy aaRS was unable to incorporate **72** into sfGFP a comparison of its aaRS sequences with HQA aaRS and pBpF aaRS proved interesting. Comparison suggests that replacement of the leucine residue at position 162 with serine may be detrimental to the aaRS ability to charge the tRNA with **72**. Similarly, a tryptophan residue at position 159 and a glutamic acid residue at position 155 may also be detrimental. As both pBiPy aaRS and pBpF aaRS have a glycine residue at position 32 this may not be necessary for incorporation. This information would be useful in the design a new library for the directed evolution of an aaRS for **72**, a potential future project that will be discussed in Chapter 6. We next looked at improving the efficiency through the directed evolution of a new aaRS specific for **72**.

5.2.2 Directed evolution of a new aminoacyl-tRNA synthetase and tRNA pair

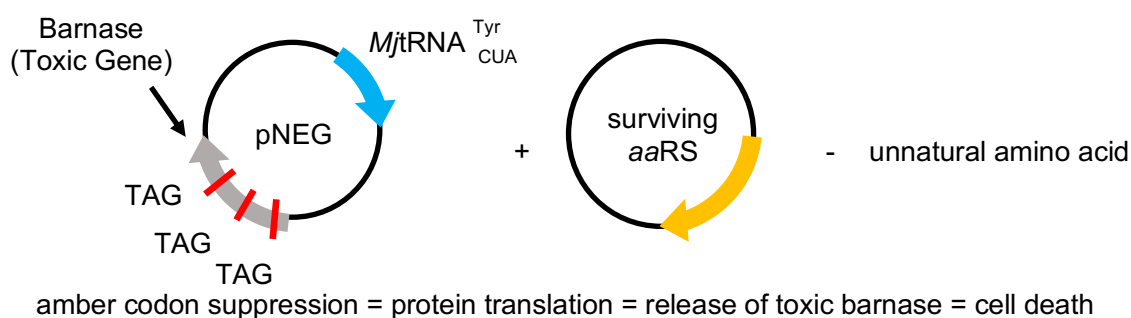
To ensure that the aaRS only charges the tRNA with the unnatural amino acid we evolved an aaRS using positive and negative rounds of selection. The positive selection was based on suppression of an amber codon at position 111 of the chloramphenicol acetyltransferase (CAT) gene. Plasmid pREP encodes the gene for the optimised *M.jannaschii* tyrosine tRNA¹⁶⁴ and the amber disrupted CAT gene.²⁰² When grown in the presence of the unnatural amino acid and chloramphenicol only those cells containing a synthetase that can effectively charge the tRNA with an amino acid, unnatural or endogenous, will survive because they are able to synthesise the CAT enzyme which protects them against chloramphenicol. To distinguish between those that can charge the tRNA with the unnatural amino acid and those that charge the tRNA with any of

the endogenous amino acids, the synthetase library is placed through a round of negative selection in the absence of the unnatural amino acid.



Scheme 5.2 Positive selection.

Negative selection was based on the lethal toxicity of barnase. Plasmid pNEG encodes the gene for the optimised *M.jannaschii* tyrosine tRNA and an amber disrupted barnase gene. This gene has two amber codons at position 2 and 44 and is under control of an arabinose promoter.²⁰³ When induced with L-arabinose, cells containing a synthetase that can effectively charge the tRNA with any of the endogenous amino acids express barnase which without its inhibitor barstar is lethal and results in cell death.



Scheme 5.3 Negative selection.

In regard to the library of aaRS, we chose to use an aaRS library that had previously been designed for direct evolution of 4-(carboxydifluoromethyl)phenylalanine (CAF2). This library was based off the wild type aaRS of *M.jannaschii* and created using PCR site-directed mutagenesis to introduce 5 NNK mutations at positions 32, 65, 108, 109 and 162. A degenerate NNK codon encodes all 20 natural amino acids and one stop codon thus, this library has a diversity of 3.4×10^7 . This library was synthesised and cloned into a pBK vector at the NdeI and PstI sites by Tan Truong, University of Virginia.

Such a large diversity increases the chances of an aaRS/tRNA pair suitable for **72** being contained within the library. However, it also means that an extremely large number of colonies need to be grown to ensure that the whole diversity of the library is covered. To account for this, the negative and positive selections, cells were grown on 150 mm agar plates rather than the standard 100 mm plates. Additionally, the cells were grown using Luria-Bertani lysogeny broth (LB). As the positive round was based on a resistance to chloramphenicol this low salt medium was used as high salt mediums limit the susceptibility of the *E.coli* cells to antibiotics, in particular to tetracycline and chloramphenicol.²⁰⁴

For the directed evolution we first subjected the CAF2 library to a round of negative selection. The pBK plasmid was transformed into competent C321.ΔA *E.coli* cells already containing plasmid pNEG. The cells were grown at 37 °C overnight on LB supplemented with carbenicillin and kanamycin to maintain the plasmids and 0.2% L-arabinose to induce barnase expression. The pBK plasmid DNA of those cells that had survived was isolated and transformed into competent C321.ΔA *E.coli* cells containing the plasmid pREP for a round of positive selection. The cells were grown at 37 °C overnight on LB supplemented with tetracycline and kanamycin to maintain the plasmids, our unnatural amino acid **72** and chloramphenicol. Again, the pBK plasmid DNA of those cells that had survived was isolated.

To ensure that only synthetases that could incorporate **72** in response to amber codons and not any of the endogenous amino acids remained a second round of negative selection was performed. The isolated pBK plasmid from the first round of positive selection was transformed into competent C321.ΔA *E.coli* cells containing plasmid pNEG. As in the first negative selection round, the cells were grown at 37 °C overnight on LB supplemented with carbenicillin and kanamycin to maintain the plasmids and 0.2% L-arabinose to induce barnase expression. This time however, the cells did not grow consistently across the whole plate (Figure 5.3 left). On repeat the same phenomenon was again observed. To determine what might be the cause of this we ran a number of controls.

In the first control C321.ΔA *E.coli* cells containing the plasmid pNEG were streaked on a LB agar plate supplemented with carbenicillin. In a second control C321.ΔA *E.coli* cells containing the plasmids pNEG and pBK were streaked on LB agar plates supplemented with carbenicillin and kanamycin. Streaking was used so that colony clusters and isolates could be observed. No abnormal growth eliminated antibiotics as the cause. Repeating these controls on 2xYT also

confirmed the use of LB was not an issue. Noteworthy, the cells grown on 2×YT were noticeably larger. We considered that a slow growth rate may be the issue and repeated the negative selection of the CAF2 library using 2×YT instead of LB. Unfortunately, we again observed abnormal cell growth (Figure 5.3 right)

Though the process of elimination it was evident that the issue lay in the addition of L-arabinose to induce barnase expression. We therefore ran a third set of controls, growing C321.ΔA *E.coli* cells containing pNEG on two 2×YT agar plates. One supplemented with carbenicillin and another with both carbenicillin and 0.2% L-arabinose. For comparison we also performed the same controls in DH10B *E.coli* cells as these cells have previously been used in the directed evolution of aaRS/tRNA pairs with the pNEG plasmid.^{199,205,206} After being left to grow overnight, only a single colony was present on the C321.ΔA *E.coli* cells plate supplemented with carbenicillin and 0.2% L-arabinose. All other plates have growth as expected (Figure 5.4).

This result was interesting as it suggests that barnase was being expressed in the C321.ΔA *E.coli* cells when L-arabinose was introduced. This concentration of L-arabinose had been used previously to induce sfGFP in these cells (Section 5.6) thus, we knew that it was not toxic to the cells. In the absence of any additional translational machinery that can suppress the amber codons in the barnase gene, C321.ΔA *E.coli* cells must therefore be able to endogenously suppress the amber codons. This does not however, seem to affect the expression of proteins when the unnatural amino acid is incorporated using an aaRS that has specifically been evolved for it.¹⁹⁷ Thus, it may be that in the absence of an optimised aaRS for the unnatural amino acid able to suppress the amber codon or RF1 to end translation an unknown stress is placed on the system. Furthermore, it brought us no closer to determining the cause of the abnormal cell growth experienced in the negative selection round. Rather this result serves to contradict what we have observed. However, since barnase is lethal without its inhibitor barstar, and even minimal suppression will result in cell death, it was clear that C321.ΔA *E.coli* cells are not suitable for the directed evolution of a new aaRS/tRNA pair and this was not explored any further.

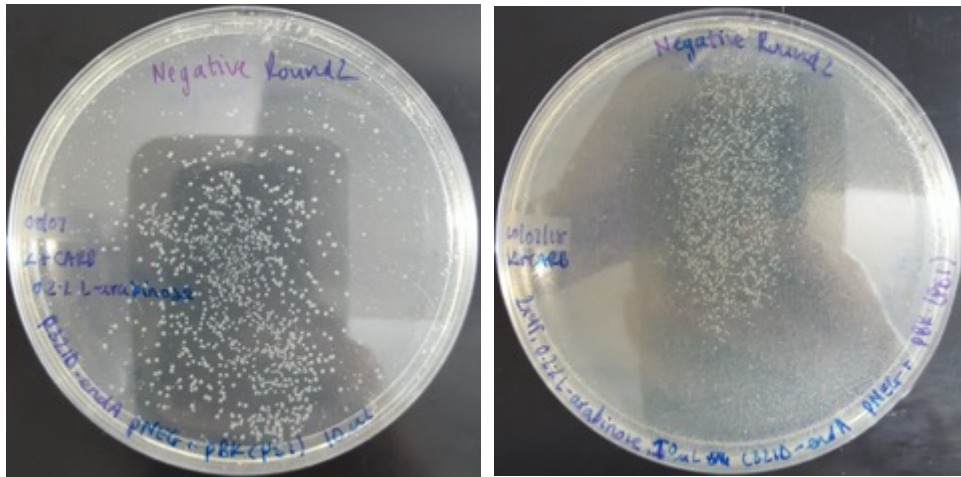


Figure 5.3 During the second round of negative selection we observed inconsistent and patchy growth of the C321.ΔA *E.coli* cells with both LB (left) and 2xYT (right) media.

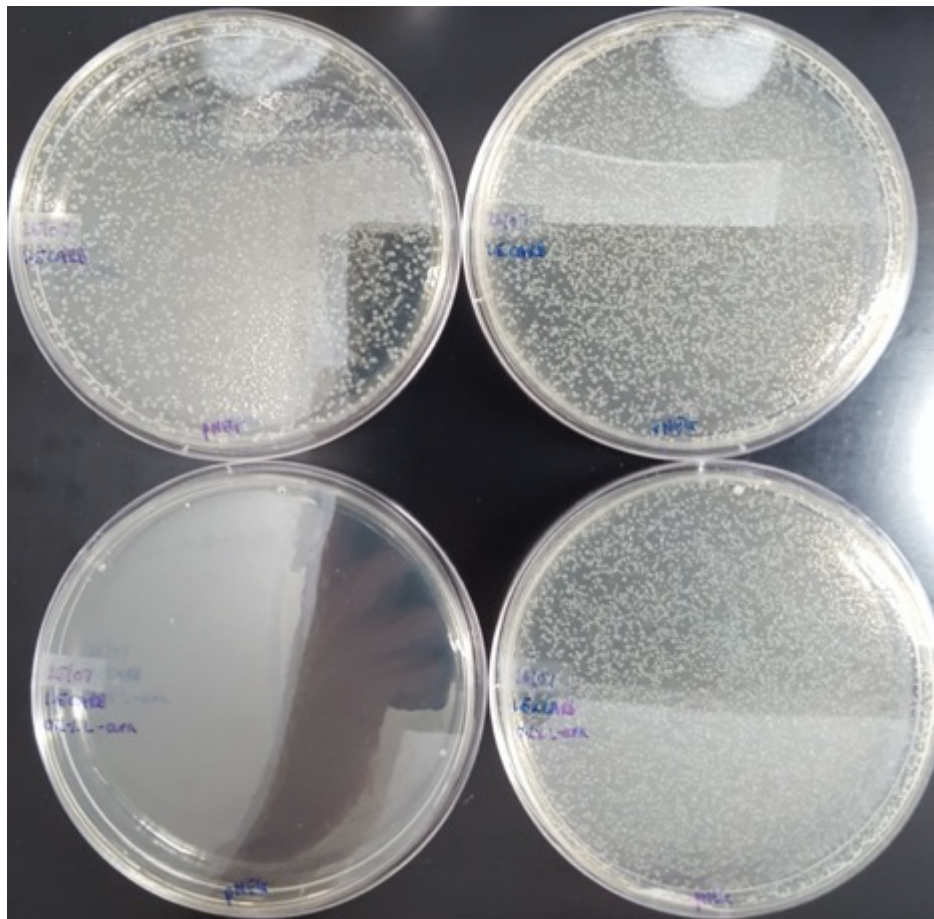


Figure 5.4 Negative selection control experiments for carbenicillin only (top) and carbenicillin and L-arabinose (bottom) in both C321.ΔA *E.coli* cells (left) and DH10B *E.coli* cells (right).

5.3 DH10B *E.coli* cells

In light of the issues experienced with C321.ΔA *E.coli* cells we decided to continue our studies in DH10B *E.coli* cells instead. This was slightly disappointing as DH10B *E.coli* cells offer lower suppression levels than what has been achieved with the C321.ΔA *E.coli* cells when the appropriate translation machinery is present.¹⁹⁷ Nevertheless, these issues could be circumnavigated by making the switch to DH10B *E.coli* cells.

5.3.1 Incorporation using existing aminoacyl-tRNA synthetase and tRNA pairs

Upon switching to the DH10B *E.coli* cells the incorporation of **72** using the existing aaRS and tRNA pairs was repeated. We had previously concluded that the decrease in protein expression observed in C321.ΔA *E.coli* cells was due to the presence of **72**. Now, however, it seemed likely that it may have actually been a result of endogenous factors.

Thus, each of the aaRS/tRNA pairs in the pEVOL plasmid were co-transformed with the pBAD plasmid encoding the amber disrupted sfGFP this time, into DH10B *E.coli* cells. The cells were grown overnight at 37 °C on agar plates supplemented with chloramphenicol and carbenicillin. Again, repeated in triplicate for each pair, a single colony was used to inoculate liquid 2×YT media supplemented with chloramphenicol and carbenicillin and grown to saturation. Two aliquots of cells from each sample were diluted to an OD₆₀₀ of 0.2 with a total volume of 1 mL. The first aliquot was diluted with a solution of liquid 2×YT media supplemented with the chloramphenicol and carbenicillin and 0.2% L-arabinose. This aliquot served as the control (–UAA). The second aliquot was with a solution of liquid 2×YT media supplemented with the chloramphenicol and carbenicillin, 0.2% L-arabinose and 2 mM of **72** (+UAA). The 42 samples were grown for 48 hours at 30 °C, 250 RPM.

Again, the ability of each of the aaRS to incorporate **72** in response to the amber codon was determined using fluorescence spectroscopy. To allow for comparisons between fluorescence each sample was diluted with liquid 2×YT media to an OD₆₀₀ of 1 with a total volume of 350 μL. The cells were then harvested via centrifugation, resuspended in phosphate buffered saline, lysed by sonication (60% amplification for 10 sec) and any solids removed via centrifugation. Finally, the fluorescence of the supernatant was recorded at an excitation of 470 nm over an emission range of 490-650 nm. The results are shown in Figure 5.5.

Experssion of sfGFP 39TAG in DH10B cells

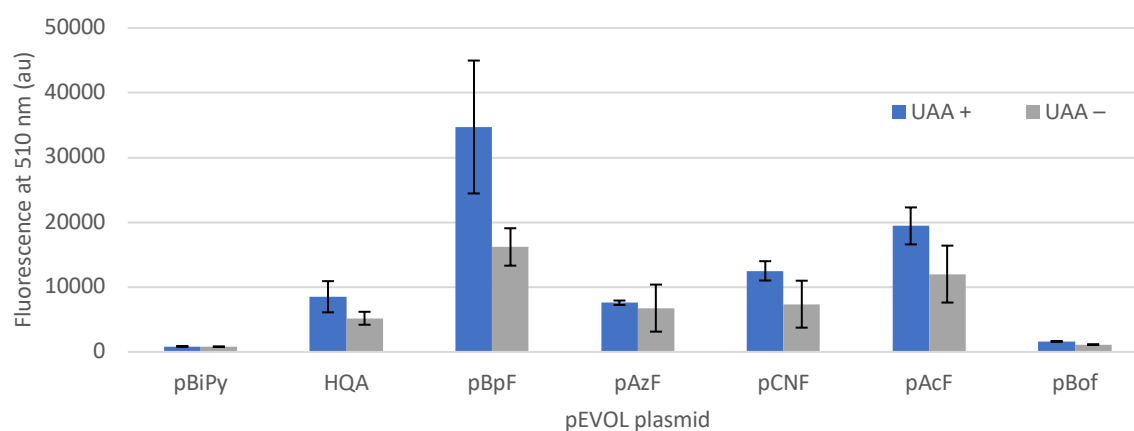


Figure 5.5 Fluorescence emitted at 510 nm with excitation at 470 nm after 48 hours of protein expression at 30 °C, 250 RPM in DH10B *E.coli* cells. The ability of existing aaRS/tRNA pairs to incorporate **72** into sfGFP was determined by monitoring expression in both the presence (blue) and absence (grey) of **72** (n=3).

Of the 7 aaRS/tRNA pairs tested the aaRS with the greatest ability to incorporate **72** was again the pBpF aaRS. It offered an ability to differentiate between **72** and endogenous amino acids that was statistically significant ($p=0.019$, $n=3$). It also offered the highest expression efficiency of those tested. Above and beyond that that was achieved in C321.ΔA *E.coli* cells, this result was exciting and further supports the likely success in the evolution of an aaRS/tRNA pair specific for **72**. The HQA, pCNF, and pAcF aaRSs were all also found have statistically significant increases in protein expression when in the presence of **72** ($p=0.046$, $p=0.043$ and $p=0.035$ respectively, $n=3$ in all cases). The increase in fluorescence observed for the pBoF aaRS was also found to be statistically significant ($p=0.0002$, $n=3$) though protein expression was very low. As was the case for the pBiPy and pAzF aaRSs in C321.ΔA *E.coli* cells, they were not able to incorporate **72** to any significant degree.

Overall, the level of protein expression in DH10B *E.coli* cells was much greater than was achieved in C321.ΔA *E.coli* cells. Most noteworthy of these results is that on all occasions the expression levels in the presence of **72** were equal to or greater than when **72** was absent. This suggests that **72** does not adversely affect protein expression in DH10B *E.coli* cells.

5.4 Concluding remarks and chapter summary

In this chapter we presented the incorporation of **72** into sfGFP in response to an amber codon at position 39. The ability of 7 existing aaRS/tRNA pairs to incorporate **72** was tested in C321.ΔA *E.coli* cells, a genomically recoded organism whereby all UAG stop codons (amber codons) have been replaced and RF1 deleted from the genome. In these cells, pBpF and HQA showed the greatest efficiency for incorporating **72**. Interestingly, for the other aaRs tested the inclusion of **72** resulted in lower levels of protein expression than when it was excluded from the experiments. This indicated that **72** may adversely affect protein translation. However, the ability of pBpF and HQA to incorporate **72** encourage the directed evolution of an aaRS specifically for **72**. During attempts to use this cell line in the directed evolution of a new aaRS/tRNA pair specifically for **72**, it was found that they have an endogenous ability to suppress amber codons. This push us to switch to the DH10B *E.coli* cells. Upon repeating experiments to assess the ability of the existing aaRS/tRNA pairs to incorporate **72**, in all cases an increase in protein expression was observed in the presence of **72**. Gratifyingly, this supported that the negative growth experienced with C321.ΔA *E.coli* cells is not explicitly related to **72**. pBpF was found to be the most efficient at incorporating **72** in response to the amber codon with an 114% increase in total fluorescence observed. It also resulted in the higher levels of protein expression. These preliminary results supported that **72** can be incorporated into proteins and encourages future studies to increase the efficiency of this incorporation through the directed evolution of an aaRS/tRNA pair specifically for **72** in DH10B cells.

5.5 Experimental procedures

5.5.1 General experimental details

All chemicals were used as supplied from commercial suppliers without further purification. All plasmids were prepared fresh from samples previously obtained by the Ai Laboratory before use. Fresh plasmids were cloned in DH10B *E. coli* cells. Plasmid DNA was isolated from cells using plasmid miniprep spin columns purchased from Syd Labs. Restriction enzymes were purchased from Thermo Scientific and antibiotics were purchased from Sigma Aldrich. All cultures were grown in 2×YT media unless stated otherwise. Absorbance and fluorescence spectroscopy were performed on a BioTek Synergy Mx Microplate Reader.

General procedure for electrocompetent Escherichia coli cells

E. coli cells were cultured on 2×YT agar plates and grown overnight at 37 °C. A single colony was picked and grown to saturation overnight in 20 mL of 2×YT liquid media in a 50 mL centrifuge tube at 37 °C, 250 RPM. The saturated culture was added to 2×YT liquid media (250 mL) and the culture grown to an OD₆₀₀ of 0.8-1.0. The cells were harvested from the culture via centrifugation in a 400 mL centrifuge bottle at 4 °C followed by removal of the supernatant. The cell pellet was carefully resuspended in a cooled 10% glycerol solution (double distilled water, ~4 °C, 150 mL) while being maintained on ice. The cells were then harvested via centrifugation at 4 °C, and the glycerol solution removed. Resuspension and centrifugation were repeated twice more before the cells were finally resuspended in 0.5 mL of a cooled 10% glycerol solution (double distilled water, ~4 °C). Aliquots (30 µL) were then transferred into 0.1 mL microcentrifuge tubes and the resuspended cells were freeze dried in a dry ice/acetone bath before being stored at -80 °C for later use. The 400 mL centrifuge tubes and the 10% glycerol solution in double distilled water were autoclaved the day before use and cooled to 4 °C in a fridge overnight.

General procedure for plasmid transformations

An aliquot of the required cells was thawed on ice. The plasmid DNA (1 µL) was added to the thawed cells with stirring. The mixture of the cells and plasmid DNA (20 µL) was placed in a pre-chilled 0.1 cm electroporation cuvette and any bubbles removed by tapping the cuvette on the bench. Any condensation on the outside of the cuvette was wiped off before the cells were shocked at 1.5 kV. The cells were immediately quenched by addition to 2×YT liquid media (0.5 mL) pre-chilled in a 1.5 mL microcentrifuge tube. The cells were then outgrown for 1 hr at 37 °C, 250 RPM.

General procedure for plasmid mini preparation

All plasmids were prepared fresh from samples previously obtained by the Ai Laboratory before use. Plasmids were transformed into DH10B cells as per the transformation procedure above and grown overnight at 37 °C on 2×YT agar plates supplemented with the appropriate antibiotic at 1000× dilution. A single colony was picked and grown overnight at 37 °C, 250 RPM in 2×YT liquid media (~5 mL) supplemented with the appropriate antibiotic at 1000× dilution in a 10 mL centrifuge tube. The cells were harvested from the culture via centrifugation followed by

removal of the supernatant. The cells were resuspended in 250 μ L P1 buffer (50 mM Tris HCl, 10 mM EDTA, pH 8.0 and 50 μ g/mL RNaseA) using a vortex mixer. P2 buffer (0.2 M NaOH, 1% SDS), 250 μ L, was added and the mixture inverted 5 times. After 2 min, 350 μ L N3 buffer (4.2 M guanidine hydrochloride and 0.9 M potassium acetate, pH 4.2) was added and the solutions mixed via inversion for 3-5 min. The solids were pelleted via centrifugation at 12000 RPM for 5 min. The supernatant was transferred to a plasmid miniprep spin column. The plasmid DNA was collected on the membrane of the column via vacuum filtration and the flow-through discarded. The plasmid DNA was washed twice with 750 μ L WS buffer (100 mM NaCl, 10 mM Tris HCl, 80 % ethanol, pH 7.5) and the WS buffer removed between washes via vacuum filtration. Residue WS buffer was removed via centrifugation at 12000 RPM for 1 min. The spin column was placed on a 1.5 mL microcentrifuge tube and 50 μ L EB buffer (10 mM Tris HCl, pH 8.5 (autoclaved)) was added directly to the membrane of the spin column. Finally, it was placed in an 80 $^{\circ}$ C heat block for 1 min before the plasmid DNA was eluted via centrifugation at 12000 RPM for 30 sec. The eluted plasmid DNA was either used straight way or stored at -20 $^{\circ}$ C for later use.

5.5.2 Plasmids used in this study

pEVOL plasmids

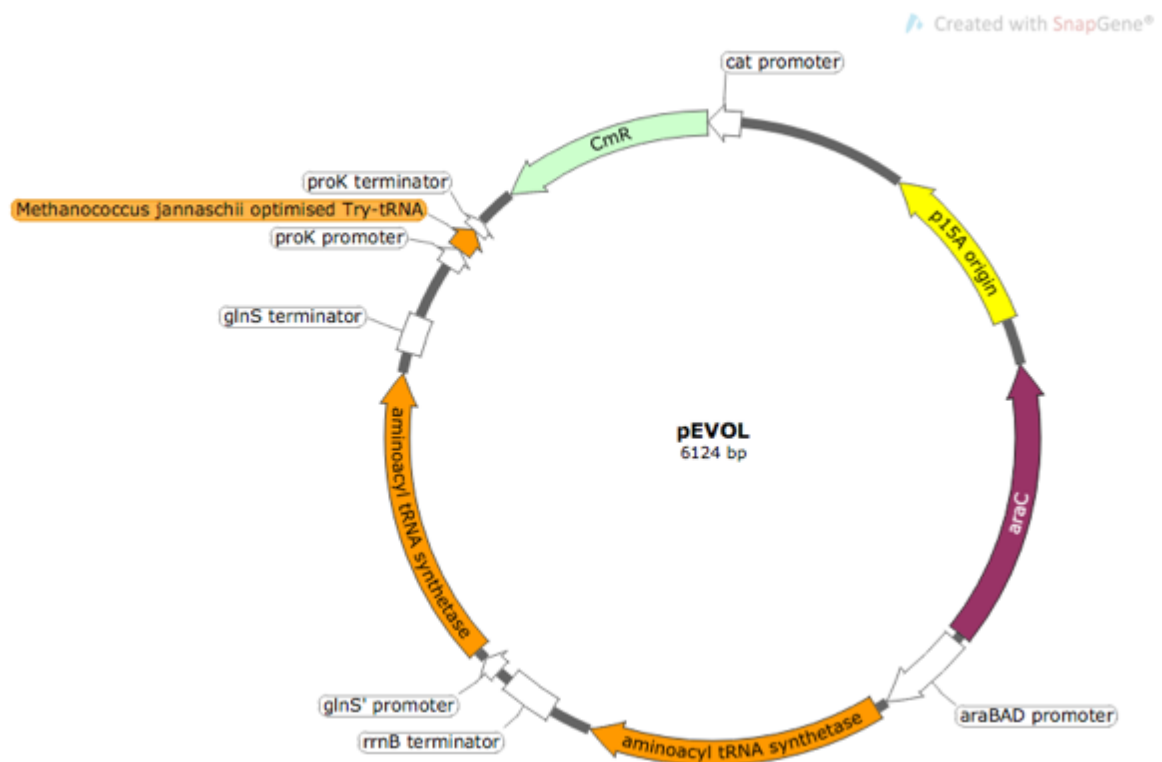


Figure S5.1. The pEVOL plasmids encode two copies of the *Methanococcus jannaschii* aminoacyl tRNA synthetase, one under control of an arabinose promoter and *rrnB* terminator and the second under a mutant *glnS* promoter where GATA is replaced with TATC in the -10 region (*glnS'*) and *glnS* terminator, one copy of the optimised *Methanococcus jannaschii* tyrosine-tRNA mutant amber suppressor under control of a *proK* promoter and terminator, a chloramphenicol resistant gene and the *araC* repressor gene.²⁰¹

Table S5.1. Amino acid mutations in the aminoacyl-tRNA synthetases used in this study.

Synthetase	Residue										Ref
	32	65	70	107	108	109	155	158	159	162	
M.jannaschii Try (wild type)	try	leu	his	glu	phe	gln	gln	asp	ile	leu	207
M.jannaschii pBiPy	gly	try	ala	–	–	–	glu	gly	trp	ser	170
M.jannaschii HQA	val	met	thr	–	arg	glu	–	ser	ser	–	171
M.jannaschii pBpF	gly	–	–	ser	–	–	–	thr	ser	–	167
M.jannaschii pAzF	thr	–	–	asn	–	–	–	pro	leu	gln	166
M.jannaschii pCNF	leu	val	–	–	trp	met	–	gly	ala	–	168
M.jannaschii pAcF	leu	–	–	–	–	–	–	gly	cys	arg	165
M.jannaschii pBoF	ser	ala	met	–	–	–	–	ser	–	glu	169

– maintains the original amino acid at this residue of Methanococcus jannaschii tyrosine-tRNA.²⁰⁷

pBAD sfGFP 39TAG

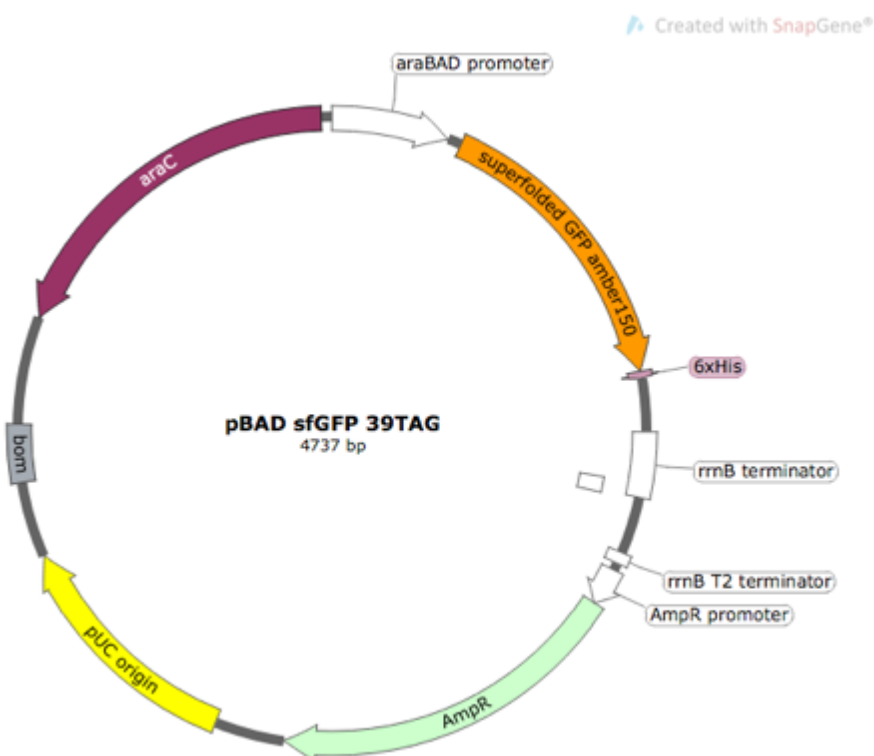


Figure S5.2 pBAD sfGFP 39TAG plasmid encodes super folded GFP disrupted with an amber (TAG) codon at position 39 and a C-terminal 6-His affinity tag controlled under and arabinose promoter and rrnB terminator, the araC repressor gene and an ampicillin resistance gene.¹⁹⁹

pREP *M.jannaschii*-Try tRNA

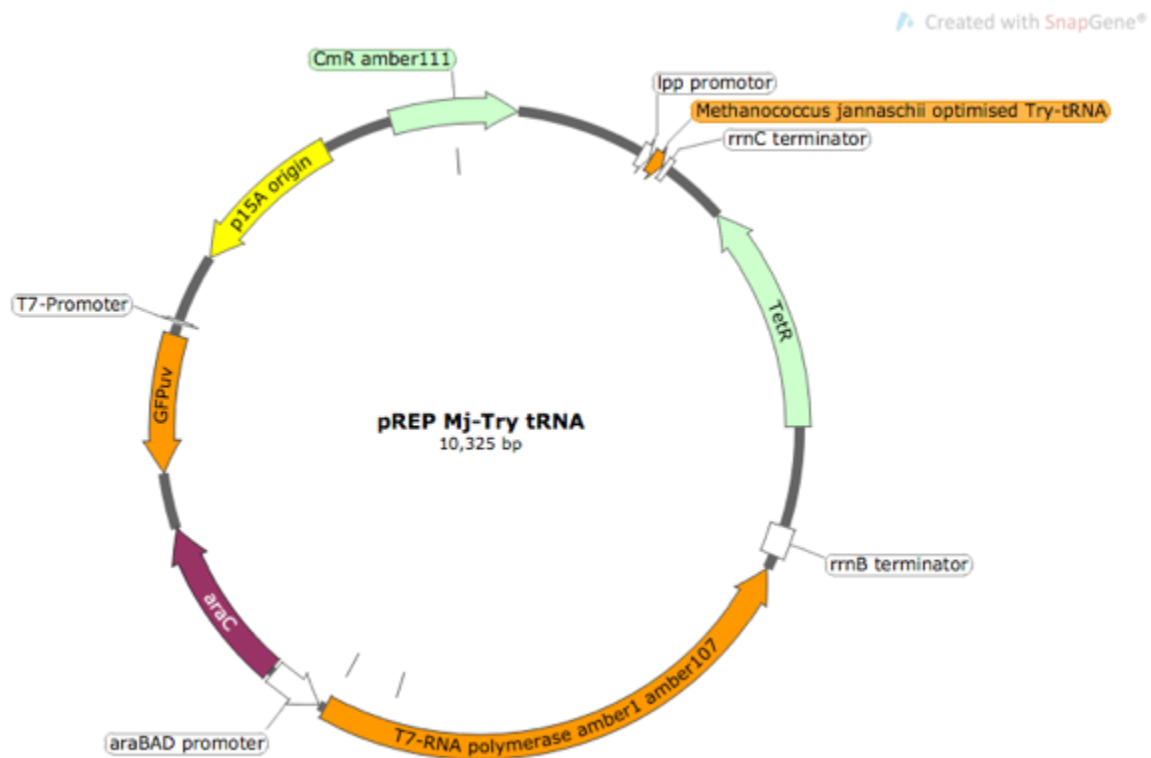


Figure S5.3 pREP *M.jannaschii*-Try tRNA plasmid encodes one copy of the optimised *Methanococcus jannaschii* tyrosine-tRNA mutant amber suppressor under control of an lpp promoter and rrnC terminator, T7 RNA polymerase disrupted with amber (TAG) codons at positions 1 and 107 under control of an arabinose promoter and rrnB terminator, GFPuv under control of a T7 promoter, a chloramphenicol acetyltransferase disrupted with an amber (TAG) codon at position 111, the araC repressor gene and a tetracycline resistance gene.²⁰²

pNEG *M.jannaschii*-Try tRNA

Created with SnapGene®

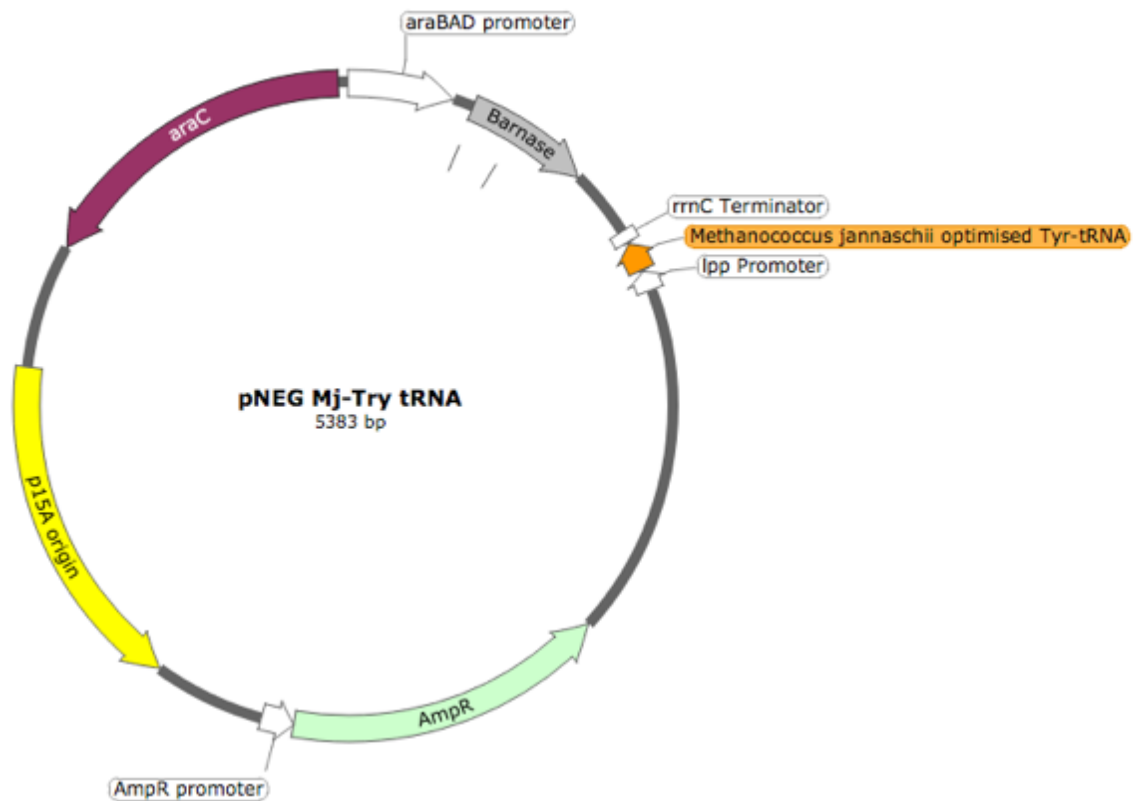


Figure S5.4 pREP *M.jannaschii*-Try tRNA plasmid encodes one copy of the optimised *Methanococcus jannaschii* tyrosine-tRNA mutant amber suppressor under control of an *ipp* promoter and *rrnC* terminator, *barnase* disrupted with amber (TAG) codons at positions 2 and 44 under control of an arabinose promoter, the *araC* repressor gene and an ampicillin resistance gene.²⁰³

pBK-CAF2 library

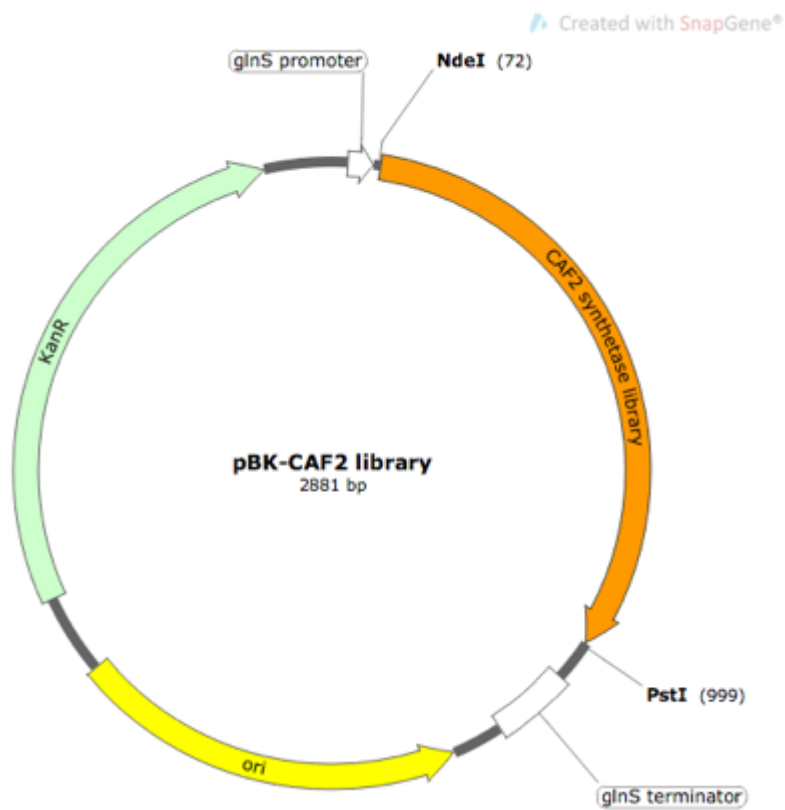


Figure S5.5 pBK-CAF2 library encodes the *Methanococcus jannaschii* aminoacyl tRNA synthetase containing NNK codons at positions 32, 65, 108, 109 and 162 under control of a glnS' promoter and terminator and a kanamycin resistance gene.

The CAF2 aminoacyl tRNA synthetase library was designed, synthesised and inserted into a pBK plasmid to yield the pBK-CAF2 library plasmid by Tan Truong, University of Virginia.

5.5.3 Genetic incorporation of the **72** using an existing aminoacyl-tRNA synthetase

Optimisation sfGFP expression in C321.ΔA *E.coli* cells

pBAD sfGFP was transformed by electroporation into C321.ΔA *E.coli* cells as per the general procedure. A 1 μL aliquot of the cells was then plated on three 100 mm 2×YT agar plates; one containing carbenicillin (100 μg/mL), one containing carbenicillin (100 μg/mL) and 0.02% L-arabinose and one containing carbenicillin (100 μg/mL) and 0.2% L-arabinose, and grown overnight at 37 °C. The cells were scraped from the plates and suspended in PBS (250 μL). Whether or not sfGFP was expressed was determined by the visual observation of fluorescence under ultraviolet light.

Table S5.2 The expression of sfGFP in C321.ΔA *E.coli* cells containing pBAD sfGFP requires the use of 0.2% L-arabinose.

L-arabinose (%)	Fluorescence
0	X
0.02	X
0.2	✓

pEVOL positive controls in C321.ΔA *E.coli* cells

General procedure: pEVOL plasmid was co-transformed with pBAD sfGFP 39TAG in a 1:1 concentration ratio by electroporation into C321.ΔA *E.coli* cells as per the general procedure. A 1 μL aliquot of the cells was then plated on 100 mm 2×YT agar plates containing carbenicillin (100 μg/mL) and chloramphenicol (50 μg/mL) and grown overnight at 37 °C. A single colony was picked and used to inoculate 4 mL 2×YT supplemented with carbenicillin (100 μg/mL) and chloramphenicol (50 μg/mL) in a falcon tube and it was grown to saturation overnight at 37 °C with shaking (250 RPM). An aliquot of cells was then diluted to a total volume of 1 mL with a final OD₆₀₀ of 0.2, chloramphenicol concentration of 50 μg/mL, carbenicillin concentration of 100 μg/mL, p-azidophenylalanine concentration of 2 mM and L-arabinose concentration of 0.2% and incubated at 37 °C with shaking (250 RPM) for 20 hr. The cells were harvested from the culture via centrifugation followed by removal of the supernatant. The cells were then resuspended in

250 μ L of PBS using a vortex mixer. Whether or not sfGFP was expressed determined by the visual observation of fluorescence under ultraviolet light.

Table S5.3 Expression of sfGFP in C321. Δ A *E.coli* cells with a different amino acyl tRNA synthetase and unnatural amino acids. All pEVOL plasmids were able to suppress the amber codon disrupted sfGFP protein and incorporated the unnatural amino acids tested.

pEVOL plasmid	Unnatural amino acid		
	pIF	pAzF	pAcF
pBiPy	✓	✓	–
HQA	✓	✓	–
pBpF	✓	✓	–
pAzF	–	✓	–
pCNF	✓	✓	✓
pAcF	–	–	✓
pBoF	✓	✓	–

✓ fluorescence observed, – not tested, X fluorescence not observed.

Incorporation of the silicon-based amino acid 72 into sfGFP

Suppression of an amber codon in sfGFP (pBAD sfGFP 39 TAG) with **72** was conducted with a number of the amino acyl tRNA synthetases (pEVOL) in both C321. Δ A and DH10B *E.coli* cells. Control experiments without the addition of **72** were conducted to determine the amount of fluorescence that is a direct result of amber suppression with **72**. The relative fluorescence was compared to that of the undisrupted sfGFP (pBAD sfGFP). All experiments were repeated in triplicate and the data is a representative of the average. Raw fluorescence data and calculated *p*-values for incorporation in C321. Δ A *E.coli* cells can be found in Appendix A. Raw fluorescence data and calculated *p*-values for incorporation in DH10B *E.coli* cells can be found in Appendix B.

Example procedure:

pEVOL pBpF was co-transformed with pBAD sfGFP 39TAG in a 1:1 concentration ratio by electroporation into C321. Δ A *E.coli* cells as per the general procedure. A 1 μ L aliquot of the cells was then plated on 100 mm 2xYT agar plates containing carbenicillin (100 μ g/mL) and

chloramphenicol (50 µg/mL) and grown overnight at 37 °C. Repeated in triplicate, a single colony was picked and used to inoculate 4 mL 2×YT supplemented with carbenicillin (100 µg/mL) and chloramphenicol (50 µg/mL) in a falcon tube and it was grown to saturation overnight at 37 °C with shaking (250 RPM). Two aliquots of cells from each replicate was then diluted to a total volume of 1 mL. One had a final OD₆₀₀ of 0.2, chloramphenicol concentration of 50 µg/mL, carbenicillin concentration of 100 µg/mL and L-arabinose concentration of 0.2% (-UAA). The other has a final OD₆₀₀ of 0.2, chloramphenicol concentration of 50 µg/mL, carbenicillin concentration of 100 µg/mL, L-arabinose concentration of 0.2% and **72** concentration of 2 mM (+UAA). The aliquots were incubated at 30 °C, 250 RPM for 48 hr. The cells were harvested from the culture via centrifugation followed by removal of the supernatant. The cells were then resuspended in 250 µL of PBS using a vortex mixer. sfGFP was lysed from the cells by sonication at 60% amplification for 10 sec. The solids were pelleted via centrifugation and the supernatant removed. Finally, the fluorescence of the supernatants was recorded in a black 96-well plate with an excitation of 470 nm over an emission range of 490-650 nm at a sensitivity of 80%.

5.5.4 Directed evolution of an orthogonal aminoacyl-tRNA synthetase/tRNA pair

Negative selection

Plasmid pBK-CAF2 was transformed via electroporation into electrocompetent C321.ΔA *E.coli* cells containing the pNEG plasmid as per the general procedure. The cells were cultured on LB agar plates supplemented with carbenicillin (50 µg/mL), kanamycin (50 µg/mL) and 0.2% w/v L-arabinose and grown overnight at 37 °C. The cells were the scrapped from the plate into LB and pelleted. Plasmid DNA was collected as per the general plasmid mini preparation procedure. Plasmid pBK was isolated through gel electrophoresis (0.7% agarose, 120 kV, 30 min). Plasmid pBK was dissolved in GEX buffer (1 mL) and transferred to a plasmid miniprep spin column. It was washed with WB buffer (2 × 750 µL). Remaining ethanol was removed via centrifugation. EB buffer (20 µL) was added to the membrane, the column heated at 80 °C for 1 min and the plasmid eluted form the column via centrifugation at 12 000 g for 30 sec.

Positive selection

The isolated pBK-CAF2 from the negative selection was transformed via electroporation into electrocompetent C321.ΔA *E.coli* cells containing the pREP plasmid as per the general procedure.

The cells were cultured on LB agar plates supplemented with tetracycline (20 µg/mL), kanamycin (50 µg/mL), chloramphenicol (50 µg/mL) and 2 mM **72** and grown overnight at 37 °C. The cells were scraped from the plate into LB and pelleted. Plasmid DNA was collected as per the general plasmid mini preparation procedure. Plasmid pBK was isolated through gel electrophoresis (0.7% agarose, 120 kV, 30 min). Plasmid pBK was dissolved in GEX buffer (1 mL) and transferred to a plasmid miniprep spin column. It was washed with WB buffer (2 × 750 µL). Remaining ethanol was removed via centrifugation. EB buffer (20 µL) was added to the membrane, the column heated at 80 °C for 1 min and the plasmid eluted from the column via centrifugation at 12 000 g for 30 sec.

Controls

A) pNEG on LB agar plates supplemented with carbenicillin

The plasmid pNEG was transformed into cells via electroporation as per the general procedure. Cells were cultured on LB and 2×YT agar plates supplemented with carbenicillin (50 µg/mL) overnight at 37 °C. This control was repeated for both C321.ΔA and DH10B *E.coli* cells.

B) pNEG on LB agar plates supplemented with carbenicillin and L-arabinose

The plasmid pNEG was transformed into cells via electroporation as per the general procedure. Cells were cultured on LB and 2×YT agar plates supplemented with carbenicillin (50 µg/mL) and 0.2% w/v L-arabinose overnight at 37 °C. This control was repeated in both C321.ΔA and DH10B *E.coli* cells. This control was repeated for both C321.ΔA and DH10B *E.coli* cells.

Chapter Six

Conclusions and future directions

6.1 Introduction

Silicon has been used extensively for the indirect fluorination of compounds. Its utility in the direct fluorination of proteins, however, remains scarce despite that silicon has long been known to react with fluorine even when in the presence of water. The research outlined in this thesis aims to address this and provide a better understanding of how silicon can be used in the direct fluorination of biomolecules where aqueous conditions are required. This work details methods to incorporate silicon site-selectively into proteins via chemical modifications at cysteine and lysine. Notably, this led to the first reported instance of using a silanol precursor in the direct fluorination of proteins. This work also established the incorporation of a silanol-based amino acid via genetic modification and amber codon suppression.

In this Chapter the overall conclusions of the work presented within this thesis will be recapped alongside the issues and limitations that were discovered, with some suggestions towards how they may be addressed in further studies. The potential in the future application of silicon for the direct radiolabelling of proteins with fluorine-18 will also be discussed.

6.2 Confirming the site of chemical modification and fluorination

In Chapter 3 we reported the site-selective modification of C2Am, annexin V and lysozyme using a number of chemical modification methods. Each modification was analysed via LC-MS to provide evidence that only a single modification had occurred. In future work, it needs to be unambiguously confirmed that these modifications occurred at the intended site. This would be done by a tryptic digest of the modified protein and subsequent MS-MS analysis. This would also be useful in confirming the site of fluorination. Using this method would allow for more rigorous studies of the fluorination as it is not limited by the high concentrations of protein required for ^{19}F NMR spectroscopy.

6.3 Direct evolution of aminoacyl-tRNA synthetase and tRNA pairs

In continuation of this research, the evolution of an aaRS/tRNA pair specific for **72** would be the next rational step. The aaRS and tRNA pair evolved for pBpF was best suited to incorporate **72** into sfGFP however, the levels of incorporation were low and there was a limited differentiation between the incorporation of **72** versus tyrosine. Evolving a pair specific for **72** would increase the fluidity of **72** incorporation and reduce the competition with tyrosine.

Our initial attempt involved the directed evolution of a pair from the CAF2 library in C321.ΔA *E.coli* cells. This was cut short due to issues with the physical growth of the cells. With the incorporation of **72** in DH10B cells showing greater levels of protein expression with less adverse effects, repeating the directed evolution from the CAF2 library in DH10B *E.coli* cells may yield a suitable pair. Ultimately, the CAF2 library has a diversity of 3.4×10^7 so statistically speaking, a suitable pair should be contained within this library.

Alternatively, an entirely new library could be synthesised. Given that pBpF was able to incorporate **72** with the highest efficiency and distinction between **72** and tyrosine a new library could be built off the sequence for the aaRS of this pair. Positions for mutations could be chosen through comparisons of the sequences of those aaRS that were able to charge the tRNA with **72** and those that were not. For example, pBpF can incorporate **72** and pBiPy cannot however, they share a commonality in a glycine residue at position 32. Thus, it may not be essential for incorporation and an NNK mutation at this position may lead to an aaRS sequence with a greater

ability to incorporate **72**. Additionally, amino acids at position 162 other than leucine found in the wild *M.jannaschii* aaRS overwhelmingly result in an inability to incorporate **72**. Thus, a mutation at this position is likely to be fruitless. The synthesis of a new library based on this information may lead to a more superior aaRS sequence than could be derived from the CAF2 library.

6.4 Hydrolytic stability studies and 2nd generation silanols

Investigations into the hydrolytic stability of the Si-F bond on a protein would provide useful insight in their suitability for PET studies. At present it is generally accepted that aryl diisopropylsilyl motifs are unsuitable for fluorine-18 PET as they often yield low Si-F hydrolytic half-lives, however, their hydrolytic stability when embedded into proteins has yet to be determined. As the hydrolytic half-lives vary widely and are highly dependent on additional functionality on the aryl, it is probable that the stability of the Si-F bond will change given its location within the protein. It is also likely to be dependent on pH and the protein microenvironment. This may make it difficult to draw general conclusions about the stability of the Si-F bond when on a protein. Nevertheless, it could provide information about favourable protein environments and inform the identification of optimal locations within proteins for the incorporation of a silanol in regard to hydrolytic stability.

If, unfortunately the aryl-diisopropylsilyl motif is found to yield unfavourable hydrolytic stability even when embedded in proteins, a 2nd generation silanols with greater hydrolytic stability could be synthesised. Along with the commonly employed *tert*-butyl substituents, *o*-methyl and *o*-dimethyl substituents on the aryl group have been shown to increase hydrolytic half-lives of Si-F bonds.⁶¹ These may be able to offer the desired increase in hydrolytic stability without a significant increase in steric hinderance that affects fluorination yields. The corresponding benzyl amines and amino acids that could be used of their chemical and genetic incorporation into proteins are shown in Figure 6.1.

All these 2nd generation silanols could be synthesised using the routes reported in this thesis. The di-*tert*-butyl substituents could be introduced and **86** and **89** synthesised with replacement of diisopropylsilyl chloride with di-*tert*-butylsilyl chloride in silylation. **87** and **88** could be synthesised from the 2-(4-bromo-3-methylphenyl)acetic acid and 2-(4-bromo-3,5-methylphenyl)acetic acid. While these starting materials are not readily available,

they can be purchased from a few niche chemical commercial suppliers. Similarly, the methylated compounds **90** and **91** could be synthesised from the 4-bromo-3-methylbenzyl alcohol and 4-bromo-3,5-dimethylbenzyl alcohol. These could be derived from the less expensive benzoic acids through reduction of the carboxylic acids to the alcohols.

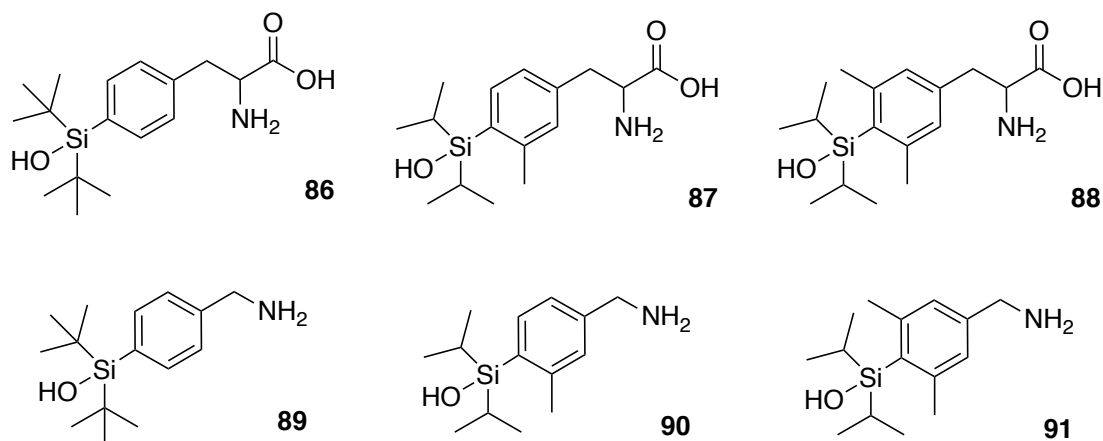


Figure 6.1 Potential 2nd generation silanols that should offer a greater hydrolytic stability.

6.5 Radiolabelling proteins with fluorine-18

Following the incorporation of silanols into proteins and their ability to be directly fluorinated which has been presented in this thesis, an obvious future application for this research is their use in the direct, aqueous radiolabelling of proteins with fluorine-18. Generally, in radiolabelling experiments fluorine is not in excess, as it has been throughout the work presented here. In future studies the radiolabelling of proteins at lower fluoride concentrations could be tested and fluorination verified by radio-HPLC analysis. Using fluorine-18 and radio-HPLC, fluorination yields will also be obtained. The most significant challenge will be obtaining the fluorination proteins in sufficient yields and specific activities for positron emission tomography studies. If fluorination can be achieved it brings about the opportunity for a much larger collaborative project aimed at the development and evaluation of fluorine-18 radiolabelled proteins as imaging biomarkers for the study and detection of disease.

6.6 Concluding remarks

This doctoral thesis details the research that led to a new method for the direct and aqueous fluorination of proteins. The method makes use of silanols that can be fluorinated under

aqueous conditions in good yields. Furthermore, it was shown that they can be site-selectively incorporated by means of both chemical and genetic methods of protein modification making their incorporation applicable to a wide range of proteins. This research has provided the base for further studies that will yield additional insight, in particular into the applicability of using silanols in the direct aqueous radiolabelling of proteins with fluorine-18.

Chapter Seven

References

- (1) Sweet, W. H. The uses of nuclear disintegration in the diagnosis and treatment of brain tumor. *New England Journal of Medicine* **1951**, 245 (23), 875–878 DOI: 10.1056/NEJM195112062452301.
- (2) Wrenn, F. R.; Good, M. L.; Handler, P. The use of positron-emitting radioisotopes for the localization of brain tumors. *Science* **1951**, 113 (2940), 525–527 DOI: 10.1126/science.113.2940.525.
- (3) Robinson, A. A.; Bourque, J. M. Emerging techniques for cardiovascular PET. *Cardiovascular Innovations and Applications* **2019**, 4 (1), 13–24 DOI: 10.15212/CVIA.2019.0004.
- (4) Driessen, R. S.; Raijmakers, P. G.; Stuijzand, W. J.; Knaapen, P. Myocardial perfusion imaging with PET. *The International Journal of Cardiovascular Imaging* **2017**, 33 (7), 1021–1031 DOI: 10.1007/s10554-017-1084-4.
- (5) Walker, Z.; Gandolfo, F.; Orini, S.; Garibotto, V.; Agosta, F.; Arbizu, J.; Bouwman, F.; Drzezga, A.; Nestor, P.; Boccardi, M.; Altomare, D.; Festari, C.; Nobili, F. Clinical utility of FDG PET in Parkinson's disease and atypical parkinsonism associated with dementia. *European Journal of Nuclear Medicine and Molecular Imaging* **2018**, 45 (9), 1534–1545 DOI: 10.1007/s00259-018-4031-2.
- (6) Chandra, A.; Valkimadi, P. E.; Pagano, G.; Cousins, O.; Dervenoulas, G.; Politis, M. Applications of amyloid, tau, and neuroinflammation PET imaging to Alzheimer's disease and mild cognitive impairment. *Human Brain Mapping* **2019**, 40 (18), 5424–5442 DOI: 10.1002/hbm.24782.
- (7) Cybulska, K.; Perk, L.; Booij, J.; Laverman, P.; Rijpkema, M. Huntington's disease: a review of the known PET imaging biomarkers and targeting radiotracers. *Molecules* **2020**, 25 (3), 482–21 DOI: 10.3390/molecules25030482.
- (8) Wu, C.; Li, F.; Niu, G.; Chen, X. PET imaging of inflammation biomarkers. *Theranostics* **2013**, 3 (7), 448–466 DOI: 10.7150/thno.6592.
- (9) Kurihara, H.; Shimizu, C.; Miyakita, Y.; Yoshida, M.; Hamada, A.; Kanayama, Y.; Yonemori, K.; Hashimoto, J.; Tani, H.; Kodaira, M.; M.; Yunokawa, M.; Yamamoto, H.;

- Watanabe, Y.; Fujiwara, Y.; Tamura, K. Molecular imaging using PET for breast cancer. *Breast Cancer* **2015**, *23* (1), 24–32 DOI: 10.1007/s12282-015-0613-z.
- (10) Dijkers, E. C.; Munnink, T. H. O.; Kosterink, J. G.; Brouwers, A. H.; Jager, P. L.; de Jong, J. R.; van Dongen, G. A.; Schröder, C. P.; Hooge, M. N. L.-D.; de Vries, E. G. Biodistribution of ⁸⁹Zr-trastuzumab and PET imaging of HER2-positive lesions in patients with metastatic breast cancer. *Clinical Pharmacology & Therapeutics* **2009**, *87* (5), 586–592 DOI: 10.1038/clpt.2010.12.
- (11) De Ruyscher, D.; Nestle, U.; Jeraj, R.; MacManus, M. PET scans in radiotherapy planning of lung cancer. *Lung Cancer* **2012**, *75* (2), 141–145 DOI: 10.1016/j.lungcan.2011.07.018.
- (12) Duncan, J. R.; Carr, D.; Kaffenberger, B. H. The utility of positron emission tomography with and without computed tomography in patients with nonmelanoma skin cancer. *Journal of the American Academy of Dermatology* **2016**, *75* (1), 186–196 DOI: 10.1016/j.jaad.2016.01.045.
- (13) Jadvar, H. Molecular imaging of prostate cancer with PET. *Journal of Nuclear Medicine* **2013**, *54* (10), 1685–1688 DOI: 10.2967/jnumed.113.126094.
- (14) Auletta, S.; Varani, M.; Horvat, R.; Galli, F.; Signore, A.; Hess, S. PET Radiopharmaceuticals for specific bacteria imaging: a systematic review. *Journal of Clinical Medicine* **2019**, *8* (2), 197–26 DOI: 10.3390/jcm8020197.
- (15) Ametamey, S. M.; Honer, M.; Schubiger, P. A. Molecular imaging with PET. *Chemical Reviews* **2008**, *108* (5), 1501–1516 DOI: 10.1021/cr0782426.
- (16) Niwa, T.; Hosoya, T. Molecular renovation strategy for expeditious synthesis of molecular probes. *Bulletin of the Chemical Society of Japan* **2020**, *93* (2), 230–248 DOI: 10.1246/bcsj.20190310.
- (17) Levin, C. S. Primer on molecular imaging technology. *European Journal of Nuclear Medicine and Molecular Imaging* **2005**, *32* (S02), S325–S345 DOI: 10.1007/s00259-005-1973-y.
- (18) Biomarkers Definitions Working Group. Biomarkers and surrogate endpoints: preferred definitions and conceptual framework. *Clinical Pharmacology & Therapeutics* **2001**, *69* (3), 89–95 DOI: 10.1067/mcp.2001.113989.
- (19) Pirart, J. Diabetes mellitus and its degenerative complications: a prospective study of 4,400 patients observed between 1947 and 1973. *Diabetes Care* **1978**, *1* (4), 252–263 DOI: 10.2337/diacare.1.4.252.
- (20) Ignatowski, A. Über die wirkung des tierischen eiweißes auf die aorta und die parenchymatösen organe der kaninchen. *Virchow's Archive European Journal of Pathology* **1909**, *198* (2), 248–270.
- (21) Waldmann, T. A. Monoclonal antibodies in diagnosis and therapy. *Science* **1991**, *252* (5013), 1657–1662 DOI: 10.1126/science.2047874.
- (22) Reivich, M.; Kuhl, D.; Wolf, A.; Greenberg, J.; Phelps, M.; Ido, T.; Casella, V.; Fowler, J.; Hoffman, E.; Alavi, A.; Som, P.; Sokoloff, L. The [¹⁸F]fluorodeoxyglucose method for the measurement of local cerebral glucose utilization in man. *Circulation Research* **1979**, *44* (1), 127–137 DOI: 10.1161/01.RES.44.1.127.
- (23) Gambhir, S. S.; Czernin, J.; Schwimmer, J.; Silverman, D. H. S.; Coleman, R. E.; Phelps, M. E. A tabulated summary of the FDG PET literature. *Journal of Nuclear Medicine* **2001**, *42* (5), 1S–93S.
- (24) Garnett, E. S.; Firnau, G.; Nahmias, C. Dopamine visualized in the basal ganglia of living man. *Nature* **1983**, *305*, 137–138 DOI: org/10.1038/305137a0.

- (25) Gharibkandi, N. A.; Hosseinimehr, S. J. Radiotracers for imaging of Parkinson's disease. *European Journal of Medicinal Chemistry* **2019**, *166*, 75–89 DOI: 10.1016/j.ejmech.2019.01.029.
- (26) Richter, S.; Wuest, F. ¹⁸F-labeled peptides: the future is bright. *Molecules* **2014**, *19* (12), 20536–20556 DOI: 10.3390/molecules191220536.
- (27) Morris, O.; Fairclough, M.; Grigg, J.; Prenant, C.; McMahon, A. A review of approaches to ¹⁸F radiolabelling affinity peptides and proteins. *Journal of Labelled Compounds and Radiopharmaceuticals* **2019**, *62* (1), 4–23 DOI: 10.1002/jlcr.3634.
- (28) Tolmachev, V.; Stone-Elander, S. Radiolabelled proteins for positron emission tomography: pros and cons of labelling methods. *Biochimica et Biophysica Acta* **2010**, *1800* (5), 487–510 DOI: 10.1016/j.bbagen.2010.02.002.
- (29) Blower, P. J. A nuclear chocolate box: the periodic table of nuclear medicine. *Dalton Transactions* **2015**, *44* (11), 4819–4844 DOI: 10.1039/C4DT02846E.
- (30) Conti, M.; Eriksson, L. Physics of pure and non-pure positron emitters for PET: a review and a discussion. *EJNMMI Physics* **2016**, 1–17 DOI: 10.1186/s40658-016-0144-5.
- (31) Buchholz, H. G.; Herzog, H.; Förster, G. J.; Reber, H.; Nickel, O.; Rosch, F.; Bartenstein, P. PET imaging with yttrium-86: comparison of phantom measurements acquired with different PET scanners before and after applying background subtraction. *Eur J Nucl Med Mol Imaging* **2003**, *30* (5), 716–720 DOI: 10.1007/s00259-002-1112-y.
- (32) Esteves, F. P.; Nye, J. A.; Khan, A.; Folks, R. D.; Halkar, R. K.; Garcia, E. V.; Schuster, D. M.; Lerakis, S.; Raggi, P.; Votaw, J. R. Prompt-gamma compensation in Rb-82 myocardial perfusion 3D PET/CT. *J. Nucl. Cardiol.* **2009**, *17* (2), 247–253 DOI: 10.1007/s12350-009-9170-1.
- (33) Braad, P. E. N.; Hansen, S. B.; Thisgaard, H.; Høiland-Carlsen, P. F. PET imaging with the non-pure positron emitters: ⁵⁵Co, ⁸⁶Y and ¹²⁴I. *Physics in Medicine & Biology* **2015**, *34* 3479–3497 DOI: 10.1088/0031-9155/60/9/3479.
- (34) Heußner, T.; Mann, P.; Rank, C. M.; Schäfer, M.; Dimitrakopoulou-Strauss, A.; Schlemmer, H.-P.; Hadaschik, B. A.; Kopka, K.; Bachert, P.; Kachelrieß, M.; Freitag, M. Investigation of the halo-artifact in ⁶⁸Ga-PSMA-11-PET/MRI. *PLoS ONE* **2017**, *12* (8), e0183329–19 DOI: 10.1371/journal.pone.0183329.
- (35) Wierts, R.; Conti, M.; Claessen, A. G. G.; Herrmann, K.; Kemerink, G. J.; Binse, I.; Wildberger, J. E.; Mottaghy, F. M.; Backes, W. H.; Jentzen, W. Impact of prompt gamma coincidence correction on absorbed dose estimation in differentiated thyroid cancer using ¹²⁴I PET/CT imaging. *Nuclear Medicine Communications* **2018**, *39* (12), 1156–1164 DOI: 10.1097/MNM.0000000000000911.
- (36) Ferguson, S.; Jans, H.-S.; Wuest, M.; Riauka, T.; Wuest, F. Comparison of scandium-44 g with other PET radionuclides in pre-clinical PET phantom imaging. *EJNMMI Physics* **2019**, 1–14 DOI: 10.1186/s40658-019-0260-0.
- (37) Levin, C. S.; Hoffman, E. J. Calculation of positron range and its effect on the fundamental limit of positron emission tomography system spatial resolution. *Physics in Medicine & Biology* **1999**, *44* (3), 781–799 DOI: 10.1088/0031-9155/44/3/019.
- (38) Kolb, A.; Sauter, A. W.; Eriksson, L.; Vandenbrouke, A.; Liu, C. C.; Levin, C.; Pichler, B. J.; Rafecas, M. Shine-through in PET/MR imaging: effects of the magnetic field on positron range and subsequent image artifacts. *Journal of Nuclear Medicine* **2015**, *56* (6), 951–954 DOI: 10.2967/jnumed.114.147637.
- (39) Abdul-Fatah, S. B.; Zamburlini, M.; Halders, S. G. E. A.; Brans, B.; Teule, G. J. J.; Kemerink, G. J. Identification of a shine-through artifact in the trachea with ¹²⁴I PET/CT. *Journal of Nuclear Medicine* **2009**, *50* (6), 909–911 DOI: 10.2967/jnumed.108.060442.

- (40) Warnders, F.-J.; Lub-de Hooge, M. N.; de Vries, E. G. E.; Kosterink, J. G. W. Influence of protein properties and protein modification on biodistribution and tumor uptake of anticancer antibodies, antibody derivatives, and non-Ig scaffolds. *Medicinal Research Reviews* **2018**, *38* (6), 1837–1873 DOI: 10.1002/med.21498.
- (41) Laboratoire National Henri Becquerel. *Library of gamma and alpha emissions*. Retrieved 11 June 2020, from <http://www.nucleide.org/Laraweb/index.php>.
- (42) Brookhaven National Laboratory. *Decay radiation information*. Retrieved 11 June 2020, from <https://www.nndc.bnl.gov/nudat2/>.
- (43) Williams, S.-P. Tissue distribution studies of protein therapeutics using molecular probes: molecular imaging. *The AAPS Journal* **2012**, *14* (3), 389–399 DOI: 10.1208/s12248-012-9348-3.
- (44) Yang, L.; Dong, T.; Revankar, H. M.; Zhang, C.-P. Recent progress on fluorination in aqueous media. *Green Chemistry* **2017**, *19* (17), 3951–3992 DOI: 10.1039/C7GC01566F.
- (45) Ehrenkauf, R. E.; Potocki, J. F.; Jewett, D. M. Simple synthesis of F-18-labeled 2-fluoro-2-deoxy-d-glucose: concise communication. *Journal of Nuclear Medicine* **1984**, *25* (3), 333–337.
- (46) Alauddin, M. M.; 2012. Positron emission tomography (PET) imaging with ¹⁸F-based radiotracers. *American Journal of Nuclear Medicine and Molecular Imaging* **2012**, *2* (1), 55–76.
- (47) Hefter, G. T.; McLay, P. J. The solvation of fluoride ions. I. Free energies for transfer from water to aqueous alcohol and acetonitrile mixtures. *Journal of Solution Chemistry* **1988**, *17* (6), 535–546 DOI: 10.1007/BF00651461.
- (48) Block, D.; Klätte, B.; Knöchel, A.; Beckmann, R.; Holm, U. N.C.A. [18F]-labelling of aliphatic compounds in high yields via aminopolyether - supported nucleophilic substitution. *Journal of Labelled Compounds and Radiopharmaceuticals* **2006**, *23* (5), 467–477 DOI: 10.1002/jlcr.2580230503.
- (49) Müller-Platz, C. M.; Kloster, G.; Legler, G.; Stocklin, G. ¹⁸F–Fluoroacetate: an agent for introducing no-carrier added fluorine-18 into urokinase without loss of biological activity. *Journal of Labelled Compounds and Radiopharmaceuticals* **1982**; Vol. 19, pp 1645–1646.
- (50) Kuhnast, B.; Dollé, F. The challenge of labeling macromolecules with fluorine-18: three decades of research. *Current Radiopharmaceuticals* **2010**, *3* (3), 174–201 DOI: 10.2174/1874471011003030174.
- (51) Schirmacher, R.; Wängler, B.; Bailey, J.; Bernard-Gauthier, V.; Schirmacher, E.; Wängler, C. Small prosthetic groups in ¹⁸F-radiochemistry: useful auxiliaries for the design of ¹⁸F-PET tracers. *Seminars in Nuclear Medicine* **2017**, *47* (5), 474–492 DOI: 10.1053/j.semnuclmed.2017.07.001.
- (52) Krall, N.; da Cruz, F. P.; Boutureira, O.; Bernardes, G. J. L. Site-selective protein-modification chemistry for basic biology and drug development. *Nature Chemistry* **2016**, *8* (2), 103–113 DOI: 10.1038/nchem.2393.
- (53) Grierson, J. R.; Yagle, K. J.; Eary, J. F.; Tait, J. F.; Gibson, D. F.; Lewellen, B.; Link, J. M.; Krohn, K. A. Production of [F-18]fluoroannexin for imaging apoptosis with PET. *Bioconjugate Chemistry* **2004**, *15* (2), 373–379 DOI: 10.1021/bc0300394.
- (54) Tait, J. F.; Smith, C.; Levashova, Z.; Patel, B.; Blankenberg, F. G.; Vanderheyden, J.-L. Improved detection of cell death in vivo with annexin V radiolabeled by site-specific methods. *Journal of Nuclear Medicine* **2006**, *47* (9), 1546–1553.

- (55) Perreault, A.; Knight, J. C.; Wang, M.; Way, J.; Wuest, F. ¹⁸F-Labeled wild-type annexin V: comparison of random and site-selective radiolabeling methods. *Amino Acids* **2015**, 48 (1), 65–74 DOI: 10.1007/s00726-015-2068-0.
- (56) Rosenthal, M. S.; Bosch, A. L.; Nickles, R. J.; Gatley, S. J. Synthesis and some characteristics of no-carrier added [F-18] fluorotrimethylsilane. *International Journal of Applied Radiation and Isotopes* **1985**, 36 (4), 318–319 DOI: 10.1016/0020-708X(85)90094-8.
- (57) Ting, R.; Adam, M. J.; Ruth, T. J.; Perrin, D. M. Arylfluoroborates and alkylfluorosilicates as potential PET imaging agents: high-yielding aqueous biomolecular ¹⁸F-labeling. *Journal of the American Chemical Society* **2005**, 127 (38), 13094–13095 DOI: 10.1021/ja053293a.
- (58) Choudhry, U.; Martin, K. E.; Biagini, S.; Blower, P. J. Alkoxysilane groups for instant labelling of biomolecules with ¹⁸F. *Nuclear Medicine Communications* **2006**, 27 (3), 293 DOI: 10.1097/00006231-200603000-00060.
- (59) Schirmacher, R.; Bradtmöller, G.; Schirmacher, E.; Thews, O.; Tillmanns, J.; Siessmeier, T.; Buchholz, H. G.; Bartenstein, P.; Wängler, B.; Niemeyer, C. M.; Jurkschat, K. ¹⁸F-Labeling of peptides by means of an organosilicon-based fluoride acceptor. *Angewandte Chemie International Edition* **2006**, 45 (36), 6047–6050 DOI: 10.1002/anie.200600795.
- (60) Mu, L.; Höhne, A.; Schubiger, P. A.; Ametamey, S. M.; Graham, K.; Cyr, J. E.; Dinkelborg, L.; Stellfeld, T.; Srinivasan, A.; Voigtmann, U.; Klar, U. Silicon-based building blocks for one-step ¹⁸F-radiolabeling of peptides for PET imaging. *Angewandte Chemie International Edition* **2008**, 47 (26), 4922–4925 DOI: 10.1002/anie.200705854.
- (61) Höhne, A.; Yu, L.; Mu, L.; Reiher, M.; Voigtmann, U.; Klar, U.; Graham, K.; Schubiger, P. A.; Ametamey, S. M. Organofluorosilanes as model compounds for ¹⁸F-labeled silicon-based PET tracers and their hydrolytic stability: experimental data and theoretical calculations (PET=positron emission tomography). *Chemistry - A European Journal* **2009**, 15 (15), 3736–3743 DOI: 10.1002/chem.200802437.
- (62) Szabó, G.; Szieberth, D.; Nyulászi, L. Theoretical study of the hydrolysis of chlorosilane. *Structural Chemistry* **2014**, 26 (1), 231–238 DOI: 10.1007/s11224-014-0543-y.
- (63) Issa, A. A.; El-Azazy, M.; Luyt, A. S. Kinetics of alkoxysilanes hydrolysis: an empirical approach. *Scientific Reports* **2019**, 9 (1), 17624 DOI: 10.1038/s41598-019-54095-0.
- (64) Glaser, M.; Iveson, P.; Hoppmann, S.; Indrevoll, B.; Wilson, A.; Arukwe, J.; Danikas, A.; Bhalla, R.; Hiscock, D. Three methods for ¹⁸F labeling of the HER2-binding affibody molecule Z_{HER2:2891} including preclinical assessment. *Journal of Nuclear Medicine* **2013**, 54 (11), 1981–1988 DOI: 10.2967/jnumed.113.122465.
- (65) Kim, S. H.; Carroll, V. M.; Zhou, D.; Dence, C. S.; Katzenellenbogen, J. A. Beyond conventional silyl acetates: strategies for one-step F-18 fluoride incorporation into aryl silanes under aqueous and organic labelling conditions to produce a useful prosthetic compound and label unprotected complex molecules. *Journal of Labelled Compounds and Radiopharmaceuticals* **2013**, 51 (S1), S157.
- (66) Tisseraud, M.; Schulz, J. X. R.; Vimont, D.; Berlande, M.; Fernandez, P.; Hermange, P.; Fouquet, E. Highly hindered 2-(aryl-di-tert-butylsilyl)-N-methyl-imidazoles: a new tool for the aqueous ¹⁹F- and ¹⁸F-fluorination of biomolecule-based structures. *Chemical Communications* **2018**, 1–4 DOI: 10.1039/C8CC01782D.
- (67) Iovkova, L.; Wängler, B.; Schirmacher, E.; Schirmacher, R.; Quandt, G.; Boening, G.; Schürmann, M.; Jurkschat, K. para-Functionalized aryl-di- tert-butylfluorosilanes as

- potential labeling synthons for ^{18}F radiopharmaceuticals. *Chemistry - A European Journal* **2009**, 15 (9), 2140–2147 DOI: 10.1002/chem.200802266.
- (68) Wängler, B.; Quandt, G.; Iovkova, L.; Schirmacher, E.; Wängler, C.; Boening, G.; Hacker, M.; Schmoeckel, M.; Jurkschat, K.; Bartenstein, P.; Schirmacher, R. Kit-like ^{18}F -labeling of proteins: synthesis of 4-(di-tert-butyl[^{18}F]fluorosilyl)benzenethiol (Si[^{18}F]FA-SH) labeled rat serum albumin for blood pool imaging with PET. *Bioconjugate Chemistry* **2009**, 20 (2), 317–321 DOI: 10.1021/bc800413g.
- (69) Kostikov, A. P.; Chin, J.; Orchowski, K.; Schirmacher, E.; Niedermoser, S.; Jurkschat, K.; Iovkova-Berends, L.; Wängler, C.; Wängler, B.; Schirmacher, R. Synthesis of [^{18}F]SiFB: a prosthetic group for direct protein radiolabeling for application in positron emission tomography. *Nature Protocols* **2012**, 7 (11), 1956–1963 DOI: 10.1038/nprot.2012.110.
- (70) Koudih, R.; Kostikov, A.; Kovacevic, M.; Jolly, D.; Bernard-Gauthier, V.; Chin, J.; Jurkschat, K.; Wängler, C.; Wängler, B.; Schirmacher, R. Automated radiosynthesis of N-succinimidyl 3-(di-tert-butyl[^{18}F]fluorosilyl)benzoate ([^{18}F]SiFB) for peptides and proteins radiolabeling for positron emission tomography. *Applied Radiation and Isotopes* **2014**, 89 (C), 146–150 DOI: 10.1016/j.apradiso.2014.02.017.
- (71) Rosa-Neto, P.; Wängler, B.; Iovkova, L.; Boening, G.; Reader, A.; Jurkschat, K.; Schirmacher, E. [^{18}F]SiFA-isothiocyanate: a new highly effective radioactive labeling agent for lysine-containing proteins. *ChemBioChem* **2009**, 10 (8), 1321–1324 DOI: 10.1002/cbic.200900132.
- (72) Askenasy, H. M.; Anbar, M.; Laor, Y.; Lewitus, Z.; Kosary, I. Z.; Guttman, S. The localization of intracranial space-occupying lesions by fluoroborate ions labelled with fluorine 18. *American Journal of Roentgenology, Radium Therapy, and Nuclear Medicine* **1962**, 88 (2), 350–354.
- (73) Entzian, W.; Aronow, S.; Soloway, A. H.; Sweet, W. H. A preliminary evaluation of F^{18} -labeled tetrafluoroborate as a scanning agent for intracranial tumors. *Journal of Nuclear Medicine* **1964**, 5 (7), 542–550.
- (74) Ting, R.; Harwig, C. W.; Lo, J.; Li, Y.; Adam, M. J.; Ruth, T. J.; Perrin, D. M. Substituent effects on aryltrifluoroborate solvolysis in water: implications for suzuki–miyaura coupling and the design of stable ^{18}F -labeled aryltrifluoroborates for use in PET imaging. *The Journal of Organic Chemistry* **2008**, 73 (12), 4662–4670 DOI: 10.1021/jo800681d.
- (75) Li, Y.; Asadi, A.; Perrin, D. M. Hydrolytic stability of nitrogenous-heteroaryltrifluoroborates under aqueous conditions at near neutral pH. *Journal of Fluorine Chemistry* **2009**, 130 (4), 377–382 DOI: 10.1016/j.jfluchem.2008.12.006.
- (76) Li, Z.; Chansaenpak, K.; Liu, S.; Wade, C. R.; Conti, P. S.; Gabbaï, F. P. Harvesting ^{18}F -fluoride ions in water via direct ^{18}F – ^{19}F isotopic exchange: radiofluorination of zwitterionic aryltrifluoroborates and in vivo stability studies. *MedChemComm* **2012**, 3 (10), 1305–4 DOI: 10.1039/c2md20105d.
- (77) Liu, Z.; Chao, D.; Li, Y.; Ting, R.; Oh, J.; Perrin, D. M. From minutes to years: predicting organotrifluoroborate solvolysis rates. *Chemistry - A European Journal* **2015**, 21 (10), 3924–3928 DOI: 10.1002/chem.201405829.
- (78) Chiotellis, A.; Ahmed, H.; Betzel, T.; Tanriver, M.; White, C. J.; Song, H.; Da Ros, S.; Schibli, R.; Bode, J. W.; Ametamey, S. M. Chemoselective ^{18}F -incorporation into pyridyl acyltrifluoroborates for rapid radiolabelling of peptides and proteins at room temperature. *Chemical Communications* **2020**, 56 (5), 723–726 DOI: 10.1039/C9CC08645E.

- (79) Ting, R.; Harwig, C.; auf dem Keller, U.; McCormick, S.; Austin, P.; Overall, C. M.; Adam, M. J.; Ruth, T. J.; Perrin, D. M. Toward [¹⁸F]-labeled aryltrifluoroborate radiotracers: in vivo positron emission tomography imaging of stable aryltrifluoroborate clearance in mice. *Journal of the American Chemical Society* **2008**, *130* (36), 12045–12055 DOI: 10.1021/ja802734t.
- (80) Harwig, C. W.; Ting, R.; Adam, M. J.; Ruth, T. J.; Perrin, D. M. Synthesis and characterization of 2,6-difluoro-4-carboxyphenylboronic acid and a biotin derivative thereof as captors of anionic aqueous [¹⁸F]-fluoride for the preparation of [¹⁸F/¹⁹F]-labeled aryltrifluoroborates with high kinetic stability. *Tetrahedron Letters* **2008**, *49* (19), 3152–3156 DOI: 10.1016/j.tetlet.2008.03.021.
- (81) Liu, Z.; Li, Y.; Lozada, J.; Pan, J.; Lin, K.-S.; Schaffer, P.; Perrin, D. M. Rapid, one-step, high yielding ¹⁸F-labeling of an aryltrifluoroborate bioconjugate by isotope exchange at very high specific activity. *Journal of Labelled Compounds and Radiopharmaceuticals* **2012**, *55* (14), 491–496 DOI: 10.1002/jlcr.2990.
- (82) auf dem Keller, U.; Bellac, C. L.; Li, Y.; Lou, Y.; Lange, P. F.; Ting, R.; Harwig, C.; Kappelhoff, R.; Dedhar, S.; Adam, M. J.; Ruth, T. J.; Bénard, F.; Perrin, D. M.; Overall, C. M. Novel matrix metalloproteinase inhibitor [¹⁸F]marimastat-aryltrifluoroborate as a probe for in vivo positron emission tomography imaging in cancer. *Cancer Research* **2010**, *70* (19), 7562–7569 DOI: 10.1158/0008-5472.CAN-10-1584.
- (83) Kommidi, H.; Tosi, U.; Maachani, U. B.; Guo, H.; Marnell, C. S.; Law, B.; Souweidane, M. M.; Ting, R. ¹⁸F-Radiolabeled panobinostat allows for positron emission tomography guided delivery of a histone deacetylase inhibitor. *ACS Medicinal Chemistry Letters* **2018**, *9* (2), 114–119 DOI: 10.1021/acsmchemlett.7b00471.
- (84) Li, Y.; Ting, R.; Harwig, C. W.; auf dem Keller, U.; Bellac, C. L.; Lange, P. F.; Inkster, J. A. H.; Schaffer, P.; Adam, M. J.; Ruth, T. J.; Overall, C. M.; Perrin, D. M. Towards kit-like ¹⁸F-labeling of marimastat, a noncovalent inhibitor drug for in vivo PET imaging cancer associated matrix metalloproteases. *MedChemComm* **2011**, *2* (10), 942–949 DOI: 10.1039/c1md00117e.
- (85) Li, Y.; Liu, Z.; Harwig, C. W.; Pourghiasian, M.; Lau, J.; Lin, K.-S.; Schaffer, P.; Benard, F.; Perrin, D. M. ¹⁸F-click labeling of a bombesin antagonist with an alkyne-¹⁸F-ArBF₃:- in vivo PET imaging of tumors expressing the GRP-receptor. *American Journal of Nuclear Medicine and Molecular Imaging* **2013**, *3* (1), 57–70.
- (86) Li, Y.; Guo, J.; Tang, S.; Lang, L.; Chen, X.; Perrin, D. M. One-step and one-pot-two-step radiosynthesis of cyclo-RGD-¹⁸F-aryltrifluoroborate conjugates for functional imaging. *American Journal of Nuclear Medicine and Molecular Imaging* **2013**, *3* (1), 44–56.
- (87) Liu, Z.; Lin, K.-S.; Benard, F.; Pourghiasian, M.; Kiesewetter, D. O.; Perrin, D. M.; Chen, X. One-step ¹⁸F labeling of biomolecules using organotrifluoroborates. *Nature Protocols* **2015**, *10* (9), 1423–1432 DOI: 10.1038/nprot.2015.090.
- (88) McBride, W. J.; Sharkey, R. M.; Karacay, H.; D'Souza, C. A.; Rossi, E. A.; Laverman, P.; Chang, C. H.; Boerman, O. C.; Goldenberg, D. M. A novel method of ¹⁸F radiolabeling for PET. *Journal of Nuclear Medicine* **2009**, *50* (6), 991–998 DOI: 10.2967/jnumed.108.060418.
- (89) McBride, W. J.; D'Souza, C. A.; Sharkey, R. M.; Karacay, H.; Rossi, E. A.; Chang, C.-H.; Goldenberg, D. M. Improved ¹⁸F labeling of peptides with a fluoride-aluminum-chelate complex. *Bioconjugate Chemistry* **2010**, *21* (7), 1331–1340 DOI: 10.1021/bc100137x.

- (90) D'Souza, C. A.; McBride, W. J.; Sharkey, R. M.; Todaro, L. J.; Goldenberg, D. M. High-yielding aqueous ^{18}F -labeling of peptides via Al^{18}F chelation. *Bioconjugate Chemistry* **2011**, *22* (9), 1793–1803 DOI: 10.1021/bc200175c.
- (91) Shetty, D.; Choi, S. Y.; Jeong, J. M.; Lee, J. Y.; Hoigebazar, L.; Lee, Y.-S.; Lee, D. S.; Chung, J.-K.; Lee, M. C.; Chung, Y. K. Stable aluminium fluoride chelates with triazacyclononane derivatives proved by X-ray crystallography and ^{18}F -labeling study. *Chemical Communications* **2011**, *47* (34), 9732–9733 DOI: 10.1039/c1cc13151f.
- (92) Kumar, K.; Ghosh, A. ^{18}F -AlF Labeled peptide and protein conjugates as positron emission tomography imaging pharmaceuticals. *Bioconjugate Chemistry* **2018**, *29* (4), 953–975 DOI: 10.1021/acs.bioconjchem.7b00817.
- (93) Fersing, C.; Bouhleb, A.; Cantelli, C.; Garrigue, P.; Lisowski, V.; Guillet, B. A comprehensive review of non-covalent radiofluorination approaches using aluminum [^{18}F]fluoride: will [^{18}F]AlF replace ^{68}Ga for metal chelate labeling? *Molecules* **2019**, *24* (16), 2866–41 DOI: 10.3390/molecules24162866.
- (94) McBride, W. J.; D'Souza, C. A.; Sharkey, R. M.; Goldenberg, D. M. The radiolabeling of proteins by the [^{18}F]AlF method. *Applied radiation and isotopes* **2012**, *70* (1), 200–204 DOI: 10.1016/j.apradiso.2011.08.013.
- (95) Lütje, S.; Franssen, G. M.; Sharkey, R. M.; Laverman, P.; Rossi, E. A.; Goldenberg, D. M.; Oyen, W. J. G.; Boerman, O. C.; McBride, W. J. Anti-CEA antibody fragments labeled with [^{18}F]AlF for PET imaging of CEA-expressing tumors. *Bioconjugate Chemistry* **2014**, *25* (2), 335–341 DOI: 10.1021/bc4004926.
- (96) Da Pieve, C.; Allott, L.; Martins, C. D.; Vardon, A.; Ciobota, D. M.; Krämer-Marek, G.; Smith, G. Efficient [^{18}F]AlF radiolabeling of $Z_{\text{HER3:8698}}$ affibody molecule for imaging of HER3 positive tumors. *Bioconjugate Chemistry* **2016**, *27* (8), 1839–1849 DOI: 10.1021/acs.bioconjchem.6b00259.
- (97) Lu, C.; Jiang, Q.; Hu, M.; Tan, C.; Yu, H.; Hua, Z. Preliminary biological evaluation of ^{18}F -AlF-NOTA-MAL-cys-annexin V as a novel apoptosis imaging agent. *Oncotarget* **2017**, *8* (31), 51086–51095 DOI: 10.18632/oncotarget.16994.
- (98) Zhou, Z.; Devoogdt, N.; Zalutsky, M. R.; Vaidyanathan, G. An efficient method for labeling single domain antibody fragments with ^{18}F using tetrazine- trans-cyclooctene ligation and a renal brush border enzyme-cleavable linker. *Bioconjugate Chemistry* **2018**, *29* (12), 4090–4103 DOI: 10.1021/acs.bioconjchem.8b00699.
- (99) Basuli, F.; Zhang, X.; Williams, M. R.; Seidel, J.; Green, M. V.; Choyke, P. L.; Swenson, R. E.; Jagoda, E. M. One-pot synthesis and biodistribution of fluorine-18 labeled serum albumin for vascular imaging. *Nuclear Medicine and Biology* **2018**, *62-63*, 63–70 DOI: 10.1016/j.nucmedbio.2018.05.004.
- (100) van der Veen, E. L.; Suurs, F. V.; Cleeren, F.; Bormans, G.; Elsinga, P. H.; Hospers, G. A. P.; Lub-de Hooge, M. N.; de Vries, E. G. E.; de Vries, E. F. J.; F Antunes, I. Development and evaluation of interleukin-2 derived radiotracers for PET imaging of T-cells in mice. *Journal of Nuclear Medicine* **2020** DOI: 10.2967/jnumed.119.238782.
- (101) Huynh, P. T.; Soni, N.; Pal, R.; Sarkar, S.; Jung, J.-M.; Lee, W.; Yoo, J. Direct radiofluorination of a heat-sensitive antibody by Al^{18}F complexation. *New Journal of Chemistry* **2019**, *43* (38), 15389–15395 DOI: 10.1039/C9NJ00722A.
- (102) Cleeren, F.; Lecina, J.; Billaud, E. M. F.; Ahamed, M.; Verbruggen, A.; Bormans, G. M. New chelators for low temperature Al^{18}F -labeling of biomolecules. *Bioconjugate Chemistry* **2016**, *27* (3), 790–798 DOI: 10.1021/acs.bioconjchem.6b00012.

- (103) Musthakahmed, A. M. S.; Billaud, E.; Bormans, G.; Cleeren, F.; Lecina, J.; Verbruggen, A. Methods for low temperature fluorine-18 radiolabelling of biomolecules. *World Intellectual Property Organisation* **2016**.
- (104) Cleeren, F.; Lecina, J.; Bridoux, J.; Devoogdt, N.; Tshibangu, T.; Xavier, C.; Bormans, G. Direct fluorine-18 labeling of heat-sensitive biomolecules for positron emission tomography imaging using the Al¹⁸F-RESCA method. *Nature Protocols* **2018**, *13* (10), 2330–2347 DOI: 10.1038/s41596-018-0040-7.
- (105) Cleeren, F.; Lecina, J.; Ahamed, M.; Raes, G.; Devoogdt, N.; Caveliers, V.; McQuade, P.; Rubins, D. J.; Li, W.; Verbruggen, A.; Xavier, C.; Bormans, G. Al ¹⁸F-Labeling of heat-sensitive biomolecules for positron emission tomography imaging. *Theranostics* **2017**, *7* (11), 2924–2939 DOI: 10.7150/thno.20094.
- (106) Russelli, L.; Martinelli, J.; De Rose, F.; Reder, S.; Herz, M.; Schwaiger, M.; Weber, W.; Tei, L.; D'Alessandria, C. Room temperature Al¹⁸F labeling of 2-aminomethylpiperidine-based chelators for PET imaging. *ChemMedChem* **2020**, *15* (3), 284–292 DOI: 10.1002/cmdc.201900652.
- (107) Bhalla, R.; Darby, C.; Levason, W.; Luthra, S. K.; McRobbie, G.; Reid, G.; Sanderson, G.; Zhang, W. Triaza-macrocyclic complexes of aluminium, gallium and indium halides: fast ¹⁸F and ¹⁹F incorporation via halide exchange under mild conditions in aqueous solution. *Chemical Science* **2014**, *5* (1), 381–391 DOI: 10.1039/C3SC52104D.
- (108) Bhalla, R.; Levason, W.; Luthra, S. K.; McRobbie, G.; Sanderson, G.; Reid, G. Radiofluorination of a pre-formed gallium(III) aza-macrocyclic complex: towards next-generation positron emission tomography (PET) imaging agents. *Chemistry - A European Journal* **2015**, *21* (12), 4688–4694 DOI: 10.1002/chem.201405812.
- (109) Monzittu, F. M.; Khan, I.; Levason, W.; Luthra, S. K.; McRobbie, G.; Reid, G. Rapid aqueous late-stage radiolabelling of [GaF₃(BnMe₂-tacn)] by ¹⁸F/ ¹⁹F isotopic exchange: towards new PET imaging probes. *Angewandte Chemie* **2018**, *130* (22), 6768–6771 DOI: 10.1002/ange.201802446.
- (110) Levason, W.; Luthra, S. K.; McRobbie, G.; Monzittu, F. M.; Reid, G. [AlCl₃(BnMe₂-tacn)] – a new metal chelate scaffold for radiofluorination by Cl/F exchange. *Dalton Transactions* **2017**, *46* (42), 14519–14522 DOI: 10.1039/C7DT02122D.
- (111) Curnock, E.; Levason, W.; Light, M. E.; Luthra, S. K.; McRobbie, G.; Monzittu, F. M.; Reid, G.; Williams, R. N. Group 3 metal trihalide complexes with neutral N-donor ligands – exploring their affinity towards fluoride. *Dalton Transactions* **2018**, *47* (17), 6059–6068 DOI: 10.1039/C8DT00480C.
- (112) Blower, P. J.; Levason, W.; Luthra, S. K.; McRobbie, G.; Monzittu, F. M.; Mules, T. O.; Reid, G.; Subhan, M. N. Exploring transition metal fluoride chelates – synthesis, properties and prospects towards potential PET probes. *Dalton Transactions* **2019**, *48* (20), 6767–6776 DOI: 10.1039/C8DT03696A.
- (113) Inkster, J. A. H.; Liu, K.; Ait-Mohand, S.; Schaffer, P.; Guerin, B.; Ruth, T. J.; Storr, T. Sulfonyl fluoride-based prosthetic compounds as potential ¹⁸F labelling agents. *Chemistry - A European Journal* **2012**, *18* (35), 11079–11087 DOI: 10.1002/chem.201103450.
- (114) Al-Momani, E.; Israel, I.; Buck, A. K.; Samnick, S. Improved synthesis of [¹⁸F]FS-PTAD as a new tyrosine-specific prosthetic group for radiofluorination of biomolecules. *Applied Radiation and Isotopes* **2015**, *104* (C), 136–142 DOI: 10.1016/j.apradiso.2015.06.021.
- (115) Matesic, L.; Wyatt, N. A.; Fraser, B. H.; Roberts, M. P.; Pham, T. Q.; Greguric, I. Ascertaining the suitability of aryl sulfonyl fluorides for [¹⁸F]radiochemistry

- applications: a systematic investigation using microfluidics. *Chem Journal of Organic Chemistry* **2013**, *78* (22), 11262–11270 DOI: 10.1021/jo401759z.
- (116) Zhang, B.; Pascali, G.; Wyatt, N.; Matesic, L.; Klenner, M. A.; Sia, T. R.; Guastella, A. J.; Massi, M.; Robinson, A. J.; Fraser, B. H. Synthesis, bioconjugation and stability studies of [¹⁸F]ethenesulfonyl fluoride. *Journal of Labelled Compounds and Radiopharmaceuticals* **2018**, *61* (11), 847–856 DOI: 10.1002/jlcr.3667.
- (117) Pascali, G.; Matesic, L.; Zhang, B.; King, A. T.; Robinson, A. J.; Ung, A. T.; Fraser, B. H. Sulfur - fluorine bond in PET radiochemistry. *EJNMMI Physics* **2017**, 1–18 DOI: 10.1186/s41181-017-0028-6.
- (118) Zheng, Q.; Xu, H.; Wang, H.; Du, W.-G. H.; Wang, N.; Xiong, H.; Gu, Y.; Noodleman, L.; Yang, G.; Sharples, K. B.; Wu, P. Click chemistry expedited radiosynthesis: sulfur [¹⁸F]fluoride exchange of aryl fluorosulfates. *ChemRxiv* **2019**, preprint, 1–312 DOI: 10.26434/chemrxiv.10314647.v1.
- (119) Kwon, Y.-D.; Jeon, M. H.; Park, N. K.; Seo, J. K.; Son, J.; Ryu, Y. H.; Hong, S. Y.; Chun, J.-H. Synthesis of ¹⁸F-labeled aryl fluorosulfates via nucleophilic radiofluorination. *Organic Letters* **2020**, *22* (14), 5511–5516 DOI: 10.1021/acs.orglett.0c01868.
- (120) Hong, H.; Zhang, L.; Xie, F.; Zhuang, R.; Jiang, D.; Liu, H.; Li, J.; Yang, H.; Zhang, X.; Nie, L.; Li, Z. Rapid one-step ¹⁸F-radiolabeling of biomolecules in aqueous media by organophosphine fluoride acceptors. *Nature Communications* **2019**, 1–7 DOI: 10.1038/s41467-019-08953-0.
- (121) Smolskaya, S.; Andreev, Y. Site-specific incorporation of unnatural amino acids into escherichia coli recombinant protein: methodology development and recent achievement. *Biomolecules* **2019**, *9* (7), 255–17 DOI: 10.3390/biom9070255.
- (122) Chalker, J. M.; Gunnoo, S. B.; Boutureira, O.; Gerstberger, S. C.; Fernández-González, M.; Bernardes, G. J. L.; Griffin, L.; Hailu, H.; Schofield, C. J.; Davis, B. G. Methods for converting cysteine to dehydroalanine on peptides and proteins. *Chemical Science* **2011**, *2* (9), 1666–1676 DOI: 10.1039/c1sc00185j.
- (123) Matos, M. J.; Oliveira, B. L.; Martínez-Sáez, N.; Guerreiro, A.; Cal, P. M. S. D.; Bertoldo, J.; Maneiro, M.; Perkins, E.; Howard, J.; Deery, M. J.; Chalker, J. M.; Corzana, F.; Jiménez-Osés, G.; Bernardes, G. J. L. Chemo- and regioselective lysine modification on native proteins. *Journal of the American Chemical Society* **2018**, *140* (11), 4004–4017 DOI: 10.1021/jacs.7b12874.
- (124) Freedy, A. M.; Matos, M. J.; Boutureira, O.; Corzana, F.; Guerreiro, A.; Akkapeddi, P.; Somovilla, V. J.; Rodrigues, T.; Nicholls, K.; Xie, B.; Jiménez-Osés, G.; Brindle, K. M.; Neves, A. A.; Bernardes, G. J. L. Chemoselective installation of amine bonds on proteins through aza-michael ligation. *Journal of the American Chemical Society* **2017**, *139* (50), 18365–18375 DOI: 10.1021/jacs.7b10702.
- (125) Corey, E. J.; Venkateswarlu, A. Protection of hydroxyl groups as tert-butyl dimethylsilyl derivatives. *Journal of the American Chemical Society* **1972**, *94* (17), 6190–6191 DOI: 10.1021/ja00772a043.
- (126) Chen, C.-H.; Chen, W.-H.; Liu, Y.-H.; Lim, T.-S.; Luh, T.-Y. Folding of alternating dialkylsilylene-spaced donor-acceptor copolymers: the oligomer approach. *Chemistry - A European Journal* **2011**, *18* (1), 347–354 DOI: 10.1002/chem.201102031.
- (127) Jones, R. G. The halogen-metal interconversion reaction with organolithium compounds. *Organic Reactions* **2011**, *6*, 339–366 DOI: 10.1002/047126418.or006.07.
- (128) Gurst, J. E. Characterization and determination of organic azides. Patai, S. *The azido group* **1971**, John Wiley & Son Ltd. DOI: 10.1002/9789479771266.

- (129) Bennett, S. M.; Tang, Y.; McMaster, D.; Bright, F. V.; Detty, M. R. A xerogel-sequestered selenoxide catalyst for brominations with hydrogen peroxide and sodium bromide in an aqueous environment. *Journal of Organic Chemistry* **2008**, *73* (17), 6849–6852 DOI: 10.1021/jo801234e.
- (130) Zubir, El, O.; Barlow, I.; Ul-Haq, E.; Tajuddin, H. A.; Williams, N. H.; Leggett, G. J. Generic Methods for Micrometer- And Nanometer-Scale Surface Derivatization Based on Photochemical Coupling of Primary Amines to Monolayers of Aryl Azides on Gold and Aluminum Oxide Surfaces. *Langmuir* **2013**, *29* (4), 1083–1092 DOI: 10.1021/la303746e.
- (131) Miseta, A.; Csutora, P. Relationship between the occurrence of cysteine in proteins and the complexity of organisms. *Molecular biology and evolution* **2000**, *17* (8), 1232–1239 DOI: 10.1093/oxfordjournals.molbev.a026406.
- (132) Rosen, C. B.; Francis, M. B. Targeting the N terminus for site-selective protein modification. *Nature Cell Biology* **2017**, *13* (7), 697–705 DOI: 10.1038/nchembio.2416.
- (133) Baldwin, A. D.; Kiick, K. L. Tunable degradation of maleimide–thiol adducts in reducing environments. *Bioconjugate Chemistry* **2011**, *22* (10), 1946–1953 DOI: 10.1021/bc200148v.
- (134) Szijj, P. A.; Bahou, C.; Chudasama, V. Minireview: addressing the retro-Michael instability of maleimide bioconjugates. *Drug Discovery Today: Technologies* **2018**, *30*, 27–34 DOI: 10.1016/j.ddtec.2018.07.002.
- (135) Chalker, J. M.; Bernardes, G. J. L.; Lin, Y. A.; Davis, B. G. Chemical modification of proteins at cysteine: opportunities in chemistry and biology. *Chemistry - An Asian Journal* **2009**, *4* (5), 630–640 DOI: 10.1002/asia.200800427.
- (136) Gunnoo, S. B.; Madder, A. Chemical protein modification through cysteine. *ChemBioChem* **2016**, *17* (7), 529–553 DOI: 10.1002/cbic.201500667.
- (137) Reddy, N. C.; Kumar, M.; Molla, R.; Rai, V. Chemical methods for modification of proteins. *Organic & Biomolecular Chemistry* **2020**, 1–35 DOI: 10.1039/D0OB00857E.
- (138) Komander, D.; Rape, M. The ubiquitin code. *Annual Review of Biochemistry* **2012**, *81* (1), 203–229 DOI: 10.1146/annurev-biochem-060310-170328.
- (139) Yau, R.; Rape, M. The increasing complexity of the ubiquitin code. *Nature Cell Biology* **2016**, *18* (6), 579–586 DOI: 10.1038/ncb3358.
- (140) Liu, J.; Chen, Q.; Rozovsky, S. Utilizing selenocysteine for expressed protein ligation and bioconjugations. *Journal of the American Chemical Society* **2017**, *139* (9), 3430–3437 DOI: 10.1021/jacs.6b10991.
- (141) Lee, B.; Sun, S.; Jiménez-Moreno, E.; Neves, A. A.; Bernardes, G. J. L. Site-selective installation of an electrophilic handle on proteins for bioconjugation. *Bioorganic & Medicinal Chemistry* **2018**, *26* (11), 3060–3064 DOI: 10.1016/j.bmc.2018.02.028.
- (142) Davletov, B. A.; Südhof, T. C. A single C₂ domain from Synaptotagmin I is sufficient for high affinity Ca²⁺/phospholipid binding. *The Journal of Biological Chemistry* **1993**, *268* (35), 26386–26390.
- (143) Alam, I. S.; Neves, A. A.; Witney, T. H.; Boren, J.; Brindle, K. M. Comparison of the C2A domain of Synaptotagmin-I and annexin-V as probes for detecting cell death. *Bioconjugate Chemistry* **2010**, *21* (5), 884–891 DOI: 10.1021/bc9004415.
- (144) Wuest, F.; Berndt, M.; Bergmann, R.; van den Hoff, J.; Pietzsch, J. Synthesis and application of [¹⁸F]FDG-maleimidehexyloxime ([¹⁸F]FDG-MHO): a [¹⁸F]FDG-based prosthetic group for the chemoselective ¹⁸F-labeling of peptides and proteins. *Bioconjugate Chemistry* **2008**, *19* (6), 1202–1210 DOI: 10.1021/bc8000112.

- (145) Suttapitugsakul, S.; Xiao, H.; Smeekens, J.; Wu, R. Evaluation and optimization of reduction and alkylation methods to maximize peptide identification with MS-based proteomics. *Molecular BioSystems* **2017**, *13* (12), 2574–2582 DOI: 10.1039/C7MB00393E.
- (146) Moody, P.; Chudasama, V.; Nathani, R. I.; Maruani, A.; Martin, S.; Smith, M. E. B.; Caddick, S. A rapid, site-selective and efficient route to the dual modification of DARPins. *Chemical Communications* **2014**, *50* (38), 4898–4900 DOI: 10.1039/C4CC00053F.
- (147) Ellman, G. L. Tissue sulfhydryl groups. *Archives of Biochemistry and Biophysics* **1959**, *82* (1), 70–77 DOI: 10.1016/0003-9861(59)90090-6.
- (148) Dawson, P. E.; Muir, T. W.; Clark-Lewis, I.; Kent, S. B. Synthesis of proteins by native chemical ligation. *Science* **1994**, *266* (5186), 776–779 DOI: 10.1126/science.7973629.
- (149) Chen, X.; Muthoosamy, K.; Pfisterer, A.; Neumann, B.; Weil, T. Site-selective lysine modification of native proteins and peptides via kinetically controlled labeling. *Bioconjugate Chemistry* **2012**, *23* (3), 500–508 DOI: 10.1021/bc200556n.
- (150) Krantz, A.; Hanel, A. M.; Strug, I.; Wilczynski, A.; Wolff, J. J.; Huang, W.; Huang, L. H.; Settineri, T.; Holmes, D. L.; Hardy, M. C.; Bridan, D. P. Site-specific labeling of a protein lysine residue by novel kinetic labeling combinatorial libraries. *Computational and Structural Biotechnology* **2014**, *9* (15), e201403001 DOI: 10.5936/csbj.201403001.
- (151) Pham, G. H.; Ou, W.; Bursulaya, B.; DiDonato, M.; Herath, A.; Jin, Y.; Hao, X.; Loren, J.; Spraggon, G.; Brock, A.; Uno, T.; Geierstanger, B. H.; Cellitti, S. E. Tuning a protein-labeling reaction to achieve highly site selective lysine conjugation. *ChemBioChem* **2018**, *19* (8), 799–804 DOI: 10.1002/cbic.201700611.
- (152) Mero, A.; Grigoletto, A.; Maso, K.; Yoshioka, H.; Rosato, A.; Pasut, G. Site-selective enzymatic chemistry for polymer conjugation to protein lysine residues: PEGylation of G-CSF at lysine-41. *Polymer Chemistry* **2016**, *7* (42), 6545–6553 DOI: 10.1039/C6PY01616B.
- (153) Adusumalli, S. R.; Rawale, D. G.; Singh, U.; Tripathi, P.; Paul, R.; Kalra, N.; Mishra, R. K.; Shukla, S.; Rai, V. Single-site labeling of native proteins enabled by a chemoselective and site-selective chemical technology. *Journal of the American Chemical Society* **2018**, *140* (44), 15114–15123 DOI: 10.1021/jacs.8b10490.
- (154) Chilamari, M.; Kalra, N.; Shukla, S.; Rai, V. Single-site labeling of lysine in proteins through a metal-free multicomponent approach. *Chemical Communications* **2018**, *54* (53), 7302–7305 DOI: 10.1039/C8CC03311K.
- (155) Zhang, Y.; Liang, Y.; Huang, F.; Zhang, Y.; Li, X.; Xia, J. Site-selective lysine reactions guided by protein-peptide interaction. *Biochemistry* **2019**, *58* (7), 1010–1018 DOI: 10.1021/acs.biochem.8b01223.
- (156) Hymel, D.; Liu, F. Selective lysine modification enabled by intramolecular acyl transfer. *Organic Letters* **2020**, *22* (8), 3067–3071 DOI: 10.1021/acs.orglett.0c00816.
- (157) Fleming, A. On a remarkable bacteriolytic element found in tissues and secretions. *Proceedings of the Royal Society of London* **1922**, *93* (653), 306–317 DOI: 10.1098/rspb.1922.0023.
- (158) Lesnierowski, G.; Kijowski, J. Lysozyme; Huopalahti, R., López-Fandiño, R., Anton, M., Schade, R., Eds.; Bioactive egg compounds **2007**, Springer Berlin Heidelberg.
- (159) Brass, S.; Chan, N.-S.; Gerlach, C.; Luksch, T.; Böttcher, J.; Diederich, W. E. Synthesis of 2,3,4,7-tetrahydro-1*H*-azepines as privileged ligand scaffolds for the design of aspartic protease inhibitors via a ring-closing metathesis approach. *Journal of*

- Organometallic Chemistry* **2006**, 691 (24-25), 5406–5422 DOI: 10.1016/j.jorgchem.2006.09.031.
- (160) Cal, P. M. S. D.; Sieglitz, F.; Santos, F. M. F.; Parente Carvalho, C.; Guerreiro, A.; Bertoldo, J. B.; Pischel, U.; Gois, P. M. P.; Bernardes, G. J. L. Site-selective installation of BASHY fluorescent dyes to annexin V for targeted detection of apoptotic cells. *Chemical Communications* **2017**, 53 (2), 368–371 DOI: 10.1039/C6CC08671C.
- (161) Young, D. D.; Schultz, P. G. Playing with the molecules of life. *ACS Chemical Biology* **2018**, 13 (4), 854–870 DOI: 10.1021/acscchembio.7b00974.
- (162) Xie, J.; Schultz, P. G. A chemical toolkit for proteins - an expanded genetic code. *Nature Reviews Molecular Cell Biology* **2006**, 7 (10), 775–782 DOI: 10.1038/nrm2005.
- (163) Xie, J.; Schultz, P. G. An expanding genetic code. *Methods* **2005**, 36 (3), 227–238 DOI: 10.1016/j.ymeth.2005.04.010.
- (164) Guo, J.; Melançon, C. E., III; Lee, H. S.; Groff, D.; Schultz, P. G. Evolution of amber suppressor tRNAs for efficient bacterial production of proteins containing nonnatural amino acids. *Angewandte Chemie International Edition* **2009**, 48 (48), 9148–9151 DOI: 10.1002/anie.200904035.
- (165) Wang, L.; Zhang, Z. W.; Brock, A.; Schultz, P. G. Addition of the keto functional group to the genetic code of *Escherichia coli*. *Proceedings of the National Academy of Sciences* **2003**, 100 (1), 56–61 DOI: 10.1073/pnas.0234824100.
- (166) Chin, J. W.; Santoro, S. W.; Martin, A. B.; King, D. S.; Wang, L.; Schultz, P. G. Addition of *p*-azido-L-phenylalanine to the genetic code of *Escherichia coli*. *Journal of the American Chemical Society* **2002**, 124 (31), 9026–9027 DOI: 10.1021/ja027007w.
- (167) Chin, J. W.; Martin, A. B.; King, D. S.; Wang, L.; Schultz, P. G. Addition of a photocrosslinking amino acid to the genetic code of *Escherichia coli*. *Proceedings of the National Academy of Sciences* **2002**, 99 (17), 11020–11024 DOI: 10.1073/pnas.172226299.
- (168) Schultz, K. C.; Supekova, L.; Ryu, Y.; Xie, J.; Perera, R.; Schultz, P. G. A genetically encoded infrared probe. *Journal of the American Chemical Society* **2006**, 128 (43), 13984–13985 DOI: 10.1021/ja0636690.
- (169) Brustad, E.; Bushey, M. L.; Lee, J. W.; Groff, D.; Liu, W.; Schultz, P. G. A genetically encoded boronate-containing amino acid. *Angewandte Chemie International Edition* **2008**, 47 (43), 8220–8223 DOI: 10.1002/anie.200803240.
- (170) Xie, J.; Liu, W.; Schultz, P. G. A genetically encoded bidentate, metal-binding amino acid. *Angewandte Chemie International Edition* **2007**, 46 (48), 9239–9242 DOI: 10.1002/anie.200703397.
- (171) Lee, H. S.; Spraggon, G.; Schultz, P. G.; Wang, F. Genetic incorporation of a metal-ion chelating amino acid into proteins as a biophysical probe. *Journal of the American Chemical Society* **2009**, 131 (7), 2481–2483 DOI: 10.1021/ja808340b.
- (172) Iovkova, L.; Könnig, D.; Wängler, B.; Schirmacher, R.; Schoof, S.; Arndt, H.-D.; Jurkschat, K. SiFA-Modified phenylalanine: a key compound for the efficient synthesis of ¹⁸F-labelled peptides. *European Journal of Inorganic Chemistry* **2011**, 2011 (14), 2238–2246 DOI: 10.1002/ejic.201100142.
- (173) Fernandes, R. A.; Kumar, P. PCC-mediated novel oxidation reactions of homobenzylic and homoallylic alcohols. *Tetrahedron Letters* **2003**, 44 (6), 1275–1278 DOI: 10.1016/S0040-4039(02)02784-3.
- (174) Lu, X.; Wan, B.; Franzblau, S. G.; You, Q. Design, synthesis and anti-tubercular evaluation of new 2-acylated and 2-alkylated amino-5-(4-(benzyloxy)phenyl)thiophene-

- 3-carboxylic acid derivatives. Part 1. *European Journal of Medicinal Chemistry* **2011**, 46 (9), 3551–3563 DOI: 10.1016/j.ejmech.2011.05.018.
- (175) Gigante, F.; Kaiser, M.; Brun, R.; Gilbert, I. H. Design and preparation of sterol mimetics as potential antiparasitics. *Bioorganic & Medicinal Chemistry* **2010**, 18 (20), 7291–7301 DOI: 10.1016/j.bmc.2010.08.007.
- (176) Piancatelli, G.; Scettri, A.; D'Auria, M. Pyridinium chlorochromate in the organic synthesis: a convenient oxidation of enol-ethers to esters and lactones. *Tetrahedron Letters* **1977**, 18 (39), 3483–3484 DOI: 10.1016/S0040-4039(01)83272-X.
- (177) Baskaran, S.; Islam, I.; Raghavan, M.; Chandrasekaran, S. Pyridinium chlorochromate in organic synthesis. A facile and selective oxidative cleavage of enol ethers. *Chemistry Letters* **1987**, 16 (6), 1175–1178 DOI: 10.1246/cl.1987.1175.
- (178) Fetizon, M.; Goulaouic, P.; Hanna, I. 1, 4-dioxene in organic chemistry. Part VII Regiospecific oxidative cleavage of 1, 4-dioxenyl carbinols with pyridinium chlorochromate. A new method for the preparation of α -hydroxy acids and α -keto acids. *Tetrahedron Letters* **1988**, 29 (48), 6261–6264.
- (179) Bijoy, P.; Subba Rao, G. S. R. An unusual C–C bond cleavage with chromium vi reagents: oxidation of primary alcohols to ketones. *Synthetic Communications* **1993**, 23 (19), 2701–2708 DOI: 10.1080/00397919308013800.
- (180) Li, M.; Johnson, M. E. Oxidation of certain 4-substituted phenethyl alcohols with collins reagent: on the mechanism of a carbon-carbon bond cleavage. *Synthetic Communications* **1995**, 25 (4), 533–537 DOI: 10.1080/00397919508011387.
- (181) Bhosale, S. M.; Momin, A. A.; Gawade, R. L.; Puranik, V. G.; Kusurkar, R. S. A new synthetic route for 1,2-diketo compounds using unexpected C–C bond cleavage by PCC. *Tetrahedron Letters* **2012**, 53 (39), 5327–5330 DOI: 10.1016/j.tetlet.2012.07.095.
- (182) Cisneros, A.; Fernández, S.; Hernández, J. E. Cleavage of vicinal diols by pyridinium chlorochromate. *Synthetic Communications* **2006**, 12 (11), 833–838 DOI: 10.1080/00397918208065960.
- (183) Norris, M. D.; Perkins, M. V. Total Synthesis of Plakilactones C, B and des-Hydroxyplakilactone B by the Oxidative Cleavage of Gracilioether Furanylidenes. *Journal of Organic Chemistry* **2016**, 81 (15), 6848–6854 DOI: 10.1021/acs.joc.6b01196.
- (184) Zhang, L.; Bi, X.; Guan, X.; Li, X.; Liu, Q.; Barry, B.-D.; Liao, P. Chemoselective oxidative C(CO)—C(methyl) bond cleavage of methyl ketones to aldehydes catalyzed by cui with molecular oxygen. *Angewandte Chemie International Edition* **2013**, 52 (43), 11303–11307 DOI: 10.1002/anie.201305010.
- (185) Liu, M.; Zhang, Z.; Shen, X.; Liu, H.; Zhang, P.; Chen, B.; Han, B. Stepwise degradation of hydroxyl compounds to aldehydes via successive C–C bond cleavage. *Chemical Communications* **2019**, 55 (7), 925–928 DOI: 10.1039/C8CC09504C.
- (186) Nishimura, T.; Onoue, T.; Ohe, K.; Uemura, S. Palladium(II)-catalyzed oxidation of alcohols to aldehydes and ketones by molecular oxygen. *Journal of Organic Chemistry* **1999**, 64 (18), 6750–6755 DOI: 10.1021/jo9906734.
- (187) Omura, K.; Swern, D. Oxidation of alcohols by "activated" dimethyl sulfoxide. a preparative, steric and mechanistic study. *Tetrahedron* **1978**, 34 (11), 1651–1660 DOI: 10.1016/0040-4020(78)80197-5.
- (188) Ley, S. V.; Norman, J.; Griffith, W. P.; Marsden, S. P. Tetrapropylammonium perruthenate, $\text{Pr}_4\text{N}^+\text{RuO}_4^-$, TPAP: a catalytic oxidant for organic synthesis. *Synthesis* **1994**, 1994 (07), 639–666 DOI: 10.1055/s-1994-25538.
- (189) Anelli, P. L.; Biffi, C.; Montanari, F.; Quici, S. Fast and selective oxidation of primary alcohols to aldehydes or to carboxylic acids and of secondary alcohols to ketones

- mediated by oxoammonium salts under two-phase conditions. *Journal of Organic Chemistry* **1987**, 52 (12), 2559–2562 DOI: 10.1021/jo00388a038.
- (190) de Nooy, A.; Besemer, A. C.; van Bekkum, H. Highly selective nitroxyl radical-mediated oxidation of primary alcohol groups in water-soluble glucans. *Archives of Biochemistry and Biophysics* **1995**, 269 (1), 89–98.
- (191) Tojo, G.; Fernández, M. TEMPO-mediated oxidations; Tojo, G. *Oxidation of primary alcohols to carboxylic acids* **2007**. Springer, New York, NY.
- (192) Xu, S.; Itto, K.; Satoh, M.; Arimoto, H. Unexpected dehomologation of primary alcohols to one-carbon shorter carboxylic acids using o-iodoxybenzoic acid (IBX). *Chemical Communications* **2014**, 50 (21), 2758–2761 DOI: 10.1039/C3CC49160A.
- (193) Strecker, A. Ueber die künstliche bildung der milchsäure und einen neuen, dem glycocoll homologen körper. *Justus Liebigs Annalen der Chemie* **1850**, 75 (1), 27–45 DOI: 10.1002/jlac.18500750103.
- (194) Ogata, Y.; Kawasaki, A. Mechanistic aspects of the Strecker aminonitrile synthesis. *Journal of the Chemical Society B: Physical Organic* **1971**, 325–325 DOI: 10.1039/j29710000325.
- (195) Guendouzi, M. E.; Faridi, J.; Khamar, L. Chemical speciation of aqueous hydrogen fluoride at various temperatures from 298.15 K to 353.15 K. *Fluid Phase Equilibria* **2019**, 499, 112244–11 DOI: 10.1016/j.fluid.2019.112244.
- (196) Lajoie, M. J.; Rovner, A. J.; Goodman, D. B.; Aerni, H. R.; Haimovich, A. D.; Kuznetsov, G.; Mercer, J. A.; Wang, H. H.; Carr, P. A.; Mosberg, J. A.; Rohland, N.; Schultz, P. G.; Jacobson, J. M.; Rinehart, J.; Church, G. M.; Issacs, F.J. Genomically recoded organisms expand biological functions. *Science* **2013**, 342 (6156), 357–360 DOI: 10.1126/science.1241459.
- (197) Zheng, Y.; Lajoie, M. J.; Italia, J. S.; Chin, M. A.; Church, G. M.; Chatterjee, A. Performance of optimized noncanonical amino acid mutagenesis systems in the absence of release factor 1. *Molecular BioSystems* **2016**, 12 (6), 1746–1749 DOI: 10.1039/C6MB00070C.
- (198) Young, D. D.; Young, T. S.; Jahnz, M.; Ahmad, I.; Spraggon, G.; Schultz, P. G. An evolved aminoacyl-trna synthetase with atypical polysubstrate specificity. *Biochemistry* **2011**, 50 (11), 1894–1900 DOI: 10.1021/bi101929e.
- (199) Miyake-Stoner, S. J.; Refakis, C. A.; Hammill, J. T.; Lusic, H.; Hazen, J. L.; Deiters, A.; Mehl, R. A. Generating permissive site-specific unnatural aminoacyl-tRNA synthetases. *Biochemistry* **2010**, 49 (8), 1667–1677 DOI: 10.1021/bi901947r.
- (200) Young, D. D.; Jockush, S.; Turro, N. J.; Schultz, P. G. Synthetase polyspecificity as a tool to modulate protein function. *Bioorganic & Medicinal Chemistry Letters* **2011**, 21 (24), 7502–7504 DOI: 10.1016/j.bmcl.2011.09.108.
- (201) Young, T. S.; Ahmad, I.; Yin, J. A.; Schultz, P. G. An enhanced system for unnatural amino acid mutagenesis in *E. coli*. *Journal of Molecular Biology* **2010**, 395 (2), 361–374 DOI: 10.1016/j.jmb.2009.10.030.
- (202) Santoro, S. W.; Wang, L.; Herberich, B.; King, D. S.; Schultz, P. G. An efficient system for the evolution of aminoacyl-tRNA synthetase specificity. *Nature Biotechnology* **2002**, 20 (10), 1044–1048 DOI: 10.1038/nbt742.
- (203) Cellitti, S. E.; Jones, D. H.; Lagpacan, L.; Hao, X.; Zhang, Q.; Hu, H.; Brittain, S. M.; Brinker, A.; Caldwell, J.; Bursulaya, B.; Spraggon, G.; Brock, A.; Rye, Y.; Uno, T.; Schultz, P. G.; Geierstanger, B. H. *In vivo* incorporation of unnatural amino acids to probe structure, dynamics, and ligand binding in a large protein by nuclear magnetic

- resonance spectroscopy. *Journal of the American Chemical Society* **2008**, 130 (29), 9268–9281 DOI: 10.1021/ja801602q.
- (204) Zhu, M.; Dai, X. High salt cross-protects *Escherichia coli* from antibiotic treatment through increasing efflux pump expression. *mSphere* **2018**, 3 (2), 230–238 DOI: 10.1128/mSphere.00095-18.
- (205) Miyake-Stoner, S. J.; Miller, A. M.; Hammill, J. T.; Peeler, J. C.; Hess, K. R.; Mehl, R. A.; Brewer, S. H. Probing protein folding using site-specifically encoded unnatural amino acids as FRET donors with tryptophan. *Biochemistry* **2009**, 48 (25), 5953–5962 DOI: 10.1021/bi900426d.
- (206) Seitchik, J. L.; Peeler, J. C.; Taylor, M. T.; Blackman, M. L.; Rhoads, T. W.; Cooley, R. B.; Refakis, C.; Fox, J. M.; Mehl, R. A. Genetically encoded tetrazine amino acid directs rapid site-specific *in vivo* bioorthogonal ligation with trans-cyclooctenes. *Journal of the American Chemical Society* **2012**, 134 (6), 2898–2901 DOI: 10.1021/ja2109745.
- (207) Ryu, Y.; Schultz, P. G. Systems for the expression of orthogonal translation components eubacterial host cells. *US 2009/0181429 A1*. July 16, **2009**.

Chapter Eight

Appendices

8.1 Appendix A

Raw fluorescence data recorded at 510 nm and t-test p -values for the incorporation of 72 into sfGFP in C321. Δ A *E.coli* cells.

pEVOL plasmid \pm UAA	Replicate			t-test p -value
	1	2	3	
Blank	0	0	8	
pBiPy + UAA	1365	1423	1178	0.423
pBiPy – UAA	1073	1379	1623	
HQA + UAA	1968	9078	7812	0.424
HQA – UAA	7710	4360	5311	
pBpF + UAA	2631	3165	1939	0.061
pBpF – UAA	1857	2085	1302	
pAzF + UAA	767	237	328	0.075
pAzF – UAA	458	1365	1290	

pCNF + UAA	1494	833	427	0.088
pCNF – UAA	1410	1246	2044	
pAcF + UAA	596	376	965	0.051
pAcF – UAA	1314	1748	849	
pBoF + UAA	1388	665	1147	0.133
pBoF – UAA	1040	1696	1618	

Raw fluorescence data recorded at 510 nm and t-test *p*-values for the incorporation of 72 into sfGFP in DH10B *E.coli* cells.

pEVOL plasmid ± UAA	Replicate			t-test <i>p</i> -value
	1	2	3	
Blank	0	0	8	
pBiPy + UAA	801	916	830	0.192
pBiPy – UAA	771	851	803	
HQA + UAA	8508	6113	10928	0.046
HQA – UAA	4074	5996	5513	
pBpF + UAA	23000	39086	42066	0.019
pBpF – UAA	19109	13335	16164	
pAzF + UAA	7212	7684	7874	0.357
pAzF – UAA	2588	9209	8489	
pCNF + UAA	13800	10878	12865	0.043
pCNF – UAA	7192	3838	11080	
pAcF + UAA	22208	19641	16507	0.035
pAcF – UAA	10307	8729	17004	
pBoF + UAA	1604	1684	1552	0.0002
pBoF – UAA	1181	1122	1090	